



The University of
Nottingham

**The Effect of Ethanol-Gasoline Blends on
SI Engine Energy Balance and
Heat Transfer Characteristics**

Taleb Alrayyes, BEng (Hons)

GEORGE GREEN LIBRARY OF
SCIENCE AND ENGINEERING

*Thesis submitted to the University of Nottingham
for the degree of Doctor of Philosophy*

September 2010

Contents

| | |
|---|-------------|
| CONTENTS | I |
| ABSTRACT | V |
| ACKNOWLEDGMENT | VII |
| NOMENCLATURE | VIII |
| ABBREVIATIONS | X |
| CHAPTER 1 INTRODUCTION | 1 |
| 1.1 Overview | 1 |
| 1.1.1 European biofuels policy | 3 |
| 1.2 Objective | 4 |
| 1.3 Thesis layout | 5 |
| CHAPTER 2 LITERATURE REVIEW | 7 |
| 2.1 Introduction | 7 |
| 2.2 Ethanol Production | 7 |
| 2.2.1 The production process | 8 |
| 2.3 Net energy and Green house gases..... | 9 |
| 2.4 Comparison of ethanol and gasoline properties | 10 |
| 2.5 Emissions..... | 14 |
| 2.6 Engine Combustion behaviour..... | 18 |
| 2.7 The use of ethanol in direct injection spark ignition engines (DISI engines)..... | 19 |
| 2.8 Other alcohol considered as alternative fuel..... | 21 |
| 2.9 Concluding comments..... | 22 |
| CHAPTER 3 EXPERIMENTAL TEST FACILITIES | 23 |
| 3.1 Introduction..... | 23 |
| 3.2 Engine description and Test Cell Facilities | 23 |

Table of contents

| | | |
|--|--|-----------|
| 3.2.1 | Fuel delivery circuit..... | 25 |
| 3.3 | Engine Data Acquisition and Sensor Calibration..... | 25 |
| 3.3.1 | Engine Pressure and Temperature | 25 |
| 3.3.2 | Engine Encoder and TDC allocation | 26 |
| 3.3.3 | Fuel Flow Measurement | 27 |
| 3.3.4 | Coolant and air flow rate Measurement:..... | 28 |
| 3.3.5 | AFR sensor | 29 |
| 3.3.6 | Exhaust gas analysis | 29 |
| 3.4 | Engine management system ATI | 30 |
| 3.5 | dSPACE control and data acquisition system | 31 |
| 3.6 | Main Measurement and calculations..... | 33 |
| 3.6.1 | In-cylinder pressure data and mean effective pressure (MEP) | 33 |
| 3.6.2 | Burned mass fraction (EGR & Residual mass fraction) | 35 |
| 3.7 | Errors and repeatability | 38 |
| 3.8 | Summary & Conclusion..... | 40 |
| CHAPTER 4 BASIC COMPARISON BETWEEN GASOLINE-ETHANOL MIXTURES..... | | 41 |
| 4.1 | Introduction | 41 |
| 4.2 | Experimental fuels | 41 |
| 4.3 | Selection of experimental comparison parameters..... | 42 |
| 4.4 | AFR_{stoich}, calorific value and adiabatic flame temperature | 42 |
| 4.5 | Power output and fuel consumption | 45 |
| 4.6 | Spark timing (ST) and MBT determination | 46 |
| 4.7 | Emissions..... | 48 |
| 4.7.1 | CO and CO ₂ emissions | 48 |
| 4.7.2 | NOx emissions..... | 49 |
| 4.7.3 | HC emissions..... | 51 |
| 4.7.4 | H ₂ O level and equivalence ratio | 52 |
| 4.8 | Combustion efficiency..... | 54 |
| 4.9 | Summary and discussion | 55 |
| CHAPTER 5 THE EFFECT OF ETHANOL ON ENGINE COMBUSTION BEHAVIOUR..... | | 57 |
| 5.1 | Introduction..... | 57 |
| 5.2 | Combustion Process characterization | 58 |
| 5.3 | Rassweiler and Withrow Method | 59 |
| 5.4 | Calculating polytropic index | 60 |

Table of contents

| | | |
|--|---|-----------|
| 5.5 | Comparison between laminar flame speed of ethanol and gasoline | 61 |
| 5.6 | Effect of ethanol blends on burning duration | 63 |
| 5.6.1 | Different speeds, loads and spark timing | 63 |
| 5.6.2 | Sensitivity to change charge composition (x_b & ϕ) | 65 |
| 5.7 | Combustion stability and tolerance to x_b | 66 |
| 5.8 | Summary and discussion | 67 |
| CHAPTER 6 OVERVIEW OF THE ENGINE ENERGY BALANCE | | 69 |
| 6.1 | Introduction | 69 |
| 6.2 | Energy balance for the engine | 70 |
| 6.3 | Exhaust gas energy | 70 |
| | Exhaust heat capacity, $\bar{c}_{p,exh}$ | 71 |
| 6.3.1 | Exhaust gas temperature measurement and correction | 72 |
| 6.4 | Heat transfer to the coolant | 74 |
| 6.4.1 | Effect of heat rejection to coolant on engine warm-up | 75 |
| 6.5 | Heat loss to ambient, \dot{Q}_{amb} | 76 |
| 6.6 | Energy balance results | 77 |
| 6.7 | Summary and discussion | 79 |
| CHAPTER 7 TIME AVERAGE ENGINE HEAT TRANSFER DURING FULLY WARM UP OPERATION | | 82 |
| 7.1 | Introduction | 82 |
| 7.2 | Background | 83 |
| 7.2.1 | Engine running on gasoline | 85 |
| 7.2.2 | Gasoline-ethanol blends | 87 |
| 7.3 | Effect of External EGR | 88 |
| 7.4 | Evaluation of the heat transfer to the exhaust port, $\dot{Q}_{exh,pt}$ | 90 |
| 7.4.1 | Measured heat transfer to the exhaust port | 91 |
| 7.4.2 | Exhaust port heat correlations | 93 |
| 7.5 | Heat conducted back to the cylinder head, \dot{Q}_{exhman} | 95 |
| 7.6 | Results and discussion | 95 |
| CHAPTER 8 IN-CYLINDER GAS PROPERTIES AND INSTANTANEOUS HEAT LOSS TO THE CYLINDER WALL | | 99 |
| 8.1 | Introduction | 99 |
| 8.2 | Calculating in-cylinder gas properties | 99 |

Table of contents

| | | |
|------------------------------------|--|------------|
| 8.2.1 | In-cylinder temperature | 99 |
| 8.2.2 | Calculating in-cylinder $\bar{\gamma}$ for different fuel mixtures..... | 102 |
| 8.3 | Charge temperature and mixture preparation..... | 104 |
| 8.4 | Instantaneous spatially-averaged heat loss to the cylinder walls | 106 |
| 8.5 | In-cylinder gas-side surface temperature..... | 107 |
| 8.6 | Calibration of the Hohenberg correlation..... | 107 |
| 8.7 | Evaluation of the Hohenberg correlation,..... | 108 |
| 8.8 | Effect of gasoline-ethanol blends at different ratios on the instantaneous heat loss.... | 109 |
| 8.9 | Further parameters variation | 111 |
| 8.9.1 | Effect of burned mass fraction, x_b | 111 |
| 8.9.2 | Effect of equivalence ratio, ϕ | 112 |
| 8.9.3 | Effect of spark timing, ST | 112 |
| 8.10 | Summary and discussion | 113 |
| CHAPTER 9 DISCUSSION..... | | 116 |
| Summary and discussion..... | | 116 |
| Future work..... | | 124 |
| CHAPTER 10 CONCLUSION | | 125 |
| APPENDICES..... | | 228 |
| A.1 | Conversion from dry to wet analysis | 228 |
| A.2 | EGR derivation..... | 231 |
| A.3 | Properties of the different fuel blends | 232 |
| A.4 | Derivation of the EGR correction factor [89] | 238 |
| A.5 | Measurements and calculation uncertainties..... | 240 |

Abstract

“The Effect of Ethanol-Gasoline Blends on SI Engine Energy Balance and Heat Transfer Characteristics”

Taleb Alrayyes

Ethanol is one of a group of hydrocarbon fuels produced from bio-mass which is attracting interest as an alternative fuel for spark ignition engines. Major producers of ethanol include Brazil, from sugar cane, and the USA, from corn. Reasons for the growing interest in ethanol include economic development, security of fuel supply and the reduction of net emissions of carbon dioxide relative to levels associated with the use of fossil fuels. Unlike gasoline, which is a mixture of hydrocarbon compounds suited to meet a range of start and operating requirements, ethanol is a single component fuel with characteristics which make engine cold starting difficult, for example. Hence, ethanol is generally used in a blend with gasoline, accounting for <5% in EU pump-grade gasoline to 85% by volume for so called flex-fuel vehicles.

Although ethanol is already available in the marketplace, there are aspects of its effects on engine behaviour that are unresolved, including its effects on engine thermal behaviour and heat transfer. These have been investigated in the experimental study presented in this thesis. The aims of this work included determining the effect of ethanol content in blends on combustion characteristics, energy balance, gas-side heat transfer rate and cylinder instantaneous heat transfer.

This study covers a range of loads, speeds, spark timings, equivalence ratios and EGR levels representative of every day vehicle use, and has been restricted to fully warm operating conditions. The investigations have been carried out on a modern design of direct injection, spark ignition engine. The performance of different ethanol-gasoline blends has been compared at conditions of matched brake power output.

The emissions data for NO, HC, CO and CO₂, which was used to calculate combustion efficiency, show a decrease in their levels proportional to the

ABSTRACT

increase in ethanol content in the fuel blend. This is owing to an increase in combustion efficiency and change in chemical structure and physiochemical properties.

Compared to gasoline, running on 85% ethanol produces slightly faster rates of burning in rapid burn stages of combustion. Typically, the reductions in rapid burn angle are 4%. Results show that the effects do not vary in proportion to the ethanol content in the fuel blend. This is attributable to the fact that, at low and medium ethanol content, the enhancement in combustion gained by oxygen availability is offset by its higher enthalpy of vaporisation and lower heat content.

Energy balance data show an improvement in thermal efficiency proportional to the increase in ethanol ratio. This is due to improvement in combustion efficiency and a reduction in coolant and exhaust losses.

Results for gas-side heat rejection show that a correlation developed for engines run on gasoline can be used without any modification. The heat rejection rate has been inferred from measurements of heat rejection to coolant adjusted to allow for the contribution of engine rubbing friction. The apparent insensitivity to ethanol content is attributed to a combination of factors. These include the increase in fuel flow rate for a given energy supply being offset in its effect on charge flowrate by a reduction in stoichiometric air/fuel ratio.

Gas-side heat transfer results from both the exhaust port and the cylinder show a clear decrease when running on 85% ethanol compare to gasoline. This reduction was also observed in the total measured heat loss to coolant.

The magnitude and phasing of instantaneous heat loss is not sensitive to the use of ethanol during combustion. However, as the combustion starts to terminate, lower heat loss for medium and high ethanol content was observed due to the reduction in the combustion product temperature. The results from the C1C2 correlation and instantaneous heat transfer are comparable.

Acknowledgment

I would like to express my sincere gratitude to Professor Paul Shayler, my supervisor at the Engines Research Group, for his support and guidance throughout the course of this researching and writing this thesis. Thanks is also given to the technical staff, Geoff Fryer and John Clarke, for ensuring that the test facility was kept in top notch working order, and especially John McGhee, for his advice and encouragement. Many thanks also go Ford Motor Company for the provision of the test engine and financial backing. I am also grateful for all the members of the engine groups, particularly Dr Theo Law for helping advising and support during much of the research.

Amongst others, special thoughts go to Dr Antonino La Rocca, the Warden of Sherwood hall, and all my fellow tutors for their endless patience and friendship.

Finally, and by no means last in importance, I would like to thank my parents and my brother Momen who have supported me throughout my education.

Nomenclature

1. Symbols

| | | |
|--------------------|------------------------------------|------------|
| A | Area | m^2 |
| CA | Crank angle | $^\circ$ |
| c_p | Specific heat at constant pressure | $J/kg\ K$ |
| c_v | Specific heat at constant volume | $J/kg\ K$ |
| d | diameter | m |
| h_c | Heat transfer coefficient | $W/m^2\ K$ |
| h_{fg} | enthalpy of vaporisation | J/kg |
| Δh_f° | molar enthalpy of formation | $kJ/kmol$ |
| k | Thermal conductivity | $W/m\ K$ |
| L | Piston stroke | m |
| m | Mass | kg |
| \dot{m} | Mass flow rate | kg/s |
| N | Engine speed | rpm |
| P | Pressure | N/m^2 |
| P_b | brake Power | W |
| Q_{ch} | Heat released due to combustion | J |
| Q_{LHV} | Fuel lower heating value | MJ/kg |
| Q_{loss} | heat loss | J/CA |
| \dot{Q} | Heat transfer rate | kW |
| \dot{q}'' | Heat flux | W/m^2 |
| t | Time | s |
| T | Temperature | K |
| $T_{g,a}$ | Effective gas temperature | K |
| T_{add} | Adiabatic flame temperature | K |
| V | Cylinder volume | m^3 |
| V_d | Swept Volume | m^3 |
| V_p | Mean piston speed | m/s |
| x_b | Burned mass fraction | $\%$ |
| \tilde{x}_i | Wet mole fraction of substance i | $\%$, ppm |
| \tilde{x}_i^* | Dry mole fraction of substance i | $\%$, ppm |
| γ (Gamma) | Ratio of specific heat | |
| η_c | Combustion efficiency | $\%$ |
| η_t | Thermal efficiency | $\%$ |

ABSTRACT

| | | |
|----------|----------------------------|-------------------|
| θ | Crank angle | ° |
| μ | Dynamic Viscosity | kg/m s |
| ρ | Density | kg/m ³ |
| ϕ | Air-Fuel Equivalence ratio | |

2. Subscripts

| | |
|----------|------------------|
| amb. | Ambient |
| b | Burned charge |
| comp | Compression |
| cyl | Cylinder |
| eff. | Effective |
| exh | Exhaust |
| exh.man. | Exhaust manifold |
| f | Friction |
| f | Fuel |
| fc | fresh charge |
| g | Gas |
| pt | Port |
| stoich | Stoichiometric |
| tot | Total |
| u | Un-burned charge |

Abbreviations

| | |
|-----------------|---|
| AFR | Air-Fuel Ratio |
| ATDC | After Top Dead Centre |
| BMEP | Brake Mean Effective Pressure |
| BSFC | Brake Specific Fuel Consumption |
| BTDC | Before Top Dead Centre |
| CA | Crank Angle |
| CO | Carbon Monoxide |
| CO ₂ | Carbon Dioxide |
| COV | Coefficient of Variability |
| CR | Compression ratio |
| DI | Direct Injection |
| DISI | Direct Injection Spark Ignition |
| DOHC | Double Over Head Cam |
| ECU | Engine Control Unit |
| EGR | External Gas Recirculation |
| EOC | End of Combustion |
| EVC | Exhaust Valve Closing |
| EVO | Exhaust Valve Opening |
| EXX | Ethanol ratio, where XX represents the volumetric fraction of ethanol in the gasoline-ethanol blend |
| FDA | Flame Development Angle (0-10% MFB) |
| FID | Flame Ionisation Detector |
| FMEP | Friction Mean Effective Pressure |
| FTP-75 | Federal Test Procedure 75 |
| GHG | Green House Gases |
| HC | Unburned Hydrocarbon |
| I/O | Input/Output |
| IMEP | Indicated Mean effective Pressure |
| IVC | Input Valve Closing |
| IVO | Inlet Valve Opening |
| KLSA | Knock Limit Spark Advance |
| MAP | Manifold Absolute Pressure |
| MBT | Maximum Brake Torque |
| MFB | Mass Fraction Burned |
| MON | Motor Octane Number |
| NO | Nitric Oxide |
| NO ₂ | Nitrogen Monoxide |
| NO _x | Nitrogen Oxides |

Abbreviations

| | |
|----------------|--|
| O ₂ | Oxygen |
| PFI | Port Fuel Injection |
| PM | Particulate Matter |
| PROMETS | PROgram for Modelling Engine Thermal Systems |
| RBA | Rapid Burning Angle (10-90% MFB) |
| RON | Research Octane Number |
| rpm | revolution per minute |
| RVP | Reid Vapor Pressure |
| SAE | Society of Automotive Engineering |
| SGDI | Spray Guided Direct Injection |
| SI | Spark Ignition |
| ST | Spark Timing |
| TDC | Top Dead Centre |
| UEGO | Universal Exhaust Gas Oxygen (Sensor) |
| ULG | UnLeaded Gasoline |
| VVT | Variable Valve Timing |
| WOT | Wide Open Throttle |

CHAPTER 1 Introduction

1.1 Overview

The topics investigated in this thesis relate to the use of ethanol mixed with gasoline at different proportions in SI engines. The use of ethanol in SI engines can be traced back to the end of the Nineteenth Century, when Henry Ford designed a car that used ethanol as fuel. Gasoline later gained prominence as fuel refined for SI engines due to the availability and cheap supply of crude oil [1]. In the last few years, however, ethanol has again attracted attention as an automotive fuel. This renewed interest in ethanol and alternative fuels in general is driven by several factors.

First, there is an increased awareness that fossil fuel reserves are finite. The International Energy Agency now estimates that world production will peak in 2010-2020 and then start to decrease sharply as illustrated in Figure 1.1 [2]. As a result, finding alternatives to fossil fuel is becoming a commercial priority.

Second, the demand for fuel in the developing world is rising, driven by emerging economic powers such as China, India, and Brazil. For instance China's demand grew at a phenomenal 7.2% annual logarithmic rate between 1991 and 2006 [3]. If that trend were to continue, by 2020 China would be consuming 20 million barrels per day (about as much as the U.S. is currently consuming), and by 2030 that amount would have doubled again to 40 million barrels per day [3].

Third, there are concerns over rising levels of greenhouse gases in the atmosphere and the potential for this to cause climate change with serious consequences on society have also focused attention on ethanol once again. Ethanol has a great potential to limit CO₂ emissions if the whole "well-to-wheel" cycle is considered, as illustrated in Figure 1.2. The CO₂ emitted when ethanol is burned in an engine can be re-captured from the atmosphere by growing crops that are then used to produce the ethanol, thus completing a cycle. It is clear that at least part of the CO₂ emissions can be avoided by using

such a renewable cycle, although the emissions associated with each stage, as well as the net reduction compared to alternative energy source must be examined with care.

Finally, increase in ethanol use has also been stimulated by concerns about oil supply disruptions due to the unstable political situation in regions that export crude oil. This came sharply into attention particularly after the 1973/74 fuel crisis [1].

Biofuels are today the only direct substitute for fossil fuels in transport that are available on a significant scale, and the most commonly produced biofuel is ethanol [1]. Ethanol can be used today in ordinary vehicle engines without major modification (unmodified for low blends or with cheap modifications to accept high blends) [4]. Whilst other fuels, or energy carrier, such as hydrogen, have not achieved large-scale viability and will require major changes to vehicle fleets and the fuel distribution system.

Ethanol production has more than doubled between 1993 and 2006 [2]. As shown in Figure 1.3, USA and Brazil are the biggest producers of ethanol, accounting for 70% of total worldwide production [2]. Both countries took serious steps towards increasing the usage of ethanol as fuel. For instance, the Brazilian government made mandatory the blending of ethanol with gasoline, at proportions fluctuating between 10% and 25%. The bulk of ethanol produced in the USA is mixed with gasoline at low proportions, 10% or E10, as oxygenate and, to a lesser extent, as fuel for E85 flex-fuel vehicles.

In the EU, the production and the use of ethanol, and biofuels in general, are still very limited compared to those of the USA and Brazil [1]. The EU is responsible for just around 7% of the global production of ethanol [2]. Most of the fuel produced in the EU is biodiesel, in which EU is the market leader [1]. At the moment, Sweden is the leading European user of ethanol [2]. Sweden has the largest E85 flexible-fuel vehicle fleet in Europe, with a sharp growth from 717 vehicles in 2001 to around 200,000 in 2010 [2]. However, most of the ethanol consumed in the country is imported [2].

1.1.1 European biofuels policy

Although Europe currently makes a modest contribution to the total production and use of biofuels, the EU has strategies and action plans in place to raise the production and promote the use of biofuels as alternative to fossil fuel [5, 6]:

- In 2003, the EU adopted Directive 2003/30/EC2 on the promotion of the use of biofuels for transport. This "biofuels directive" urged Member- States to set indicative targets for a minimum proportion of biofuels to be put in place in the market. These targets were set at 2% in 2005 then growing by 0.75 annually, to reach 5.75% in 2010. These percentages were calculated on the basis of the energy content of the fuel.
- Directive 2003/96/EC3, in 2003, which was the EU's framework for the taxation of energy products and electricity, was amended to allow Member States to grant tax reductions and/or exemptions in favour of renewable fuels under certain conditions.
- In February 2006, the EU Commission published a new Communication entitled "An EU Strategy for Biofuels", preparing the ground for a review of the Biofuels Directive by the end of 2006 that might include mandatory targets instead of the indicative ones set in 2003. The aim of the strategy was to further promote biofuels in the EU, to prepare for their large-scale use, and to explore opportunities for developing countries to build plants producing biofuels.

Although the Biofuels Progress Report [7] showed that the 5.75% target set by the EU was not reached, those measures and action plans did increase biofuels usage tenfold between 2003 and 2010, as shown in Figure 1.4. Between 2008 and 2009, ethanol consumption increased by 31.9%, representing a share of 19.3% of the total biofuels consumption as shown in Figure 1.5.

Although ethanol has been used as fuel for spark ignition engines since the earliest days of the automotive industry, its recent increasing use in the EU in blends with gasoline raises question about its effects on engine performance and emissions. Modern engines for the EU market are required to meet most of the stringent emissions regulations in the world. EU customers demands high level of refinement, performance and reliability of their vehicles. Meeting

regulations and customer expectations leaves little room for unknown effects of fuel quality and it is this area which the author work has focused on.

1.2 Objective

The objective of this thesis is to establish the effect of different gasoline-ethanol blends, containing up to 85% ethanol, on engine performance, combustion speed, energy balance and heat transfer characteristics of a SGDI engine. In order to achieve these objectives, a number of specific tasks were undertaken, which include:

- The design and commission of a test rig used to carry out all the experimental tests included in this thesis.
- Several tests were carried out on a wide range of engine running conditions to evaluate the effects of increasing ethanol content in a gasoline-ethanol blend on:
 - the physicochemical and combustion properties of the fuel, including stoichiometric AFR, calorific value, MBT, and adiabatic flame temperature. Also, the subsequent effect of these properties on power output and fuel consumption.
 - the main regulated emissions and combustion efficiency
 - combustion duration, combustion stability and EGR tolerance.
 - exhaust temperature and heat capacity.
 - energy balance inside the engine, including the thermal efficiency, heat loss to coolant, heat loss to ambient and heat loss to exhaust.
 - gas-to-wall heat transfer, and any required modifications to the C1C2 correlation to allow for changes in the fuel heating value and other fuel properties.
 - other sources contributing to the heat rejection to coolant including: exhaust port, heat conducted back from exhaust manifold, and friction.
 - instantaneous heat loss to coolant and in-cylinder temperature and properties.

1.3 Thesis layout

Chapter 2 describes a review of the published literature relevant to the study presented in this thesis, with a focus on ethanol production, main properties, and effects on engine performance and emissions.

Chapter 3 covers details of the test engine and the experimental facilities developed to meet the objective of the thesis.

The main body of the thesis is concerned with heat transfer characteristics and the combustion behaviour of the engine. The physiochemical and combustion properties of the fuel blends, which are important to understand these characteristics, are examined in Chapter 4. Calorific values, AFR_{stoich} , adiabatic flame temperatures as well as MBT (and its effect on engine power, output and fuel consumption) were calculated. Also, emission levels for different fuel blends were measured at different running conditions, and used to calculate combustion efficiency.

In Chapter 5, the Rassweiler and Withrow method was used to calculate and compare burn durations for different fuel blends. Several methods to calculate appropriate polytropic index values were assessed. Gasoline and ethanol laminar flame speeds were calculated and compared. The effects of changing an engine's running conditions such as speed, load and spark timing (or charge composition by changing EGR or equivalence ratio) were evaluated for the different fuel blends. Finally, the effect of increasing ethanol ratios on combustion stability and tolerance to EGR was studied.

The manner in which the total energy released by the fuel is distributed between brake output, coolant energy, and exhaust loss for different fuel blends is described in Chapter 6. The chapter also establishes the effect of increasing ethanol content on key characteristics that will affect engine performance and power output, including thermal efficiency, exhaust temperature and coolant heat rejection rate.

In Chapter 7, the validity of using the C1C2 correlation to predict gas-side heat rejection to coolant when the engine runs on ethanol-gasoline blends is assessed. Different sources that contribute to the total heat transfer to coolant were also indentified which include: exhaust port, friction, and heat conducted

back to the engine block. The contributions of each of these sources, as well as the effects of adding ethanol, were evaluated.

Heat rejection to the coolant is examined further in Chapter 8, which includes predictions of the instantaneous heat loss value and phasing for different gasoline-ethanol blends using an empirical correlation (the Hohenburg correlation). This chapter also investigates the in-cylinder charge preparation (the temperature between IVC and ST) that is expected to be affected by differences in ethanol physiochemical properties.

A discussion of the findings of these investigations, as well as recommendations for further work that could enhance these findings, are included in Chapter 9. A series of conclusions drawn from the work are also presented.

CHAPTER 2 Literature review

2.1 Introduction

This chapter contains a detailed overview of the current knowledge surrounding the subject of production, properties and consequences of ethanol use in SI engines.

An important factor when consider the relative merits and drawbacks of any fuel product is its sustainability, both in terms of the dependability of its supply and the robustness of its production process. For that reason, the first section of this literature review will cover the production and net energy balance of the complete ethanol cycle. The properties of ethanol, which must be well understood in order to fully comprehend their effects, will be examined in the second section of this review.

The chapter will then proceed to review the effect of using ethanol on the engine characteristics, including its emissions and combustion behaviour. This will be approached with a specific focus on the use of ethanol in Direct Injection SI engines. Finally, the last section will look into the use of other alcohol-based blends as alternative fuels.

Despite the extensive research literature that has been produced over the past few years, no material was found that directly investigates the effects of ethanol on energy balance, or on heat transfer characteristics. This highlights a notable gap in the current body of knowledge on the topic, which this study endeavours to address.

2.2 Ethanol Production

The main barrier to the commercialisation of ethanol is its high cost of production compared to that of gasoline. This cost is largely determined by that of biomass feedstock, which can account for up to 40% of the final price of ethanol [8]. However, recent increases in the price of crude oil in the last few years have helped close the gap between gasoline and ethanol prices [9].

Various types of feedstock are used to produce ethanol; the majority are either sugar crops, such as sugar cane and sweet sorghum, or starchy crops such as corn and cassava. Sugar cane is the preferred raw material for ethanol production in Brazil, India, and South Africa, whereas corn is used in the USA and sugar beet in France [10]. Current research efforts in the field of ethanol production are focused on using lignocellulosic materials as feedstock, otherwise known as “second-generation” production techniques. This includes agricultural residuals (e.g. wheat straw, corn stalks, soybean residues, and sugar cane bagasse), forest residues, industrial waste (from the pulp and paper industry) and municipal solid waste [10]. The main reason for promoting a shift to ethanol production from lignocellulosic biomass is the latter’s availability and its low prices compared to food crops. Furthermore, it has a higher net energy balance, which makes it more attractive from an environmental point of view. However, the complex structure of lignocellulosic biomass is a barrier to its utilization, as it makes it resistant to degradation (thus more difficult to convert into sugar) [1].

2.2.1 The production process

Ethanol production methods depend on the feedstock used, as shown in Figure 2.1. Ethanol production from sugar crops is relatively simple: micro-organisms use the sucrose present in sugar crops directly without any external hydrolysis [9]. Starchy crops such as corn, however, contain larger and more complex carbohydrates that need to be broken down by hydrolysis into simpler sugar prior to fermentation [1, 10]. For the lignocellulose transformation, the degree of complexity is higher. The three major components of any cellulosic material are cellulose (40% to 60% of the dry weight), hemicellulose (20% to 40%), and lignin (10 to 25%). Only Cellulose and Hemicellulose can be converted into sugar, whereas Lignin cannot because of its resistance to biological degradation. However, it can be used to produce electricity and/or heat [10]. For both crops and lignocellulosic biomass, the fermentation and distillation steps are basically identical. If the ethanol is to be used in automotive engines, its water content must be close to zero in order to reduce the corrosive effect of the fuel. An extra step in ethanol fuel production is therefore needed to dehydrate the alcohol [1].

2.3 Net energy and Green house gases

The net energy of ethanol and the green house gases, GHG, produced during its whole production cycle (Figure 1.2) has been the subject of extensive scholarly debate [11]. The main question has always been “how much energy from non-renewable sources does ethanol production consume compared to the energy generated by the ethanol fuel produced?” [12]. Results addressing this question have varied significantly between different researchers. Indeed, whereas some researchers found that a negative net GHG, others found a positive net energy, ranging from small to significant improvement in both net energy and GHG [11]. The difference in net energy results is mainly attributed to the different types of feedstock used to produce ethanol and/or the assumptions about the system boundaries and key parameters during the net energy calculations [13, 14].

Farrel *et al.* [11] and Kim [15] found that including the input energy of co-products, which are inevitably generated when ethanol is produced, would significantly and positively affect the net energy as well as reduce the calculated GHGs. Co-products that are generated include CO₂ (during fermentation), distillers grains, corn gluten feed, and corn oil. These co-products have a positive economic value. For example, CO₂ can be marketed for use in the food processing industry, including the production of carbonated beverages and flash-freezing applications. Distillers’ grains and corn gluten feed can also be used for animal feed, thereby saving the energy required to produce ethanol, and positively affecting the energy shift [11].

Feedstock also has a significant effect on both GHG and net energy. Farrell [11] compared the net energy and GHG of ethanol that is produced from different feedstock, across data obtained from different researchers. These data showed clearly that ethanol produced from cellulosic material has a much higher net energy and lower GHG than the one produced from corn crops. Although using cellulosic material showed a significant improvement in net energy, the amount of petroleum that is required to produce ethanol is higher than when using other feedstock where other non-renewable source such as coal and natural gases are also used. This could be disadvantageous since one of the objectives of using ethanol is to reduce dependence on foreign oil [11].

2.4 Comparison of ethanol and gasoline properties

While gasoline is complex and contains variable mixtures of hydrocarbon and additives [16], ethanol is a single alcohol. The lower molecular weight, change in H/C ratio, and the presence of oxygen will cause a significant difference in the properties of ethanol compared to gasoline. Table 2.1 shows a comparison between the respective properties of ethanol and gasoline [17]. Table 2.1 shows that ethanol has a lower RVP, heat content and AFR_{stoich} , but a higher enthalpy of vaporisation, RON, and MON compared to conventional gasoline. Two characteristics that differ between ethanol and gasoline, and would have a significant effect on engine performance, are volatility and octane number.

Volatility

The volatility of the fuel is of extreme importance since the combustion inside the engine occurs when the fuel is at vapour state. Fuel with low volatility is often associated with liquid fuel being inducted into the cylinder especially at cold start or at low ambient temperature [17]. The liquid fuel inducted into the cylinder can be responsible for an increase in HC and CO emissions and thus poor efficiency. Volatility also influences cold-start fuel economy. This is because spark-ignition engines start on very rich mixtures and continue to run on rich mixtures until they reach their normal operating conditions, this is to ensure adequate vaporisation of fuel. Consequently, increasing the volatility of the fuel will decrease the fuel consumption at cold start, and thus HC emissions [16].

The volatility of the fuel is expressed in terms of either a distillation curve or Reid vapour pressure (RVP). Adding ethanol to gasoline will have a profound effect on both these measures.

Wallner *et al.* [18] compared the distillation curve of ethanol and gasoline. The results showed that gasoline, as a mixture of hydrocarbons, exhibited typical evaporation behaviour, with an initial boiling point of around 25 °C and a final boiling point of 215 °C. In contrast, ethanol, being a single alcohol, has a defined boiling point temperature of 78 °C. As a result, adding ethanol to gasoline will alter the fuel distillation curve. Topgu *et al.* [19] measured the effect of increasing ethanol content up to 60% on the distillation curve using the standard test method for distillation, ASTM D-86.

The results showed that the initial boiling point at 10%, 90%, and final distillation are almost independent of ethanol content levels, while the other distillation temperature decreased as ethanol content rose. The same results were also obtained by He *et al.* [20], D'Ornellas [21] and Hsieh *et al.* [22], who studied the effect of increasing ethanol content up to 30%.

Reid vapour pressure (RVP) is the most common measure of the volatility of gasoline, the higher the RVP of the fuel, the more volatile it is. Although ethanol has a lower molecular weight than gasoline, it has a lower RVP because of the hydrogen bonding in the hydroxyl group [23].

In a study carried out by Kar *et al.* [24], the ATSM standard test method was adapted to measure the RVP for different ethanol-gasoline blends. The results illustrated that RVP does not correlate linearly with ethanol content levels in the blend. As shown in Figure 2.2, initially as the ethanol proportion increased in the blend, RVP also rose. This was the case for all ethanol ratios up to 10%-20%, but then RVP falls eventually as the blend nears pure ethanol value. Ethanol in general does not mix well with hydrocarbon due to its polar intermolecular force. When ethanol is added to gasoline in low proportions, the non-polar species of gasoline disperse the polar alcohol molecules, thus disturbing the stabilizing hydrogen bonding network, and causing the alcohol to behave as if its RVP was much higher [23]. Such an effect is at its strongest for blends with a 10-20% ethanol concentration [24].

As ethanol ratios increase further, a positive azeotrope is formed between ethanol and some of the hydrocarbons in the gasoline, for instance, benzene, cyclohexane and n-heptane, which results in a lower RVP [24]. The results also illustrate that the maximum value of RVP is affected by temperature. Thus, as temperature increases, the Reid vapour pressure value also increases for all different fuel blends. The same trend was also obtained by Pumphrey *et al.* [25], Silva *et al.* [26] and Hsieh [22]. However, the maximum value of RVP was found to lie at between 5 and 10% of ethanol content. The values of RVP were found to be slightly higher in these studies than the aforementioned one, as measured by Kar *et al.* [24], especially at low ethanol content levels. This is presumably due to the different gasoline types used by the various research teams. Gasoline has different Reid vapour pressure values depending on weather conditions. In hot weather, those gasoline components with a higher

molecular weight (and thus lower volatility) are used in order to avoid vapour lock in the fuel lines and pre-ignition behaviour. In contrast, in cold weather, gasoline will have a higher Reid vapour pressure so as to avoid problems related to cold start [16].

Volatility characteristics can also be affected by the enthalpy of vaporisation, h_{fg} , of the fuel. As shown in Table 2.1, ethanol has a much higher h_{fg} than typical gasoline (three times higher). Surprisingly, little research has been published on the effect of adding ethanol to gasoline. Balbin *et al.* [27] found that increasing ethanol content level up to 20% of the total blend will linearly increase the enthalpy of vaporisation. The enthalpies of vaporisation for different fuel blends were derived from vapour pressure data using the Clausius-Clapeyron equation. Kar *et al.* [24] used the same methodology to calculate the effect of increasing ethanol content until the fuel blend is pure ethanol as shown in Figure 2.3. From zero and up to a 20% ethanol content level, the results of their study correspond to the findings of Balbin *et al.* [27]. However, at higher levels the value first decreases then appears to flatten out between 30% and 60% ethanol content levels. Beyond the 60% ethanol content mark, the value begins to increase again.

Resistance to knock

Abnormal combustion can take several forms, principally pre-ignition and self-ignition. Pre-ignition occurs at hot surfaces such as the exhaust valve. Self-ignition, which can be characterised as knocking, occurs when the remaining unburned gas mixture ignites spontaneously as a result of an increase in pressure and temperature due to the advancing flame front. Pre-ignition can lead to self-ignition and vice versa [16]. Abnormal combustion, if severe, can cause major damage, and even when not severe, it can cause undesirable noise, which can be perceived as a 'knocking' sound by the vehicle operator [17]. Furthermore, energy released by a knock is not converted into useful work. Instead, it is dissipated through pressure waves and increased radiant heat. Knock will also affect the power output by limiting the compression ratio, CR, and spark timing. Increasing the CR should improve the engine's performance and power output. Increasing CR is limited by engine knock characteristics. A knock will also affect spark timing by retarding it from its Minimum advance

for Best Torque ignition timing, MBT. Retarding ignition timing to avoid a knock is referred to as knock limit spark advance (KLSA) [16].

The Research Octane Number (RON) and Motor Octane Number (MON) are the most common measures of a fuel resistance to knock [17]. The higher their values are, the better anti-knock characteristics of the fuel. As shown in Table 2.1, RON and MON for gasoline are typically in the range 92-98 and 80-90 respectively. RON and MON values for pure ethanol are 107 and 89 respectively. The effect of adding ethanol at low ratios was studied by several research teams. Hsieh *et al.* [22] showed that increasing ethanol content will linearly increase the octane number of the fuel. The tests were carried on gasoline-ethanol blends containing up to 30% ethanol (low ethanol content), increasing ethanol content to 30% increased RON by 7.5%. The same results were also obtained by Silva *et al.* [26], Palmer [28], Wu *et al.* [29] and Abdel *et al.* [30]. Szybist [31] measured MON and RON for E10, E50 and E85, and compared the results to those of regular unleaded gasoline. The results illustrated that the blending response of RON and MON as a function of ethanol content is highly nonlinear at high ethanol content levels. There was a substantial octane improvement between gasoline and E10, and between E10 and E50. However, between E50 and E85 there was very little difference in either RON or MON; surprisingly, until the writing of this work, no literature was found of RON and MON measurements for high ethanol content that could either support or refute these results.

Some of the previous research investigated the effect ethanol has on some engine variables and parameters relating to knock engine characteristics, including the CR limit and the knock limit spark advance (KLSA). Nakata *et al.* [32] investigated the effect of adding ethanol on KLSA in engines running at low speed, with WOT and a CR of 13.5 [32]. The results illustrated that increasing ethanol content allowed a more advanced KLSA. E10 advanced KLSA by 4°. At E50 and E85, there was no need to advance ignition from MBT. The same results were also found by Yucesu *et al.* [33]. In their study, KLSA was allocated for different gasoline-ethanol blends containing ethanol ratios of up to 60% at various CRs ranging between 8 and 13. For all CRs, KLSA advanced as ethanol content increased. At E40 and E60 ethanol content, spark timing reached MBT without spotting any knocks.

Caton *et al.* [34] studied the performance and knock characteristics of E10 and E85 in comparison to regular gasoline. The results showed that for E85, MBT can be maintained up to a CR of about 13.5, whereas MBT could not be maintained for gasoline and 10% ethanol blend past a CR of 9.0. The same results were also found by Szybist *et al.* [31], who investigated knock-limited CR of ethanol-gasoline blends to identify the potential for improved operating efficiency. CRs ranged between 9.2 and 12.87, with the engine running at different loads and speeds. The test results illustrated that while high ethanol blends, E85 and E50, were not knock-limited under any running conditions, gasoline and E10 became knock-limited as the compression ratio increased. Under knock-limited conditions, retarding ST will reduce power output. Stein *et al.* [35], evaluated a dual-fuel system, where gasoline as primary engine fuel, was delivered through PFI injectors, whereas E85, as the secondary engine fuel, was delivered as needed to prevent knock. It was found that under turbocharged conditions with a 12.0 compression ratio configuration. The maximum amount of E85 required to prevent knocking at peak load was about 60% of the total fuel delivered, which is effectively about E50.

2.5 Emissions

Current European legislation sets limits on the amount of regulated emissions that can be produced by motor vehicles. Those legislations were driven by their toxicity and concerns over human health, in addition to the emissions' detrimental impact on the environment and their potential global warming effect. These limits have been getting tighter over the last 20 years, as shown in Table 2.2 [36]. As illustrated in Table 2.2, the main regulated emissions are CO, NO_x, and HC emissions.

The environmental and health concerns, as well as issues regarding the engine emissions have led to increasingly tighter emission regulations in Europe as stated above. In Euro 4 and earlier regulations, the manufacturers of flexible-fuelled vehicles were allowed to use only the conventional (gasoline) fuel in the certification testing. From Euro 5, which took effect in September 2009, both fuels (gasoline with 5 and 85 % ethanol mixtures) must be used at the certification testing. Testing at low ambient conditions will also be demanded

for both fuels from 2011 [36]. All of these regulations required a clear understanding of the effect of ethanol on emissions produced.

Many studies concentrated on the effect of using ethanol as oxygenate to enhance combustion on regulated emissions [20, 22, 28, 29, 37] with gasoline ethanol blends containing up to 30% ethanol. Ethanol was perceived as a viable substitute for MTBE, which was widely used as oxygenate during the 90s but was later proven to cause contamination of drinking water aquifers [38]. Several studies have also been carried out to examine the emissions characteristics of engines running on higher ethanol ratios, in the range from 50% to pure ethanol [18, 32, 39-45].

The effect of ethanol content on the level of CO produced was very evident in the literature reviewed [20, 22, 37, 42, 44, 45]. Indeed, when ethanol was used, CO production was reduced dramatically compared to when using gasoline. The decrease was significant even for low ethanol content (5 and 10%). He *et al.* [20], in a study carried out on a port-injection gasoline engine, illustrated that adding 10% ethanol in a gasoline ethanol mixture would decrease the level of CO by 4.8% to 7%, depending on the speed and equivalence ratio. The study also shows the effect of ethanol to be more significant at rich fuel charges. The same trend was also obtained by Palmer *et al.* [28]. Some studies [22, 45] showed that CO levels will be reduced even more significantly, by up to 30% with 10% ethanol content, when an open loop fuel system was employed, as a result of the leaning effect of ethanol. Increasing ethanol percentage in gasoline-ethanol blends will affect CO further. The literature reviewed [42, 44] illustrated a linear relation between an increasing ethanol ratio in ethanol-gasoline blends and the decrease in the level of CO emissions, until the blend is entirely made up of pure ethanol.

NO_x and HC results, on the other hand, showed a clear variation among the different research studies [18, 20, 22, 29, 41, 42, 44, 45].

In a study carried out by Wallner *et al.* [18], NO_x emissions were found to be decreasing as ethanol percentages increased. The decrease was observed even at low ethanol percentages. The scale of the NO_x emission reduction was dependent on engine load; at high load, there was up to a 45 % decrease in NO_x emissions between gasoline and E85. The same result was reached by

other researchers who studied the effect of using ethanol at low [20] and high [42, 44] content on NO_x emissions produced.

The same results were also obtained by Varde *et al.* [43] at high ethanol percentage. However, with mixtures containing low ethanol content (E10 and E22), the produced NO_x emissions were comparable to those produced from gasoline

Some studies [22, 37, 45] showed a completely different trend between increasing ethanol content and NO_x emission levels under particular running conditions. In other cases, increasing ethanol content led to an increase in NO_x values.

The main reason for the variation in NO_x results is that some of these studies were carried out for engines operating on specific cycles [22, 45]. This means that relative air-to-fuel ratios were not controlled directly to ensure it was kept constant for different fuel blends (open loop system). As a result, introducing ethanol will cause a leaning effect on the engine, which will in turn affect NO_x emissions. NO_x level in the exhaust is greatly influenced by the relative air-to-fuel ratio inside the cylinder, its maximum value thus occurs when the charge is slightly lean, but decreases as the charge becomes richer or leaner [17].

The different fuelling systems inside the engines under investigation could be another reason for the variation in NO_x results. For instance, the one equipped with a carburetion system will have a wider range relative air-to-fuel ratio than those with port-injection or direct injection systems. In addition, using a carburetion system is going to limit the cooling effect of ethanol compared to engines equipped with a port-injection system, and to an even larger extent compared to those equipped with a direct-injection system. The cooling effect of ethanol as a result of its higher heat of vaporisation is considered to be the primary reason for the decrease in NO_x emissions (lower in-cylinder temperature) [20, 22, 41, 42, 44].

HC also showed a variation in the results amongst different researchers; while some studies [18, 20, 22, 42, 43, 45] showed a decrease in HC as a result of increasing ethanol content in the fuel blends, other studies [39-41] showed a different trend.

The reasons for the variation in the NO_x emission results mentioned above are also applicable to variations in HC results. The increase in RVP [24] as ethanol

content also increases (especially at higher ethanol ratio) will have a more significant effect on those engines equipped with a carburetion fuel system than on those equipped with a port-injection or a direct-injection system. Less fuel is evaporated in a carburetion system at high ethanol ratios, and some fuel drops might even reach the combustion stroke without being vaporized. As a result, HC increases due to insufficient combustion at high ethanol ratios. The above can thus explain the results obtained by Huang *et al.* [40]. Their study was carried out on a single-cylinder SI engine equipped with a carburetted fuel system. The fuel blends investigated included gasoline, E15, E30 and E50. The results illustrated an initial decrease in HC levels at low ethanol concentrations (E15 and E30) which was then followed by an increase in HC levels at E50.

Another reason for the variation in results is injection timing. Advance injection timing in a direct injection engine, aimed at increasing the amount of fuel injected to compensate for the lower heat content of ethanol, will also lead to an increase in HC as a result of piston wetting, as shown in Price *et al.* [41].

FID is used to measure HC. The FID response is proportional to C atoms in each molecule. In alcohol, the C is bonded to an O in an R-O-H group, where R is an Alkyl radical, and gives a response of about 50 to 85% of a C atom [41]. The same is true for the FID response to aldehydes. Failure to recognize this and to determine relative response factors properly, contributed to the variation in results among researchers [23].

As shown in Table 2.2, gasoline engines are exempted from particulate matter (PM) standards through to the Euro 4 stage, but direct-injection engines will be subjected to regulations for Euro 5 and Euro 6. Price *et al.* [41] explored the effect of adding ethanol and methanol to gasoline on emissions of ultra-fine PM. Particulate number concentration and size distribution were measured using a combustion DMS500. The data were presented for different AFR, loads, ignition timings and injection timings. The results illustrated that the accumulation mode number PM concentration was significantly lower for an 85% alcohol blend than for the 30% one or gasoline, particularly for rich fuel mixtures. In addition, the PM response to relative AFR was found to be less pronounced for the 85% alcohol blends than the rest of the blends.

So far, aldehydes were not designated as regulated pollutant emissions, presumably because aldehyde levels in SI engine emissions running on pure

gasoline are relatively small [23]. Although aldehyde emissions are not regulated, aldehydes are one of the products of the photochemical reaction between hydrocarbons and nitrogen oxides that causes the smog phenomenon. For that reason, understanding the effect of ethanol on aldehyde emissions is of extreme importance. The aldehydes are formed from the partial oxidation of fuel that had remained after flame extinction at low temperatures. Aldehyde composition is dependent on the fuel that has been used. While the oxidation of ethanol at low temperatures (270°C-300°C) will mainly produce acetaldehyde as an initial product, the oxidation of methanol will produce formaldehyde [23].

Several studies have shown a clear increase in aldehyde emissions when alcohol fuels are used [43, 46-50]. For example, Varde *et al.* [43] investigated the effect of using ethanol as fuel on acetaldehyde, which is the main aldehyde produced by ethanol. The result showed that E85 showed a significant increase in acetaldehyde compared to pure gasoline and lower ethanol blends, particularly at low loads.

2.6 Engine Combustion behaviour

The use of ethanol in SI engines is expected to affect the engine performance and combustion behaviour. This is due to ethanol's physical and chemical properties, which differ from those of gasoline, as stated above.

Several researchers studied the effect of ethanol on engine combustion behaviour. Malcolm *et al.* [51] examined the combustion behaviour of blends of gasoline, isooctane and a variety of alcohols under part-load engine operation at 1500 rpm, with port fuel injection. The tested fuels were gasoline, E85 and isooctane, with ethanol content levels at 25% and 85%, as well as a blend with 25% butanol content. The tests were carried out in an optical SI engine and the combustion duration was tested using high-speed crank-angle resolved natural light imaging in conjunction with in-cylinder pressure analysis over batches of 100 cycles. It was found that E85 shows a faster mass fraction burned traces and faster flame radius growth than the rest of the fuel for most test cases, irrespective of the change in spark timing. The same results were also obtained by Yeliana *et al.* [52], who studied the effects on combustion duration of blending ethanol with gasoline at different proportions (up to 85%

ethanol content, in 20% gradual increments). One-dimensional single zone and two zone analyses have been conducted to calculate the mass fraction burned using the cylinder pressure and volume data. In both analyses, E85 showed a decrease in the combustion duration compared to that for all other fuel blends. The decrease was clear at both FDA and RBA. For the other fuel mixtures, with low and medium ethanol content FDA showed a linear decrease as ethanol ratio increased. RBA on the other hand, show very little difference between the various fuel blends.

The same FDA results were also obtained by Cairns *et al.* [53]. However, RBA showed comparable results between different fuel blends, including E85.

Other researchers (Varde *et al.* [43], Yoon *et al.* [42] and Wallner *et al.* [18]) found different results where ethanol, whether at high or low content levels, exhibited no effects on either FDA or RBA.

2.7 The use of ethanol in direct injection spark ignition engines (DISI engines)

Until recently, the vast majority of flexi-fuel engines were equipped with port-fuel injection systems (PFI) [53]. Currently, however, there is significant and growing interest in the use of DISI engines. The DISI engine has the potential to improve engine performance through changing volumetric efficiency and increasing the compression ratio. This is achieved through better use of the enthalpy of vaporisation and of the anti-knock characteristics, as compared to a conventional PFI engine [54]. Since ethanol has a higher octane number and a higher enthalpy of vaporisation compared to gasoline, the use of ethanol is expected to enhance the thermodynamics benefits of DI engines [44].

Brewster [55] studied the potential benefits of using ethanol in a turbocharged DI research engine powered by a centrally mounted air assistant injector. It was suggested that the injector used could offer improved low-temperature starting characteristics for ethanol. In addition, the system will allow a disconnection between fuel metering and fuel delivery, allowing for the increase in the fuel consumption required for ethanol direct injection at a high specific output. Based on the current production turbocharged SI engine torque levels, ethanol results indicated a lower boost pressure, a lower exhaust temperature, more optimized ignition timing, and a higher thermal efficiency.

Furthermore, using ethanol demonstrated a significant reduction in excess fuelling at higher speeds and loads.

In another recent study, carried out by the same researcher, Brewster *et al.* [56] evaluated the performance of a spray-guided direct injection, SGDI, when anhydrous ethanol (E100) and hydrated ethanol (E93h, E87h, E80h) are used as fuels. The SGDI engine had a compression ratio of 10.4:1, the experiments were carried out at high loads. The results illustrated that the key differences arising from fuel water content were reduced burn rate requiring an advance in ignition timing. Another effect of increasing ethanol water content was an increased fuel mass flow rate and a decrease in engine emissions of NO_x, as well as an increase in HC. The results also illustrate that higher ethanol content blends would have a higher potential for running at increased compression ratio.

The cold start problem associated with using ethanol was also another driving factor behind the increased interest in the gasoline DI engine as a way to improve cold start performance. Kapus *et al.* [57] performed a comparison between E85 and E100 in an optical single cylinder powered by a direct injection system at a crank speed of 200 rpm and with fluids controlled at 20°C. The results illustrated that by using multiple pulse fuel injections during the induction and compression strokes will improve the start on ethanol.

Cairns *et al.* [53] carried out a study to evaluate the performance of a potential future biofuel during advanced spark SI engine. This was conducted on a multi-cylinder DI research engine. Three gasoline/ethanol blends and three gasoline/butanol blends were considered in this study. Some of the conclusions drawn up from the study include: firstly, alcohol blends generally perform better at slightly later injection timings and marginally lower fuel pressures. Secondly, while increasing ethanol content will increase EGR tolerance at low and high loads, due to the decrease in combustion duration, it will not have any effect on excess air tolerance. Finally, there was a strong synergy between SI engine downsizing and fuel containing low to moderate amounts of alcohol. Such a combination allowed a significant improvement in fuel economy to be made over the engine's driving cycle.

Cairns *et al.* [53] also studied the effect of ethanol on deposit formation in the injector, which is an important factor in a DI engine. The results illustrate that

E10 produces a relatively thicker layer of deposit on the injector face compared to gasoline. E85 tests, on the other hand, showed relatively immaculate fuel injectors. The same results were also obtained by Taniguchi *et al.* [44]. Their study showed that E100 suppressed injector deposit formation. The reduction in injector deposit formation starts to manifest itself when the engine is running on E50. The reduction in injector deposit when ethanol is used is presumably caused by the reductions in both injector nozzle temperature and the amount of aromatics and sulphur contents in the fuel.

2.8 Other alcohol considered as alternative fuel

Early interest in biofuels concentrated on methanol usage [53, 58]. However, problems such as corrosive behaviour, vapour lock and lower energy density compared to both gasoline and ethanol (50% and 24% less than gasoline and ethanol respectively) turned the attention more towards ethanol [53, 59]. There is an increased interest in higher alcohol such as propanol (C3), butanol (C4) and pentanol (C5) [47]. Higher alcohol fuels generally have a higher energy density (and hence better fuel economy), better water tolerance, volatility control, and lower RVP compared to ethanol. However, some benefits associated with ethanol, such as enthalpy of vaporisation and anti-knock behaviour will typically reduce [46, 53]

Some research studies were carried out to look into the effect of higher alcohol blends on engine performance. Yacoub *et al.* [47] compared a wide range of C1-C5 alcohol fuel blends' effects on anti-knock behaviour. The engine operating conditions were optimized for each (C1-C5) blend with two different values of matched oxygen mass content (2.5 and 5.0 per cent). It was concluded that, whilst adding lower alcohols (C1, C2, and C3) to UTG96 improved knock resistance, blends with higher alcohols (C4, C5) showed degraded knock resistance when compared to neat gasoline. The same results were also obtained by Gautam *et al.* [60]. The study also concluded that increasing oxygen content by adding any alcohol will increase the flame speed. Bata *et al.* [61] studied the effect of various butanol/gasoline blends on the performance of a 2.2l naturally-aspirated research engine. The results showed a 6.4 % increase in specific fuel consumption when using 20% butanol, but under limited test conditions. The fuel blends illustrated a higher thermal

efficiency and lower specific fuel consumption compared to both methanol and ethanol.

In another recent study [51] carried out in an optical SI engine to examine the effect of alcohol blends on combustion behaviour. The addition of 25% butanol to *iso*-octane did not affect appreciably the combustion characteristics of *iso*-octane for fixed-ignition timings. However, for lean conditions, the combustion process slowed down marginally with butanol addition. When ignition timing is optimized, the addition of 25% butanol to *iso*-octane was shown to make it burn faster than pure *iso*-octane.

2.9 Concluding comments

The literature review covers a wide range of subjects related to ethanol. These subjects are related, either directly or indirectly, to the study presented in this thesis and intended to set the study in context.

There has been extensive research on the effect of using ethanol blended with gasoline at different proportions on engine characteristics such as emissions and combustion behaviour. These two characteristics were also covered in this thesis. The variation in previous literature meant that a more thorough and robust understanding of the effect of ethanol is required. In addition most of these research studies were carried out on engines equipped with either port-fuel injection system or carburettors. Limited number of studies were carried on a direct-injection engine, particularly a spray-guided direct-injection engine such as the one that was used in this study.

Despite extensive research by the author, no literature was found investigating the effect of using ethanol-gasoline blends on energy balance and heat transfer characteristics. This indicates a gap in the knowledge relating to this subject that this thesis is trying to tackle.

CHAPTER 3 Experimental test facilities

3.1 Introduction

The experimental data presented in the thesis were recorded on an engine test facility developed by the author. This chapter deals with the development of the test facility, data acquisition and test rig control systems based on dSPACE, Simulink and ATI softwares.

The analysis of combustion behaviour, energy balance and heat transfer characteristics are the main focus of this work. The main experimental considerations were the accurate measurement of coolant and fuel flow rate, in-cylinder pressure and coolant, exhaust and inlet air temperature under fully warm conditions. For that reason a standard reference point was chosen for regular repeatability tests to ensure that the accuracy of the data was maintained across the course of the experimental tests. In addition, several techniques were used to eliminate any noise which could affect the readings. The engine was also instrumented to measure brake output, speed, manifold pressure and emissions.

3.2 Engine description and Test Cell Facilities

The experimental studies was carried out on a prototype, four cylinders inline, 1.6L Spray Guided Direct Injection, SGDI, gasoline engine manufactured by Ford motor company as shown in Figure 3.1 the engine specification can be found in detail in Table 3.1.

SGDI engines are currently being proposed as the next generation of Direct Injection Spark Ignition, DISI, engine because of their expected fuel economy advantages and lower emissions over their corresponding wall-guided DI engine and PFI engines [54]. The spray guided combustion process is characterised by the way the fuel is injected to the combustion chamber. As illustrated in Figure 3.2, the fuel injected forms a hollow cone at the injection nozzle [62]. DISI engines in general have a fuel economy advantage over

corresponding PFI engines; this is largely due to lower pumping loss resulting from higher MAP, better mixture properties due to lean/dilute operation, lower heat losses due to charge cooling effects and the higher compression ratio enabled by charge cooling effects. Potential disadvantages of the DISI engine include higher friction losses, which increase due to higher peak pressure, lower combustion efficiency and higher combustion phasing losses [54]. In the case of SGDI engines combustion efficiency is higher and combustion phasing losses is lower, which result in a significant improvement in the fuel economy for SGDI engine over that of wall- guided system [63].

A Froude Consine eddy current dynamometer was coupled to the engine via a 'straight through' gearbox supplied by Ford (running in top gear) and prop-shaft. The dynamometer offered two modes of operation: constant speed and constant load.

The standard starter motor in the engine was retained for cranking but the alternator was disconnected to allow it to run without external electrical errors. The waste heat generated by both the engine and the dynamometer were dissipated via an external cooling system. The external cooling system consisted of a Carter M/3 series external forced convection cooling tower, water pump and a Bowman heat exchanger that replaces the standard vehicle radiator as shown in Figure 3.3.

The basic engine coolant circuit consists of a thermostat and a bypass system. During the warm up period, coolant is circulated round the engine by means of a water pump and fed back to the inlet through a bypass line in the thermostat housing. The thermostat opens at a coolant temperature of approximately 90°C, and at that point a portion of the coolant flow is diverted to the external cooling system. The two coolant paths are shown in Figure 3.3. The engine coolant is a 50:50 mixture of water and ethylene glycol.

Exhaust gases were vented to the atmosphere via the laboratory extraction system using a standard exhaust pipe with minimum re-routing to suit the layout of the test bed. A dummy closed coupled catalyst body was used purely to provide the connection between the exhaust manifold and exhaust pipe.

Two 12V 70Ah batteries were used on the test facilities. One was used solely to crank the engine and the other was used to power the ECU and other engine ancillaries.

3.2.1 Fuel delivery circuit

As shown in Figure 3.4, the fuel system in the engine under investigation consists of low and high pressure circuits. The low pressure system is used to provide an initial pressure in order to prevent vapour bubble formation during hot start and high pressure operation. The system consists of the electrical fuel pump with an integrated pressure limiting valve and low pressure regulator. A pressure gauge was used to adjust the pressure regulator to a pressure between 5 to 6 bar. The high pressure system includes a cam driven high pressure pump which able to generate an injection pressure ranging between 40-120 bar, a fuel rail which acts as a pressure accumulator for the injected fuel, a high pressure regulator which limits the pressure in the fuel rail and finally a fuel rail pressure sensor which measures the actual pressure inside the fuel rail.

The pressure inside the rail was fixed to 70 bar pressure and the change in amount of fuel supplied occurred only through change the injectors pulse width.

The engine employs a gasoline direct injection strategy, with injection fixed to an early value of 60° ATDC. The early injection results in a fairly homogeneous fuel air mixture at ignition in order to avoid retaining any unburned fuel in the exhaust.

Ethanol is a strong aggressive solvent which has the potential to cause failure to fuel system rubber components. In addition, in higher concentrations it can cause corrosion to fuel system components made from brass, steel and aluminium. These problems are exacerbated when the ethanol is left inside the engine for a long period of time, if the engine was not modified for the use of ethanol. For that reason and as the engine under investigation was not modified to operate as a flexi-fuel engine, two fuel tanks were used; one for pure gasoline and the other for an ethanol-gasoline mixture. After each test the engine was flushed with gasoline to make sure that no ethanol was retained.

3.3 Engine Data Acquisition and Sensor Calibration

3.3.1 Engine Pressure and Temperature

In-cylinder pressure was measured in two out of the four cylinders using Kistler 6123A piezoelectric pressure transducer (250 bar range). Each

transducer was connected to a Kistler 5011 charge amplifier. The transducer was flush mounted in the cylinder head to prevent any 'ringing' effect induced by a narrow passage between combustion chamber and sensing element. The transducers and amplifiers were calibrated in pairs to 150 bar on a Budenberg dead weight tester as shown in Figure 3.5.

All other engine pressures were measured using cost effective Kulite *PT 2054* pressure transducers employing a silicon diaphragm and a strain gauge bridge. Pressure measurements were taken in the intake and exhaust manifold. These low power transducers had an accuracy of 0.01% and a resolution of 0.001%. The Kulite pressure sensors were calibrated on the dead weight tester.

All temperatures, for oil, coolant, fuel and exhaust gas were measured using Nickel-Chromium (K type) thermocouples probes, these were used owing to their vast junction measuring range and the relatively large emf sensitivity per 1°C change [64]. For most temperature measurements, a 3 mm diameter insulated hot junction which has 5 seconds response time was used. 0.5 mm diameter wires, which have a response time of 1 second, were used to measure the exhaust port surface. The thinner thermocouples were used purely for installation purposes. The response times for both thermocouples types are acceptable for steady state tests. The signals from the thermocouples were passed through AD595 thermocouple amplifiers which also act as cold junction compensation.

The thermocouples were calibrated in a thermostatic oil bath, the reading from the thermocouples was monitored using the data acquisition system and compared to a platinum resistance thermocouple (PRT) reading also placed within the oil bath. Figure 3.6 shows an example of the thermocouple's calibration.

3.3.2 Engine Encoder and TDC allocation

To monitor and record the crank shaft position, a Hohner W4D91R (W series) incremental optical encoder was connected to the crank shaft. The encoder has two outputs; the first creating one pulse every half a degree of a crankshaft rotation to trigger the data acquisition system, and one creating a single pulse every complete revolution (i.e. every 360° rotation). The encoder one pulse every revolution marker was set to match TDC in the cylinder. TDC represents

a datum which all angular measurement refers to. Any error in its location will obviously be passed through as a constant offset for such a measurement. The exact location of TDC is of extreme importance for in-cylinder pressure related measurement.

The TDC was calibrated for cylinder 1. Initially, TDC was set manually via the dial guage indicator and extension bar resting on the piston crown. Then, an AVL 428 tool was used to obtain a more accurate impression of the position of TDC. The AVL sensor was installed in place of the spark plug in cylinder 1. The sensor evaluates the distance between the sensor tip and the piston crown by measuring the varying capacitance between the two. The sensor then generates a voltage that represents the relative distances. The location of TDC can be then interpolated from the data. The TDC location obtained from the sensor was aligned with the TDC location given by shaft encoder. Figure 3.7 shows the difference between TDC according to the AVL tool and the signal from the encoder.

The correction of the TDC location obtained from the encoder was made through an offset in the data acquisition software.

In order to distinguish between TDC at intake stroke and at exhaust stroke, a comparison between the pressures at both points were carried out as part of the Simulink model. The TDC point with higher pressure is the combustion stroke TDC.

3.3.3 Fuel Flow Measurement

An accurate fuel flow measurement is essential as the heat transfer measurement and the overall energy balance determination and quantification within the engine depend largely upon the fuel delivered to the engine. An Elite CMF025 Coriolis type flow meter was used to measure the fuel flow rate. The flow meter is connected to an Elite RFT9739 transmitter which has an output current proportional to the mass flow rate of fuel in kg/hour in ranges of 4-20mA. These currents were converted to a voltage by connecting four $100\ \Omega$ resistors in parallel across the current outputs to give a voltage output of 0.1V at zero flow rate (4mA).

The flow meter uses the Coriolis effect to measure the mass flow of a fluid. The fluid travels through dual curved tubes. A vibration is applied to the tubes

at their natural frequency using a drive coil and a feedback circuit. As the liquid flows through the tube, it is forced to take on the vertical movement of the tube as shown in Figure 3.8. When the tube is moving upward during half of its cycle, the liquid flowing into the meter pushes down on the tube. Having been forced upward, the liquid flowing out of the meter resists having its vertical motion decreased by pushing up on the tube. This action causes the tube to twist, as shown in Figure 3.8. The biggest advantage of the Coriolis design is that it measures mass flow instead of volumetric flow. Since mass is unaffected by changes in pressure, temperature, viscosity and density, reasonable fluctuations of these parameters in the fluid line have no effect on the accuracy of the meter, which can approach 0.05% of mass flow. It is of particular importance in this study to be able to measure the mass flow rate of different fuel mixtures.

In order to calibrate the Coriolis flow meter, the gasoline from a header tank passed through the Coriolis flow meter and was collected in a container placed on a weighing scale, while the filling process was timed. The corresponding voltage was recorded using the data acquisition system. This process was repeated at different flow rates. The flow rate was changed using a needle valve placed at the entrance of the Coriolis flow meter. The mass flow rate was calculated and plotted as the function of the recorded voltage output and a linear relation between the voltage output and mass flow rate was drawn from the graph.

3.3.4 Coolant and air flow rate Measurement:

The coolant flow rate was measured using an Endress and Hauser electromagnetic type flow meter. In the electromagnetic flow meter, voltage is induced when coolant flow crosses the lines of a magnetic field, which provides a direct indication of the volumetric flow rate, as shown in Figure 3.9. The main advantage of these flow meters is that they do not create any resistance to the coolant flow, since they do not use any moving part within the coolant passage.

The electromagnetic flow meter was calibrated using the same technique used to calibrate Coriolis flow meter (see section 3.3.4). However, a Peristaltic pump was used to pump the coolant into the electromagnetic flow meter owing

to the high flow rate of the coolant inside the engine which cannot be matched by a header tank.

A standard mass air flow (MAF) sensor was used to measure the mass air flow at the air intake manifold. This is a hotwire anemometer monitored by the ECU [62].

3.3.5 AFR sensor

AFR is monitored primarily using a MEXA-700 Lambda portable A/F analyzer which measures air-to-fuel ratio (A/F), excess air ratio (Lambda) and oxygen concentration with a wide range UEGO sensor. The sensor was mounted in the exhaust system in the pre-cat exhaust. The system can be calibrated to be used with different fuels by adjusting the fuel coefficient, i.e. H/C and O/C ratio. This will prove beneficial in acquiring data for different gasoline-ethanol blends.

3.3.6 Exhaust gas analysis

Engine exhaust gas composition was analysed using a Horiba MEXA-7000 engine emissions analysis system which comprised of a number of individual analysers. The exhaust sample was drawn through heated lines using a heated pump. These lines are kept at a constant temperature of 190°C to ensure that the exhaust samples arrive to the emissions analysis system in a fully vaporised state.

A flame ionisation detector (FID) was used to detect the concentration of the unburned HCs in the exhaust gas. NO_x Level was measured using a heated vacuum chemiluminescence analyzer. CO and CO₂ concentration were measured using the well-established infrared gas filter type analyser, and finally exhaust gas oxygen (O₂) was measured using a paramagnetic oxygen analyzer. Because of the nature of the CO₂, CO and O₂ analysers, water vapour in the exhaust must be kept to a minimum before entering the analyzers. For this reason, the exhaust sample passes through a cooler drier unit to cool the gases and condense the majority of the water content in the exhaust gas. The gas that passes through the cooler drier is cooled to 5°C and a portion of the exhaust gas's mass in the form of water is lost before being analysed by the CO, CO₂ and O₂ analysers (dry analysis). To obtain true values for the

concentration in the raw 'dry' exhaust system, a correlation is applied in the post processing of the raw data. The correlation is a function of lambda value and the ethanol ratio inside the fuel as following,

$$\tilde{x}_i = \frac{\tilde{x}_i^*}{(0.0733 E + 0.1287)\lambda^{(3E-1.1678)}} \quad (3.3.1)$$

Where \tilde{x}_i^* is the dry mole fraction, \tilde{x}_i is the true value (wet mole fraction) and E is the ethanol ratio. For more detail about the methods used to develop the correlation, see Appendix 1.

All gas analyzers must be calibrated regularly. The analyzers require zero calibration and span calibration. The zero calibration is performed with a gas that contains none of the analyte gas to which the analyzer responds. For example, pure nitrogen is perfect for zeroing either oxygen or carbon dioxide analyzers, because it contains neither oxygen nor carbon dioxide. Calibration grade span gases, with a precisely defined concentration of the analyte gas to which the analyzer responds, were used to calibrate each individual analyser. Table 3.2 shows the different span gases used to calibrate each analyser.

3.4 Engine management system ATI

An Electronic system in a car consists of an Electronic Control Unit (ECU), sensors, setpoint generators and actuators. The sensors are used to detect the parameters of the electronic system, such as mass air flow rate, coolant temperature and engine temperature. The setpoints register the settings which the driver has specified with his or her operating control, such as pedal position; the sensors and set points produce the input signals to the ECU which then analyses and processes them. Actuators (e.g. ignition coil and fuel injectors) receive the electrical signals produced by the ECU and convert it into physical variables [62]. The command centre of the engine's ECU is a small microprocessor (function processor) with a program memory (EPROM), which stores all algorithms for control processes.

The ATI system, used in the test rig, is an integrated calibration measurement solution which allows access to the ECU for calibration, logging measurement

data and managing calibration data changes [65]. A specially constructed ECU is used for the test rig; the lab ECU differs from the production ECU version in the fact that the flash EPROM was replaced by an IC socket. The M5 emulator module is plugged into this socket with the aid of a custom Tool Adapter Board (TAB) which has been tailored to the ECU's micro processor to simulate the EPROM by means of a RAM. This will provide direct access to ECU calibration parameters and make it possible to modify the different parameters both directly and online. A PC, connected to the M5 emulator via high speed USB port (12MB/s at full speed), was used to perform the control operation through an ATI software package known as ATI's VISION™ as shown Figure 3.10. ATI's VISION™ is a graphical interface software which allows its operator to calibrate, monitor and control the different Engine variables in the strategy file [65]. Among the engine operating variables which were most frequently changed were throttle position, ignition timing, required lambda value and EGR. In order to change any of these variables, some of the management structures related to this particular variable must be disabled first, in order to enable alteration of the variable without any external effect. For example, all new engines are torque based system structures which means that all performance demands placed on the engine are converted into torque requirements. The torque coordinator prioritizes the torque demands from internal and external power consumers. The resulting required torque is proportional to fuel, air and ignition timing. The torque is adjusted by calculating the required cylinder charge and subsequently the required throttle valve angle. Therefore, in order to allow for straight control of the throttle position, the torque structure which is related to so many variables has to be disabled first.

3.5 dSPACE control and data acquisition system

dSPACE is a hardware and software package [66]. The basic concept of the dSPACE system is task sharing. While the software package provides experimental environment and serves for the user interface, the dSPACE hardware takes over the real time calculation.

MATLAB/Simulink was used for modelling, analysis and offline simulation. It provides an interactive graphical environment and a customizable set of block

libraries. Within Simulink, Real-Time Workshop, RTW, was used to generate and execute stand-alone C code for the Simulink model. Real time interference, RTI, blocks are the link between dSPACE's real-time hardware and the MATLAB/Simulink development software. It extends the C code generator RTW so that the Simulink model can be easily implemented on dSPACE real-time hardware. The interaction between dSPACE software, hardware and Simulink is shown in Figure 3.11.

Communication with the test rig occurred through the appropriate I/O cards, described in the following section. Signals produced by the engine sensor were received by I/O cards and displayed for the user via a network communication link between the dSPACE system and a PC, using a dSPACE software package known as ControlDesk. ControlDesk provides the interface which allows the user to interact with the system. Using a variety of virtual instrumentation, data was captured at user-specified lengths and intervals. An example of a ControlDesk page is shown in Figure 3.12

Here is the list of the boards which were used as part of the dSpace hardware system.

DS 1005 PPC Processor

The board featured a Motorola PowerPC 750 processor running at 480 MHz. The DS1005 board provides the computing power for the real-time system and also function as an interface to the I/O boards and the host PC. It communicates to the I/O boards via 32 bit peripheral high speed (PHS) bus that has a transfer rate up to 20 Mbyte/s.

Slow A/D converter (DS2003)

The system comprises of two DS2003 multi channel A/D converters; they include two independent A/D converters with 32 A/D input channels (single-ended). The A/D converter resolution is programmable over a range of 4-16 bit. Each channel is software programmable for a range of $\pm 5V$ or $\pm 10V$. The sampling time is dependent on the number of channel used; while sampling two channels will give a sample time of 5.7 μs , sampling 32 channels will increase the sample rate to 72.5 μs (16 bit).

The two boards were used for time-based sampling. On the first board, the temperature thermocouple signals were sampled. On the other board, pressure transducers, dynamometer load and speed and fuel flow rate were sampled.

Fast A/D converter (DS 2004)

The DS2004 board has 16 parallel independent A/D converter channels, with a resolution of 16 bits. The sampling rate is 800 ns per channel. The measurement modes plus four external trigger inputs enable the conversion of both single measurement values and whole sample bursts. The board was used for the in-cylinder pressure transducers. The data acquisition system was triggered every half-degree of crank shaft rotation by the optical shaft encoder. The hardware trigger block from RTI was used to trigger the crank resolved sampling, by half degree encoder signal to sample the in-cylinder pressure.

Ds4002 timing and Digital I/O

DS4002 timing was primarily used to calculate engine speed using the 0.5 degree square wave output from the encoder. The frequency-to-digital RTI block was used to time sample each rising and falling edge, and then output a digital signal proportional to the frequency of the pulses. The data is then processed to obtain a value for engine rotational speed.

The arrangement of the individual boards, together with an explanation of how they are integrated in the system is shown in Figure 3.13.

3.6 Main Measurement and calculations**3.6.1 In-cylinder pressure data and mean effective pressure (MEP)**

In-cylinder pressure was measured over 100 cycles by the piezoelectric sensors. The piezoelectric sensors are differential sensors and need to be referenced to a known pressure at a given point in order to obtain an absolute pressure. Therefore, in-cylinder pressure at BDC during the intake stroke was sensibly assumed to be equal to the pressure in the intake manifold.

In order to reduce sensitivity to noise, single cycle smoothing of the pressure data was carried out using a simple 3-point rectangular (un-weighted) Algorithm. The algorithm replaces each data point with an average of adjacent points:

$$P_i(\text{smooth}) = \frac{P_{i+1}(\text{raw}) + P_i(\text{raw}) + P_{i-1}(\text{raw})}{3} \quad (3.6.1)$$

For $i=2$ to $m-1$, the reduction in random noise is approximately \sqrt{m} , where m = smooth width. Figure 3.14 illustrates an example of a log pressure vs. log volume graph, for both raw pressure and smooth averaged data.

While torque is an important technique for measuring the ability of an engine to perform work, the difference in engine size makes it hard for the researcher or reader to understand the significance of a particular torque compared to the maximum torque inside the cylinder. For example, while 100 Nm torque is almost the maximum torque for a 1.4L SI engine; it is a medium torque for a 2.0L SI engine. For that reason, mean effective pressure, MEP, is considered to be a more useful way to express work output. MEP is a relative performance measurement which scales the engine/gas work output to the engine displacement. Details of the calculation of brake, indicated, gross and pump mean effective pressure are described below,

BMEP is defined the engine work out per cylinder to the engine displacement as following,

$$P_b = \frac{2\pi NT}{60} \quad (3.6.2)$$

$$BMEP = \frac{2P_b}{V_d N / 60} = \frac{4\pi T}{V_d} \quad (3.6.3)$$

where P_b is brake power output, T is the torque (Nm), N is the engine speed (rpm) and V_d is the swept volume. *IMEP* is defined as the work transfer from gas to piston per cylinder per unit swept volume. In-cylinder pressure is used to calculate the work transferred from the gas to the piston. *IMEP* is calculated using the following equation,

$$IMEP = \frac{W_{c,i}}{V_d} = \frac{\int_{x_1}^{x_2} P dV}{V_d} \quad (3.6.4)$$

where $W_{c,i}$ is delivered per cycle, P is the instantaneous cylinder pressure measured and dV is the change in the cylinder volume from the previous

sample. The values of x_1 and x_2 vary depending on whether gross or net *IMEP* is measured.

IMEP_{net} includes all four strokes with $x_1=0^\circ$ and $x_2=720^\circ$. *IMEP_{gross}* includes only the compression and expansion stroke with $x_1=180^\circ$ and $x_2=540^\circ$.

The difference between *IMEP_{net}* and *IMEP_{gross}* represents the pumping loss during inlet and exhaust stroke,

$$PMEP = IMEP_{net} - IMEP_{gross} \quad (3.6.5)$$

The accuracy of *IMEP* calculations is mainly dependent on pressure/volume phasing. Figure 3.15 demonstrates that an error of 1° in TDC location can cause an error as high as 6% on the *IMEP_n* at low load and 4.5% at high load. This highlights the importance of accurately locating TDC, as detailed in section 3.3.2.

Other sources of error which could affect pressure readings and *IMEP* calculation include error in pressure pegging, clearance volume estimation and transducer temperature variation (which can change the transducer calibration factors) [17].

3.6.2 Burned mass fraction (EGR & Residual mass fraction)

Residual mass fraction, x_r , is defined as fraction of the exhaust gas that is left in the cylinders from previous cycle,

$$x_r = \frac{m_r}{m_{tot} + m_r} \quad (3.6.6)$$

where m_r is residual mass and m_{tot} is the total intake charge,

$$m_{tot} = m_{air} + m_{EGR} + m_{fuel} \quad (3.6.7)$$

The main factors which affect the residual fraction magnitude are inlet and exhaust pressure, valve timing, compression ratio, exhaust system dynamics and engine speed [17]. Its magnitude will have a significant effect on the

engine volumetric efficiency, performance and emissions produced by the change in the thermodynamics properties of the in-cylinder charge. For that reason, accurate knowledge of the x_r is required.

Although the engine has variable valve timing, VVT, technical problems in the signal coming from the VVT sensors forced the author to fix the IVO and EVC at 0°BTDC which means zero overlap between exhaust and inlet valves.

The most common way to quantify cylinder residual fraction is by extracting an in-cylinder charge sample during compression, however, this would require complex instrumentation, and it was beyond the scope of this work to perform such an experiment. Instead, x_r was determined through the ideal gas law. Since both IVO and EVC are fixed at 0°BTDC x_r will be trapped at the clearance volume with temperature equal to the exhaust temperature before the exhaust port T_{exh} , the pressure, P , was assumed to be equal to in-cylinder pressure just before IVO. Hence, m_r can be calculated from the following equation,

$$m_r = \frac{PV_{clearance}}{RT_{exh}} \quad (3.6.8)$$

In order to verify equation 3.9, it was compared with correlations developed by Heywood [17] and Winborn [67], and measured values obtained from Bonatesta [68] at 0 overlapping between EVC and IVO.

Heywood [17] use the following equation to calculate x_r as part of engine cycle simulation,

$$x_r = \left(1 + \frac{T_{exh}}{T_m} \left[r_c \left(\frac{P_m}{P_{exh}} \right) - \left(\frac{P_m}{P_{exh}} \right)^{(\gamma-1)/\gamma} \right] \right) \quad (3.6.9)$$

Where T_{exh} , T_m , p_m , p_{exh} and r_c are exhaust temperature, manifold temperature, manifold pressure, exhaust pressure and compression respectively

Winborn [67] developed the following correlation,

$$x_r = \frac{1}{(1 + 2(r_c - 1)\eta_v C)} \quad (3.6.10)$$

Where η_v is the volumetric efficiency,

$$\eta_v = \frac{m_{air}}{\rho_{air} V_d} \quad (3.6.11)$$

$$C \text{ is constant} = \frac{AFR + 1 - EGR}{AFR - AFR \cdot EGR}$$

Figure 3.16 shows a comparison between equation 3.9, Heywood [17] and Winborn [67] equations, and measured values. The data illustrates that there is a small difference between the results from the different equations, especially between Winborn and equation 3.9; the measured value showed a 2% higher value on average than that calculated by equation 3.9. The difference can be attributed to a difference in the compression ratio between the two engines, 11.5:1 compared to 9:1 for the engine used by Bonatesta [68]. Equation 3.9 was assumed to be accurate to calculate x_r inside the engine during this study. All data demonstrated a decrease in x_r as the load increase. This was due to the increase in inlet to exhaust pressure ratio.

EGR can be defined as the ratio of the mass flow rate of the recycled gas and the total induced mixture, expressed as percentage.

$$EGR(\%) = \left(\frac{\dot{m}_{EGR}}{\dot{m}_{EGR} + \dot{m}_{air}} \right) \times 100 \quad (3.6.12)$$

The EGR percentage was calculated using Horiba emission equipment. A sample of the intake gas was drawn using a vacuum pump, filtered and sent to the cooler dryer travelling going through a carbon oxide analyser to measure the concentration of CO₂ present. The EGR level can be obtained by comparing the CO₂ concentration in the manifold subtracted by atmospheric CO₂ (~0.03%) with that of the exhaust (minus atmospheric):

$$EGR \% = \left(\frac{\tilde{x}_m^* - x_{amb}}{\tilde{x}_e^* - x_{amb}} \right) \times 100 \quad (3.6.13)$$

where \tilde{x}_m^* is the dry percentage of CO₂ in the inlet manifold, x_{amb} is the CO₂ in the ambient air (~0.03%) and \tilde{x}_e^* is the dry amount in the exhaust. See Appendix 2 for more detail about the method used to develop equation 3.14. The burned gas mass in the fresh charge before combustion is the sum of the circulated and residual gas masses

$$m_b = m_r + m_{EGR} \quad (3.6.14)$$

Hence, the burned mass fraction, x_b can be expressed as following,

$$x_b = \frac{m_b}{m_a + m_{fuel} + m_b} \quad (3.6.15)$$

3.7 Errors and repeatability

The test rig which is used in this study was constructed and instrumented by the author. Most of these instrumentations has been used for the first time or has not been used for a period before its use in the current rig. Reliability of the results is the most important part of any experiment, and several potential sources of error could be present in the data acquisition system. Some of these errors can be quantified and sorted, such as noise. The reliability of the test, nevertheless, can be influenced by external factors which will affect the measurement. Ambient temperature, pressure and engine aging are the most obvious factors which can have an effect on the accuracy of the measurement. In this study, a standard reference point at BMEP of 4.7 bar, 2000 rpm speed, MBT spark timing (14 °BTDC) and AFR_{stoich} was chosen to perform a repeatability test. A total of 20 repeatability tests were carried out during the course of the 18 months of experimental tests. The main aim of the repeatability test is to quantify the effect of any external influence and to make

sure that all instrumentations are working in a satisfactory manner before commencing any test.

Figure 3.17 shows an example of the data measured during the repeatability tests. Table 3.3 details the parameters measured and calculated during 18 months of experiments. Air temperature was found to vary a lot during the course of the experiment with COV=10%, temperature varying between 20-30°C depending on the time of the year, weather conditions and the number of engines running inside the lab.

Engine speed, load output, fuel rail pressure and lambda all displayed less than 1% COV which indicates that engine operating conditions are well controlled and repeatable.

The greatest variation was found to concern HC and NOx emissions measurement, with COV = 7 and 4.3 % respectively. This variation can be attributed to the low values being measured and the sensitivity of both emissions to change in inlet air temperature.

The overall results illustrate a reasonable repeatability with COV < 3%, especially regarding heat transfer to coolant and fuel mass flow rate, which have a significant influence on the heat transfer characteristics comparisons. In real world applications, an even greater variation will naturally occur.

Random error related to noise could have significant effect on the data derived from the experiment. For that reason, eliminating or at least reducing noise effect is vital. During the course of this study, several techniques, such as low pass filter for some transducers, were used to eliminate and reduce noise. Both crank and time domain trigger systems data were acquired over long periods. Pressure data was acquired from 100 consecutive cycles. The data was averaged and the moving average technique was used, as explained in detail in section 3.6.1, to eliminate the effect of noise on pressure data related calculations.

The rest of the readings were acquired over 75 seconds with time samples of 0.1s, which means that there were 750 samples for each test point. Before averaging the samples, the noise spike was removed from the data sets to avoid any shift in the data. This was achieved by removing any data point outside the domain ($\bar{x} \pm fS_D$), where \bar{x} is the samples mean, S_D is the standard deviation of

the mean, and the degree of freedom “f” is determined as 2 for 95% confidence level.

Estimate of the uncertainties in some of the measurements and calculations are shown in Appendix A.5.

3.8 Summary & Conclusion

The chapter has described the engine test facilities developed to calculate combustion behaviour, heat transfer and energy balance with different ethanol ratio inside the engine. The repeatability test showed a reasonable degree of accuracy with $COV < 3\%$. The test rig performed in a satisfactory manner during the data acquisition phase. The data has been processed analysed and presented in the following sections.

CHAPTER 4 Basic comparison between gasoline-ethanol mixtures

4.1 Introduction

The most obvious difference between gasoline and ethanol is that the latter is a single species that might be viewed as partially oxidized hydrocarbon [69], the former is complex and composed of variable mixtures of hydrocarbons [23]. The presence of oxygen in ethanol, coupled with its lower molecular weight and H/C ratio, will cause substantial differences physiochemical and combustion properties for ethanol compared to gasoline. In this study, the effect of adding ethanol on gasoline to form different fuel blend on fundamental parameters including AFR_{stoich} , adiabatic flame temperature and heating value will be investigated.

In addition, this section is concerned with the evaluation of the engine performance including power output, BSFC, MBT, emissions and combustion efficiency while operating at various gasoline-ethanol blends.

The above characteristics will have a significant effect on the engine's combustion behaviour, energy balance and heat transfer characteristics that are the main concern of this thesis.

4.2 Experimental fuels

Experiments were carried out on different gasoline-ethanol blends. Ethanol and gasoline were mixed on a volume basis. The blends were mixed just before carrying out the test in order to avoid any absorption of moisture from atmosphere, which can cause phase separation. Phase separation can occur because ethanol is miscible with water while gasoline is not [69]. Phase separation between ethanol and gasoline occurs when the amount of water absorbed exceeds a tolerance level, which will depend on the ethanol ratio of the fuel blend [70]. Water contamination of fuel has a destructive effect on lubricants. It attacks additives, induces base oil oxidation and interferes with oil film production. It also results in corrosion of mechanical components.

Four blends were tested including 10% (E10), 20% (E20), 50% (E50) and 85 % (E85) ethanol ratio. The volume fractions were chosen for several reasons. E10 was of interest as it is already of use in US markets and is being considered for the EU market [1]. E20 and E50 were selected to provide fuels with moderate content which are already used by countries such as Brazil [1]. Finally, E85 has already emerged in some markets, such as USA and Sweden [1], and was required to provide information about the effect fuel with high ethanol content on the engine performance. In addition, a wide range of ethanol ratios were used to aid characterisation of the physical and the chemical properties that might not be linear.

The key properties of the different fuel mixtures are summarized in Table 4.1. The gasoline used in this study is a premium unleaded gasoline which was referred to as ULG in all the figures. For simplicity and for the purpose of the calculation, gasoline was assumed to have a chemical structure of $C_{8.26}H_{15.5}$ [71].

4.3 Selection of experimental comparison parameters

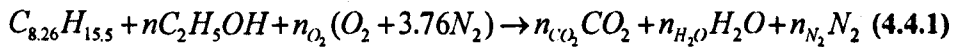
Several potential bases for comparison were considered before starting the experimental work, including constant mass charge, fixed throttle position and constant brake power output. Constant brake power output was selected. Speed, load, spark timing and equivalence ratio were kept constant. This is to insure a direct comparison between the different fuel blends, with change in ethanol content in the fuel as the only variable. Running the engine on different fuel blends with either throttle position or in-cylinder charge mass fixed would affect the power output, as discussed in more detail in the following sections. This means that, in addition to increasing ethanol content in the gasoline-ethanol mixtures, there will be other factors that would affect the engine performance.

4.4 AFR_{stoich} , calorific value and adiabatic flame temperature

AFR_{stoich} , adiabatic flame temperature and calorific value of the fuel are fundamental parameters that have an effect on the engine combustion and performance. This section is concerned with calculating the effect of adding ethanol at different ratios on all these parameters.

Stoichiometric air/ fuel ratio, AFR_{stoich}

AFR_{stoich} , is defined as the ratio of air (oxidizer) to fuel by mass needed to completely burn a quantity of fuel [71]. Mixing of gasoline/ethanol at various ratios will have an effect on fuel composition and thus AFR_{stoich} . The AFR_{stoich} of the different fuel mixture was determined by considering simple atomic balance for the overall chemical equation for complete combustion as follows,



where n , n_{O_2} , n_{CO_2} , n_{H_2O} and n_{N_2} are number of moles of ethanol, air, CO_2 , H_2O and N_2 , respectively. More detail of the calculation are shown in Appendix 3.

Figure 4.1 shows the calculated effect of increasing ethanol ratio on AFR_{stoich} , H/C ratio and O/C ratio. The data illustrate that AFR_{stoich} will decrease as the ethanol percentage increase in the fuel mixture. The decrease in AFR_{stoich} is mainly due to the increase in O_2 content and change in H/C ratio in the fuel mixture. Comparing the gradients of O/C ratio and H/C ratio curves in Figure 4.1 illustrates that O/C ratio has far greater effect on AFR_{stoich} than H/C ratio.

Calorific value

Calorific value or heating value, Q_{HV} , of a fuel is defined as the magnitude of the heat of reaction at constant pressure or constant volume at standard temperature (usually 25°C) for a complete combustion of a unit mass of the fuel. The heating value at constant pressure is more commonly used, the different between the heating values is small [17].

The heating value is divided into upper or higher heating value, Q_{HHV} , and lower heating value, Q_{LHV} . Q_{HHV} is the heat of combustion calculated assuming that all of the water vapour formed in the products has condensed into water. On the other hand, Q_{LHV} is calculated assuming that there is no water condensed in the products. Q_{LHV} is more commonly used to express the energy content of the fuel. The heating value of the different fuel mixture was determined from the heat of enthalpy of reaction, thus [71],

$$Q_{LHV} = -(\text{enthalpy of reaction}) = -(H_{prod} - H_{reac}) \quad (4.4.2)$$

Detailed calculation of the Q_{LHV} for different fuel blends is found in Appendix 3. Calculated data are plotted in Figure 4.2. The data illustrate a linear relation between ethanol content and Q_{LHV} of the fuel. Increasing ethanol content in the fuel blend will decrease Q_{LHV} . Q_{LHV} has decreased from 42 to 29 MJ/kg from gasoline to Ethanol. The value of Q_{LHV} can be related to ethanol volume percentage in the mixture, E, by

$$Q_{LHV} = -16.474E + 42.863 \text{ (MJ / kg)} \quad (4.4.3)$$

Adiabatic flame temperature, T_{add}

The definition of T_{add} is dependent on how the combustion process is completed, constant volume or constant pressure process. The constant volume adiabatic flame temperature, $T_{add,vol}$, is a result of a complete combustion inside the engine without any work transferred into the piston, and with no heat transfer or changes in kinetic or potential energy (constant internal energy). The constant pressure adiabatic flame temperature, $T_{add,press}$, is the temperature that results from a complete combustion process that takes place with no heat transfer or changes in kinetic or potential energy (constant enthalpy process). $T_{add,vol}$ is higher than $T_{add,press}$ because some of the energy in $T_{add,press}$ is used to change the volume of the system (i.e. generate work).

Internal combustion engines cover several degrees of crank shaft rotation during the combustion process, so there will be a change in volume. For that reason, the constant pressure definition was used to calculate T_{add} for the different fuel blends. For the constant pressure definition, the absolute enthalpy of the reactants at the initial state equals the absolute enthalpy of the products at the final state as follows:

$$H_{react}(T, P) = H_{prod}(T_{add}, P) \quad (4.4.4)$$

The enthalpy is calculated by,

$$H = \sum_{total} n_i [\bar{h}_{f,i}^o + \bar{c}_{p,i} (T_i - 298)] \quad (4.4.5)$$

The enthalpies of the reactants were calculated assuming an initial temperature T_i of 298 K. The enthalpy of formation of air is equal to zero, $\bar{h}_{f,i}^o = 0$, at $T_{init} = 298$ K. $\bar{h}_{f,i}^o$ for fuel, for both gasoline and ethanol, is calculated from a polynomial function from Turns [71] for a reference state of zero enthalpy at 298 K and 1 atm,

$$\bar{h}_f^o = 4184 \left(a_1 \theta + a_2 \frac{\theta^2}{2} + a_3 \frac{\theta^3}{3} + a_4 \frac{\theta^4}{4} - a_5 \frac{\theta^{-1}}{5} + a_6 \right) \quad (4.4.6)$$

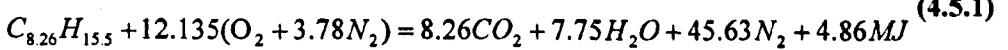
where the coefficients for gasoline and ethanol are shown in Table 4.3. The enthalpy of the combustion products, which is based on temperature, was taken from Rogers and Mayhew [72].

The calculated data were plotted in Figure 4.2. The data illustrates a small decrease in adiabatic temperature between gasoline and ethanol ($\approx 3\%$).

4.5 Power output and fuel consumption

The energy output of the engine is largely a function of the amount of heat released in the combustion chamber; heat release is dependent on the properties of the fuel burned and the amount of air available. Q_{LHV} of ethanol (27.74 MJ/kg) is approximately 63% that of gasoline (43.66 MJ/kg), while AFR_{stoich} of ethanol and gasoline is 9 and 14.52, respectively. The amount of energy that can be released per unit mass of air is proportional to the Q_{LHV} divided by AFR_{stoich} . Consequently in this case, despite the lower heat content of ethanol compared to gasoline, its lower AFR_{stoich} enables an equivalent or even greater amount of energy to be released for a given amount of air, as illustrated in the equations below;

Gasoline :



Ethanol:



Figure 4.3 shows an example of the effect of increasing ethanol ratio in the fuel blend on the engine brake output at WOT, constant speed and fix ST. WOT and constant speed creates a constant mass flow of air for the different fuel blend tests, assuming constant temperature conditions. The results illustrate that as ethanol ratio increases, BMEP output also increases. The data shows a 4.8% improvement in BMEP between gasoline and E85. The improvement in BMEP is also obvious for small ethanol percentages, such as E10 and E20, that are currently commonly used as oxygenates and octane boosters. The improvement in brake output can also be attributed to cooling effect of ethanol as a result of its higher enthalpy of vaporisation. The cooling effect will increase the air density and hence increase the mass of air introduced.

The combined effect of AFR_{stoich} and Q_{LHV} illustrate also that less air is required for ethanol to get the same power output as gasoline. This will affect internal dilution especially at low load, as shown in Figure 4.4, due in the decrease in MAP.

This increase in brake output will be at the expense of BSFC due to the lower Q_{LHV} of ethanol as shown in Figure 4.5. The results show a clear increase in BSFC as ethanol ratio increases.

4.6 Spark timing (ST) and MBT determination

Spark timing, ST, has significant effects on combustion behaviour, energy balance and emissions. If combustion starts too late, peak pressure and temperature will reduce and work transfer from gas to piston during the expansion stroke decreases, consequently reducing brake work output. On the other hand, if combustion starts early in the cycle, a large amount of work will transfer from the piston to the gases at the end of the compression stroke, thus reducing work output. The ST that gives maximum engine torque and minimum brake specific consumption at fixed speed is referred to as maximum brake torque timing, MBT [17]. MBT is mainly dependent on speed and load.

As the speed increases, MBT will advance from TDC since combustion duration, in crank angle degrees, will increase. Increasing load will retard MBT due to the reduction in the combustion duration [17].

MBT was determined at fixed load by changing the mixture flow (increasing or decreasing throttle position) to maintain constant speed for different ST. Figure 4.6 shows the effect of changes in ST location on BSFC and manifold air pressure, MAP. As shown in Figure 4.6, minimum MAP is quite flat and it is hard to allocate exactly where MBT is. In general, the engine is calibrated so that ST is slightly retarded (at the beginning of the flat line).

An alternative approach to determine MBT was used to verify the previous method. A ST sweep was carried out at constant MAP (minimum MAP obtained from previous method was chosen) and constant speed. The test started from significantly retarded ST until a drop in torque or the knock limit was encountered. A comparison between the two methods is shown in Figure 4.7. The data show a torque increase as ST is advanced until the curve is flat at maximum load. Both methods yield the same result.

In order to investigate the effect of adding ethanol on MBT, ST sweeps were conducted for different fuel blends at constant speed and torque as shown in Figure 4.8. The data illustrate that there was very little change in ST as ethanol ratio increase. Table 4.2 shows the MBT location for different fuel mixtures at part and high load. MBT location in the table was obtained from fitting a quadratic polynomial to the ST sweeps with $R^2 > 0.9$. The data illustrate again that there is no significant difference between MBT for different fuel blends. E85 had a very slightly retarded MBT compared to gasoline.

The introduction of EGR has an effect on MBT location due to the change in combustion duration of the in-cylinder charge. As EGR increased in the mixture, ST has to advance in order to maintain MBT timing and thermal efficiency. The relation between MBT with no EGR, θ_0 , and MBT when EGR is introduced, θ , for both E85 and gasoline is plotted in Figure 4.9. From the plotted data, θ_0 and θ are related by,

$$\text{For gasoline: } \theta_{EGR} = \theta_0 e^{3.23EGR} \quad (4.6.1)$$

$$\text{For E85: } \theta_{EGR} = 0.99\theta_0 e^{3.0EGR} \quad (4.6.2)$$

4.7 Emissions

The SI engine is a major source of emissions; the regulated emissions that are produced by SI engine are CO, HC and NO_x emissions. In addition there are aldehyde emissions that are not yet regulated and particulate matter, PM, that are regulated for DISI engines. Increasingly tighter regulations mean that greater understanding of the effect using ethanol on those emissions is required. Although the effect of using ethanol has been extensively studied by several researchers, there was variation in the results as discussed in detail at the literature review in Chapter 2. Furthermore, the majority of these tests were carried out on PFI engine, and the rest were carried out in a wall guided DISI engine. The only exception is Price *et al.* [41] who looked at the effect of ethanol in an SGDI engine. The study investigated PM without looking at any of the other emissions. For that reason, it was essential to understand the effect of using ethanol in SGDI engines. In addition, the exhaust composition was used to calculate the combustion efficiency for different fuel blends.

The work here focused on comparing the emissions produced when the engine is running on different fuel blends. The tests we carried out at different running conditions, varying ϕ , EGR and ST.

The introduction of ethanol was expected to have an effect on the emissions produced due to the change in the chemical composition of the different fuel blends including the higher H/C ratio and the availability of oxygen in the fuel. Regulated emissions were sampled using a Horiba exhaust gas analyzer, see section 3.3.6 for more details.

4.7.1 CO and CO₂ emissions

While CO₂ is formed as a result of complete combustion of fuel, CO is formed at high temperature when there is insufficient oxygen to form CO₂. That is why CO mainly forms during the combustion stroke where rich fuel/air mixtures and high temperature products are available, and then freezes in the expansion stroke as temperature reduces.

It is well established that fuel/air equivalence ratio, ϕ , is the main parameter that affects CO and CO₂ emissions in an SI engine [17]. Figure 4.10 shows CO and CO₂ emissions as function of ϕ for different fuel blends. The results demonstrate that on the lean side, CO₂ level rise as ϕ decreases due to the reduction in fuel quantity. At the rich side, CO₂ mass fraction drops as ϕ increases due to the reduction in the oxygen available for complete combustion. CO emissions, on the other hand, are very small at the lean charge but not zero due to the high temperature inside the combustion chamber. However, as ϕ increases over 1, CO mass fraction increases steadily due to insufficient O₂ for combustion. This result indicates that high concentration of CO can be avoided by running lean or even at stoichiometric. However, SI engine has to run rich at starting up to avoid stalling especially at low temperatures (which appears to be particularly a problem when running with ethanol) and at WOT to increase maximum power.

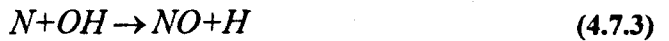
Adding ethanol to the fuel had a significant effect on both CO and CO₂ as illustrated in Figure 4.10. Increasing ethanol percentage in the mixture decreases CO₂ mass fraction for lean mixtures until ϕ reaches 1.1, then CO₂ does not change between the different fuel blends. The reduction in CO₂ is attributed to the change in H/C and O/C ratios. The effect of H/C ratio change on CO₂ emissions was calculated from the atomic balance in chemical equation 4.1, assuming complete combustion. The calculated data were plotted in Figure 4.11. The data illustrate a decrease in CO₂ as ethanol ratio rises (H/C ratio increase). As shown later in this chapter, when $\phi > 1$, increasing ethanol ratio improves the combustion efficiency as shown in Figure 4.19, therefore increasing CO₂ fraction. The combined effect of H/C ratio and combustion efficiency can explain the unchanged CO₂ at rich fuel/air ratio.

The reduction in CO at rich fuel/air ratio as ethanol content increase is a direct result of the increase in combustion efficiency.

4.7.2 NO_x emissions

Oxides of Nitrogen (NO_x) are harmful emissions that contribute to the formation of acid rain and photochemical smog [17]. NO_x refer to both NO and NO₂ emissions. In SI engines, NO dominates NO_x composition with contributions between 70-90% of the total [17]. The most widely approved

mechanism for the thermal formation of NO emissions is that of Zeldovich [17]. The mechanism comprise of three different steps,



High combustion temperature causes the oxygen molecules to dissociate to atomic oxygen which initiates nitric oxide formation; subsequently in-cylinder temperature and availability of oxygen are the main parameters that affect NO formation. In other words, higher burned gas temperature results in higher rate of NOx formation. The rate of the reaction in equation 4.11 to 4.13 is slower than the combustion rate and for that reason the majority of NO is formed behind the flame [17]. NO₂ is generated through the conventional mechanism as follows,



NOx emissions are mainly influenced by EGR, ignition timing and equivalence ratio; all of which have a direct impact on in-cylinder temperature and oxygen availability.

Figure 4.12 shows NOx emissions as a function of equivalence ratio for different fuel blends. For all fuel mixtures, the maximum formed NOx is found near $\phi = 0.9$. Reducing peak temperature can significantly reduce NOx emissions. This can be achieved by re-circulating some of the exhaust back to the combustion chamber using EGR. The effect of EGR is to increase the heat capacity of the charge, thus, reducing the peak combustion temperature. The reduction in temperature will cause a reduction in NOx emissions, as shown in Figure 4.13. However, EGR also decreases the combustion rate, making stable combustion more difficult to achieve. This results in increased HC emissions, as shown in Figure 4.15 [73].

Another method to reduce NO_x emissions is by retarding ignition timing. Retarding ignition timing moves the peak pressure away from TDC, thus, reducing peak pressure and temperature due to the increase in volume. The effect of ignition timing is shown in Figure 4.14.

Data in Figure 4.12, Figure 4.13 and Figure 4.14 illustrate clearly that NO_x is decreasing as ethanol ratio increases. The decrease is small between gasoline and E50 followed by a large decrease between E50 and E85. The decrease in NO_x emissions is mainly attributed to the decrease in local flame temperature. While it was beyond the scope of this study to measure the combustion temperature directly, adiabatic flame temperature was calculated using the emission constituent. See appendix 3 and section 4.4 for more details. Figure 4.2 shows a clear reduction of adiabatic flame temperature as ethanol ratio increase. Previous research showed a clear correlation between adiabatic flame temperature and NO_x emissions [74]. Furthermore, increasing ethanol content will decrease h_{fg} as shown in Figure 2.3. This will create a cooling effect before combustion and subsequently decrease in in-cylinder temperature.

Another minor factor to consider is that, for the same load and speed, internal dilution will increase slightly as ethanol ratio increases, as shown in Figure 4.4.

4.7.3 HC emissions

HC emissions are formed as a result of incomplete combustion of the hydrocarbon fuel. As mentioned in Chapter 2 and Chapter 3, a FID is used to measure HC. FID response is proportional to C atoms in each molecule. In alcohol, the C is bonded to O in R-O-H group where R is an Alkyl radical gives a response of about 50 to 85% of a C atom [41]. A correction factor based on the average of FID response to alcohol, 65%, was used. A linear relation between ethanol content and FID response was assumed.

Figure 4.15 & Figure 4.16 illustrate that increasing ethanol ratio will cause a significant decrease in HC emissions for all equivalence ratios conditions. There was up to a 30% decrease in HC emissions between gasoline and E85.

There are several mechanisms that could cause the formation of HC emissions for SI engines [17] such as flame quenching, filling of the crevice with unburned mixture, oil layer absorbing the fuel vapour during intake and

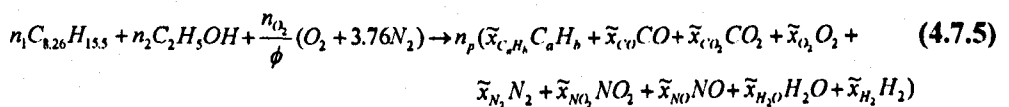
compression then releasing these vapours during expansion and exhaust and finally incomplete combustion or total misfire that could occur as a result of poor combustion quality.

Flame quenching and crevice volume do not change significantly between different blends. The polar nature of ethanol molecules means that they cannot be absorbed easily by lubricating oil that has a non-polar nature. However, this is not expected to be significant enough to explain the obvious trend for the decrease in HC emissions. Although ethanol is an oxygenate fuel, the oxygen availability for the different blends was the same since the comparison was based on fixed equivalence ratio, ϕ . However, the fact that oxygen is contained within the fuel might have enhanced the HC oxidation due to higher surface connection and better mixing between fuel and oxygen. The fuel chemical components of ethanol and gasoline are quite different. The increase of ethanol ratio in fuel blend will lead to the reduction of aromatics and olefins and other hazardous high-octane additives commonly used to replace TEL lead in gasoline. Studies indicated that fuel with higher aromatic and olefins will produce higher concentrations of reactive hydrocarbons [17] and subsequently increasing ethanol ratio will decrease HC.

4.7.4 H_2O level and equivalence ratio

H_2O is produced from the combustion process. Although there are no health risks or environmental concerns associated with the production of H_2O , the level of H_2O in the exhaust will affect exhaust temperature and subsequently some of the engine operations; this will be discussed in more detail in the following chapters.

H_2O was not measured directly; instead, it was calculated from the measured exhaust constituents (HC, CO, O_2 , CO_2 and NOx). Based on combustion balance, the overall reaction can be written as follows [17],



where n_1 and n_2 are the number of moles for gasoline and ethanol respectively, \tilde{x}_i^* is the dry mole fraction and is related to the wet mole fraction \tilde{x}_i by $\tilde{x}_i = (1 - \tilde{x}_{H_2O})\tilde{x}_i^*$. From the combustion balance H_2O can be calculated using the following equation,

$$\tilde{x}_{H_2O} = \frac{A}{2B} \frac{\tilde{x}_{CO}^* + \tilde{x}_{CO_2}^*}{[1 + \tilde{x}_{CO}^* / (K\tilde{x}_{CO_2}^*)] + (A/2B)(\tilde{x}_{CO}^* + \tilde{x}_{CO_2}^*)} \quad (4.7.6)$$

Where A & B is the number of H and C moles respectively in the products and equal to:

$$B = 8.26n_1 - 2n_2$$

$$A = \frac{15.5n_1 - 6n_2}{2}$$

A comparison of H_2O emissions for different gasoline-ethanol blends is plotted in Figure 4.17. H_2O increased as ethanol ratio increased in the fuel. This is due to changing chemical composition, namely increase in H/C and O/C ratio. Figure 4.11 shows the effect of H/C and O/C ratio change on H_2O mass fraction calculated from the atomic balance in chemical equation 4.1, assuming complete combustion.

The engine is fitted with a UEGO sensor that is linked to the ECU and is used to measure directly the equivalence ratio. However the accuracy of the sensor varies across different operating conditions; for this reason a calculation of equivalence ratio based on combustion balance, equation 4.15, is performed. The fuel/ air equivalence ration is given by:

$$\phi = \frac{2n_{o_2}}{n_p \tilde{x}_{H_2O} + n_p (1 - \tilde{x}_{H_2O}) (\tilde{x}_{CO}^* + 2\tilde{x}_{CO_2}^* + \tilde{x}_{CO}^* + 2\tilde{x}_{O_2}^* + \tilde{x}_{NO}^*) - Xr} \quad (4.7.7)$$

Where,

$$n_{o_2} = \frac{24.27 - 18.27 X}{2}$$

$$n_p = \frac{n_c}{\tilde{x}_{HC_{bls}} + (1 - \tilde{x}_{H_2O})(\tilde{x}_{CO}^* + \tilde{x}_{CO_2}^*)}$$

$$n_p = \frac{B}{\tilde{x}_{HC} + \tilde{x}_{CO} + \tilde{x}_{CO_2}}$$

Figure 4.18 shows a comparison between calculated and measured value, the results show good agreement with less than 5% variation.

4.8 Combustion efficiency

Engine combustion efficiency is an important parameter showing the quality of combustion inside the cylinder; it defines the fraction of chemical energy that has been released inside the combustion chamber:

$$\eta_c = \frac{\dot{Q}_f}{\dot{m}_f Q_{LHV}} \quad (4.8.1)$$

The combustion inefficiency, and subsequently the efficiency, was calculated using combustible emissions i.e. CO, H₂ and HC. The chemical energy of these combustible emissions represents the combustion inefficiency [17],

$$1 - \eta_c = \frac{\sum x_i Q_{LHV_i}}{[\dot{m}_f / (\dot{m}_f + \dot{m}_a)] Q_{LHV_f}} \quad (4.8.2)$$

where the lower heat value of CO and H₂ are 10.1 MJ/kg and 120 MJ/kg respectively. The composition of unburned HC is not known. However, in this study H/C ratio was assumed to be the same as the fuel blend used to run the engine and the heating value can be assumed to be between (29-43MJ/kg) depending on the fuel blend.

Figure 4.19 shows the combustion efficiency of the different fuel blend as function of equivalence ratio, ϕ . Increasing ethanol content in the fuel blends gives an increase in the combustion efficiency. This increase in efficiency becomes more significant as ϕ increase and the charge becomes richer. There was a 10% increase in combustion efficiency between gasoline and E85 at $\phi = 1.2$. The data also illustrate that there is a non-linear relationship between

increasing ethanol content and combustion efficiency. While there was not any significant change in efficiency between gasoline and E10 or E50 and E85, there was an obvious improvement in efficiency for E10 and E20, then E20 and E50.

The improvement in combustion efficiency is due to the oxygen availability in ethanol. Increasing ethanol ratio in the mixture increases oxygen availability in the fuel, thus, oxygen mass fraction in the fuel will increase as shown in Figure 4.20. Figure 4.20 illustrates that the increase in oxygen mass fraction as ethanol ratio increases is even higher as ϕ increases. This can explain the bigger improvement in combustion efficiency at higher ϕ .

Also, the data clearly show that for all fuel blends, combustion efficiency is substantially affected by equivalence ratio ϕ . On the rich side, there was rapid decrease in combustion efficiency due to lack of the oxygen available for complete combustion.

4.9 Summary and discussion

The aim of this chapter was to perform a basic comparison between the different fuel blends that were used through the course of this study. This included the effect of ethanol on AFR_{stoich} , Q_{LHV} , T_{add} , MBT, BSFC, power output, emissions and combustion efficiency. All these characteristics will have a significant effect on the engine's combustion behaviour, energy balance and heat transfer which are going to be discussed in more detail in the following chapters.

The change in the chemical composition of the fuel mixture as ethanol content increase, particularly the increase in H/C ratio and Oxygen content, was expected to affect the above properties.

An increase in ethanol ratio leads to decrease in AFR_{stoich} , Q_{LHV} , and to lesser extent T_{add} . The reduction in Q_{LHV} value was illustrated in the increase in BSFC as ethanol ratio rise. The lower ethanol Q_{LHV} did not affect the engine power output. On the contrary, engine power output, for a fixed throttle position, increased slightly as ethanol ratio increased. This is attributed to the decrease of AFR_{stoich} .

MBT location, which is important for future calibration of flexi-fuel engine, did not change among the different fuel blends.

The change in chemical composition was expected to affect the emissions produced by the engine. Increasing ethanol ratio shows a decrease in CO, CO₂, HC and NO_x emissions for most running conditions. H₂O, on the other hand, showed a clear rise in its level.

Change in CO₂ and H₂O levels is a direct result to the increase in H/C ratio. CO and HC mass fraction reduce due to the improvement in combustion efficiency as ethanol ratio increases. HC mass fraction also decreases as a result of other factors including the polar nature of ethanol that will reduce the amount of fuel absorbed by the lubricating oil and the reduction in high octane booster additives such as aromatics and olefins that contribute to HC emissions. NO_x formation is mainly influenced by the local peak temperature that was affected by both lower adiabatic flame temperature and the higher enthalpy of vaporisation for ethanol.

The decrease in emissions level, particularly with higher ethanol ratio, indicates that using ethanol has the potential to contribute to the effort to comply with increasingly tight emissions regulations.

As mentioned previously, increasing ethanol will increase combustion efficiency as particularly at rich mixtures. This is attributed to the oxygen content of ethanol that enhances combustion.

CHAPTER 5 The effect of ethanol on engine combustion behaviour

5.1 Introduction

The main objective of the work presented in this chapter is to understand the effect of ethanol on combustion behaviour. Although the effect of ethanol on combustion behaviour was studied by several researchers, the variation in the results among those researches (see section 2.6) illustrated a need for a better understanding of ethanol effects. This is particularly important in this thesis since combustion behaviour has a significant effect on the energy balance and heat transfer characteristics that are studied in more detail in later chapters. This will happen through the effect of combustion duration on in-cylinder gas and exhaust temperature.

Burning rate and burn duration in CA have a significant effect on the combustion behaviour. There is a clear agreement among researchers that faster burn duration is a favourable characteristic [17]. Shorter burn duration produce more robust and repeatable combustion pattern since it allows a higher level of EGR and leaner mixture within the normal constraints of engine smoothness and response. Higher EGR and lean mixture will allow more emission control by reducing NO_x emissions without increasing HC level. In addition, at part load, fuel consumption will reduce due to the reduction in pumping work and decrease in gas temperature and hence heat transfer [17].

In this chapter, the effect of changing unburned gas composition by increasing ethanol percentage in the fuel blend will be evaluated. Experimental data was obtained for different running conditions including different speeds, loads, ST, equivalence ratio and EGR as shown in Table 5.1. The Rassweiler and Withrow [75] method was used to estimate the burn duration in the engine.

Furthermore, the effect of increasing ethanol concentration on combustion stability and EGR tolerance was evaluated

5.2 Combustion Process characterization

A Mass fraction burned (MFB) profile as a function of crank angle provides a convenient basis for defining various stages of combustion processes by their crank angle duration. MFB can be defined as the percentage of the cylinder charge that has been burned at a certain instant after spark discharge.

At the initial part of the curve, immediately after the spark discharge, the air fuel mixture burns at a low rate. The charge burn rate starts to increase until it reaches its maximum about half way through the burning process, and then decreases to zero as the burning process ends. The previous stages of combustion process and energy release can be characterized in three main definitions [17]:

Flame development angle, FDA is the crank angle duration that starts immediately after spark discharge until a small but significant fraction of the cylinder charge has been burned or fuel energy has been released. This fraction is usually 10% [17]. However, some researchers used 2% or 5 % MFB [17]. In this study a 10% MFB limit is used to avoid errors associated with small fuel heat release at early stages of MFB.

Rapid burn angle, RBA is the crank angle interval where the bulk of the cylinder charge is burned. It starts after the FDA stage and continues until the end of the flame propagation process. Heywood [17] defines the RBA as crank angle interval that covers 10% to 90% of the MFB. The Heywood definition is adopted in this thesis. 90% MFB limit was chosen to avoid errors associated with locating the end of combustion since the final stage of combustion is hard to identify[68]. In addition, the fuel energy released by the fuel as the combustion terminates is comparable to other heat process that occur at the same time and the MFB only increases slightly over a large number of CA degrees.

Overall burning angle is defined as the sum of the two previous burn angles.

5.3 Rassweiler and Withrow Method

In this study, the method developed by Rassweiler and Withrow [75] was used to calculate the MFB from experimental pressure and volume variation data. This approach is based on two main observations from a constant volume bomb experiment; firstly, it was noticed that the mass fraction burned is approximately equal to the fraction pressure rise.

$$x_b = \frac{m_b}{m_{tot}} \approx \frac{P_b}{P_{tot}} \quad (5.3.1)$$

Secondly, they observed that for a given amount of energy release, combustion pressure rise is inversely proportional to the volume $P_C \propto \frac{1}{V}$. In order to apply this equation to SI engine conditions, the change in total pressure, P_{tot} across a discrete crank angle interval is considered to be the sum of pressure changes due to volume, P_V , and combustion, P_C .

$$\Delta P_{tot} = \Delta P_C + \Delta P_V \quad (5.3.2)$$

The pressure rise from change in volume can be calculated at small crank angle intervals assuming polytropic process.

$$\Delta P_V = \Delta P_\theta \left[\left(\frac{V_\theta}{V_{\theta+1}} \right)^n - 1 \right] \quad (5.3.3)$$

In order to compensate for the change in the volume of the combustion chamber compared to a constant volume of the bomb used by Rassweiler and Withrow, the combustion pressure has to be related to reference volume.

$$\Delta P_C' = \Delta P_C \times \frac{V_\theta}{V_{ref}} \quad (5.3.4)$$

V_{ref} was assumed to be equal the combustion chamber volume at TDC. The MFB at a particular crank angle θ is therefore,

$$MFB = \frac{m_b}{m_{tot}} \approx \frac{\sum_{\theta_0}^{\theta} \Delta P'_C}{\sum_{\theta_0}^{EOC} \Delta P'_C} \quad (5.3.5)$$

The estimated uncertainty in Rassweiler and Withrow approach in Appendix CHAPTER 9A.5 concluded that Rassweiler and Withrow is a robust method to calculate combustion duration and it is not very sensitive to pressure or to pressure-volume phasing errors. The maximum errors in FDA and RBA are 0.6° and 0.4° respectively.

5.4 Calculating polytropic index

The major difficulty with using the Rassweiler and Withrow method is selecting appropriate polytropic index values to calculate P_V . The sensitivity of pressure to the polytropic index increases with increasing in-cylinder pressure. For this reason the sensitivity of the MFB profile to the compression index, n_{comp} , is relatively low. The expansion index, n_{exp} , is more important since the pressure reaches its maximum after TDC. MFB profile sensitivity to the change in n_{exp} is shown in Figure 5.1.

Prior to spark ignition, during the compression stroke, the process was assumed to be polytropic that starts from IVC. The polytropic index was calculated from slope of $(\log P, \log V)$ diagram over 30 degrees before ST as shown in Figure 5.2. However, during the expansion stroke, the value of n_{exp} varied due to heat transfer, work exchange and turbulent intensity. The use of the correct n_{exp} will keep the burn rate at 100% once the combustion is over until EVO. This will satisfy the zero combustion pressure conditions [76].

Several techniques have been developed to calculate n_{exp} . The iterative method is the most common. This starts from a value of $n_{exp} = 1.3$, changing the value of n_{exp} and EOC location accordingly until a reasonable MFB S-shape profile is reached, as show in Figure 5.1. EOC, at which n_{exp} was chosen, was determined from the calculated combustion pressure, P_C . Several methods were

proposed to determine EOC including 'first negative index', 'sum negative index' and 'negligible P_C fraction index'. 'First negative index' assumes that EOC is located when the first negative P_C occurs. 'Sum negative index' assumes that EOC occurred when three consecutive negative P_C take place. The second method is seen as more robust since it reduces the influence of noise. Finally, with 'negligible P_C fraction index', EOC is defined when P_C becomes a negligible fraction of the total pressure ($P_C \leq 0.02 P_{tot}$). Any of the previous methods can be used as part of the iterative method.

Another method to calculate n_{exp} is $PV^{1.15}$ index [77] which is a simple alternative technique to iterative method. $PV^{1.15}$ index simply uses the point where $PV^{1.15}$ reaches its maximum then adds 10°CA to allocate EOC and subsequently determine a value of n_{exp} that satisfies the S-shape profile.

Wiseman *et al.* [76] also proposed a method where n_{exp} is calculated without the need to determine EOC. Wiseman calculated the value of n_{exp} over small interval just before EVO that satisfies P_C equal to zero after combustion terminates.

Figure 5.3 shows a comparison between the different techniques proposed to calculate n_{exp} for different running conditions. With the exception of Wiseman method, there was not a significant change among the different methods. The Wiseman index appears to be overestimating the combustion duration especially for medium and high loads.

In this study, the iterative method was used to determine n_{exp} , with EOC was allocated using 'negligible P_C fraction index'. EOC was determined when P_C becomes a negligible fraction of the total pressure ($P_C \leq 0.02 P_{tot}$) at three consecutive steps. This method was seen to be more robust since it reduced the influence of noise and it was easier to use to define EOC.

5.5 Comparison between laminar flame speed of ethanol and gasoline

Burning rate is often expressed in terms of a turbulent burning velocity. Turbulent flames can be treated as an array of laminar flamelets with no turbulence structure residing within them [17]. Therefore, understanding of laminar combustion is important to understand flame turbulent combustion.

Laminar flame speed can be defined as the rate of propagation of a flame through a gaseous fuel-and-oxidizer mixture relative to a fixed reference point [17].

Laminar burning velocity of gasoline and ethanol has been measured using a spherical combustion bomb by various researchers. The gas motion of the spherical bomb can illustrate the features of the induced motion in an engine. Data at higher pressure and temperature have been fitted to a simple empirical correlation of the form [17].

$$S_L = S_{L,0} \left(\frac{T_u}{T_0} \right)^\alpha \left(\frac{P}{P_0} \right)^\beta \quad (5.5.1)$$

where $T_0 = 298$ K and $P_0 = 1$ atm are the reference temperature and pressure, and $S_{L,0}$, α and β are constant for given fuel, equivalence ratio and burned gas diluents fraction. For gasoline these constants can be represented by [78]:

$$\begin{aligned} \alpha &= 2.4 - 0.271\phi^{3.51} \\ \beta &= -0.357 + 0.14\phi^{2.77} \\ S_{L,0} &= B_m + B_\phi(\phi - \phi_m)^2 \end{aligned}$$

where $\phi_m = 1.21$ is the equivalence ratio at which $S_{L,0}$ is a maximum with value of B_m . For gasoline $B_m = 30.5$ cm/s and $B_\phi = -54.9$.

For ethanol these constants can be represented by [79, 80]:

$$\begin{aligned} \alpha &= 1.783 - 0.375(\phi - 1) \\ \beta &= \begin{cases} -0.17\sqrt{\phi} & \phi \geq 1 \\ -0.17/\sqrt{\phi} & \phi \leq 1 \end{cases} \\ S_{L,0} &= Z.W.\phi^\eta \exp[-\varepsilon(\phi - 1.075)^2] \end{aligned}$$

where $Z=1$, $W=0.465$, $\eta = 0.25$ and $\varepsilon = 6.34$

Equation 5.6 was used to calculate laminar flame speed for ethanol and gasoline, with appropriate constants used for each fuel. Figure 5.4 shows a comparison between the laminar flame speed of gasoline and ethanol as a function of ϕ at a different initial pressured and temperatures. For all pressure conditions, the data illustrate clearly that ethanol has higher laminar flame speed than gasoline for most ϕ values. The maximum difference in laminar flame speed between ethanol and gasoline occurs at stoichiometric conditions. Ethanol seems to be more sensitive to the change in ϕ . Subsequently, the difference in laminar flame speed starts to decrease as ϕ moves away from stoichiometric, particularly as it becomes richer. As the charge becomes richer the difference in laminar flame speed between the two fuels decreases significantly up to point where gasoline will have a higher laminar speed than ethanol, at $\phi=1.2-1.3$ depending on the pressure.

Laminar burning speed is influenced by several factors including molecular structure of the fuel, T_{add} , pressure, upstream temperature and EGR [17]. Although T_{add} has a strong influence on laminar burning velocity, and ethanol has a lower T_{add} due its lower Q_{LHV} (see section 4.4), the molecular structure of ethanol includes an oxygen molecule that will significantly increase laminar flame speed.

5.6 Effect of ethanol blends on burning duration

Several tests were carried out at wide range of running conditions in order to examine the repeatability and the sensitivity of the effect of ethanol on burn duration across those conditions. In addition, the effect of those running conditions on burn duration in an SGDI engine was investigated. The different running conditions are summarized in Table 5.1.

5.6.1 Different speeds, loads and spark timing

In order to evaluate the effect of ethanol on combustion characterises, several tests were carried out with engine running at different loads, speeds and spark timing.

Figure 5.5, Figure 5.6 and Figure 5.7 show the effect of ethanol on the FDA and the RBA for various loads, speeds and spark timing, respectively.

For all engine running conditions, the results illustrate very little difference in FDA among different fuel blends. RBA results illustrate that there is not a linear relation between increasing ethanol ratio and RBA. Initially E10 showed a slight decrease in the RBA. Then, there was a very small difference or no trend in RBA between E10, E20 and E50. E85, on the other hand, clearly showed a clear faster combustion speed, shorter RBA, compared to all fuel blends and particularly gasoline.

The decrease in RBA for E85 compared to gasoline ranged between 2% at low load to 6 % at high load. The lower decrease in RBA at low load compared to high load is attributed to different internal dilution among fuel mixtures. At low BMEP, for fix cam timing and power output, internal dilution increases as ethanol ratio increases as shown in Figure 4.4.

The observed similarities in FDA value for the different gasoline-ethanol blends were not expected, because of the higher laminar flame speed of ethanol. This however, can probably be explained by the design of the engine under investigation. It is a high compression ratio engine (11.5:1), and consequently properties associated with high compression work, charge density and in-cylinder turbulence dominated the early stages of combustion.

The non-linear relation between increasing ethanol and the RBA is explained by the ethanol properties that influence the combustion. Ethanol has different properties, some of which may be beneficial to combustion while others have the opposite effect. The high laminar burning velocity and oxygen availability will improve combustion and reduce its duration. However, ethanol higher enthalpy of vaporisation and lower Q_{LHV} will decrease gas temperature during compression resulting in slower combustion duration. The combined influence of the two factors will affect the burn duration inside the cylinder. Consequently, the improvement in the laminar speed as a result of adding ethanol to the fuel blend will not have any apparent effect on RBA until high ethanol content.

Changing the running conditions also influences the combustion speed in the same manner for all fuel blends. Increasing load or advance ST decreases the combustion speed. This is due to the increase in pressure and temperature at the time of combustion. Furthermore, increasing load will decrease the internal dilution due to the reduction in the difference between MAP and exhaust

manifold pressure. Increasing speed, on the other hand, will decrease slightly the combustion speed. The increase in piston speed will cause an increase in combustion duration in CA domain. However, increasing the speed will increase in-cylinder gas velocity and introduce swirl which will increase the turbulent intensity and subsequently increase combustion duration [17]. For that reason burn duration will only increase slowly with increasing engine speed.

5.6.2 Sensitivity to change charge composition (x_b & ϕ)

Changing the charge composition, through factors such as x_b and ϕ will affect burn duration. The sensitivity of different gasoline-ethanol blends to these changes is evaluated in this section.

The burned mass fraction, x_b , is defined as the sum of EGR and internal dilution, x_r (See section 3.6.2 for more detail). x_b was chosen instead of EGR because x_r changes for different gasoline-ethanol blends at fixed cam positions as shown in Figure 4.4.

Figure 5.8 shows the effect of x_b on RBA and FDA. For all fuel blends, both RBA and FDA increase x_b increases. Once again, FDA shows no trend between the different fuel mixtures for all x_b conditions. RBA, on the other hand, appears to be more sensitive to the change in x_b as ethanol ratio increases. At low x_b , there was an obvious reduction in RBA as ethanol ratio increases. However, the difference in RBA between the fuels blends starts to decrease as x_b increases. At high x_b level, the fuel blends show a comparable RBA.

The increase in FDA and RBA as x_b values increases is attributed to the reduction in temperature and pressure during combustion, and thus the laminar flame speed. The effect of x_b on laminar flame speed was studied by Rhodes *et al.* [81], a correlation to calculate the effect of x_b on laminar flame speed was developed as follows,

$$S_L(\tilde{x}_b) = S_L(\tilde{x}_b = 0) (1 - 2.06 \tilde{x}_b^{0.77}) \quad (5.6.1)$$

Equation 5.7 was used to calculate the effect of x_b on laminar flame speed for both ethanol and gasoline as shown in Figure 5.9. The plotted data demonstrate

that the laminar flame speed of ethanol is more sensitive to changes in x_b than it is for gasoline. Subsequently, the difference in laminar flame speed starts to decrease as x_b value increases. This corresponds well with the data showed in Figure 5.8 and can explain the reduction in the difference in RBA value between the fuel mixtures as x_b increases.

Equivalence ratio, ϕ , will also have an effect on burn duration as shown in Figure 5.10. For all fuel blends, FDA and RBA increases as the in-cylinder charge becomes leaner. The increase becomes more significant after $\phi=1$. Comparing between the different fuel mixtures, at $\phi = 1$ the burn duration is clearly decreasing as ethanol ratio increases. However, when the mixture becomes leaner or richer, the RBA duration difference between the different fuel mixtures slightly decreases. This corresponds well with the laminar flame speed results shown at Figure 5.4. The difference between gasoline and ethanol laminar flame speed starts to reduce as the charge moves away from stoichiometric. Other factors such as lower heat content and lower adiabatic flame temperature for ethanol begin to become more dominant especially when the charge is rich.

5.7 Combustion stability and tolerance to x_b

In order to evaluate x_b tolerance of the different fuel blends, x_b sweeps were carried out at both low and medium load and constant speed. The ST was set to MBT for each running condition (see section 4.5).

Increasing x_b will decrease combustion speed, which makes stable combustion harder to achieve. The level of x_b that the engine can tolerate will depend on the level of the resulting decrease in combustion speed. The increase in combustion speed associated with high ethanol content in the fuel, as shown the previous sections, illustrates a potential to increase the x_b tolerance. The combustion stability is expressed as the coefficient of variation of IMEP, COV_{IMEP} . Figure 5.11 and Figure 5.12 show COV_{IMEP} as a function of x_b for the different fuel blends. Both figures illustrate that for low and medium load, running at x_b less than 17% and 14% , for E85 and gasoline respectively, COV_{IMEP} remains unchanged and at a reasonable value (<5%) among the different fuel blends, which indicates excellent cyclic variability. However, as x_b level increases COV_{IMEP} starts to increase significantly and wider

distribution of COV_{IMEP} between the different fuel blends starts to appear. While there is no clear trend between E10 to E50, there is a reduction in COV_{IMEP} between gasoline and E85 for high x_b levels. The plotted data was used to obtain the maximum x_b that the engine can tolerate for each fuel mixture, assuming that drivability issues occur at $COV > 10\%$, i.e combustion stability limits. Table 5.2 shows x_b tolerance for each fuel blend. E85 tolerance to x_b has improved.

5.8 Summary and discussion

The main aim of the work presented in this chapter was to investigate the effect of adding ethanol at different proportions on the combustion behaviour of the engine. Combustion behaviour of the different fuel blends will have a significant effect on the in-cylinder and exhaust temperatures, and consequently, on the energy balance and heat transfer characteristics that are going to be investigated in more detail in later chapters.

Despite the lower T_{add} for ethanol due to its lower heat content, calculated laminar flame speed for ethanol demonstrated a higher value compared to gasoline for most conditions. The increase in laminar burn speed of ethanol is attributed to the availability of oxygen in the ethanol chemical structure. Laminar flame speed for ethanol and gasoline were calculated at a different ϕ , pressures and temperatures. The peak difference in laminar flame speed between ethanol and gasoline occurs at stoichiometric. Ethanol is more sensitive to the change in ϕ than gasoline. Subsequently the difference in laminar flame speed decreases as the charge starts to move away from stoichiometric.

The increase in the laminar flame speed was not demonstrated in the FDA results obtained from the engine running at various running conditions. FDA data show comparable results between all ethanol/gasoline blends. This might be explained by the design of the engine under investigation. The engine is high compression engine (11.51:1). The effect of compression work and therefore charge density and temperature at the time of ignition becomes the dominant factor over laminar flame speed.

The RBA results show a non linear relation between increasing ethanol content and combustion speed. The fuel blend with highest ethanol content (E85)

illustrates an increase in combustion speed compared to other fuel blends, which correspond well with the increase in laminar flame speed for ethanol. Fuel blends with low and medium ethanol content (E10, E20 and E50) showed a slight rise compared to gasoline. However, no significant difference or trend was found in RBA among those fuel blends. The difference in RBA between E85 and gasoline is between 1°C to 2.5°C which is higher than the estimated experimental error (0.4°C); see Appendix 5 for more details. This indicates that the decrease in RBA is due to addition of ethanol rather than any experimental error.

Increasing ethanol content was expected to increase laminar flame speed and hence enhance combustion and reduce duration. On the other hand, increasing ethanol content will also increase h_{fg} and decrease Q_{LHV} which will have a negative effect on combustion. The combination of those effects will determine the combustion speed of the mixture. For that reason, the advantage of having higher laminar flame speed will not appear until high ethanol content, or E85. Those results were consistent over various engine speeds and loads.

The same effect of increasing ethanol content was also observed with changing in-cylinder composition (through x_b and ϕ). Once again, E85 RBA results follow similar pattern to laminar flame speed results. Increasing x_b will decrease the difference in burn speed between gasoline and E85. Laminar speed difference between ethanol and gasoline decrease as x_b increase.

Due to the change in combustion duration, increasing ethanol ratio was expected to have an effect on the engine tolerance to x_b . This tolerance is mainly influenced by combustion stability. Fuel with high ethanol ratio, E85, increased tolerance to x_b as a result of the decrease in combustion duration and subsequent increase in combustion stability.

CHAPTER 6 Overview of the engine energy balance

6.1 Introduction

The main objective of this chapter is to evaluate the impact of using different ethanol-gasoline blends on the energy balance inside the engine.

Knowledge of the way energy released from the fuel is distributed between brake power output, coolant energy, exhaust energy and unmeasured heat losses are crucial to understanding the total thermal behaviour of the engine. Although coolant, exhaust and unmeasured heat losses are unavoidable, more understanding of the energy balance can aid in reducing those losses to a minimum through improving and/or optimizing engine-running conditions. Any decrease in those losses will be translated into an improvement of thermal efficiency. The thermal efficiency is improved by increasing the proportion of energy that is transferred into useful brake power.

The increase in the ethanol content of the fuel mixture is expected to affect the energy balance inside the engine due to the incurred change in its chemical properties and combustion behaviour, as discussed in more detail in previous chapters. In the present work, total heat-rejection rate to coolant was measured and comparisons between the different fuel blends were undertaken. The evaluation of exhaust heat-loss included determining the effect of an increase in ethanol ratio on both exhaust temperature and heat capacity. Exhaust temperature itself has an impact on HC level, CO level, exhaust after treatment system and the amount of power obtained from the exhaust recovery devices such as turbochargers [17].

A considerable part of the energy released by fuel is also turned into unmeasured heat losses including ambient heat loss, crevice loss and unburned fuel. The effect of ethanol on heat transfer to ambient was investigated. The unburned fuel effect was examined in Chapter 4 by calculating combustion efficiency.

Finally, energy balance comparison between the different fuel blends was carried out. Furthermore, the effect of different running conditions on energy balance was studied.

6.2 Energy balance for the engine

The distribution of the energy released by the fuel combustion is given by the energy balance. For a control volume which surrounds the engine, the steady flow energy conservation equation is [17],

$$\dot{m}_f Q_{LHV} = P_b + \dot{Q}_{coolant} + \dot{Q}_{amb.} + \dot{H}_{exh,s} + \dot{H}_{exh,ic} \quad (6.2.1)$$

where $\dot{m}_f Q_{LHV}$ is the rate of the fuel energy input, P_b is the brake power, $\dot{Q}_{coolant}$ is the heat transferred to the coolant, $\dot{Q}_{amb.}$ is the ambient heat loss, $\dot{H}_{exh,ic}$ represents the exhaust enthalpy loss due to incomplete combustion and $\dot{H}_{exh,s}$ is the sensible exhaust energy flux relative to a datum of zero at a reference temperature, T_{ref} . A datum state of 298 K and 1atm pressure was chosen. The estimated error in energy balance calculation is shown in Appendix A.5.

Under constant engine running conditions, the rate of fuel energy input is dependent on the fuel mixture used by the engine. Q_{LHV} and the mass flow rate of the fuel vary between the different mixtures, as shown in chapter 4. P_b was calculated from the dynamometer torque output using equation 3.3. $\dot{H}_{exh,ic}$ was determined from the combustion efficiency calculated in section 4.8. The methods that have been used to calculate $\dot{Q}_{coolant}$, $\dot{H}_{exh,s}$ and $\dot{Q}_{amb.}$ are explained in detail in the following sections.

6.3 Exhaust gas energy

The exhaust gas energy flux is calculated from the following equation:

$$\dot{H}_{exh,s} = \dot{m}_{exh} \bar{c}_{p,exh} (T_{exh} - T_{ref}) \quad (6.3.1)$$

where T_{exh} is the exhaust temperature at the exhaust port exit and $\bar{c}_{p,exh}$ is the mean specific heat capacity of the exhaust gas. The method that was used to measure and calculate the different variables and the effect of increasing ethanol ratio are presented in the following sections.

Exhaust heat capacity, $\bar{c}_{p,exh}$

The heat capacity of the exhaust gases, $\bar{c}_{p,exh}$, has an effect on the thermal condition inside the engine by affecting the exhaust gas temperature. Subsequently, $\bar{c}_{p,exh}$ affect exhaust energy and the amount of heat lost to the exhaust port. $\bar{c}_{p,exh}$ can be determined from the exhaust gas composition, as follows:

$$\bar{c}_{p,exh} = \sum_i x_i c_{p_i} \quad (6.3.2)$$

Where x_i and c_{p_i} are mass fraction and heat capacity of the exhaust constituent, respectively. The values of c_{p_i} for the exhaust constituent was obtained from Roger and Mayhew [72]. Figure 6.1 shows the effect of increasing ethanol ratio on $\bar{c}_{p,exh}$ as a function of T_{exh} . The data illustrate clearly that there is an increase in $\bar{c}_{p,exh}$ as the ethanol ratio increases. This increase is attributed to the change in exhaust composition and particularly to the increase in water composition inside the exhaust, as explained in detail in Chapter 4 and illustrated in Figure 4.17.

The increase in water content is due to the change in the H/C ratio of fuel and the increase in oxygen content when the ethanol ratio increases.

The data also illustrates that the rise in T_{exh} will increase $\bar{c}_{p,exh}$ for all fuel blends.

The estimated error in $\bar{c}_{p,exh}$ calculation is around 1.9 % as show in Appendix A.5.6. On Average, $\bar{c}_{p,exh}$ increases by 4% between ULG and E85 which is higher than any experimental error.

6.3.1 Exhaust gas temperature measurement and correction

T_{exh} has a significant effect on the engine's performance and heat transfer characteristics. T_{exh} will influence the amount of heat rejected to the coolant, either through the exhaust port, or conducted back into the cylinder. In addition, it gives an indication of the in-cylinder gas temperature especially after combustion.

T_{exh} can also affect other parts of the engine, such as the turbocharger's performance (if used) and, further down the stream, on the after-treatment system. T_{exh} has an effect on the time needed for the catalytic converter to reach operating temperature; this is particularly significant in the case of a cold start. Koehlen *et al.* [82] suggested that 80% of the HC emissions measured over the entire FTP-75 drive cycle are emitted within the first 20 seconds after the engine is started.

T_{exh} was measured using a thermocouple located at the exhaust port exit in two cylinders as described in Chapter 3.

Correction of exhaust temperature measurements

The thermocouple tips were inserted into the centre of the gas flow. The equilibrium temperature of the thermocouple is reached when the heat transfers by radiation to the exhaust walls, and the conduction along the supporting wires is balanced by convective heat-transfer from the gas. Since the exhaust wall and the thermocouple mount are generally cooler than the gas, the heat transfer by conduction and radiation will be from the thermocouple to the connecting leads and to the exhaust port wall respectively. As a result, this equilibrium temperature will be lower than true time-averaged temperature. This is referred to as radiation and conduction error.

Rogers and Mayhew [72] suggested that errors in thermocouple readings can be compensated for by using the energy balance between convection gain and radiation loss using the following formula:

$$h_c (T_{exh_true} - T_{exh_meas}) = h_r (T_{exh_meas} - T_{exh_wall}) \quad (6.3.3)$$

Rearranging the equation, we find:

$$T_{ex_true} = \frac{h_r}{h_c} (T_{ex_meas} - T_{ex_wall}) + T_{ex_meas} \quad (6.3.4)$$

where T_{ex_true} is the true exhaust temperature, T_{ex_meas} is the actual measured value, T_{ex_wall} is the exhaust port wall temperature, and both h_r and h_c are, respectively, effective radiative and convective heat transfer coefficients for the thermocouple tips.

For a turbulent flow perpendicular to a wire, the convective coefficient is determined to be [72]:

$$Nu_d = 0.5 Re_d^{0.5} \quad (6.3.5)$$

where the characteristic dimension is the thermocouple's diameter and the gas properties are evaluated according to the measured exhaust temperature.

For a special case of a grey body radiation within a black or large enclosure (which represents the thermocouple within the exhaust port), the radiative heat transfer is given as [72]:

$$h_r = \sigma \varepsilon (T_{ex_meas}^2 - T_{ex_wall}^2) + (T_{ex_meas} - T_{ex_wall}) \quad (6.3.6)$$

where σ is the Stefan-Boltzman constant, ε is the emissivity of the thermocouple surface. The value of ε is in the 0.2 to 0.8 range. An ε value of 0.5 was used for the purpose of this study. Figure 6.2 shows a comparison between the measured T_{exh} value and the true T_{exh} value for different fuel mixtures. The results illustrate that the real value is typically 8.5-10% higher than the measured equivalent. These results correspond perfectly to the findings of Yuen [83] and Caton [84], where it has been established that the average temperature is typically 10% higher than the measured value. For that reason, the average temperature used in this thesis is going to be estimated by multiplying the measured T_{exh} by a factor of 1.1.

Figure 6.3 shows the effect of an increasing ethanol ratio on T_{exh} . The result illustrates clearly that increasing an ethanol ratio will decrease T_{exh} . This can be

attributed to the increase in the water content in the exhaust, as shown in Figure 4.17 and, subsequently, $\bar{c}_{p,exh}$, as shown in section 0.

The results also illustrate that the change in the engine's operating condition has a significant effect on T_{exh} . Increasing the speed or retarding ST decreases T_{exh} , due to the decrease in the time available for the burned products to cool during the expansion and exhaust strokes. Increasing EGR levels will also decrease T_{exh} due to the increase in exhaust heat capacity. T_{exh} is also influenced by changes ϕ . T_{exh} peaks at AFR_{stoich} and decreases as the charge becomes leaner or richer.

6.4 Heat transfer to the coolant

The heat transfer to coolant $\dot{Q}_{coolant}$ was calculated by fixing a thermocouple before and after the bowman heat exchanger. The heat removed by the heat exchanger was assumed to be equal to the heat rejected to the coolant, as described by the following equation:

$$\dot{Q}_{coolant} = \dot{m}_{coolant} c_p (T_{coolant_before} - T_{coolant_after}) \quad (6.4.1)$$

where $\dot{m}_{coolant}$ is the coolant flow-rate, c_p is the coolant heat capacity at average coolant temperature, as shown in Table 6.1, and $T_{coolant_before}$ and $T_{coolant_after}$ are coolant temperature values before and after heat exchanger respectively.

An amount of heat is lost through the copper pipes of the cooling circuit into the ambient air by forced convection. Calculations have shown that this amount is negligible compared to the heat dissipated by the exchanger, and thus contributes between 0.8-1.5 percent of the total heat rejected to the coolant. Figure 6.4 shows the effect of an increasing ethanol ratio on the amount of heat lost to the coolant. The data illustrate that, for most conditions, at low ethanol levels, there is very little difference in $\dot{Q}_{coolant}$ compared to gasoline. At a higher ethanol ratio, $\dot{Q}_{coolant}$ decreases considerably. E85 show a clear decrease in $\dot{Q}_{coolant}$ compared to gasoline, between 3 to 7%, when the engine is running

under exactly the same conditions in terms of speed, load, ST and EGR. This decrease might be attributed to that in in-cylinder temperature, itself a result of a higher h_{fg} value for ethanol. It is also caused by the decrease in the combustion product temperature during the expansion stroke and the exhaust stroke, as demonstrated from the T_{exh} results shown in section 6.3. Different sources contributing to total heat rejection to coolant and the effect of ethanol are explained in more detail in Chapter 7.

6.4.1 Effect of heat rejection to coolant on engine warm-up

A change in the amount of heat rejected to coolant is expected to affect the warming up characteristics of the engine. A reduction in the amount of heat transferred to coolant means that more time is required to fully reach the warmed-up condition. A major proportion of driving consists of short trips during which the engine is still in its warming up period [85].

The performance of the engine during warm-up is very important. Indeed, the warm-up period affects the engine's performance by determining its power output, emission levels and friction [85]. In addition, it can influence the passengers' comfort levels since passenger heating cannot operate until the engine coolant has sufficiently warmed up.

It was not possible to investigate the effect of using ethanol on the warm-up characteristics of the engine under investigation. The management system does not allow for a change in the amount of fuel supplied during start-up. This made it hard to start using fuel with a high ethanol content. To overcome this problem, the engine was initially started on gasoline then switched to different gasoline-ethanol blends after being warmed up.

In order to demonstrate the effect that ethanol might have on the time required to reach fully warmed-up conditions, data collected by another researcher [86] were used. The data were collected from a 1.4L PFI engine. Direct access to the engine management system allowed for a change in the amount of fuel injected at the engine's start up. The amount of gasoline injected during the warm-up tests was based on information from the engine strategy files. During E75 and E50 tests, the amount of fuel injected, during start-up, was scaled up proportionally to the decrease in Q_{LHV} compared to gasoline. Figure 6.5 shows

the temperatures of the oil, the coolant inside the engine and the coolant at the engine's exit ($T_{c, exit}$) during warm-up for various fuel blends.

After engine starts, $T_{c, exit}$ remains constant until the thermostat is open. When that happens, the coolant starts to circulate inside the engine and through the heat exchanger as shown in Figure 3.3. As a result, $T_{c, exit}$ does not start to increase until the engine reaches its operating temperature.

The time that takes place between the start-up of the engine and for $T_{c, exit}$ to start increasing was assumed to be equal to the time needed for the thermostat to open, $t_{thermostat}$. The results show that $t_{thermostat}$ increases slightly as ethanol content rises. There is a 6-seconds difference between gasoline and E75 inside the engine. The time periods required to reach a particular T_{oil} is summarized in Table 6.3. The results demonstrate, as before, that increasing ethanol content increases the time required to reach a specific T_{oil} . T_{oil} is of particular importance since the higher viscosity of cold oil will increase friction. Subsequently, the longer the time needed for oil to reach its fully warmed-up operation, the higher the warm-up friction.

6.5 Heat loss to ambient, \dot{Q}_{amb} .

The heat loss to the ambient, \dot{Q}_{amb} , occurs as a result of the free convection heat transfer from the engine's surface to its surroundings. In order to investigate the engine's external surface heat loss to ambient, the engine was split into blocks to simplify the calculations, as shown in Figure 6.6. These blocks covered the vast majority of the engine area. The engine's skin temperature, T_w , was measured at different locations of the engine block using a PRT probe (Platinum Resistance Temperature sensor).

Natural turbulent convection heat transfers from vertical and horizontal planes of the engine's different blocks were calculated using the following correlation [87]:

$$Nu_f = C(Gr_f Pr_f)^m \quad (6.5.1)$$

where Gr and Pr are Grashof and Prandtl numbers respectively. The Prandtl numbers is constant based on T_f and Grashof number is defined as

$$Gr = \frac{g\beta(T_{wall} - T_{amb})L^3}{\nu^2} \quad (6.5.2)$$

where g is gravity, L is dimension length, ν is kinematic viscosity and $\beta = \frac{1}{T_f}$

The subscript f indicates that the properties in the dimensionless groups are evaluated at film temperature.

$$T_f = \frac{T_{amb} + T_{wall}}{2} \quad (6.5.3)$$

The product of Grashof and Prandtl numbers is called the Rayleigh number:

$$Ra = GrPr \quad (6.5.4)$$

The C and m constants were determined by several researchers [87]. These constants are dependent on several factors such as the Rayleigh number and the position of the planes, as shown in Table 6.2.

Figure 6.7 shows \dot{Q}_{amb} as a function of BMEP for gasoline and E85. The data illustrate that the \dot{Q}_{amb} is small with value ranges between 400 and 600 Watt this represents approximately 1 to 2 % of the total heat released by the fuel. The data also illustrate that there was very little difference in \dot{Q}_{amb} between the two fuels. The tests, on the two fuels, were carried out in the same day to make sure that the ambient temperature is approximately constant. The ambient temperature was checked regularly to evaluate any external effect such as other engines start to run in the lab.

6.6 Energy balance results

The effect of increasing the ethanol ratio on the energy balance inside the engine is plotted in Figure 6.8 and Figure 6.9. For all engine running conditions, the ratio of brake work output to total heat released by the fuel rises as ethanol content in the fuel blend increases, i.e. as thermal efficiency, η_t ,

improves. The increase in η_t ranges between 0.5% to 3%. The increase in η_t suggests that the penalty in BSFC associated with the increase in the Q_{LHV} of ethanol has the potential to decrease. Figure 6.10 shows a comparison between the reduction in Q_{LHV} and the increase in BSFC compared to gasoline as ethanol content increases. The results illustrate that the reduction in BSFC is less than that expected by the reduction in Q_{LHV} . While E85 has 40% lower heat content, it shows 28% to 32% lower BSFC. This can be explained by improvements in thermal efficiency.

Exhaust and coolant energy levels showed comparable results between the different fuel blends. The improvement in combustion efficiency, η_c , demonstrated in section 4.8 is the main reason for the increase in η_t . In order to evaluate the effects of combustion efficiency on thermal efficiency, the former was taken into consideration in the energy balance ($(m_f \cdot Q_{LHV} \cdot \eta_c)$) as shown in Figure 6.11 and Figure 6.12. In addition, η_c was taken into account when comparing the distribution of heat released as a result of combustion, rather than the expected total heat released by the fuel.

These results clearly show that the combustion efficiency contributed to the majority of the improvements in thermal efficiency, especially at low and medium ethanol ratios. Nevertheless, there was still an improvement in thermal efficiency particularly when comparing between E85 and gasoline. Thermal efficiency values still increased from 0.5% to 1.5% between E85 and gasoline. This is explained by the decrease in the coolant and exhaust energy losses as shown in Figure 6.11 and Figure 6.12. The decrease in these energy losses is ultimately transferred into useful brake work and subsequently into an improvement in thermal efficiency. The variation in the levels of decrease in exhaust and coolant energy losses and, in some cases, the absence of this decrease, is attributed to experimental error. The level of decrease in the engine losses between E85 and gasoline is small (ranging between 0.5 % and 2 %.) Subsequently, any small errors in the measurements could influence the results.

The results show a small difference between the various fuel blends. These differences could be due to experimental errors instead of the effect of fuel content. The experimental error was estimated in Appendix A5.8. The results show that the inaccuracy is around $\pm 1\%$, $\pm 1.25\%$ and $\pm 0.7\%$ for thermal

efficiency, coolant energy percentage and exhaust energy percentage respectively.

Although the difference in energy balance between the fuel blends was, in some cases, lower than the experimental error, there was consistency in the results over the different engine running conditions. The tests at those running conditions were taken at different days. In addition, the improvement in thermal efficiency was obvious in BSFC results.

The results in Figure 6.11 and Figure 6.12 also illustrate that changes in the engine's running conditions influence the in-cylinder energy balance for all fuel blends. By increasing speed, coolant-loss percentage decreases, whereas the exhaust energy percentage increases. This is due to the reduction in the time available for the charge to cool and the increase in the exhaust temperature. Increasing the load leads to a significant rise in the percentage of brake load, a decrease in coolant energy losses and an increase in the percentage of energy lost to the exhaust. This is attributed to an increase in combustion efficiency, peak in-cylinder temperature and exhaust temperature.

6.7 Summary and discussion

The main objective of this chapter was to investigate the effect of ethanol on the energy balance inside the engine. The energy released by the fuel is distributed between brake output, coolant energy, exhaust energy and unmeasured heat loss. The unmeasured heat loss includes the un-combusted fuel, crevice losses and heat losses to ambient.

Section 4.7 show that increasing ethanol content influences the exhaust's different constituent levels. The change meant that the exhaust's heat capacity, $\bar{c}_{p,exh}$, changes accordingly. The $\bar{c}_{p,exh}$ results, calculated in this chapter, illustrate a marked rise as ethanol content increases as a result of increasing water level in the exhaust.

The increase in $\bar{c}_{p,exh}$ is also demonstrated in the measured exhaust temperature values, T_{exh} . Increasing ethanol content illustrates a clear decrease in T_{exh} at various engine running conditions. T_{exh} is also affected by the engine's running conditions. Retarding ST or increasing speed increases T_{exh} due to the reduction in the time available for the in-cylinder charge to cool

down. Increasing BMEP or EGR level, on the other hand, decreases exhaust temperatures due to a rise in the $\bar{c}_{p,exh}$ values.

A reduction in T_{exh} could have a considerable effect on emission levels, particularly at warming-up. The reduction in exhaust temperature levels would increase the time needed for the catalyst to reach its operating temperature. This would increase the level of the engine's tail pipe emissions, especially at cold start. The reduction in T_{exh} also affects HC and CO after flame combustion. T_{exh} can additionally have an effect on the amount of heat loss to the coolant. T_{exh} affects the levels of exhaust-port heat loss and heat conducted back into the engine through the exhaust manifold.

The decrease in T_{exh} and the higher h_{fg} of ethanol suggest that heat transfer to coolant will decrease as ethanol content increases. The results confirmed this expectation. However, the effect of ethanol appears only at medium and high ethanol content (E50 & E85). Low ethanol content fuel blends show comparable results to gasoline ones. At low ethanol content, the oxygen availability dominates the combustion more than the increase in h_{fg} , which would eliminate the cooling effect of ethanol. The decrease in heat rejection to coolant will affect the warm-up characteristics of the engine. By increasing ethanol content, more time is required to reach normal operation temperature. This would be reflected as an increase in fuel consumption, friction and emissions.

Heat lost to ambient shows comparable results between E85 and gasoline. This was expected, since the coolant inside the engine will keep the engine's skin temperature at approximately constant levels. The change in coolant temperature and flow rate, when running on E85, was not big enough to affect the engine's skin temperature.

Energy balance is affected by the changes in exhaust temperature and heat transfer to coolant. The energy balance data illustrate a considerable improvement in the thermal efficiency as ethanol content increases. This improvement in thermal efficiency was consistent over various engine running conditions. This is attributed mainly to the increase in combustion efficiency, as was demonstrated in section 4.8. The decrease in exhaust energy and coolant energy percentages also contribute to an improvement in thermal

efficiency, particularly at E85. The increase in thermal efficiency decreases the penalty in BSFC as a result of the lower Q_{LHV} of ethanol.

CHAPTER 7 Time average engine heat transfer during fully warm up operation

7.1 Introduction

A detailed understanding of the heat transfer to coolant is essential, The amount of heat transfer to cylinder wall will have an impact on the work transferred to the piston and, subsequently, on specific power and efficiency levels. Engine knock behaviour will also be influenced by both heat transfer to the cylinder wall during the compression stroke, and by heat transfer from the hot exhaust valve and piston. The emission formation will be affected as a result of the change in gas temperature, due to heat transfer both within the engine cycle and in the exhaust system, where after burning of CO and HC occurs. Friction will also contribute to heat rejection to coolant and get affected by it. Friction will be influenced by both changes to oil temperature, and thus to its viscosity, and by piston and liner thermal distortion [17].

As shown in Chapter 6, running the engine on ethanol-gasoline blends containing medium and high ethanol levels affected the heat rejection rate to coolant, $\dot{Q}_{coolant}$.

$\dot{Q}_{coolant}$ is the sum of various instances of heat transfer from the combustion chamber, the exhaust port and other engine components, each of which has a different heat transfer mechanism. In the present work, the effect of ethanol levels on the different heat sources that contribute to $\dot{Q}_{coolant}$ was evaluated.

The gas-side heat rejection rate to coolant was predicted using C1C2 correlation, and then compared to the measured values. The C1C2 correlation is a time-averaged heat transfer correlation that was developed by The University of Nottingham for thermal modelling, using the PROMETs software [88, 89]. The main advantage of using time-averaged heat transfer correlation is its simplicity compared to instantaneous spatially-averaged heat

release and instantaneous local heat release correlations, where specific engine calibration and unavailable supporting data are required. One of the main objectives of this chapter is to evaluate the validity of using the C1C2 correlation in the prediction of heat transfer to coolant for an SGDI engine running on different gasoline-ethanol blends, and whether any modification in C1C2 correlation is required.

The experimental work was carried out on a variety of running conditions including different speeds, loads, ϕ and EGR, as shown in Table 5.1.

7.2 Background

Taylor and Toong [90] developed an empirical correlation based on heat transfer data from 19 different engines, both gasoline and diesel-based. Their correlation was expressed in the form of a Nusselt-Reynolds number relationship. This can be expressed to give the heat transfer rate \dot{Q}_T from the gas-side, per cylinder, as:

$$\dot{Q}_T = 10.4 \left(\frac{\pi B^2}{4} \right) \frac{k_g}{B} (T_{g,a} - T_c) \text{Re}_g^{0.75} \quad (7.2.1)$$

The effective gas-side Reynolds number can be determined by:

$$\text{Re} = \frac{4\dot{m}_f(1 + AFR)}{\pi B \mu_g} \quad (7.2.2)$$

where $T_{g,a}$ is the effective gas temperature, determined by Taylor and Toong [90] as a function of the equivalence ratio, as shown in Figure 7.1. $T_{g,a}$ was evaluated by measuring the heat transfer to the coolant, $\dot{Q}_{coolant}$, and the mean gas-side surface temperature, $T_{s,g}$, under conditions where h_g and $T_{g,a}$ were either known or believed to be constant. $\dot{Q}_{coolant}$ and $T_{s,g}$ were measured at the cylinder head to avoid the complication caused by the change of cylinder surface area due to piston motion. The variations in $T_{s,g}$ occurred through the variation in coolant flow rate and temperature. $T_{g,a}$ was obtained by solving the heat convection relationship, where $T_{g,a}$ and h_g were assumed to be the intercept

and slope, respectively [90]. k_g and μ_g are conductivity and viscosity values, respectively. T_c is the coolant temperature, which is taken as the arithmetic mean of the inlet and outlet coolant temperature. Finally, \dot{m}_f is the fuel mass flow rate per cylinder.

The Taylor and Toong equation has been successfully applied, and gave a reasonably good prediction of the total gas-side heat transfer from both spark ignition and diesel engines [83, 91]. However, there were obvious weaknesses to the above derivation. Shayler *et al.* [88] identified these weaknesses and suggested some improvements. Taylor and Toong estimated the gas-side heat transfer, \dot{Q}_T , from the heat rejected to the coolant, $\dot{Q}_{coolant}$ and friction losses \dot{Q}_f as follows:

$$\dot{Q}_T = \dot{Q}_{coolant} - \dot{Q}_f \quad (7.2.3)$$

A modified correlation was developed as a result of a more detailed energy balance. Shayler *et al.* [88] identified the main sources for the heat loss to the engine coolant, $\dot{Q}_{coolant}$, to include in-cylinder gas-side heat transfer, \dot{Q}_{cyl} , heat transfer from the exhaust port, $\dot{Q}_{exh.pt}$, heat generated from engine friction, \dot{Q}_f , and heat conduction from the exhaust manifold back into the engine structure, $\dot{Q}_{ex.man}$ as expressed in the following equation:

$$\dot{Q}_{coolant} + \dot{Q}_{amb.} = \dot{Q}_{cyl} + \dot{Q}_{exh.pt} + \dot{Q}_f + \dot{Q}_{ex.man} \quad (7.2.4)$$

The equation above shows that gas-side heat transfer is the sum of the heat transfers from the gas-side to the structure surrounding the cylinder and from the exhaust gas flow to the exhaust port's surface. This can be expressed as follows: $\dot{Q}_{C1C2} = \dot{Q}_{cyl} + \dot{Q}_{exh.pt}$

$$= C_1(A_{cyl.eff} + C_2 A_{exh.pt}) \frac{k_g}{B} (T_{g,a} - T_c) Re_g^{0.7} \quad (7.2.5)$$

Equation 7.5 can be separated into two components, one for the heat transfer rates in the cylinder and another for the exhaust port:

$$\dot{Q}_{cyl} = C1 A_{cyl,eff} \frac{k_g}{B} (T_{g,a} - T_c) Re_g^{0.7} \quad (7.2.6)$$

And

$$\dot{Q}_{exh.pt} = C1C2 A_{exh.pt} \frac{k_g}{B} (T_{g,a} - T_c) Re_g^{0.7} \quad (7.2.7)$$

The port surface area, $A_{exh.pt}$, is multiplied by a factor C2 to account for the difference between heat-flux values in the cylinder and in the exhaust port. If the characteristic heat flux is:

$$\dot{q}'' = \frac{\dot{Q}_{cyl}}{A_{cyl,eff}}$$

Then the corresponding heat flux in the exhaust port is $C2 \dot{q}''$. The factors C1 and C2 are constants that minimise error in the experimental results. For an SI engine at MBT spark timing, C1 and C2 were determined to be 1.8 and 1.5 respectively.

7.2.1 Engine running on gasoline

Equation 7.5 was initially evaluated for the engine under investigation running on pure gasoline without any ethanol addition. Running conditions ranged from BMEP 1.61 to 7.9 Bar, the speeds going from 1500 to 4000 rpm, and different ST advanced and retarded from MBT as shown in Table 5.1.

The energy balance equation 7.4 was re-arranged as follows:

$$\dot{Q}_{coolant} = \dot{Q}_{cyl} + \dot{Q}_{exh.pt} + \dot{Q}_f + \dot{Q}_{exh.man} - \dot{Q}_{amb} \quad (7.2.8)$$

$\dot{Q}_{coolant}$ represents the total heat transfer to coolant, both directly and through the oil. Gas-side heat transfer from both \dot{Q}_{cyl} and \dot{Q}_{exhpt} was determined using equation 7.5. The effective gas cylinder area, $A_{cyl,eff}$, used in the equation is defined in [92]. $A_{cyl,eff}$ is smaller than the combustion chamber area at the point when the piston is at its lowest position, because the liner is not always exposed to the cylinder gas. The $A_{cyl,eff}$ is defined as:

$$A_{cyl,eff} = A_{pc} + A_{head} + \int_0^L f\left(\frac{x}{L}\right)\pi B dx \quad (7.2.9)$$

Where A_{pc} and A_{head} are the piston-crown area and the cylinder-head combustion chamber area respectively. $f(x/L)$ is a polynomial function that relates the local heat flux at any point down the liner to the same value as calculated at the top of the liner (which is always exposed to the cylinder gas), where x is the distance of a given point down the line from TDC, and L is the cylinder stroke.

May *et al.* [92] solved the polynomial function and found it be:

$$A_{cyleff} = A_{pc} + A_h + 0.29\pi BL \quad (7.2.10)$$

To evaluate the heat generated due to friction, \dot{Q}_f , mechanical friction losses have to be predicted. Mechanical friction losses can be obtained from IMEP and BMEP calculations where:

$$FMPEP = IMEP_{net} - BMEP \quad (7.2.11)$$

$IMEP_{net}$ was obtained from the in-cylinder pressure data (see section 3.6.1). BMEP was obtained from measuring the torque absorbed by the dyno. Therefore \dot{Q}_f is calculated as:

$$\dot{Q}_f = FMEP \times V_d \times N / 60 \quad (7.2.12)$$

$\dot{Q}_{exh.man}$ is the rate of heat conduction to the head from the exhaust manifold flange. In a study carried out by Imabeppu *et al.* [93] on a 2.0L DOHC SI engine operating at fully warm-up conditions, it was found that $\dot{Q}_{exh.man}$ is related to the exhaust port's heat flux $\dot{q}_{exh.pt}''$, through the following expression:

$$\dot{Q}_{exh.man} = a \dot{q}_{ex.pt}'' \quad (7.2.13)$$

Where a is constant and equal to 0.0042 m^2 for a cast-iron exhaust manifold. The result from Imabeppu *et al.* [93] suggested that $\dot{Q}_{exh.man}$ accounts for 8-12% of the total heat transferred to the engine structure. However, the value of the constant a and the percentage of heat conducted back will depend on the exhaust manifold and gasket material. For example, Hayden [94] found that using a fibre gasket can reduce the heat transfer to as little as $\frac{1}{4}$ of the rate measured when a metal gasket is used. The engine used in this study has a steel exhaust manifold and a metal gasket that conform well with the predictions of Imabeppu *et al.* [93].

Finally, heat transfer to the ambient, \dot{Q}_{amb} , generally has a small effect on overall energy balance, accounting typically for 400 to 600W under natural convection conditions, as shown in section 6.5.

The rate of heat rejection to the coolant, $\dot{Q}_{coolant}$, is a value measured as shown in section 6.4.

Figure 7.2 illustrates a comparison between the actual measured heat transfer to coolant and the predicted equivalent from equation 7.8 for pure gasoline. The results show a good agreement between the predicted and the measured values within a 10% accuracy limit.

7.2.2 Gasoline-ethanol blends

The main aim of this section is to establish the validity of using the C1C2 correlation to predict the gas-side heat loss rate to the coolant, \dot{Q}_{C1C2} , and to

determine whether any modification is required when ethanol at different blends is used. \dot{Q}_{C1C2} was predicted using equation 7.2 in exactly the same manner explained in the preceding section 7.2.1, as such, C1 and C2 remain constant. The $T_{g,a}$ value used was the same as the one developed by Taylor and Toong [90], as shown in Figure 7.1.

When the engine was running on pure gasoline, the values used for k_g and μ_g , which are both highly dependent on temperature, were assumed to be the same as those of air at $T_{g,a}$. When running on ethanol mixtures, however, the AFR_{stoich} is going to decrease as the ethanol ratio increases in the fuel. Consequently, this would affect the chemical properties of the in-cylinder charge and the validity of this assumption has to be examined.

A comparison between the conductivity and viscosity of air and ethanol-air mixtures for different AFR equivalence ratios is plotted in Figure 7.3. The results illustrate that there is no significant difference in conductivity between the air and ethanol-air mixtures. The viscosity of air, on the other hand, appears to be slightly higher than that of an air-ethanol mixture at rich fuel mixtures. Air viscosity is around 4.5% higher at equivalence ratio 1.5 and around 2.5% higher at AFR_{stoich} . The difference is, nonetheless, still relatively small. In addition, the majority of the engine cycle is dominated by the properties of the exhaust that are closer to air properties. For this reason, the assumption that μ_g is equal to that of air at different ethanol ratios is still valid.

Comparisons between the predicted values of $\dot{Q}_{coolant}$, obtained using equation 7.2, and the measured values for different ethanol-gasoline blends, are plotted in Figure 7.4. The results illustrate a good agreement between predicted and measured values.

The previous results show clearly that the C1C2 correlation is able to predict heat transfer to coolant values without any need to modify C1, C2 or $T_{g,a}$. The reason for this is discussed in more detail in section 7.6.

7.3 Effect of External EGR

Introducing EGR will have a significant effect on the heat loss rate to the coolant. To investigate the effect of EGR on heat rejection rate, several tests were undertaken at both MBT, where ST needed to be advanced, and different

ST. The tests were performed with the BMEP ranging from 1.61 to 4.75 Bar and the EGR ranging from 5 to 30 % depending on the load.

The introduction of EGR to the SI engine will affect the heat rejection rate through the increase in the overall charge mass, the increase in the inlet gas temperature and, finally, the increase in the thermal capacity per unit mass of charge.

Increasing the intake charge temperature will increase the gas-side heat rejection rate. Lundin *et al.* [95] and Povolny *et al.* [96] studied the effect of variation in inlet charge temperatures on $\dot{Q}_{coolant}$. They found that the effective in-cylinder gas temperature needed to be corrected to a reference inlet manifold temperature according to the relation:

$$T_{g,a} = T_{g,a,298} + 0.35(T_i - 298) \quad (7.3.1)$$

where T_i is the gas temperature at the intake manifold and $T_{g,a,298}$ is the average effective gas temperature for an inlet gas temperature of 298K. The variation of $T_{g,a,298}$ is shown in Figure 7.1.

The increase in charge mass as a result of EGR is taken into account through the redefining of the Reynolds number as follows:

$$Re = \frac{4\dot{m}_f(1 + AFR)/(1 - EGR)}{\pi B \mu_g} \quad (7.3.2)$$

The increase in inlet charge temperature and mass will increase the heat transfer to the coolant as accounted for in equations 7.14 and 7.15. However, the use of EGR will also increase the thermal capacity of the cylinder charge and, hence, reduce the heat rejected to coolant. The effect of an increase in thermal capacity can therefore be accounted for by applying a correction factor F_{EGR} to the prediction [89], as follows:

$$\dot{Q}_{CIC2_EGR} = F_{EGR} \dot{Q}_{CIC2} \quad (7.3.3)$$

where $F_{EGR} = 1 - EGR$. The method that has been used to develop F_{EGR} is explained in detail in Appendix 4.

A comparison between measured and predicted $\dot{Q}_{coolant}$ values at different EGR percentages for an engine running on gasoline is plotted in Figure 7.5. The results clearly shows an improvement in the prediction when the correction factor, F_{EGR} , was used.

Several tests were carried out in order to evaluate the validity of using the F_{EGR} to predict $\dot{Q}_{coolant}$ values for different gasoline-ethanol fuel blends, as shown in Figure 7.6 and Figure 7.7.

The engine was running on E50 and E85, with the BMEP ranging from 1.61 to 4.75 Bar and the EGR ranging from 5 to 30 %, depending on the load. The data illustrate clearly that the prediction values correspond well to measured values within the 10% limit.

7.4 Evaluation of the heat transfer to the exhaust port, \dot{Q}_{ex_pt}

The heat transfer to coolant through the exhaust port, \dot{Q}_{ex_pt} , represents a considerable percentage of the total heat transfer to coolant due to the high exhaust speed and temperature. Taylor [97] suggested that around 20% of the total heat transferred to the coolant is through the exhaust port, Imabeppu [93] suggested that it is more typically between 24-27%. With the stricter emissions regulations, understanding \dot{Q}_{ex_pt} is becoming increasingly essential. The energy loss through the exhaust affects the ability to get the after-treatment system to the required temperature, especially at cold temperatures i.e. losing energy will cause the system to take longer to reach its maximum effectiveness and will result in higher tail-pipe emissions.

This section is concerned with the effect of ethanol on the heat loss to the exhaust port. The heat transfer to the exhaust port has a pulsating nature. When the exhaust valves are open the heat transfer is treated as a forced convection, while it is treated as a natural convection when the exhaust valves are closed.

Heat transfer by natural convection can be ignored since it is small compared to the forced convection equivalent.

7.4.1 Measured heat transfer to the exhaust port

In order to evaluate the heat loss to the cylinder wall, two thermocouples were fitted at the start and the exit of the exhaust port of cylinder 1 and cylinder 3 as shown in Figure 7.8. $\dot{Q}_{exh.pt}$ was calculated from the temperature difference between the start and the exit of the exhaust port. The drop in temperature was assumed to be due to the $\dot{Q}_{exh.pt}$. This is assuming that kinetic energy loss and the heat generated by flow resistance in the piping is insignificant compared to $\dot{Q}_{exh.pt}$. Hence, $\dot{Q}_{exh.pt}$ was calculated using the following:

$$\dot{Q}_{exh.pt} = \dot{m}_{exh} \bar{c}_{p,exh} (T_{exh_outlet} - T_{exh_inlet}) \quad (7.4.1)$$

T_{exh_outlet} & T_{exh_inlet} are measurable values, the exhaust mass flow rate, \dot{m}_{exh} was calculated from knowing the fuel flow rate, AFR and x_b levels. $\bar{c}_{p,exh}$ was calculated from the exhaust constituents and exhaust temperature (both measurable values) as shown in section 6.4.3. Tests were carried out with the engine running at different speeds, loads, ignition timings, equivalence ratios and EGR levels as shown in Table 5.1. Those ranges were chosen to investigate not only the effect of the different fuel blends over a wide range of running condition but also the consistency and the repeatability of the results. Figure 7.9 shows the $\dot{Q}_{exh.pt}$ for different fuel blends as a function of load, speed, EGR and ϕ . Data for all running conditions illustrate a decrease in $\dot{Q}_{exh.pt}$ as ethanol ratios increase; this decrease is more obvious at higher ethanol ratios, i.e. E50 and E85, where there is approximately a 5% decrease in $\dot{Q}_{exh.pt}$ between gasoline and E85.

The main factors that are affecting $\dot{Q}_{exh.pt}$ are the exhaust mass flow rate, the surface temperature and the exhaust temperature, T_{exh} . Figure 7.10 illustrates that the exhaust surface temperature does not change with increasing ethanol

levels due to coolant circulation, which keeps the engine's surface temperature constant. Exhaust surface temperature was taken at three different locations of the exhaust port and on two different cylinders. Mass flow rate decreased slightly for higher ethanol contents as shown in Figure 7.11. Finally, with increasing ethanol content, T_{exh} decreased considerably due to the increase in $\bar{c}_{p,exh}$ of the exhaust (i.e. an increase in the water content of the exhaust) as shown in Figure 6.3. The decrease T_{exh} is the main reason for the reduction in $\dot{Q}_{exh,pt}$. The small decrease in exhaust mass flow rate also contributed to this decrease.

The change in engine running conditions also affects $\dot{Q}_{exh,pt}$. For all fuel mixtures, increasing load and speed shows an increase in the $\dot{Q}_{exh,pt}$ due to the increase in exhaust mass flow rate and temperature. Equivalence ratio up to AFR_{stoich} does not show any change in $\dot{Q}_{exh,pt}$. However, as the charge becomes rich, $\dot{Q}_{exh,pt}$ start to decrease. This is mainly due to the decrease in T_{exh} and in the exhaust mass flow rate. Increasing EGR level does not show any effect on $\dot{Q}_{exh,pt}$. The combined effect of decreasing T_{exh} and increasing mass flow rate as EGR levels increase explains the unchanged heat loss between different EGR percentages.

The contribution of the measured $\dot{Q}_{exh,pt}$ to the total heat released to the coolant is shown in Figure 7.12, the results illustrate that the contribution level remained between 15 to 20 % of the total heat rejected to the coolant. These results are lower than would have been suggested by previous studies (Taylor [90] suggested around 20% and Imabeppu [93] suggested between 24-27%). The lower value of the measured exhaust port heat loss can be explained by the thermocouple readings at the exhaust port inlet. Due to the complex geometry of the exhaust port, it was hard to place the thermocouple accurately at the exhaust port inlet; instead it was placed as close as possible. This meant that the exhaust gas might have already cooled slightly before reading the thermocouples. In addition, it is hard to place the thermocouples accurately in the middle of the exhaust port, the closer the thermocouple to the surface the

more the readings are affected by the cooling of the surface. Furthermore, the exhaust port has a pulsating nature while the thermocouples have a time-based one. This might cause an error in the thermocouples' reading.

The underestimated measurements of the heat lost to the exhaust port are acceptable for the purpose of this study since a comparison between the different fuel blends is the main objective.

7.4.2 Exhaust port heat correlations

Several correlations have been developed over the years to predict the heat transfer to the exhaust port. These correlations were developed assuming a quasi-steady forced convection heat transfer to the exhaust port. The heat transfer coefficient can be defined from the Nusselt Reynolds relation as follows:

$$h = a \frac{k_{exh}}{d_{exh,pt}} Re^b \quad (7.4.2)$$

And:

$$Re_{pt} = \frac{4\dot{m}_f(1 + AFR)}{\mu_{exh}\pi d_{exh,pt}} \quad (7.4.3)$$

where k_{exh} is thermal conductivity and μ_{exh} is dynamic viscosity. Both values are dependent on exhaust temperature, the properties of air were used for simplicity. The coefficients a and b are dependent on the correlation used. The variation in correlation coefficients can be attributed to the difference in the geometry of each engine that the correlation was developed on [98]. The variation in geometry will alter the flow pattern inside each engine and, subsequently, affect $\dot{Q}_{exh,pt}$. In addition, the pulsating nature based on valve events, as well as the pipe length, can significantly change the flow pattern and heat transfer relationship [98].

In order to determine the best correlation for predicting $\dot{Q}_{exh,pt}$, the heat transfer calculated from the different correlations in Table 7.1 was compared to

the total heat transfer to the coolant as shown in Figure 7.13, for gasoline and E85. The data show that correlations from Meisner and Sorenson [99] and Shayler and Chick [88] are the most suitable correlations to predict $\dot{Q}_{exh.pt}$ since they are more consistent with Taylor [90] and Imabeppu's [93] results (20% to 27% of the total heat transfer to the coolant).

$\dot{Q}_{exh.pt}$ for different gasoline-ethanol blends as functions of speed and load were calculated using Meisner and Sorenson [99] and Shayler and Chick [88] correlations as shown in Figure 7.14 and Figure 7.15. The results illustrate a decrease in $\dot{Q}_{exh.pt}$ as ethanol ratio increased in the fuel blends.

The results correspond well with the measured data obtained in section 7.4.1. A comparison between measured and predicted $\dot{Q}_{exh.pt}$ using different correlations is shown in Figure 7.16. The data demonstrates a linear relation between predicted and measured values for the different correlations. However, while the measured values fit well with the Shayler and Chick correlation, they are lower than the predicted values using C1C2 as well as those predicted by the Meisner and Sorenson correlation. The underestimated measurements of the exhaust port heat loss (see section 7.4.1) can explain the difference between measured and predicted values. In addition these correlations were developed on a different engine and this could affect the values they predicted.

The measured heat loss was used to plot a relation between Re and Nu as shown in Figure 7.17. Nu was calculated assuming forced convection heat transfer process such as:

$$Nu = \frac{\dot{Q}_{exh.pt} d_{exh.pt}}{k_{exh} (T_{exh} - T_{exh.pt_surface})} \quad (7.4.4)$$

A trend line was fitted to the data and a relation between Nu and Re was found to be:

$$Nu \propto 0.25Re^{0.654}$$

7.5 Heat conducted back to the cylinder head, \dot{Q}_{exhman}

As mentioned previously, part of the exhaust energy is conducted across the cylinder head/exhaust manifold flange face. The magnitude of \dot{Q}_{exhman} will be dependent on the type of gasket used. Imabeppu *et al.* [93] found that \dot{Q}_{exhman} is a function of the exhaust port heat flux, \dot{q}_{exhpt}'' , as shown in equation 7.13. As a result, the decrease in \dot{Q}_{exhpt} for medium and high ethanol content fuels will reduce the amount of heat conducted back to the engine as shown in Figure 7.18. The data in figure 7.18 was calculated using equation 7.13.

To confirm these findings, \dot{Q}_{exhman} was also calculated using the coolant energy balance shown in equation 7.4. A comparison between the different fuel mixtures for various running conditions is shown in Figure 7.19. The results illustrate that up to E50 there is no clear trend between increasing ethanol ratios and heat conducted back to the cylinder. E85, on the other hand, shows a slight decrease in \dot{Q}_{exhman} for different engine running conditions. The results correspond well to the data obtained from equation 7.13.

Figure 7.20 shows \dot{Q}_{exhman} , as calculated from the coolant energy balance, as a function of \dot{q}_{exhpt}'' . The results illustrate that there was an approximate linear relationship between \dot{Q}_{exhman} and \dot{q}_{exhpt}'' . These results agree with the findings of Imabeppu *et al.* [93]. The value of a , however, varied between 0.0048 m^2 and 0.0053 m^2 , depending on the fuel blends. The change in the value of a can be attributed to the change in T_{exh} among the different fuel blends which will change the relation between \dot{q}_{exhpt}'' and \dot{Q}_{exhman} . In addition, the experimental error associated with the C1C2 correlation, FMEP, and $\dot{Q}_{coolant}$ calculations can contribute to the variations in the value of a .

7.6 Results and discussion

The main aim of the work presented in this chapter was to investigate the effect of gasoline-ethanol blends at different proportions on the gas-side heat transfer to coolant, both from the cylinder and exhaust port. Furthermore, it

was desired to establish whether the C1C2 correlation requires any modification to allow for changes in fuel heating values and other fuel properties.

Results obtained in section 6.4 demonstrate a clear decrease in the total heat rejection to coolant, $\dot{Q}_{coolant}$, for high and medium ethanol content fuel blends (E50 & E85). The reasons for this decrease were investigated in this chapter by examining the different heat sources that contribute to $\dot{Q}_{coolant}$ as shown in Figure 7.21. Different sources include the in-cylinder gas-side heat transfer (\dot{Q}_{cyl}), exhaust port heat loss ($\dot{Q}_{exh.port}$), heat generated from engine friction (\dot{Q}_f) and heat conduction from the exhaust manifold ($\dot{Q}_{exh.man}$).

Both the predicted and measured results showed that $\dot{Q}_{exh.port}$ and $\dot{Q}_{exh.man}$ decrease for fuel blends with medium and high ethanol contents as a result of the decrease in T_{exh} . This decrease will contribute to the total decrease in the measured $\dot{Q}_{coolant}$.

The in cylinder gas side heat transfer, \dot{Q}_{cyl} , is expected to change as ethanol content increases in the fuel blends due to the physical properties of ethanol. Indeed, ethanol has a higher enthalpy of vaporisation. As a result, increasing ethanol will have a cooling effect on the in-cylinder charge leading to a decrease in in-cylinder peak temperature. However, using ethanol will also increase combustion speed, as illustrated in chapter 5, resulting in higher peak pressure and temperatures. The combined effect of these two factors will determine the in-cylinder temperature and hence \dot{Q}_{cyl} .

The NOx emission results in section 4.6.3 show a reduction in NOx levels when ethanol ratios increase in the fuel blend. This reduction indicates a decrease in the local in-cylinder peak temperatures. Furthermore, the decrease in T_{exh} illustrates a decrease in the product of combustion or the in-cylinder gas temperatures later on in the combustion stroke, which has a considerable effect \dot{Q}_{cyl} . Both the NOx emissions and T_{exh} data illustrate a decrease in in-cylinder temperature at high ethanol content and, subsequently, in \dot{Q}_{cyl} . This decrease

is expected to contribute to the total decrease in $\dot{Q}_{coolant}$. The \dot{Q}_{cyl} for different fuel blends were predicted using equation 7.6 as part of C1C2 correlation as shown in Figure 7.22. The C1C2 correlation was found to agree well with the measured values within the 10% limit range without any need for modification for C1 or C2 values. The data in Figure 7.22 illustrate that, in most cases, E85 showed a lower \dot{Q}_{cyl} than the rest of the fuel mixtures. Using E85 reduces heat rejection rates to between 0.5 and 3% compared to gasoline. These results correspond well with the author's prediction of the effect of ethanol as mentioned above.

The decrease in \dot{Q}_{cyl} is accounted for through the change in Re without the need to change C1 or $T_{g,a}$. The Re number decreases when the engine is running on E85 compared to the rest of the fuel blends as shown in Figure 7.23. Although E85 showed a decrease in \dot{Q}_{cyl} , the results do not illustrate any clear trend between increasing ethanol ratios and \dot{Q}_{cyl} . This might be explained by the confidence limit and experimental discrepancy associated with C1C2 correlation where change in \dot{Q}_{cyl} can be too small to be resolved by the C1C2 correlation. \dot{Q}_{C1C2} can be predicted within an accuracy of a 10% limit. In addition, the increase in combustion efficiency for low ethanol ratios can have a more dominant effect on increasing in-cylinder temperatures than the cooling effect of ethanol or the decrease in T_{exh} .

$\dot{Q}_{exh.port}$ was also predicted using the C1C2 correlation in equation 7.7. C2 in equation 7.7 represents the ratio of exhaust port heat flux and cylinder heat flux. C2 will remain constant since the ratio is constant for all fuel blends as shown in Figure 7.24. The measured $\dot{Q}_{exh.port}$ value was used to calculate C2.

In summary, it is believed that the C1C2 correlation can be used to predict gas-side heat transfer without any modification. The change that is expected in \dot{Q}_{cyl} is accounted for through a decrease in Re without the need to change C1 or $T_{g,a}$. C2 remains constant since the ratio of exhaust port heat flux and cylinder heat flux show very little difference between the various gasoline-ethanol blends.

Finally, \dot{Q}_f shows comparable results between the different fuel blends and will not affect the change in $\dot{Q}_{coolant}$

EGR affects the gas-side heat transfer through increasing the heat capacity of the charge, the inlet charge temperature and the mass flow rate of the charge. The effect of EGR was accounted for by using correlations to account for the increase in heat capacity and inlet temperatures. A modified Reynolds definition was also used to account for the increase in mass fraction. This kept the accuracy of the prediction within the 10% limit. This modification for EGR also appeared also to correspond well to the predictions of heat transfer to the coolant when gasoline-ethanol blends at different percentages were used.

CHAPTER 8 In-cylinder gas properties and instantaneous heat loss to the cylinder wall.

8.1 Introduction

Heat transfer to the coolant from different engine components was discussed in detail in Chapter 7. However, these investigations have all been based on cycle-averaged heat transfer. In this chapter, the effect of ethanol on the instantaneous spatially-averaged heat loss is investigated. The temporal change in heat loss across the cycle is important in explaining the effect that the ethanol has on some of the engine's characteristics, such as power output, engine efficiency and thermal NO_x formation. The effect of higher ethanol content on some of the in-cylinder charge properties and charge preparation was also studied.

The heat loss was predicted from the pressure data using a correlation developed by Hohenberg [100]. The Hohenberg correlation has been used extensively to predict heat loss for both gasoline and diesel engines. The use of this correlation to predict heat loss for different gasoline-ethanol blends has never been examined until this work was undertaken. In this chapter, the validity of the Hohenberg correlation for different gasoline-ethanol mixtures is going to be evaluated.

8.2 Calculating in-cylinder gas properties

8.2.1 In-cylinder temperature

The cyclic variation of average the in-cylinder gas temperature, T_g , is required to calculate the heat loss to the cylinder wall. The measurement of T_g is extremely difficult as it requires access to the cylinder. In addition, the gas temperature also varies according to location, with the biggest difference in temperature between burned and un-burned areas. It was beyond the scope of this work to measure T_g directly. Instead, the average temperature was

estimated. In order to estimate T_g , the engine cycle was divided into three separate parts as shown in Figure 8.1. Firstly, the induction cycle until IVC. Secondly, the close part of the cycle between IVC to EVO and, finally, the exhaust stroke, starting from EVO until the end of the cycle.

In the induction stroke, the T_g is small and will be close to the cylinder's surface temperature. Heat loss to the cylinder wall during induction is small compared to the compression, combustion or exhaust part of the cycle. T_g during the induction stroke is assumed to be constant and equal to the T_g at IVC.

The ideal gas law was used to calculate the gas temperature during the close part of the cycle, i.e. between IVC and EVO, thus

$$T_g = \frac{PV}{m_{charge}R} \quad (8.2.1)$$

In-cylinder pressure, P , is a measurable value as shown in section 3.6.1. Instantaneous cylinder volume, V , is calculated from our knowledge of the engine's geometry. The mass of the in-cylinder charge, m_{charge} , includes the inducted air and fuel as well as any external EGR and any internal dilution.

During the exhaust stroke, when the exhaust valve is open, the in-cylinder pressure drops considerably until they reach exhaust manifold pressure. The charge temperature during the exhaust stroke was determined by assuming the process during blowdown to be isentropic, thus:

$$T_g = T_{EVO} \left(\frac{P}{P_{EVO}} \right)^{\frac{\gamma-1}{\gamma}} \quad (8.2.2)$$

The pressure variation is known and T_{EVO} can be calculated from ideal gas law as described above. Although the exhaust stroke is not isentropic, it is believed to be a good approximation of the real value. The temperature trend obtained in this study was similar to that obtained by previous studies such as May *et al.* [92] and Caton and Heywood [84].

A comparison between the different fuel blends is shown in Figure 8.2 and Figure 8.3. The results illustrate that, in both cylinders, there is not a clear trend between increasing ethanol content and the calculated in-cylinder temperature. In cylinder 1, however, there was a small increase in T_g for E85 when compared with gasoline.

The results of the calculated bulk in-cylinder gas temperature, T_g , do not correspond to the expectation of the author. Indeed, the increase in ethanol content in the fuel blend was expected to decrease T_g . This expectation was based on the reduction in the total measured heat transfer to the coolant, $\dot{Q}_{coolant}$, decreases in NOx level, decreases in T_{exh} and increases in h_{fg} as ethanol content rises, as discussed in detail in section 7.6.

The calculated T_g is a function of the measured pressure and the mass of the charge, m_{charge} . The pressure reading does not show any significant variation either in the measured 100 consecutive cycle pressure data or at the standard reference point, as shown in section 3.7. m_{charge} was calculated from the measurement of the total fuel flow rate to the engine and the measured Lambda value. The fuel flow rate was assumed to be equally divided between the four cylinders. The Lambda value was measured at the exhaust manifold and assumed to be equal in the four cylinders. However, the assumption that m_{charge} is equal in the different cylinders is not necessarily accurate. There might be differences in the m_{charge} and AFR values among the different cylinders. This is due to the variation in the amount of fuel injected into each cylinder (which might be caused by the injectors' manufacturing tolerances) or the amount of air drawn by each cylinder. For that reason, in this section, m_{charge} is going to be calculated using ideal gas law instead, which would be as follows:

$$m_{charge,calc} = \frac{P_{EVO} V_{EVO}}{RT_{EVO}} \quad (8.2.3)$$

where T_{EVO} was assumed to be equal to the measured temperature before the exhaust port. Since the temperature at EVO is higher than the one measured before the exhaust port, the calculated mass charge, $m_{charge,calc}$ will be higher

than the actual value. However, this study is a comparative study and the main purpose is to compare the different fuel mixtures.

$m_{charge,calc}$ was used to calculate the in-cylinder bulk temperature, $T_{g,calc}$, using equation 8.1. The results illustrate that, during combustion, there is no correlation between ethanol content and temperature magnitude and phasing as shown in Figure 8.4. However, by the end of combustion, the combustion products' temperature slightly decreases at high and medium ethanol ratios (E50 and E85), this corresponds well to the measured decrease in T_{exh} .

Peak calculated temperature; however, does not appear to be in line with the NOx emissions as there was no clear decrease in peak T_g with higher ethanol levels. This can be attributed to the fact that NOx is affected by the local temperature rather than the bulk average temperature. The decrease in adiabatic flame temperature as ethanol content increase, as shown in Figure 4.2, could explain the reduction in NOx level.

8.2.2 Calculating in-cylinder $\bar{\gamma}$ for different fuel mixtures

As shown in Chapter 4, higher ethanol content in the gasoline/ethanol blend will affect the fuel's physiochemical properties and the exhaust composition. These changes might have an effect on the in-cylinder charge heat capacity and, subsequently, on the in-cylinder charge heat capacity ratio, $\bar{\gamma}$, used in net heat release calculations. This section is concerned with the method used to calculate $\bar{\gamma}$ and the potential effect of increasing ethanol levels on the $\bar{\gamma}$ value. The calculation of $\bar{\gamma}$ was based on dividing the cylinder into two zones: a fresh charge zone and a burned zone. The fresh charge consists of the fuel-air mixture and the unburned region consists of the products of the combustion. Heat capacity, c_p , calculated for the fresh charge and the products of combustion was based on polynomial correlations as detailed in Appendix 3. Although ethanol has a higher c_p than gasoline and subsequently a different γ , as shown in Figure 8.5; nonetheless, Figure 8.6 illustrates that this difference in c_p between gasoline-air and ethanol-air mixtures is very small. This is explained by the change in AFR_{stoich} between gasoline and E85. As a result, the γ difference between the two mixtures is very small as shown in Figure 8.7. On average, E85-air mixtures had around a 0.3% increase in γ value over that of a gasoline-air mixture. A correlation that relates γ to temperature was developed,

by the author, based on the γ average between the E85-air mixture and the gasoline-air mixture, calculated as follows:

$$\gamma_{fc} = 6 \times 10^{-8} T^2 - 0.0002T + 1.4063 \quad (8.2.4)$$

where T is the temperature in Kelvin (K). The burned gas heat capacity, $c_{p,b}$, was calculated from the emissions composition measured at different running conditions. Figure 8.8 shows $c_{p,b}$ as a function of temperature for the engine running on different loads, at gasoline, E50 and E85. The results illustrate clearly that $c_{p,b}$ is sensitive to changes in temperature and fuel composition. Increasing ethanol content produces a clear increase in the $c_{p,b}$ of the emissions for a given temperature. The results also show that $c_{p,b}$ is not sensitive to a change in load. A correlation was developed based on the average emission produced at different loads, as follows:

If $275 < T(K) < 1000$

$$c_{p,b} = A1T + A2 \quad (8.2.5)$$

If $T(K) > 1000$

$$c_{p,b} = B1 \ln T - B2 \quad (8.2.6)$$

Where,

$$A1 = 0.0003$$

$$A2 = 0.0222E + 0.955$$

$$B1 = 0.0205E + 0.2063$$

$$B2 = 0.1159E + 0.1776$$

where E is the ethanol ratio and T is the temperature in K. The methods that were used to develop these correlations are described in detail in Appendix 3. Subsequently, the heat capacity ratio for the burned charge, γ_b , can be calculated using the following equation:

$$\gamma_b = \frac{c_{p,b}}{c_{p,b} - R_b} \quad (8.2.7)$$

At each CA degree, the mass average heat capacity ratio of the fresh charge and the burned charge, $\bar{\gamma}$, is calculated through the following equation:

$$\bar{\gamma} = \frac{\gamma_{fc}(1 - MFB)m_{fc} + \gamma_b MFB m_{fc} + \gamma_b x_b m_{charge}}{m_{charge}} \quad (8.2.8)$$

where x_b is the burned gas fraction in fresh charged, which includes internal dilution and EGR. MFB is the mass fraction burned.

The temperature of the diluted unburned gas, T_u , is calculated by assuming a polytropic compression after IVC. The temperature of the burned gas, T_b , was calculated assuming that when an element burns it instantaneously mixes with the already-burnt gas, hence the average mean temperature for the burned gas is [17]:

$$\bar{T}_b = \frac{R_u}{R_b} \bar{T}_u + \frac{pV - mR_u \bar{T}}{mR_b MFB} \quad (8.2.9)$$

Figure 8.9 shows an example of γ during the engine cycle for different fuel mixtures when the engine is running at constant BMEP 4.75 bar and 2000 rpm.

8.3 Charge temperature and mixture preparation

In the DISI engine, there is a limited amount of time for fuel to evaporate and mix with the air to form a combustible charge. The evaporation of the fuel happens in two stages [41]:

- When the liquid fuel is injected directly into the cylinder during the induction stroke, part of it evaporates by absorbing heat from the surrounding air and the combustion chamber's surfaces which will decrease in-cylinder temperature as a result.
- During the compression stroke, the rest of the liquid fuel evaporates as a result of the increase in temperature and pressure.

The two temperature parameters (the drop in temperature after injection and its rise during compression) were considered by several studies [24, 41] in an attempt to evaluate the mixture preparation characteristics. Price *et al.* [41] and Dodge [101] found that in a DISI engine running at homogenous operation, the

majority of the fuel is vaporised during the compression stroke. For this reason, an increase in temperature during the compression stroke can be considered as an indication of the amount of heat required to evaporate the fuel. In this section, the effect of higher levels of ethanol content on the fuel vaporisation process and its potential cooling effect are assessed by calculating T_{comp} , the temperature increase between IVC and ST, as shown in Figure 8.10 and Figure 8.11. The results illustrate that, for all running conditions, whilst E10 and E20 show comparable T_{comp} values to that of gasoline, the results for E50 and E85 show a clear decrease in T_{comp} with E85 showing the lowest T_{comp} . The non-linear relation between T_{comp} and an increase in ethanol content can be explained by the fact that T_{comp} is proportional to several relations that are themselves inter-related. During the compression stroke, the piston work exerted on the charge is divided into three components: latent heat used to vaporise the liquid fuel, a change in internal energy and the heat transferred to the coolant through cylinder walls. Heat transferred to the wall can be ignored due to the small difference between the wall temperature and the charge temperature during compression, thus:

$$-W = \Delta U + h_{fg} \quad (8.3.1)$$

$$\text{where } \Delta U = m_{charge} c_v (T_{ST} - T_{IVC}) \text{ or } \Delta U = m_{charge} c_v (T_{comp}) \quad (8.3.2)$$

From equations 8.10 and 8.11, and from assuming constant work, ΔU and subsequently T_{comp} is a function of the mass of the charge, m_{charge} , the constant volume-specific heat capacity, c_v , and the enthalpy of vaporisation, h_{fg} . The increase in h_{fg} as ethanol content increases, as shown in Figure 2.3, means that a higher percentage of the piston work is going into vaporizing the fuel than turned into a gain in internal energy and, hence, T_{comp} will decrease. However, the increase of c_v as ethanol content increases will have an opposite effect, as shown in Figure 8.12. The combined effect of these two factors means that the cooling effect of increasing ethanol content will not manifest itself until medium ethanol contents, as is indicated by the decrease in the compression stroke temperature, T_{comp} .

8.4 Instantaneous spatially-averaged heat loss to the cylinder walls

The idea of the instantaneous spatially-averaged heat loss, Q_{loss} , to the cylinder wall is based on the assumption that the in-cylinder heat transfer is a quasi-steady process, i.e. a uniform instantaneous in-cylinder gas temperature and, thus, the heat transfer to the cylinder is proportional to the difference between the working fluid and metal surface temperatures, T_{wall} . The heat lost through the cylinder wall can be calculated as follows:

$$\frac{\delta Q_{loss}}{\delta \theta} = \frac{h_c A (T_g - T_{wall})}{6N} \quad (8.4.1)$$

where h_c is the heat transfer coefficient (averaged over the chamber surface area), A is the instantaneous cylinder area, and N is the engine speed (rpm). Equation 8.12 was divided by $6N$ to transfer the change of heat transfer from time-based into crank-based. h_c can be estimated from the engine heat transfer correlations. The two most common correlations are the Woschni [102] and Hohenberg [100] correlations. The main disadvantage of using Woschni is the need to evaluate the motored pressure during the combustion and the expansion strokes. The motored pressure is not available since the dynamometer used in this study can only be used for power absorption and not to motor the engine. The Hohenberg correlation, however, is a simplified expression based on experimental observations from four different direct-injection diesel engines, and was obtained after a detailed examination of Woschni's original formula.

$$h_c = A_1 V^{-0.06} P^{0.8} T_g^{-0.4} (V_p + A_2)^{0.8} \quad (8.4.2)$$

where P is the indicated pressure, V is the in-cylinder instantaneous volume and V_p , the piston mean velocity, represents the gas velocity inside the engine where:

$$V_p = 4LN/60 \quad (8.4.3)$$

The mean value of the constants A_1 and A_2 were found to be 130 and 1.4 respectively. A_2 represents the effect of combustion-produced turbulence and heat loss due to radiation.

8.5 In-cylinder gas-side surface temperature

The gas-side surface temperature, T_{wall} , is maintained below a certain temperature though coolant circulation in order to avoid thermal stress that could lead to fatigue cracking and the deterioration of the oil film [17]. T_{wall} varies with the location, cycle variation and engine running condition. The swing in surface temperature during the engine cycle is very small, it being around 7 K [17]. Spatially-averaged in-cylinder gas-side surface temperatures typical range between 370 K and 450 K depending on the running condition [17]. T_g between ST to EVO during the engine cycle lies between 750 K and 2500 K. Thus, the temperature difference between gas and wall is large and changes in wall temperature will have only a small influence on the predicted gas-to-wall heat transfer. For that reason, it is safe to assume the surface temperature to be constant and averaged between 370 K and 450 K.

8.6 Calibration of the Hohenberg correlation

As mentioned above, the Hohenberg correlation was originally developed for diesel engines. Consequently, A_1 and A_2 need to be recalculated in order to calibrate the correlation for the engine under investigation.

Assuming a constant A_2 , A_1 was determined by directly relating the amount of fuel chemical energy released to heat transfer into: work, sensible energy and heat loss to the chamber wall, assuming negligible crevice losses such as:

$$\int Q_{gross} = \eta_c (\dot{m}_f Q_{LHV}) = \int Q_{net} + \int Q_{loss} \quad (8.6.1)$$

where Q_{gross} , Q_{net} and Q_{loss} are gross heat release, net heat release and heat loss respectively. Q_{net} is defined as the energy that is transformed into sensible

energy and real work within the combustion chamber. Assuming that the chamber's contents are a semi-perfect gas, Q_{net} can be calculated from [17]:

$$\delta Q_{net} = \frac{\gamma}{\gamma - 1} p \delta V + \frac{1}{\gamma - 1} V \delta p \quad (8.6.2)$$

As shown in Figure 8.13, A_1 was found to have an average of 68.2 to satisfy equation 8.15 for different running conditions and different fuel blends.

8.7 Evaluation of the Hohenberg correlation,

The Hohenberg correlation was initially developed for diesel engine and has been widely used to predict Q_{loss} in SI engines running on gasoline. The validity of using Hohenberg to predict heat loss for an SI engine running on different ethanol ratios has never been properly examined. The main aim of this section is to evaluate the robustness of the Hohenberg correlation in predicting Q_{loss} at different ethanol ratios. This was carried out through three different techniques.

Firstly, the proportion of the total gross heat release energy to the total energy released by the fuel ($\dot{m}_f \times Q_{LHV}$) for different fuel mixtures was calculated as shown in Figure 8.14. The total gross heat profile is obtained through the integration of Q_{gross} in equation 8.15 from ST to EVO.

For all fuel blends, the percentage of gross heat release ranged from 92% to 78% as the charge become richer, $\phi > 1$. E85 appears to have higher percentage of gross heat release compared to the rest of the fuel mixtures, particularly at rich charge. The results correspond well with combustion efficiency results, as shown in Figure 4.19. The difference between the combustion efficiency values and the percentage of gross heat release values is probably due to crevice losses.

Secondly, the Q_{loss} value, as predicted using the Hohenberg correlation, was compared to the measured heat loss rate to the coolant. The heat transfer to coolant as a result of friction, exhaust port and heat conducted back into the

cylinder head were all subtracted from $\dot{Q}_{coolant}$ to leave only the contribution of the cylinder wall (see section 7.2 for more detail) as follows:

$$\dot{Q}_{cyl} = \dot{Q}_{coolant} + \dot{Q}_{amb.} - (\dot{Q}_{exh.pt} + \dot{Q}_f + \dot{Q}_{exh.man}) \quad (8.7.1)$$

Q_{loss} was transferred from the instantaneous CA domain heat loss ($J/^\circ CA$) to the time-domain-averaged heat loss (J/s), \dot{Q}_{cyl} , using the following equation:

$$\dot{Q}_{cyl} = \int_0^{720} \frac{Q_{loss}(\theta) \times N}{60 \times 2} \quad (8.7.2)$$

Figure 8.15 shows a comparison between measured and predicted heat loss. The results show a good agreement between the two values, within the 10% limit. All fuel mixtures showed approximately the same trend during the various running conditions.

Finally, the heat predicted from the Hohenberg correlation was compared to the one predicted using the C1C2 correlation (equation 7.6 in section 7.2) as shown in Figure 8.16. The results show a good agreement between the two correlations in most predicted heat loss values. At high heat loss, however, the Hohenberg prediction appears to be around 10% higher than the equivalent C1C2 correlation prediction. All fuel blend results show approximately the same relation between the two correlations.

The three techniques illustrate clearly that the Hohenberg correlation can be used to predict instantaneous heat loss to the cylinder wall for all gasoline/ethanol blends.

8.8 Effect of gasoline-ethanol blends at different ratios on the instantaneous heat loss

Several tests were carried out with the engine running at a wide range of speeds and loads (with speeds ranging from 1500 to 4000 rpm and loads ranging from 1.26 to 8 bar BMEP,) in order to evaluate the effect of ethanol on heat loss magnitude and phasing.

These ranges of speeds and loads were chosen to investigate the sensitivity and consistency of the effect of the different fuel blends across a wide range of running conditions. For all fuel blends, the engine was running at constant ST (gasoline MBT) and AFR_{stoich} . This allowed for a direct comparison between the different fuel blends by eliminating any other factors.

The instantaneous heat loss to the cylinder wall, Q_{loss} , was predicted using the Hohenberg correlation as mentioned earlier, m_{charge} is calculated from AFR and \dot{m}_f measurements.

Figure 8.17 and Figure 8.18 show the predicted Q_{loss} for different speeds and loads in two different cylinders (cylinders 1 and 3). Neither cylinder showed any trend between an increase in ethanol ratio and Q_{loss} . The Q_{loss} results contradicted the author's expectations and the results of the measured heat rejected to coolant (see section 6.4). A reduction in Q_{loss} was expected to accompany increases in ethanol content, as discussed in detail in section 7.6. The heat loss to the cylinder walls is dependent on T_g , T_{wall} and heat transfer coefficient, h_c , which is itself dependent on T_g and on in-cylinder pressure. T_{wall} was assumed to remain constant, as explained in section 8.5. Therefore, the main factor that affects heat loss to cylinder wall is T_g . As explained in section 8.2.1, the assumption that m_{charge} is equal among the cylinders is not necessarily accurate. This will affect T_g and subsequently Q_{loss} . Furthermore, it must be assumed to be the reason for the variation in Q_{loss} results between the two different cylinders, where cylinder 3 appears to be less sensitive to the increase in ethanol content.

For the comparative purposes of this study, Q_{loss} was recalculated based on the calculated in-cylinder mass charge, $m_{charge,calc}$, and $T_{g,calc}$ (see section 8.2.1).

The recalculated Q_{loss} for the different fuel mixtures is shown in Figure 8.19. The results show that, during combustion, there was no change in heat loss peak value or phasing as ethanol ratios increases. However, as the combustion starts to terminate, the heat loss appears to decrease slightly at higher ethanol ratios (E50 & E85). This is attributed to the reduction in of the products of combustion temperature.

Q_{loss} data was used to calculate the time-averaged heat transfer, \dot{Q}_{cyl} , using equation 8.18. As shown in Figure 8.20, in both cylinder and for all running

conditions, there is a clear decrease in \dot{Q}_{cyl} for E50 and E85 compared with gasoline. \dot{Q}_{cyl} for E85 is 5 to 7% lower than that for gasoline. These results agree with the measured decrease in $\dot{Q}_{coolant}$ and the author's own expectation.

8.9 Further parameters variation

So far, it was found that increasing ethanol content does not show any significant effect on the instantaneous heat loss, Q_{loss} , magnitude or phasing during combustion. Altering x_b , ϕ , or ST might change this. The main aim of this section is to evaluate whether altering any of these variables can affect the behaviour of the Q_{loss} when ethanol ratios increase. In addition, the effect on Q_{loss} of changing these variables was investigated. For all calculations in this section, m_{charge} was calculated from equation 8.3 (see section 8.2.1).

8.9.1 Effect of burned mass fraction, x_b

Tests were performed on an engine running on low and medium loads and at a constant speed at 2000 rpm. The change in x_b levels took place through changing EGR percentage between 5 and 15%. ST was set to MBT for each x_b level as shown in section 4.3.

Altering x_b levels affects Q_{loss} as shown in Figure 8.21. Increasing x_b percentage reduces the magnitude and the peak value of Q_{loss} for all fuel mixtures. The decrease in Q_{loss} is attributed to the increase in in-cylinder charge heat capacity and a decrease in combustion speed as x_b percentage increases. The x_b phasing did not change despite the ST being advanced to MBT as x_b percentage increased. This can be explained by the decrease in the burn speed (see section 5.6.2). The effect of x_b is consistent over all the fuel blends.

A comparison of Q_{loss} between the different gasoline-ethanol blends for different x_b levels, at low and medium loads, is plotted in Figure 8.22 and Figure 8.23. The results illustrate that, for all running conditions, there is no clear trend between the increase in ethanol content and the Q_{loss} magnitude or phasing during combustion. E85, in most cases, shows a lower Q_{loss} than the rest of the mixtures where it shows a lower peak Q_{loss} and a lower Q_{loss} at a later stage of the combustion stroke. An apparent difference between the

different fuel blends is observed when Q_{loss} was transferred into time domain using equation 8.18, \dot{Q}_{cyl} (J/s), as shown in Figure 8.24. The results show clearly that fuel containing medium and high ethanol content has a lower \dot{Q}_{cyl} compared to the rest of the fuel blends. E85 results show a significant decrease in \dot{Q}_{cyl} compared to all other fuel blends (including E50). The decrease in \dot{Q}_{cyl} for E85 compared to that for gasoline ranged between 4% and 8.5%.

8.9.2 Effect of equivalence ratio, ϕ

Several tests were carried out with ϕ ranging between 0.833 to 1.25. The engine was running at a constant speed of 2000 rpm, a medium BMEP of 4.75 bar, and a constant ST (MBT). For all fuel blends, peak Q_{loss} decreased as the in-cylinder charge became leaner, as shown in Figure 8.25. This can be explained by the increase in the heat capacity (an increase in the charge mass) and the decrease in combustion speed (section 5.6.2) as the charge becomes leaner. A direct comparison between the different fuel blends at different ϕ is plotted in Figure 8.26. The data illustrate that, during combustion, Q_{loss} values do not show any trend between the different fuel blends. By the end of combustion, Q_{loss} decreases for E50 and E85 compared to other fuel blends. Once again, calculated \dot{Q}_{cyl} from equation 8.18 shows a more apparent effect of ethanol than Q_{loss} . E85 shows a lower \dot{Q}_{cyl} than the rest of the fuel blends for all ϕ conditions. There is approximately a 5% decrease in \dot{Q}_{cyl} for E85 compared to gasoline. \dot{Q}_{cyl} results also illustrate that, despite the decrease in peak Q_{loss} as the charge becomes leaner, peak \dot{Q}_{cyl} occurs at the slightly lean side of AFR_{stoich} . This is due to the higher Q_{loss} at the early stage of combustion. The increase in Q_{loss} is attributed to the enhancement in combustion as result of oxygen availability.

8.9.3 Effect of spark timing, ST

Figure 8.28 shows the effect of spark timing on the instantaneous heat loss to the cylinder walls for different fuel blends, averaged over two cylinders. The Q_{loss} has a higher magnitude and earlier phase as the spark timing advances. During the late stage of the compression stroke and early stage of the

combustion stroke, the advanced ST has a higher Q_{loss} but then falls rapidly and has a lower magnitude in the late combustion stroke. This is due to the increase in pressure and temperature, as the combustion occurs closer to TDC. As the ST is retarded, the combustion occurs when the cylinder volume is larger. This trend is consistent among the different gasoline-ethanol blends. The peak Q_{loss} increases by around 8-9% as ST advances from 8 °BTDC to 18 °BTDC. This earlier phasing as spark timing is advanced can be explained by the early start of combustion and the faster combustion speed (see section 5.6.1). The heat transfer rate to the cylinder wall, \dot{Q}_{cyl} is shown in Figure 8.29. The results, once again, show a decrease in \dot{Q}_{cyl} at high and medium ethanol ratios (E50 and E85). Advancing ST will increase \dot{Q}_{cyl} to the cylinder as illustrated earlier in the Q_{loss} results.

8.10 Summary and discussion

The main aim of the present work is to study the effect of adding ethanol at different proportions on the spatially-averaged instantaneous heat loss to the cylinder wall. Furthermore, it is to investigate its effect on some of the in-cylinder gas properties and charge preparation before combustion.

Despite the fact that ethanol has a lower c_p than gasoline, the ethanol-air mixture c_p at AFR_{stoich} demonstrates a comparable value to that of the gasoline-air mixture due to the change in AFR_{stoich} . The c_p for the product of combustion, on the other hand, will be lowered as ethanol content increases due to the change in its composition, particularly an increase in H₂O content. This will affect the total heat capacity ratio, γ_{tot} and, subsequently, the net heat release calculations.

The in-cylinder bulk gas temperature, T_g , was calculated using the ideal gas law. The results show that increasing ethanol content does not have any effect on either the phasing or the magnitude of T_g during combustion. However, T_g at a late stage of the combustion stroke and the exhaust stroke, shows a clear decrease for high and medium ethanol ratios particularly when compared to gasoline. This agrees with the T_{exh} measured data where E85 and E50 data shows a clear decrease in T_{exh} due to the increase in the exhaust heat capacity.

The higher enthalpy of vaporisation, h_{fg} , for ethanol is expected to increase the cooling effect inside the cylinder before combustion. In DISI engines, the majority of fuel is expected to vaporise during the compression stroke. The heat required to vaporise the fuel will affect the increase in temperatures during the compression stroke, T_{comp} . For that reason, T_{comp} was used as an indication of the amount of heat required to vaporise the fuel. T_{comp} was calculated from the temperature difference between IVC and ST. High and medium ethanol contents show a clear decrease in T_{comp} . E85, in particular, showed a significant decrease in T_{comp} compared to the rest of the fuels, including E50. This is explained by the increase in h_{fg} and in the fuel flow rate (higher BSFC).

The Hohenberg correlation was used to predict instantaneous heat loss to cylinder. The correlation, which was originally developed for diesel engines, was calibrated by comparing gross heat released, as calculated from the first law of thermodynamics, to the heat released from the combusted fuel. Several techniques were used to validate the use of the Hohenberg correlation to predict the heat loss for different gasoline-ethanol mixtures. That included comparing the gross heat release to the heat release by the fuel, and comparing the predicted heat transfer rate to the measured one as well as to that predicted using the C1C2 correlation. The results illustrate that the Hohenberg correlation can be used to predict the instantaneous heat loss for the different gasoline-ethanol mixtures.

The results also illustrate that there is very little difference in the heat loss magnitude, peak value, and phasing between the different fuel blends during combustion. E85 shows, in some cases, a slight decrease in peak heat loss. The heat loss magnitude at both the later stages of the combustion stroke and then at the exhaust stroke, shows a decrease for medium and high ethanol contents. These results were consistent over different running conditions, including different speeds, BMEPs, x_b and ϕ .

The heat transfer in the time domain (J/s) shows a clearer effect of ethanol than the heat loss in the crank angle domain. Both E85 and E50 show a clear decrease in heat transfer rate. However, E85 shows a more significant reduction in heat transfer rate than E50. This reduction is attributed to the reduced product of combustion temperature.

The more pronounced effect of E85 compared to E50 might explain the C1C2 correlations results in Chapter 7. While the C1C2 correlation shows a clear decrease in the predicted heat transfer for E85. E50 predictions show comparable results to the rest of the fuel blends. The decrease in heat transfer rate for E50 might be too small to be observed within the confidence limit of C1C2 correlation.

CHAPTER 9 Discussion

Summary and discussion

This thesis describes the effects of using ethanol/gasoline blends at different proportions on the engine's combustion behaviour, energy balance and heat transfer characteristics.

The contribution of the presented work to knowledge could be divided into two categories: firstly the effect of ethanol on

- energy balance inside the engine.
- cycle average heat transfer characteristics including the effect different sources.
- the validity of using C1C2 correlation and whether any modification is required to compensate for the change in heating value and other fuel properties.
- crank angle resolved heat transfer and charge preparation.

Despite the extensive research literature that has been produced over the past few years, no material was found that directly investigates the effects of ethanol on the abovementioned subjects. This highlights a notable gap in the current body of knowledge on the topic, which this study endeavours to address.

Secondly, the effect of ethanol on:

- in-cylinder combustion behaviour.
- exhaust composition, heat capacity and temperature.

As shown in Chapter 2, several researchers studied the effect of ethanol on the aforementioned characteristics. However, there was variation in the results among researchers. This variation might be attributed to the use of different engines particularly different fuelling systems and compression ratios. The majority of these studies were carried out on a port fuel injection engine. Some were carried out on a wall guided direct injection engine. This study was carried on a spray guided direct injection engine with high compression ratio (11.5:1) that has never been examined before.

Discussion

For the purpose of this study, an engine test rig was designed and commissioned. Accurate measurements of the engine's power-out (load and speed), fuel consumption, coolant flow rate, temperatures and in-cylinder pressure were prerequisites of the design. Since the objective of this study was to evaluate the effect of different ethanol/gasoline blends on various engine characteristics, the engine was operated at a steady state, with all running conditions and engine variables kept constant. This permitted a direct comparison between the different fuel blends, with change in ethanol content in the fuel as the only variable. Direct access to the ECU, in order to modify, adjust and fix different engine variables was possible through ATI software and hardware. Among variables that were most commonly modified were EGR, spark timing, and equivalence ratio.

The addition of ethanol to gasoline changes the chemical composition of the fuel blends; particularly, it increases the H/C ratio and O₂ content of the fuel. This change was expected to affect the physiochemical and combustion properties of the fuel. The work presented in this thesis starts by assessing the effects of increasing ethanol content in gasoline/ethanol blends on the combustion properties, including AFR_{stoich} , Q_{LHV} and T_{add} . The results indicate a decrease in all three properties. The reduction in Q_{LHV} is also illustrated by a measured BSFC rise that accompanies increases in ethanol content. However, the decrease in Q_{LHV} did not affect the power output of the engine. On the contrary, for high ethanol content, the effect of the combined reduction in AFR_{stoich} and Q_{LHV} was to produce a slightly higher engine power output for the same throttle position. Hence, higher total power output can be achieved using ethanol compared to standard gasoline at the expense of BSFC.

The effect of increasing ethanol content on emission and H₂O levels was evaluated at different engine running conditions. Increasing the ethanol ratio shows a decrease in CO, CO₂, HC and NO_x emissions for most running conditions. H₂O level, on the other hand, clearly rises for higher ethanol content. CO₂ and H₂O levels change as a direct result of differing chemical structure between gasoline and ethanol; in particular increase in H/C ratio and O₂ content. The reduction in NO_x levels is attributed to the lower T_{add} and the higher h_{fg} of ethanol. The levels of CO and HC emissions decrease due to the improvement in combustion efficiency that is observed as ethanol content

Discussion

increases. Plotting the combustion efficiency of the different fuel blends as a function of ϕ shows a clear increase in combustion efficiency as ethanol content increases, particularly for rich mixtures. This is attributed to the oxygen content of the fuel. Oxygen mass fraction in the fuel increases from approximately 0% for gasoline to 35% for E85.

Decreased emissions level, particularly at higher ethanol ratios, indicate that using ethanol can contribute to the wider efforts of ensuring compliance with increasingly tight emission regulations.

The combustion characteristics and, subsequently, the engine's heat transfer characteristics were also expected to be affected by changes in the physiochemical properties associated with the increase in ethanol content. Despite lower T_{add} of ethanol due to its lower Q_{LHV} , the calculated laminar flame speed for ethanol is found to be higher than that of gasoline, with the peak difference occurring at AFR_{stoich} . This increase is attributed to the presence of oxygen in ethanol chemical's structure. The effect of using ethanol on both FDA and RBA was investigated at various engine running conditions. The combustion duration was determined using the Rasweiler and Withrow methods based on the in-cylinder pressure data. The data illustrate that, despite the higher laminar flame speed of ethanol, FDA values were comparable for all fuel blends. This can be explained by the high compression ratio engine under investigation (11.5:1).

Indeed, as a result of this high compression ratio, the effects of compression work and, therefore, charge density and temperature dominated flame initiation. RBA data, on the other hand, show a clear increase in combustion speed, decrease in RBA, for E85 compared to gasoline and other fuel blends, which corresponds well with the rise in laminar flame speed of ethanol. The RBA results, nevertheless, do not show a linear relation between increasing ethanol content and RBA. Fuel blends with low and medium ethanol content (E10, E20 and E50) show a slight reduction in RBA compared to gasoline. However, there is no significant difference, nor trend, in RBA amongst those fuel blends.

The non-linear relation between RBA and ethanol content can be explained by the differences in ethanol's properties. Indeed, whilst ethanol with a higher laminar flame speed and oxygen content will decrease RBA, lower Q_{LHV} and

higher h_{fg} levels in ethanol will have the opposite effect. For that reason, the effect of increasing ethanol will only appear for blends with high ethanol content.

Changing the in-cylinder charge composition, either by changing ϕ or x_b , shows a significant effect on laminar flame speed for both ethanol and gasoline. Ethanol laminar flame speed appears to be more sensitive to variation in any of these two variables. As a result, the peak difference in laminar flame speed between the two fuels occurs at AFR_{stoich} and low x_b level. This difference starts to decrease as the charge moves away from AFR_{stoich} or x_b level increases. The RBA results correspond well to the laminar flame speed trend where, once again, E85 has a lower RBA than gasoline at AFR_{stoich} and low x_b level. As x_b levels rise or the charge moves away from AFR_{stoich} , the difference in RBA between the two fuels decreases.

The tolerance for x_b when using different fuel blends, which is mainly affected by combustion duration, was studied using COV of IMEP. The results showed a slight increase in x_b tolerance for E85 compared to other fuel blends. This indicates that, in addition to the reduction in NOx levels for E85, further decreases in NOx can occur due to the increase in tolerable x_b ratio.

The study of the heat transfer characteristics inside the engine started with an engine energy balance evaluation for different fuel mixtures. There was an investigation of how the energy released by the fuel was distributed between brake output, coolant energy, exhaust energy and heat loss to ambient. As ethanol content increases, exhaust heat capacity, $\bar{c}_{p,exh}$, also increases due to exhaust composition, particularly the increase in H₂O content. For all running conditions, lower $\bar{c}_{p,exh}$ was also manifested in a marked decrease in the exhaust temperature, T_{exh} , as ethanol content increased. Lower T_{exh} can have significant effects on various engine characteristics. A reduction in T_{exh} could considerably effect emission levels, particularly during warm-up. The decrease in T_{exh} would increase the time needed for the catalyst to reach its operating temperature. This would increase tail-pipe emissions, especially at low temperature start. Reduced T_{exh} will also affect HC and CO after flame combustion. Nevertheless, the increase in ethanol content shows a decrease in HC and CO levels regardless of T_{exh} . Decreasing T_{exh} can also affect the

exhaust energy-powered devices such as the turbocharger (if used). Finally T_{exh} has an effect on total heat rejected to coolant by affecting the amount of heat transferred through the exhaust port, conducted back to the engine head and heat transferred to the cylinder wall after end of combustion, during the expansion and the compression strokes. The decrease in T_{exh} and the higher h_{fg} of ethanol, which will have a cooling effect on the charge before combustion, indicate a potential decrease in the heat rejection to coolant. The measured heat rejection to coolant, $\dot{Q}_{coolant}$, confirms this expectation. However, the effect of ethanol on heat rejection to coolant appeared only at medium and high ethanol content (E50 & E85). E85 particularly showed a marked decrease in $\dot{Q}_{coolant}$ compared to all other fuel blends. Low ethanol content fuel blends exhibited comparable results to gasoline. At low ethanol content, oxygen availability, which enhances combustion, dominates the combustion more than the increase in h_{fg} . This eliminates the cooling effect of ethanol.

Although lower total heat rejection to coolant was not significant enough to require a radical change in the design of the cooling system, it was expected to change the warm up characteristics. Data obtained from the PFI engine show a clear increase in the time required by the thermostat to open as well as the time required to reach a particular oil temperature, i.e. an increase in the time required to reach the engine's operating temperature. This would be reflected in an increase in friction, fuel consumption and emissions. This effect could be more extensively quantified in future work. Measurements of heat lost to ambient produced comparably similar results for both E85 and gasoline. This was expected since the coolant inside the engine maintains the engine's skin temperature at an approximately constant level.

Energy balance results showed a clear increase in thermal efficiency as ethanol content increased for all running conditions. This is noticeable even for low ethanol content. The results also illustrate that the improvement in combustion efficiency is the primary reason for the increased thermal efficiency. In addition, the slight decrease in heat loss to exhaust and coolant, at high ethanol content, was translated into an improvement in thermal efficiency as more work was transferred to the piston.

Discussion

The improvement in thermal efficiency is reflected in the BSFC. The results show that the increase in the BSFC associated with a decrease in the Q_{LHV} of ethanol was less than expected. In addition, the reviewed literature shows that using ethanol has the potential of increasing the compression ratio due to its high anti-knock resistance relative to gasoline. This will increase thermal efficiency even further. Indeed, the thermal efficiency of an SI engine running on ethanol has the potential to be comparable to that of a diesel engine.

The C1C2 correlation was used to predict gas-side heat transfer to coolant, \dot{Q}_{cyl} and $\dot{Q}_{exh,port}$. C1C2 is a time-averaged correlation that was developed at The University of Nottingham and proved to be reliable in predicting $\dot{Q}_{coolant}$ for both diesel and SI engines. The correlation has been used extensively for engine thermal modelling as part of the PROMETs software package. One of the objectives of this thesis was to evaluate the validity of the C1C2 correlation in predicting heat transfer for different gasoline-ethanol blends, as well as establishing whether any modifications in the C1, C2 or $T_{g,eff}$ constants were required. This would be useful in future work when modelling engine thermal conditions when running on different ethanol-gasoline blends. Comparisons of the measured and predicted values of $\dot{Q}_{coolant}$ show that the C1C2 correlation can be used to predict gas-side heat transfer without any need to modify the correlation. This was unexpected since \dot{Q}_{cyl} was anticipated to decrease as ethanol content increased and, subsequently, produce a change in C1 and $T_{g,eff}$. The expected reduction in \dot{Q}_{cyl} was based on the following reasons:

firstly, the increase in h_{fg} as ethanol content increases, results in a cooling effect inside the cylinder. Secondly, reduced NOx emission levels observed with increasing ethanol content indicates lower peak in-cylinder temperature. Finally, the decrease in T_{exh} illustrates a corresponding decrease in the temperature of the products of combustion, which has a considerable effect on total heat loss. Using the C1C2 correlation to predict \dot{Q}_{cyl} for different gasoline-ethanol blends showed that the \dot{Q}_{cyl} for E85 was lower than for other fuel mixtures, which corresponds well with the author's expectations. The decrease in \dot{Q}_{cyl} is accounted for by a lower Re number without the need to

Discussion

modify either C1 or $T_{g,a}$. Although E85 showed a decrease in \dot{Q}_{cyl} , the results do not illustrate any clear correlation between a higher ethanol ratio and the \dot{Q}_{cyl} value. This might be explained by the confidence limit associated with the C1C2 correlation where change in \dot{Q}_{cyl} can be too small to be resolved by this correlation. In addition, the increase in combustion efficiency for low ethanol content can have more a dominant effect on increasing in-cylinder temperature than the cooling effect of ethanol, or the decrease in T_{exh} .

The 'C2' constant in the C1C2 correlation represents the ratio of exhaust port heat flux to cylinder heat flux. C2 will thus remain constant since the ratio is found to be constant for all fuel blends. As mentioned previously, the results illustrate a clear decrease in $\dot{Q}_{coolant}$ for medium and high ethanol contents. The decrease in \dot{Q}_{cyl} contributes to the total decrease in $\dot{Q}_{coolant}$. Other sources that contribute to $\dot{Q}_{coolant}$ are heat transfer from the exhaust port, $\dot{Q}_{exh.port}$, heat generated from engine friction, $\dot{Q}_{friction}$, and heat conducted from the exhaust manifold back into the engine structure, $\dot{Q}_{ex.man}$. A significant proportion of total heat transfer to coolant is from the exhaust port. The exhaust port heat transfer was both measured and predicted using empirical correlations. The effect of increasing ethanol content was evaluated. Both predicted and measured results showed a clear decrease in $\dot{Q}_{exh.port}$ as ethanol content increased. This is attributed mainly to the decrease in T_{exh} . The slight decrease in the Re number for medium to high ethanol content is another reason for the decrease in $\dot{Q}_{exh.port}$. The calculated $\dot{Q}_{ex.man}$ value also decreased as ethanol content increased. $\dot{Q}_{friction}$, on the other hand, showed similar results for different fuel blends. The decrease in both $\dot{Q}_{exh.port}$ and $\dot{Q}_{ex.man}$ contributed to the total decrease in $\dot{Q}_{coolant}$.

Further investigation of the heat transfer to the cylinder wall was carried out. Pressure data was used to predict instantaneous heat loss to the cylinder walls (J/CA), Q_{loss} using the Hohenburg empirical correlation. Q_{loss} gives an insight into the temporal heat flux variation during the engine cycle, which includes

heat loss magnitude and phasing. The validity of using the Hohenburg correlation, which had been calibrated for the engine under investigation, to calculate the instantaneous heat transfer coefficients for the different ethanol-gasoline blends had to be examined. Several techniques were used, including comparing the predicted heat loss using the Hohenburg correlation to both the actual measured value, and to the one predicted by the C1C2 correlation. Furthermore, gross heat release was compared to the expected heat released by the fuel. The results from the different techniques confirmed the validity of using the Hohenburg correlation.

During combustion, heat loss magnitude and phasing showed comparable values for the different fuel blends. E85, in some cases, showed a lower peak heat loss than the rest of the ethanol-gasoline blends. After combustion, during the later stage of the combustion stroke and the exhaust stroke, E85 and E50 heat loss decreased slightly relative to other fuel blends. The increase in heat loss is attributed to the lower temperature of the product of combustion. This was indicated by the decrease in measured exhaust temperature and an increase in the calculated heat capacity. Reduced heat loss later on in the combustion stroke is reflected in decreased heat rejection rate in the time domain (J/s) where the effect of ethanol was more obvious. Both E85 and E50 showed a clear decrease in heat transfer rate. However, E85 exhibited a more significant decrease in the heat transfer rate than that seen with E50.

The more pronounced effect of E85 on heat transfer rate compared to E50 would explain the C1C2 correlation results. While the C1C2 correlation showed a clear decrease in the predicted heat transfer for E85, its E50 prediction indicated results that were comparable to the other fuel blends. The decrease in the heat transfer rate for E50 is probably too small to be observed within the confidence limit of the C1C2 correlation.

In a DISI engine, most of the injected fuel is vaporised during the compression stroke, causing a cooling effect on the charge. The use of ethanol is expected to increase this cooling effect due to its higher enthalpy of vaporisation and rise in the amount of fuel injected. The effect of ethanol was assessed by calculating the temperature increase, T_{comp} , between IVC and ST. E50 and E85 show a reduction in T_{comp} compared to the rest of the fuel blends. This

reduction illustrates that bigger portion of the piston work during the compression stroke is going to vaporise E85 than gasoline.

Future work

The work presented in the thesis concentrates on the effect of gasoline-ethanol mixtures on the combustion behaviour and heat transfer characteristics during fully warmed-up conditions only. Further work investigating the effect of ethanol on heat transfer characteristics during warming-up conditions is of extreme importance. Indeed, the presence of ethanol is expected to affect the time and the amount of fuel required for the engine to reach its fully warmed-up conditions. Moreover, changing the engine's warm up characteristics will have a significant effect on emissions, friction levels, power output and fuel consumption. A clear understanding of the effect of ethanol on those characteristics would greatly assist in developing strategies for a more rapid flexi-fuel engine warm-up.

A more detailed understanding of the effect of ethanol on in-cylinder heat transfer characteristics can also be achieved through measurement of instantaneous wall temperature. Wall temperature should be measured at different locations inside the combustion chamber using fast-response thermocouples. The different locations can include the cylinder liner, piston and cylinder head. Temperature measurements can be used to provide the heat flux profile. This will allow for an assessment of the impact of increasing ethanol content on instantaneous spatial variation of heat transfer flux. The results would provide a qualitative insight into differences between different fuel mixtures, and would also illustrate the quantitative differences in heat transfer rates. It also could validate the use of classical heat transfer correlations when applied to different fuel mixtures.

Further work investigating the heat transfer characteristics and combustion behaviour for different fuel blends should be carried out for other engine designs, with a particular focus on alternative fuelling systems, namely port-fuel injection or wall-guided DISI engines. In addition, engines with different compression ratios, either turbocharged or naturally aspirated, could be used. The sensitivity of ethanol to all these changes should be properly investigated.

CHAPTER 10 Conclusion

The principle conclusion of this thesis includes:

- Increasing ethanol ratio showed a clear improvement in the engine performance including decreasing in the main regulated emissions, improvement in combustion efficiency and increase in maximum BMEP. This improvement was obvious even at low ethanol ratio.
- While FDA is comparable for all fuel blends, increasing ethanol decrease RBA compare to pure gasoline. However, this decrease is not linear. A small decrease is observed at E10, but no further decrease occurs until E85. E85 exhibits a lower RBA compared to all other fuel blends particularly gasoline.
- Increasing ethanol content improves thermal efficiency, mainly due to the increase in combustion efficiency. Also, due to the decrease in exhaust and coolant losses.
- The decrease in the heat transfer rate to the coolant, as ethanol ratio increase, is due to the decrease in cylinder heat loss, exhaust heat loss and heat conducted back to the engine block.
- The C1C2 correlation can be used to predict heat loss without need for any modification.
- Instantaneous heat loss during combustion does not change among different fuel mixtures, however it decrease later on in the combustion stroke .

The following details the conclusion of each chapter in the thesis:

Chapter 4

- Increasing ethanol ratio in the gasoline-ethanol blend causes an obvious decrease in AFR_{stoich} , the calorific value and, to a lesser extent, the adiabatic flame temperature.

Conclusion

- Although ethanol has a lower calorific value, increasing ethanol content increases the power output for a constant throttle position due to the decrease in AFR_{stoich} . This will be at the expense of BSFC.
- Increasing ethanol ratio has a significant influence on exhaust composition. Increasing ethanol ratio decreases CO, CO₂, HC and NO_x emission levels for most running conditions. H₂O levels, on the other hand, increase.
- Significant improvements in combustion efficiency are obtained as ethanol ratios increase, particularly using rich mixtures.

Chapter 5

- Despite the higher laminar flame speed of ethanol, different gasoline-ethanol blends have comparable FDA values under different running conditions. The compression work, turbulent flow and charge density dominate flame initiation in the high compression ratio engine under investigation (11.5:1).
- There is no linear trend between increasing ethanol content and RBA. A small decrease is observed at E10, but no further decreases occur until E85. E85 exhibits a lower RBA compared to all other fuel blends, particularly gasoline.
- Ethanol's laminar flame speed is more sensitive to changes in charge composition, such as ϕ and x_b , than gasoline. As a result, the difference in laminar flame speeds start to be reduced as x_b increases or the charge moves away from AFR_{stoich} . The RBA data show the same trend where the E85 data indicate a reduction in RBA compared to gasoline at AFR_{stoich} . The difference between the two fuels starts to decrease as ϕ or x_b changes.
- High ethanol ratios will slightly increase x_b tolerance as a result of shorter combustion duration.

Chapter 6

- Increasing ethanol ratios increases exhaust heat capacity as a result of changes in exhaust composition, in particular, higher water content. This is responsible for reduction in exhaust temperature.

Conclusion

- The heat rejection rate to coolant decreases at medium and high ethanol ratios.
- The decreases in heat rejection to coolant, and in the exhaust temperature, affect the engine's warm up characteristics. Running on fuel containing medium and high ethanol content increases the time required for the engine to reach operating temperature.
- Increasing ethanol content improves the engine's thermal efficiency considerably compared to gasoline. This is attributed mainly to the increase in combustion efficiency. The decrease in heat losses to the exhaust and coolant also contribute to the improvement in thermal efficiency.

Chapter 7

- The C1C2 correlation can be used to predict gas-side heat transfer to coolant for different gasoline-ethanol blends without need for modification.
- In the C1C2 correlation, the decrease in Re for E85 compensated for the expected decrease in the cylinder heat loss to coolant without the need to modify either C1 or $T_{g,a}$. The expected decrease in cylinder heat loss is attributed to the decrease in the total heat rejection to coolant, NOx emission levels, and exhaust temperature.
- The ratio of the heat flux-to-exhaust to the heat-flux-to-cylinder remains constant. Subsequently, C2, which represents this ratio in the C1C2 correlation, is unchanged.
- Other coolant heat sources also contribute to the total decrease in heat rejection to coolant for medium and high ethanol content fuel mixtures. Both measured and predicted exhaust heat loss and heat conducted back into the engine decrease for medium and high ethanol content as a result of reduced exhaust temperature.

Chapter 8

- There is little difference in instantaneous heat loss magnitude and phasing among the fuel blends during combustion. As the combustion

Conclusion

terminates and into the exhaust stroke, heat loss becomes lower for medium and high ethanol content.

- The predicted heat loss in the time domain (J/s) shows a more apparent effect of ethanol compared to the heat loss in the CA domain (J/CA). Both E50 and E85 show a clear decrease in the heat loss with E85 exhibiting a more pronounced decrease.
- Due to ethanol's higher enthalpy of vaporisation and the increase in the amount of fuel injected, E50 and E85 blends show a higher cooling effect in the compression stroke than the other fuel blends.

In summary, the use of ethanol in SI engines has the advantage of reducing most regulated emissions, as well as improving combustion and thermal efficiency. This effect is noticeable even at low ethanol contents. However, contrary to assumptions, there is no linear trend between increasing ethanol content and any change in combustion and heat transfer characteristics. The effect of ethanol on these characteristics manifests itself only at medium to high ethanol levels. E85 has the most pronounced effect on increasing combustion speed and decreasing heat losses to coolant and exhaust. Finally, the C1C2 correlation can be used, without any modification, to predict gas-side heat loss for different gasoline-ethanol mixtures. This is particularly important for future modelling of engine running on different gasoline-ethanol blends.

Apart from Sweden, the use of ethanol in the EU is still limited to low proportion ethanol-gasoline blends (ranging from 5% to 10%). According to the finding of this thesis, the current level of ethanol use does not affect the combustion and heat transfer characteristics. However, plans towards reducing dependence on fossil fuels push towards the use of alternative fuels such as ethanol. The changes in engine combustion and heat transfer characteristics, when running on high percentage ethanol blends, should be taken into account in future flexi-fuel engine design.

References

1. E.V. Thuijl, C.J. Roos, and L.W.M. Beurskens, "An overview of biofuel technologies, market and policies in Europe". Energy research centre of the Netherlands: Amsterdam 2003.
2. Renewable Fuel Association, RFA. (2006). "FROM NICHE TO NATION, ETHANOL INDUSTRY OUTLOOK", http://www.mda.state.mi.us/renewablefuels/documents/RFAoutlook_2006.pdf, Accessed Feb. 2010.
3. J.D. Hamilton, "Understanding Crude Oil Prices", NBER Working Paper No. w14492 2008.
4. EurObserv'ER Website. "Biofuels Barometer", <http://www.eurobserv-er.org/pdf/baro198.pdf>, Accessed Feb. 2010.
5. The European Association for Bioindustries Website. (June 2007). "Biofuels in Europe", http://www.europabio.org/positions/Biofuels_EuropaBio%20position_Final.pdf, Accessed Feb. 2010.
6. R. Schnepf, "European Union Biofuels Policy and Agriculture: An Overview". Congressional Research Service, 2006.
7. European Commission Website. (2007). "Biofuels Progress Report", http://ec.europa.eu/energy/energy_policy/doc/07_biofuels_progress_report_en.pdf, Accessed Feb. 2010.
8. Z.G. Sivers M, Olsson L, B Hahn-Hägerdal "Cost analysis of ethanol from willow using recombinant *Escheri-chia coli*", *Biotechnol Prog*, **10**: p. 555-560, 1994.
9. J.R. Mielenz, "Ethanol production from biomass: technology and commercialization status", *Current Opinion in Microbiology*, **4**: p. 324-329, 2001.
10. J. Zaldivar, J. Nielsen and L. Olsson, "Fuel ethanol production from lignocellulose: a challenge for metabolic engineering and process integration", *Applied Microbiology and Biotechnology*, **56**: p. 17-34, 2001.
11. A.E. Farrell, R.J. Plevin, B.T. Turner, A.D. Jones, M. O'Hare and D.M. Kammen, "Ethanol Can Contribute to Energy and Environmental Goals", *Science*, **311**: p. 506 - 508.

References

12. H. Shapouri, J. Duffield and M. Wang, "The energy balance of corn ethanol revisited", *TRANSACTIONS OF THE ASAE*, **46** (4): p. 959-968, 2003.
13. R.S. Chambers, R.A. Herendeen, J.J. Joyce and P.S. Penner, "Gasohol: Does It or Doesn't It Produce Positive Net Energy?" *Science*, **206**(4420): p. 789 - 795, 1979.
14. C. Cleveland, "Net energy from the extraction of oil and gas in the United States", *ENERGY*, **30**(5): p. 769-782, 2005.
15. S. Kim and B.E. Dale, "Life cycle assessment of various cropping systems utilized for producing biofuels: Bioethanol and biodiesel", *Biomass and Bioenergy*, **29**: p. 426-439, 2005.
16. R. Stone, "Introduction to Internal Combustion Engines" Palgrave, 1999.
17. J.B. Heywood, "Internal Combustion Engine Fundamentals" McGraw-Hill Book Company, 1988.
18. T. Wallner and S.A. Miers, "Combustion Behaviour of Gasoline and Gasoline/Ethanol Blends in a modern Direct-Injection 4-Cylinder Engine", SAE Technical Paper No. 2008-01-0077, 2008.
19. T. Topgul, H. Yucesu, C. Cinar and A. Koca, "The effects of ethanol-unleaded gasoline blends and ignition timing on engine performance and exhaust emissions", *Renewable Energy*, **2006**: p. 2534-2542, 2006.
20. B. He, J. Wang, J. Hao, X. Yan and J. Xiao, "A study on emission characteristics of an EFI engine with ethanol blended gasoline fuels ", *Atmospheric Environment*, **37**: p. 949-957, 2003.
21. C.V. D'Ornellas, "The effect of ethanol on gasoline oxidation stability", SAE Technical Paper No. 2001-01-3582, 2001.
22. W. Hsieh, R. Chen, T. Wu and T. Lin, "Engine performance and pollutant emission of an SI engine using Ethanol-gasoline blend fuels", *Atmospheric Environment*, **36**: p. 403-410., 2002.
23. R.M. Bata, A.C. Elrod and R.W. Rice, "Emissions From IC Engines Fueled With Alcohol-Gasoline Blends: A Literature Review", *Journal of Engineering for Gas Turbines and Power*, **111**(3): p. 424-431, 1989.
24. K. Kar, T. Last, C. Haywood and R. Raine, "Measurement of Vapor Pressure and Enthalpies of Vaporization of Gasoline and Ethanol Blends and Their effects on Mixture Preparation in an SI Engine", SAE Technical Paper No. 2008-01-0317, 2008.

References

25. J.I.B. J. A. Pumphrey, and W. A. Scheller, "Vapour pressure measurements and predictions for alcohol-gasoline blends", *Fuel*, **79**: p. 1405-1411, 2000.
26. R.d. Silva, R. Cataluña, E.W.d. Menezes, D. Samios and C.M.S. Piatnicki, "Effect of additives on the antiknock properties and Reid vapor pressure of gasoline", *Fuel*, **84**: p. 951-959, 2005.
27. R.M. Balabin, R.Z. Syunyaeva and S.A. Karpova, "Molar enthalpy of vaporization of ethanol-gasoline mixtures and their colloid state", *Fuel*, **86**(3): p. 323-327, 2007.
28. F.H. Palmer, "Vehicle performance of Gasoline containing oxygenates". IMeche conference publication: London, UK, International conference on petroleum based and automotive applications, 1986.
29. C.-W. Wu, R.-H. Chenb, J.-Y. Pua and T.-H. Lina, "The influence of air-fuel ratio on engine performance and pollutant emissions of an SI engine using ethanol gasoline blended fuel", *Atmospheric Environment*, **38**(40): p. 7093-7100 2004.
30. A.A. Abdel-Rahman and M.M. Osman, "Experimental investigation on varying the compression ratio of SI engine working under different ethanol-gasoline fuel blends", *International Journal of Energy Research*, **21**: p. 31-40., 1997.
31. J. Szybist, M. Foster, W.R. Moore, K. Confer, A. Youngquist and R. Wagner, "Investigation of Knock Limited Compression Ratio of Ethanol Gasoline Blends", SAE Technical Paper No. 2010-01-0619, 2010.
32. K. Nakata, S. Utsumi, A. Ota and K. Katsunori, "The Effect of Ethanol fuel on Spark Ignition Engine ", SAE Technical Paper No. 2006-01-3380, 2006.
33. H. Yücesu, T. Topgül, C. Çinar and M. Okur, "Effect of ethanol-gasoline blends on engine performance and exhaust emissions in different compression ratio", *Applied Thermal Engineering*, **26**: p. 2272-2278, 2006.
34. P.A. Caton, L.J. Hamilton and J.S. Cowart, "An Experimental and Modelling Investigation into the Comparative Knock and Performance Characteristics of E85, Gasohol [E10] and Regular Unleaded Gasoline [87 (R+M)/2]", SAE Technical Paper No. 2007-01-0473, 2007.
35. R.A. Stein, C.J. House and T.G. Leone, "Optimal Use of E85 in a Turbocharged Direct Injection Engine", *SAE International Journal of Fuels and Lubricants*, **2**: p. 670-682, 2009.

References

36. C. Sandstrom, "Measurement Technology for Emissions from Ethanol Fuelled Vehicles". AVL, 2009.
37. K. Knapp, F.D. Stump and S.B. Tejada, "The Effect of Ethanol Fuel on the Emissions of Vehicle Over a Wide range of Temperature", Journal of the Air & Waste Management Association, **48**: p. 646-653, 1998.
38. F. Nadim, P. Zack, G.E. Hoag and S. Liu, "United States experience with gasoline additive", Energy Policy, **29**(1): p. 1-5, 2001.
39. R. Bechtold and J.B. Pullman, "Driving cycle economy, emissions and photochemical reactivity using alcohol fuels and gasoline", SAE Technical Paper No. 800260, 1980.
40. Z. Huang, H. Miao, L. Zhou and D. Jiang, "Combustion characteristics and hydrocarbon emissions of a spark ignition engine fuelled with gasoline-oxygenate blends", Proceedings of the IMEche, Part D: Journal of Automobile Engineering, **214**: p. 341-346 2000.
41. P. Price, B. Twiney, R. Stone, K. Kar and H. Walmsley, "Particulate and Hydrocarbon Emissions from a Spray Guided Direct Injection Spark Ignition Engine with Oxygenate Fuel Blends", SAE Technical Paper No. 2007-01-0472, 2007.
42. S.H. Yoon, S.Y. Ha, H.G. Roh and C.S. Lee, "Effect of bioethanol as an alternative fuel on the emissions reduction characteristics and combustion stability in a spark ignition engine", Proceedings of the IMEche, Part D: Journal of Automobile Engineering, **223**: p. 941-951, 2009.
43. K. Varde, A. Jones, A. Knutsen, D. Mertz and P. Yu, "Exhaust emissions and energy release rate from a controlled spark ignition Engine using ethanol blends", Proceedings of the IMEche, Part D: Journal of Automobile Engineering, **221**: p. 933-941, 2006.
44. S. Taniguchi, K. Yoshida and Y. Tsukasaki, "Feasibility study of Ethanol Applications to A Direct Injection Gasoline Engine", SAE Technical Paper No. 2007-01-2037 2007.
45. D. Bresenham and J. Reisel, "The effect of High Ethanol Blends on Emissions from Small Utility Engines", SAE Technical Paper No. 1999-01-3345, 1999.
46. M. Gautam, D.W.M. II and D. Carder, "Emissions characteristics of higher alcohol/gasoline blends", Proceedings of IMEche, Part A: Journal of Power and Energy, **214**: p. 165-182, 2000.
47. Y. Yacoub, R. Bata and M. Gautam, "The performance and emission characteristics of C1-C5 alcohol-gasoline blends with matched oxygen

References

- content in a single-cylinder spark ignition engine", *Proceedings of IMeche, Part A: Journal of Power and Energy*, **212**: p. 363-379, 1998.
48. S.G. Pouloupoulos, D.P. Samaras and C.J. Philippopoulos, "Regulated and unregulated emissions from an internal combustion engine operating on ethanol-containing fuels", *Atmospheric Environment*, **35**(26): p. 4399-4406, 2001.
 49. R. Magnusson, C. Nilsson and B. Andersson, "Emissions of aldehydes and ketones from a two-stroke engine using ethanol and ethanol-blended gasoline as fuel", *Environmental Science and Technology*, **36**(8): p. 1656-1664., 2002.
 50. L.H. Browning, J.F. Nebolon and R.K. Pefley, "Research Investigation of Alcohol Usage in Spark Ignition Engines", *Society of Automotive Engineers, Inc.* p. 367-376, 1983
 51. J.S. Malcolm, P.G. Aleiferis, A.R. Todd, A. Cairns, A. Hume, H. Blaxill, H. Hoffmann and J. Rueckauf, "A Study of Alcohol Blended Fuels in a New Optical Spark-Ignition Engine". *IMEchE: London, Internal Combustion Engines:Performance, Fuel Economy and Emissions*, 2007.
 52. Y. Yeliana, C. Cooney, J. Worm and J.D. Naber, "The Calculation of Mass Fraction Burn of Ethanol-Gasoline Blended Fuels Using Single and Two-Zone Models", *SAE Technical Paper No. 2008-01-0320* 2008.
 53. A. Cairns, P. Stansfield, N. Fraser, H. Blaxill, M. Gold, J. Rogerson and C. Goodfellow, "A Study of Gasoline-Alcohol Blended Fuels in an Advanced Turbocharged DISI Engine." *SAE Technical Paper No. 2009-01-0138*, 2009.
 54. A.C. Alkidas and S.H.E. Tahry, "Contributor to the fuel economy advantage of DISI engine over PFI engine." *SAE Technical Paper No. 2003-01-3101*, 2003.
 55. S. Brewster, "Initial Development of a Turbo-charged Direct Injection E100 Combustion System", *SAE Technical Paper No. 2007-01-3625*, 2007.
 56. S. Brewster, D. Railton, M. Maisey and R. Frew, "The Effect of E100 Water Content on High Load Performance of a Spray Guide Direct Injection Boosted Engine", *SAE Technical Paper No. 2007-01-2648*, 2007.
 57. P.E. Kapus, A. Fuerhapter, H. Fuchs and G.K. Fraidl, "Ethanol Direct Injection on Turbocharged SI Engines - Potential and Challenges". *SAE Paper Technical No. 2007-01-1408*, 2007.

References

58. T. Suga and Y. Hamazaki, "Development of Honda Flexible Fuel Vehicle", SAE Technical Paper No. 922276, 1992.
59. J.S. Cowart, W.E. Boruta, J.D. Dalton, R.F. Dona, F.L. Rivard II, R.S. Furby, J.A. Piontkowski, R.E. Seiter and R.M. Takai, "Powertrain Development of the 1996 Ford Flexible Fuel Taurus", SAE Technical Paper No. 952751.
60. M. Gautam and D.W. Martin, "Combustion characteristics of higher-alcohol/gasoline blends", *Proceedings of IMechE, Part A: Journal of Power and Energy*, **214**, 2000.
61. R.M. Bata, C. Elrod and T.P. Lewandowski, "Butanol as a Blending Agent with Gasoline for I. C. Engines", SAE Technical Paper No. 890434, 1989.
62. Bosch, "Gasoline-Engine Management" Professional Engineering Publishing Ltd., 2004.
63. G.A. Szekey and A.C. Alkidas, "Combustion Characteristics of a Spray-Guided Direct-Injection Stratified-Charge engine with a High-Squish Piston", SAE Technical Paper No. 2005-01-1937, 2005.
64. "Manufacture handbook, Guide to Thermocouple and resistance thermometry". Issue 6, TC limited. ,
65. Accurate Technologies Inc company website. <http://www.accuratetechnologies.com>, Accessed May 2007.
66. dSPACE GmbH company website. <http://www.dspaceinc.com/ww/en/inc/home.cfm>, Accessed Jan. 2007.
67. L.D. Winborn, "The Cold operation of SI engines and the significance of fuel losses, oil dilution, and mixture gas/fuel ratio", PhD Thesis, University of Nottingham, 2001.
68. F. Bonatesta, "The charge burn characteristics of a gasoline engine and the influence of valve timing", PhD Thesis, University of Nottingham, 2006.
69. F. Yüksel and B. Yüksel, "The use of ethanol-gasoline blend as a fuel in an SI engine", *Renewable Energy*, **29**: p. 1181-1191., 2004.
70. Mónica B. Gramajo de Doz, Carlos M. Bonatti and H.N. Sólamo, "Water Tolerance and Ethanol Concentration in Ethanol-Gasoline Fuels at Three Temperatures", *Energy & Fuels*, **18** (2): p. 334-337, 2004.
71. S.R. Turns, "An introduction to combustion, concepts and applications" McGRAW-HILL Book Company, 2000.

References

72. G.F.C. Rogers and Y.R. Mayhew, "Thermodynamic and Transport Properties of Fluids" Blackwell Publishers Ltd, 1975.
73. N.J. Darnton, "Fuel Consumption and Pollutant Emissions of Spark Ignition Engines During Cold-Started Drive Cycles", PhD thesis Thesis, University of Nottingham, 1995.
74. N. Nabi, H. Ogawa and N. Miyamoto, "Nature of Fundamental Parameters Related to Engine Combustion for a Wide Range of Oxygenated Fuels", SAE Technical Paper No. 2002-01-2853, 2002.
75. G.M. Rassweiler and L. Withrow, "Motion Pictures of Engine Flame Propagation Model for SI Engines", SAE Journal (Trans), 42: p. 185-204, 1938.
76. P.J. Shayler and M.W. Wiseman, "SI engine combustion processes ", SAE Technical Paper No. 900351, 1990.
77. M.F.J. Burnt and A. Emtage, "Evaluation of Burn Rate Routines and Analysis Errors ", SAE Technical Paper No. 970037, 1997.
78. M. Metghalchi and J.C. Keck, "Laminar flame velocity Propane-Air mixtures at high temperature and pressure", Combustion and Flame, 38: p. 143-154, 1980.
79. S.Y. Liao, D.M. Jiang, Z.H. Huang, K. Zeng and Q. Cheng, "Determination of the laminar burning velocities for mixtures of ethanol and air at elevated temperatures", Applied Thermal Engineering, 27(2-3): p. 374-380, 2007.
80. O.L. Gulder, "Correlation of Laminar Combustion Data for Alternative S.I. Engine Fuels", SAE Technical Paper No. 841000, 1984.
81. D.B. Rhodes and J.C. Keck, "Laminar Burning Speed Measurements of Indolene-Air-Diluent Mixtures at High Temperature and Pressure", SAE Technical Paper No. 850047, 1985.
82. C. Koehlen, E. Holder and G. Vent, "Investigation of Post Oxidation and Its Dependency on Engine Combustion and Exhaust Manifold Design." SAE Technical Paper No. 2002-01-0744, 2002.
83. H.C.R. Yuen, "An Investigation of Thermal Condition in Spark Ignition Engines", PhD Thesis, University of Nottingham, 1995.
84. J.A. Caton and J.B. Heywood, "An Experimental and Analytical Study of Heat Transfer in an Engine Exhaust Port", Int. J. Heat Mass Transfer, 24(4): p. 581-595, 1981.

References

85. J.A. Kaplan and J.B. Heywood, " Modeling the Spark Ignition Engine Warm-Up Process to Predict Component Temperatures and Hydrocarbon Emissions", SAE Technical Paper No. 910302 1991.
86. B. Waters, "Personal Communication". University of Nottingham, 2010.
87. J.P. Holman, "Heat Transfer" McGraw Hill Book Company, 1989.
88. P.J. Shayler, J.P. Chick and T. Ma, "Correlation of Engine Heat Transfer for Heat Rejection and Warm-Up Modelling ", SAE Technical Paper No. 971851, 1997.
89. P.J. Shayler, W.S. Baylis and J.P. Chick, "The Effect of EGR and turbocharging on Engine Heat Rejection Rate". IMechE conference, 1999.
90. C.F. Taylor and T.Y. Toong, "Heat Transfer in Internal Combustion Engines", SAE Technical Paper No. 670931, , 1967.
91. P.J. Shayler, S.J. Christian and T. MA, "A Model for the Investigation of the Temperature, How flow and Friction Characteristics During Engine Warm-up", SAE Technical Paper No. 931153, 1993.
92. P.J. Shayler, S.A. MAY and T. Ma, "Heat Transfer to the Combustion Chamber Walls in Spark Ignition Engine", SAE Technical Paper No. 950686, 1995.
93. S. Imabeppu, H. Shimonosono, Y. Hirano, K. Fujigaya and K. Inoue, "Deveopment of a Method for Predicting Heat Transfer to Engine Coolant", SAE Technical Paper No. 931114, 1993.
94. D.J. Hayden, " Investigation and Modelling of Thermal Condition in Spark Ignition Engine and after Treatment Systems", PhD thesis Thesis, University of Nottingham, 1995.
95. B.T. Lunden, J.H. Povolny and L.J. Chelko, "Correlation of Cylinder Head Temperature and Coolant Heat Rejection of a Multi-Cylinder Liquid Cooled Engine of 1710 cubic inch Displacement,". NASA report 931, 1949.
96. J.H. Povolny, L.J. Bogdan and L.J. Chelko, "Cylinder Head Temperatures and Coolant Heat Rejection of a Multi-Cylinder Liquid Cooled Engine of 1650 cubic inch Displacement", NACA TN 2069, 1950
97. C.F. Taylor, "The Internal Combustion Engine in Theory and Practice" MIT Press, 1985.

References

98. C. Depcik and D. Assanis, "A Universal Heat Transfer Correlation for Intake and Exhaust Flows in an Spark-Ignition Internal Combustion Engine", SAE Technical Paper No. 2002-01-0372, 2002.
99. S. Meisner and S.C. Sorenson, "Computer Simulation of Intake and Exhaust Manifold Flow and Heat Transfer", SAE Technical Paper No. 860242, 1986.
100. G.F. Hohenberg, "Advance approaches for heat transfer calculation." SAE Technical Paper No. 790825, 1979.
101. L.G. Dodge, "Fuel Preparation Requirements for Direct-Injected Spark-Ignition Engines", SAE Technical Paper No. 962015, 1996.
102. G. Woschni, "A Universally Applicable Equation for the Instantaneous Heat Transfer Coefficient in the Internal Combustion Engine", SAE Technical Paper No. 670931, 1967.
103. S.D. Hires and G.L. Pochmara, "An Analytical Study of Exhaust Gas Heat Loss in Piston Engine Exhaust Port", SAE Technical Paper No. 760767, 1976.
104. J.A.Caton and J.B. Heywood, "An Experimental and Analytical Study of Heat Transfer in an Engine Exhaust Port", *Int. J. Heat Mass Transfer*, **24**(4): p. 581-595, 1981.
105. National Institute of Standards and Technology (NIST) <http://www.physics.nist.gov/cuu/Uncertainty/>, Accessed Dec. 2010.
106. "Product Information: Micro Motion Coriolis Flow meter". Fisher-Rosemount, 1995.
107. "Technical Information: Promag F Electromagnetic Flow Measuring System". Endress+Hauser, 1996.
108. "Instruction Manual". Horiba, 2001.
109. A.L. Randolph, "Methods of Processing Cylinder-Pressure Transducer Signals to Maximize Data Accuracy", SAE Technical Paper No. 900170, 1990.
110. M.F.J. Brunt and C.R. Pond, "Evaluation of Techniques for Absolute Cylinder Pressure Correction", SAE Technical Paper No. 970036, 1997.

Tables

CHAPTER 2

| Fuel properties | Gasoline | Ethanol |
|--|-----------------------|------------|
| Chemical formula | C_8H_{15} (typical) | C_2H_5OH |
| Molecular weight (kg/kmol) | 111.21 | 46.07 |
| Oxygen contents (wt %) | 0.00 | 34.73 |
| RON | 92-98 | 107 |
| MON | 80-90 | 89 |
| Reid vapour Pressure [kPa] | 61.4 | 19.3 |
| Enthalpy of vaporisation [kJ/kg] | 305 | 840 |
| Calorific value [MJ/kg] | 31.2 | 26.9 |
| Stoichiometric air/fuel ratio [kg air/kg fuel] | 14.51 | 9.0 |
| Boiling temperature [°C] | 34-207 | 78.3 |

Table 2.1. A comparison between the physiochemical properties of gasoline and ethanol[17].

| | | Limit values for passenger cars (Category M) and light commercial vehicles (Category N1-I) | | | | |
|--------|-----------|--|------|-------|-----------------|--------|
| | | CO | THC | NMHC | NO _x | PM |
| | | g/km | g/km | g/km | g/km | g/km |
| Euro 4 | Jan 2005 | 1.00 | 0.1 | | 0.08 | |
| Euro 5 | Sept 2009 | 1.00 | 0.1 | 0.068 | 0.060 | 0.005* |
| Euro 6 | Sept 2014 | 1.00 | 0.1 | 0.068 | 0.060 | 0.005* |

*Applies only to vehicles with direct injection engines

Table 2.2. European emissions limits for gasoline fuelled passenger cars and light commercial vehicles[36].

CHAPTER 3

| Specification | |
|---------------------------|--------------------------------|
| Displacement | 1.6 L |
| Cylinder configuration | Inline 4-cyl |
| Injection type | Direct |
| Number of valves | 16 |
| Valve train configuration | DOHC |
| Block material | Aluminium |
| Compression ratio | 11.51:1 |
| Bore | 79mm |
| Piston Stroke | 81.4mm |
| Con-rod length | 133mm |
| Firing order | 1-3-4-2 |
| Injection timing | 300 °BTDC (homogeneous charge) |
| IVO | 0° BTDC |
| EVC | 0° BTDC |

Table 3.1. Test Engine Specification.

| Emission Measured | Analyzer | Span gas used |
|---------------------|-----------------------------------|---|
| HCs | Flame Ionisation Detector (FID) | Propane or Methane equivalence. |
| NO _x | Heated vacuum chemiluminescence | 5000ppm NO |
| CO, CO ₂ | Infrared gas filter type analyser | 10% CO ₂ or 1% CO |
| O ₂ | paramagnetic oxygen analyzer | Zero grade air (20.9% O ₂ by volume) |

Table 3.2. Span gas used for different analyzers.

| Parameter | Mean | Standard Deviation | COV (%) |
|-------------------------------|--------|--------------------|---------|
| Load (Nm) | 60.6 | 0.58 | 1.0 |
| Speed (rpm) | 2008.5 | 7.78 | 0.4 |
| BMEP (bar) | 4.8 | 0.04 | 0.9 |
| Rail Pressure (bar) | 70.1 | 0.004 | 0.1 |
| MAP (bar) | 0.61 | 0.02 | 2.6 |
| Fuel mass flow rate (mg/s) | 1.02 | 0.04 | 3.9 |
| Coolant Heat transfer (kWatt) | 13.97 | 0.39 | 2.8 |
| Lambda | 1.00 | 0.01 | 0.8 |
| IMEPn (bar) | 5.18 | 0.15 | 2.8 |
| IMEPg (bar) | 5.64 | 0.14 | 2.6 |
| Peak Pressure (bar) | 29.03 | 1.14 | 3.9 |
| Exhaust port temp. (°C) | 632.1 | 14.04 | 2.2 |
| Intake air union temp. (°C) | 26.3 | 2.57 | 9.8 |
| Oil temp. (°C) | 101.8 | 3.83 | 3.8 |
| NOx (ppm) | 2067.5 | 89.51 | 4.3 |
| HC (ppm C1) | 2439.9 | 171.00 | 7.0 |
| CO (%) | 1.26 | 0.03 | 2.3 |
| O ₂ (%) | 1.28 | 0.04 | 3.3 |
| CO ₂ (%) | 13.31 | 0.39 | 2.9 |

Table 3.3. Standard reference point data variation over 20 tests.

CHAPTER 4

| Fuel properties | Gasoline | E10 | E20 | E50 | E85 | E100 |
|--|----------|--------|--------|-------|-------|-------|
| Molecular weight (kg/kmol) | 111.21 | 107.76 | 100.90 | 80.31 | 56.29 | 46.07 |
| AFR _{stoich} [kg air/kg fuel] | 14.54 | 13.95 | 13.08 | 11.66 | 9.75 | 9.00 |
| Oxygen contents (wt %) | 0.00 | 3.2% | 9.9% | 24.1% | 34.7% | 34.7% |
| H/C ratio | 1.88 | 1.95 | 2.03 | 2.31 | 2.76 | 3.00 |
| Calorific value[MJ/kg] | 43.66 | 42.98 | 42.21 | 39.10 | 32.60 | 27.74 |
| Boiling temperature [°C] | 34-207 | - | - | - | - | 78.3 |
| Density [kg/l] | 0.742 | 0.747 | 0.752 | 0.766 | 0.783 | 0.785 |

Table 4.1. Properties of tested fuel blends.

| | BMEP 4.72 bar/2000rpm °BTDC | BMEP 7.87bar/2000rpm °BTDC |
|-----------------|--------------------------------|-------------------------------|
| Gasoline | 14.3 | 12.25 |
| E10 | 14.5 | 12.7 |
| E20 | 13.5 | 12.5 |
| E50 | 13.75 | 12.8 |
| E85 | 13.9 | 11.7 |

Table 4.2. MBT spark timings at different loads and constant speed.

| | Gasoline C _{8.26} H _{15.5} | Ethanol C ₂ H ₅ OH |
|----------------------|---|---|
| a₁ | -24.078 | 6.99 |
| a₂ | 256.63 | 39.741 |
| a₃ | -201.68 | -11.926 |
| a₄ | 64.75 | 0 |
| a₅ | 0.5808 | 0 |
| a₆ | -27.562 | -60.214 |

Table 4.3. Coefficients for calculation of enthalpy of formation $\bar{h}_{f,i}^o$ from polynomial equation 4.6 for gasoline and ethanol [71].

CHAPTER 5

| Variable | Range |
|---------------------------|---------------|
| Speed | 1500-4000 rpm |
| BMEP | 1.57-8 bar |
| Equivalence ratio, ϕ | 0.8-1.25 |
| EGR | 0-20% |

Table 5.1. Engine running conditions.

| | Low load | Medium load |
|----------|----------|-------------|
| Gasoline | 19.60% | 20.01% |
| E10 | 21.02% | 21.5% |
| E20 | 21.2% | 20.5% |
| E50 | 21.2% | 18.99% |
| E85 | 21.8% | 21.8% |

Table 5.2. Maximum EGR allowed for a stable combustion assuming COV_{IMEP_n} limit of 10%.

CHAPTER 6

| Coolant Temp. (°C) | Specific Heat, c_p (kJ/kg °C) |
|-----------------------|------------------------------------|
| 40 | 3.385 |
| 50 | 3.432 |
| 60 | 3.474 |
| 70 | 3.515 |
| 80 | 3.556 |
| 90 | 3.598 |
| 100 | 3.637 |
| 110 | 3.677 |
| 120 | 3.703 |
| 130 | 3.730 |
| 140 | 3.753 |
| 150 | 3.776 |

Table 6.1. Heat capacity c_p for engine coolant (50% water and 50% Ethylene Glycol by volume).

| Geometry | $Gr_f Pr_f$ | C | m |
|--|------------------|-------|-----|
| Vertical planes | 10^4-10^9 | 0.59 | 1/4 |
| | 10^9-10^{13} | 0.021 | 2/5 |
| Horizontal upper surface of heat plates | $2*10^4-8*10^6$ | 0.54 | 1/4 |
| | $8*10^6-10^{11}$ | 0.15 | 1/3 |
| Horizontal lower surface of heated plate | 10^5-10^{11} | 0.27 | 1/4 |

Table 6.2. Constants for use in equation 6.6 developed by several researchers and obtained from Holman [87].

| Fuel | Time to oil 40 °C, s | Time to oil 60C, s | Time to oil 80C, s |
|-----------------|----------------------|--------------------|--------------------|
| E100 | 287.5 | 454.5 | 751 |
| E75 | 280 | 450 | 745 |
| E50 | 277.5 | 445.5 | 749 |
| Gasoline | 269.5 | 433 | 725.5 |

Table 6.3. Time in seconds needed for each fuel to reach a particular oil temperature.

CHAPTER 7

| Author(s) | Nusselt-Reynolds Relation | Notes |
|----------------------------|----------------------------|---------------------------|
| Hires and Pochmara [103] | $Nu = 0.258 Re^{0.8}$ | SI Engine exhaust port |
| Caton and Heywood [104] | $Nu = 0.358 Re^{0.6}$ | SI Engine exhaust port |
| Meisner and Sorenson [99] | $Nu = 0.0774 Re^{0.769}$ | SI Engine exhaust port |
| Shayler <i>et al.</i> [88] | $Nu \approx 0.18 Re^{0.7}$ | Both diesel and SI engine |

Table 7.1. Summary of the main exhaust port correlations.

Figures

CHAPTER 1

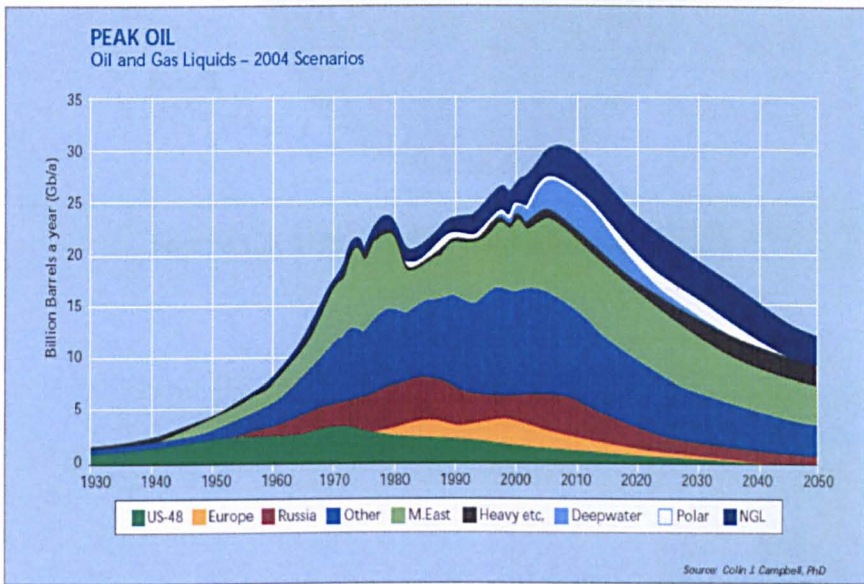


Figure 1.1. Historical world oil production and projection of trend [2].

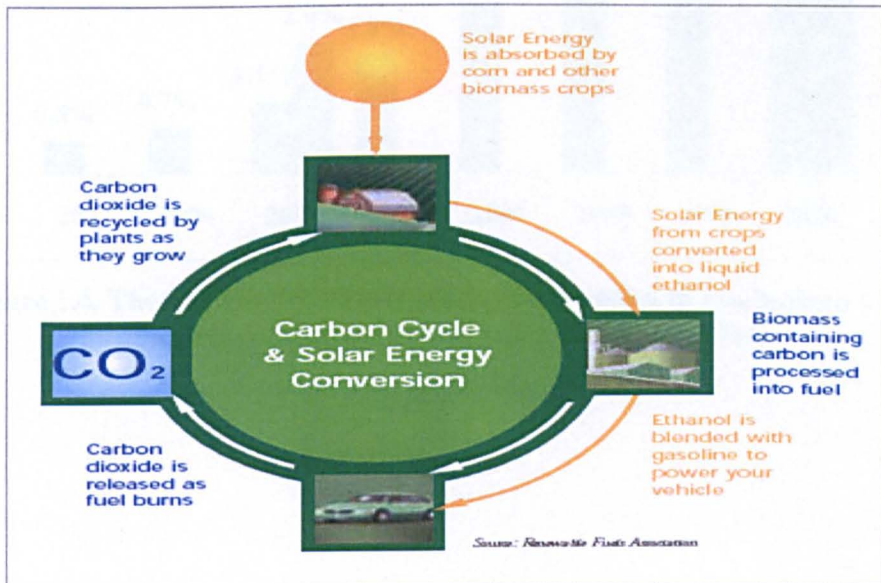


Figure 1.2. Schematic diagram showing the complete well-to-wheel cycle of ethanol [2].

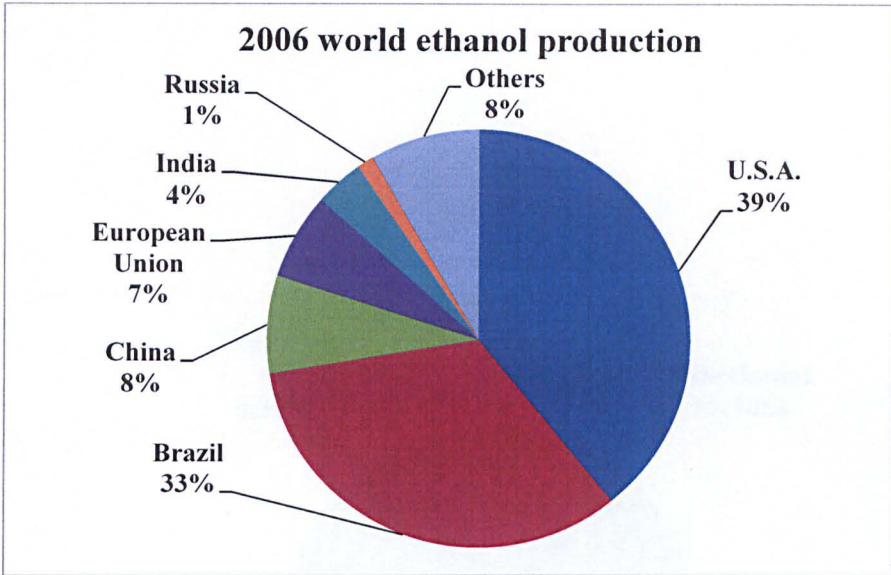


Figure 1.3. 2006 ethanol world production [2].

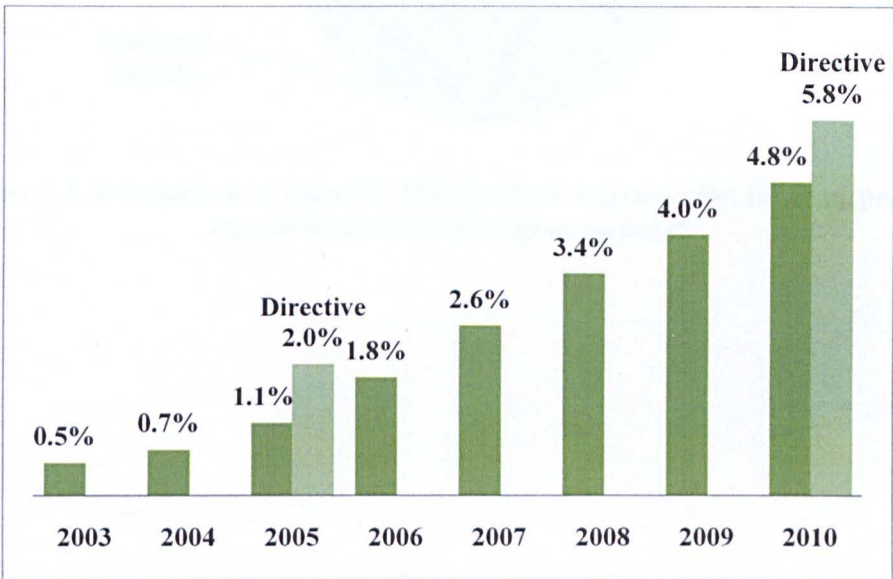


Figure 1.4. The increase trend in biofuels consumption in comparison to the objectives of the biofuels directive (2003/30/EC) [4].

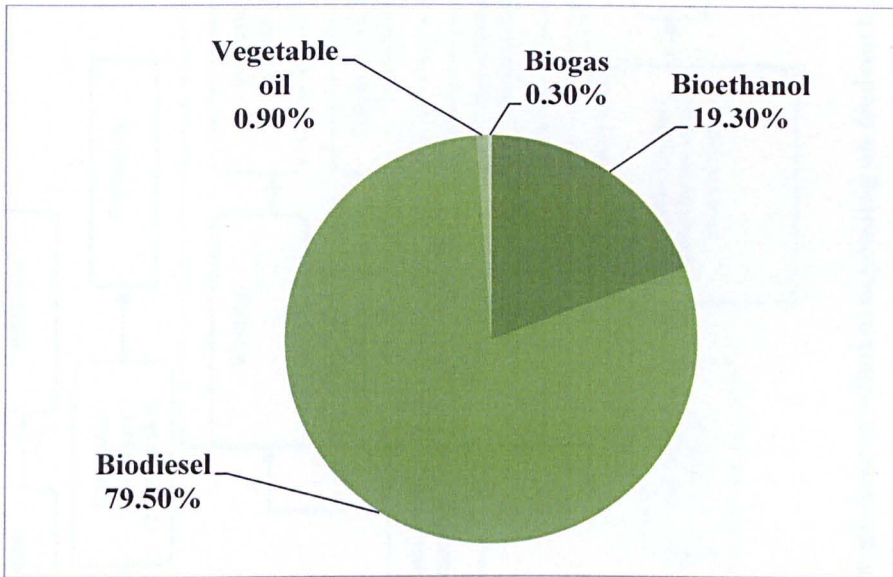


Figure 1.5. Breakdown of total EU 2009 biofuels consumption for transport by type of biofuel and energy content.[4].

CHAPTER 2

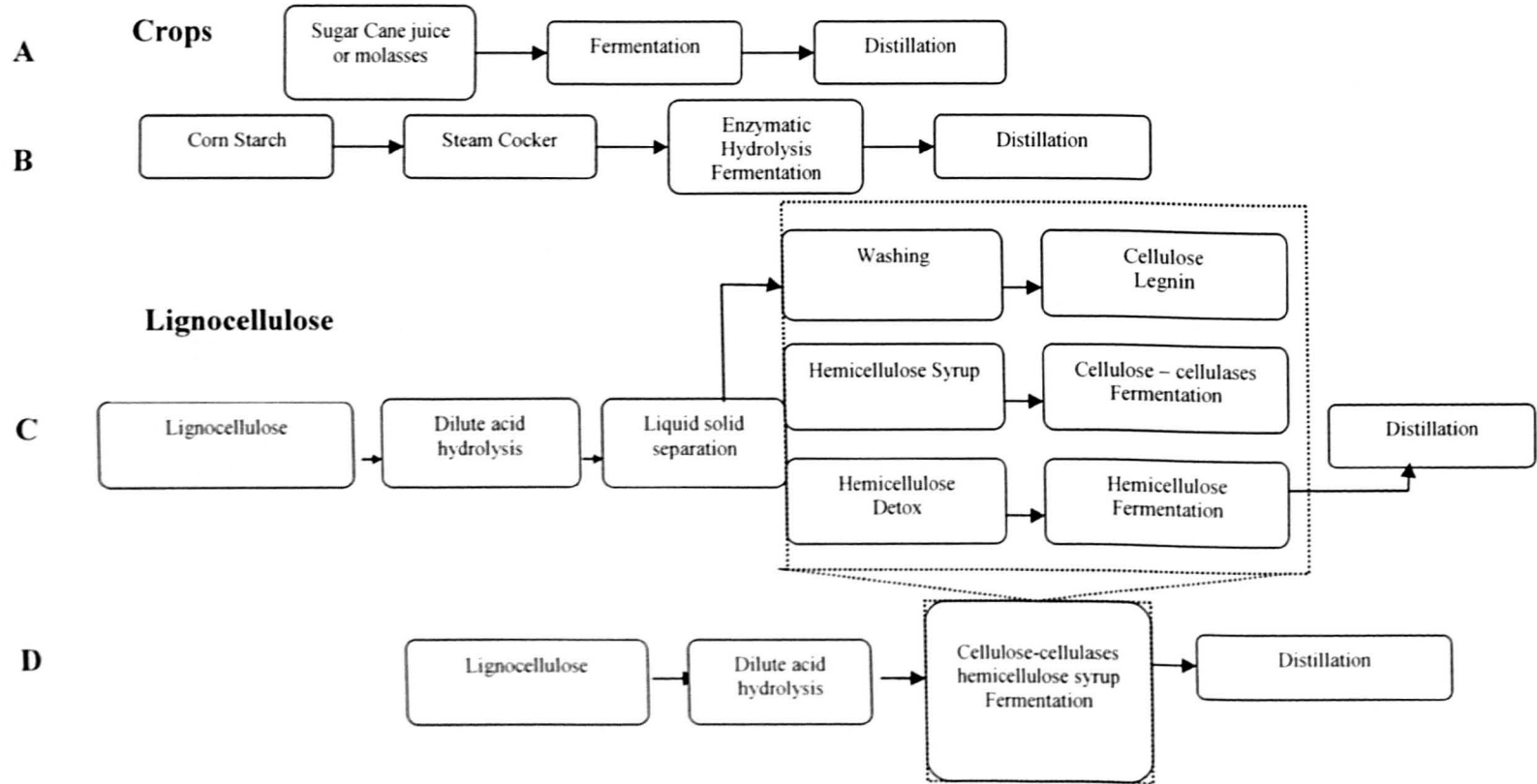


Figure 2.1. Illustration of different production methods of ethanol depending on feedstock [1].

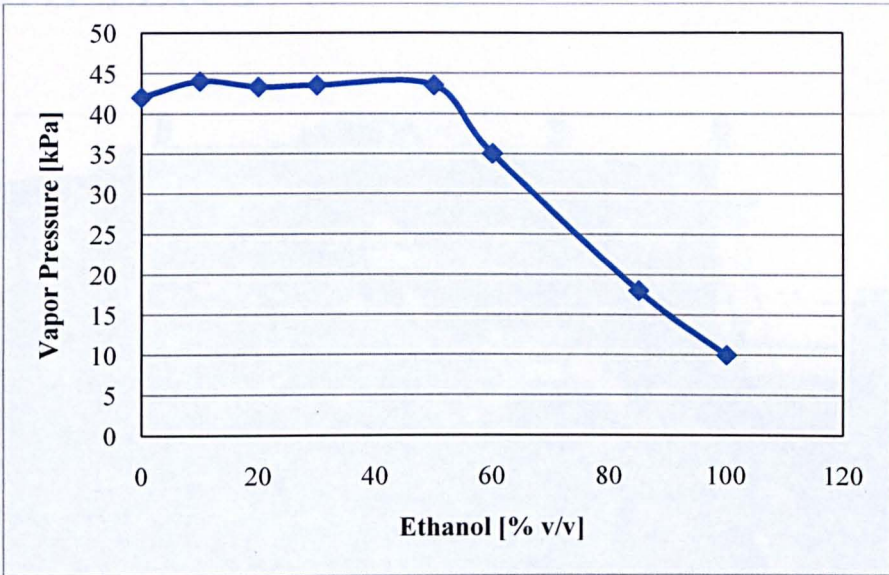


Figure 2.2. Vapour pressure as a function of ethanol content plotted from data obtained from Kar et al [24].

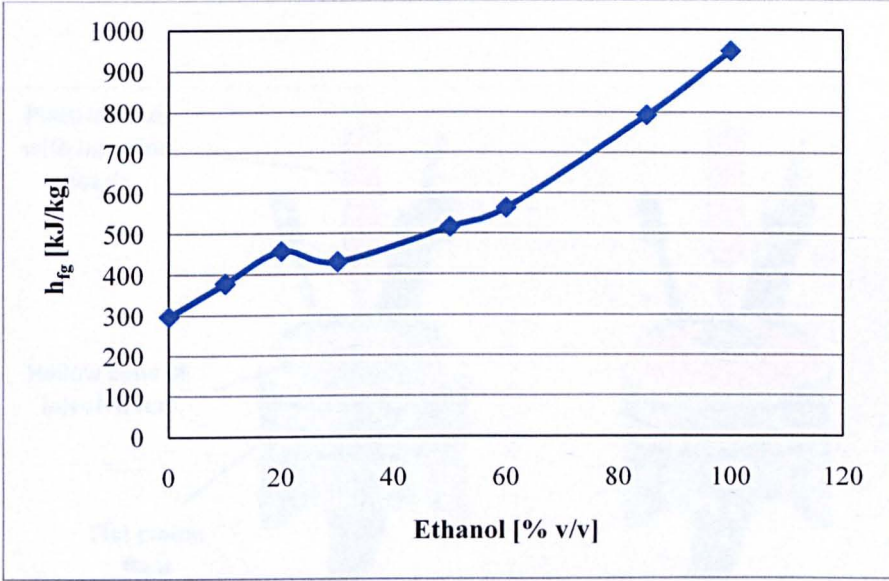


Figure 2.3. Enthalpy of vaporisation as a function of ethanol content, data obtained from Kar et al [24].

CHAPTER 3

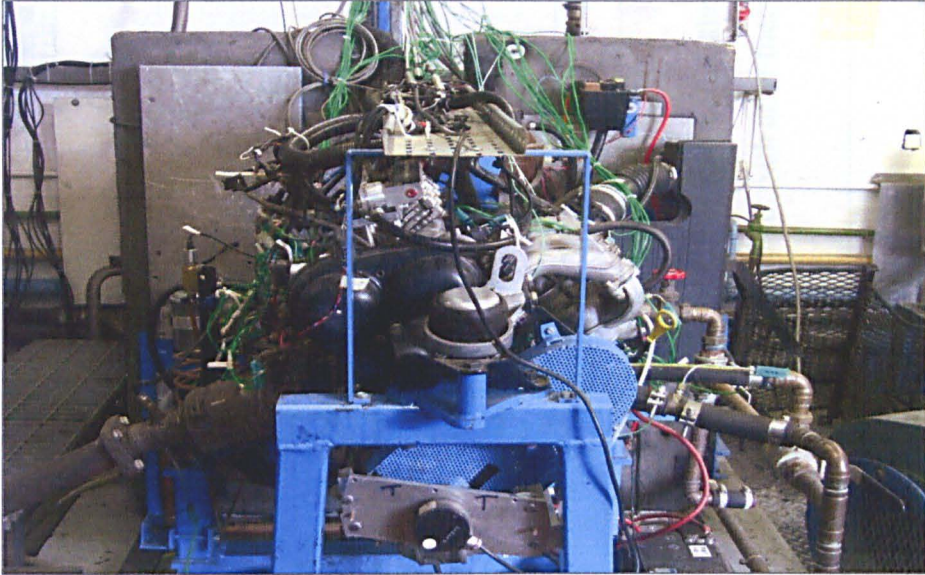


Figure 3.1. SGDI Engine Research Facility.

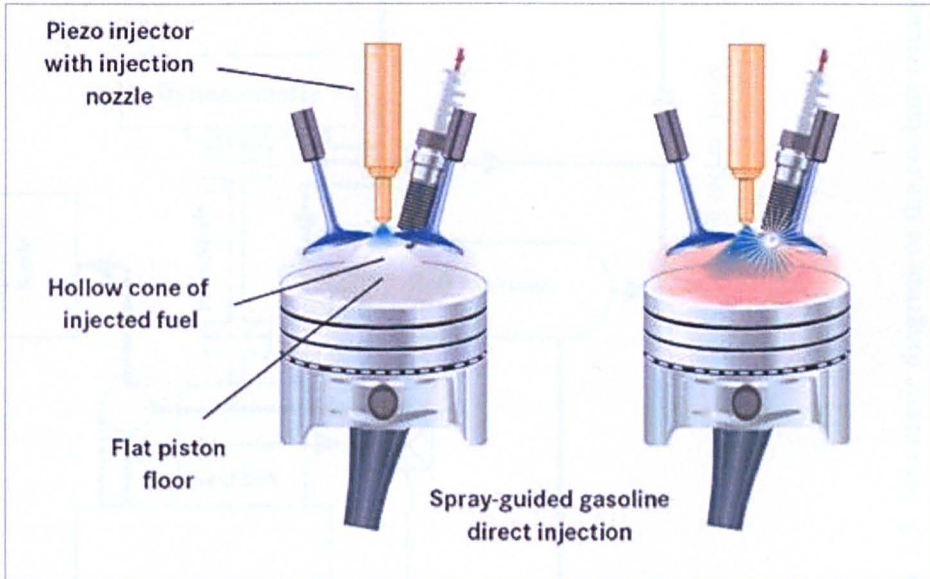


Figure 3.2. Spray-guided gasoline direct injection system, SGDI, a hollow cone of fuel forms at the injection nozzle. This cloud of fuel and air remains stable up until the precise moment when it is required to ignite [45].

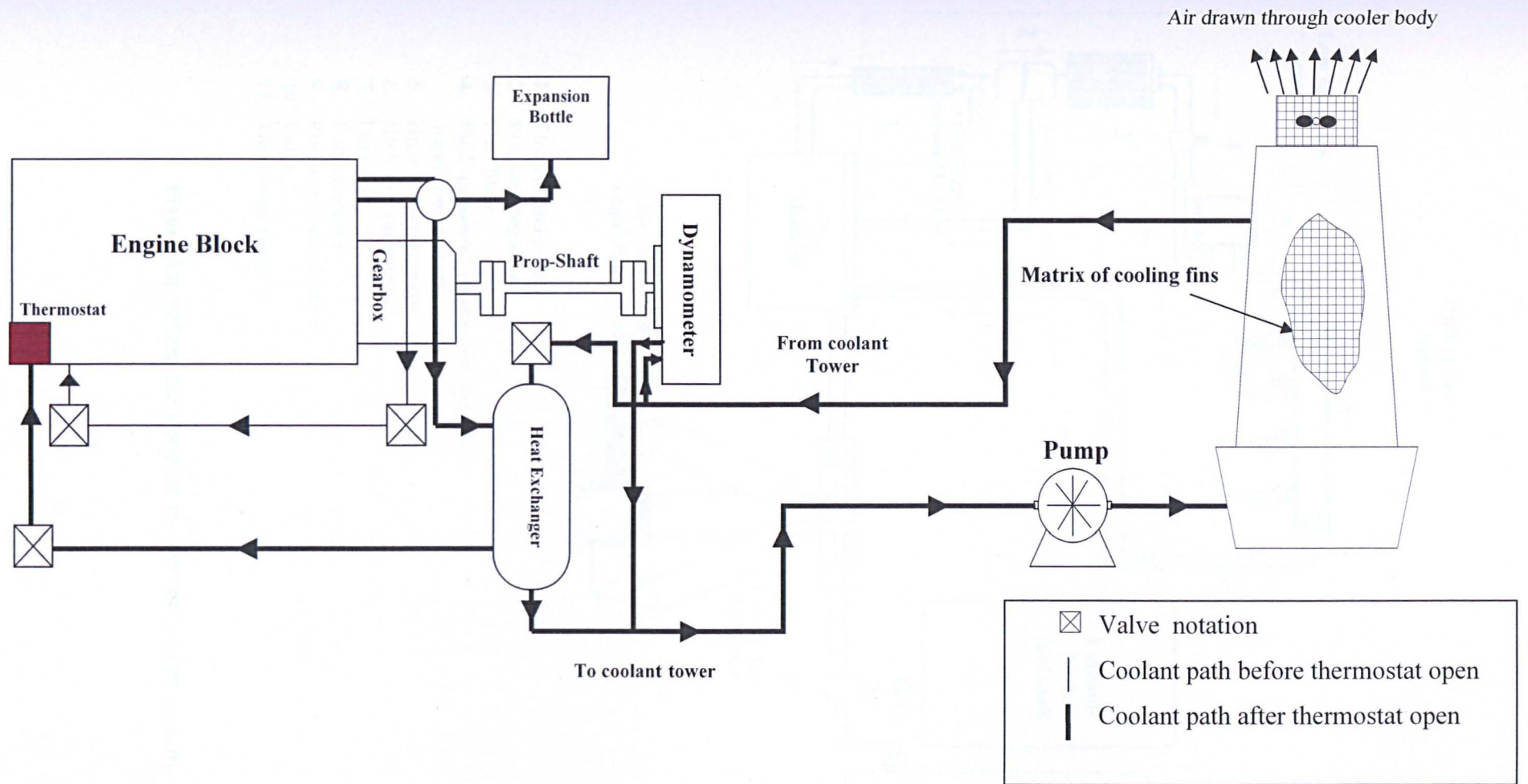
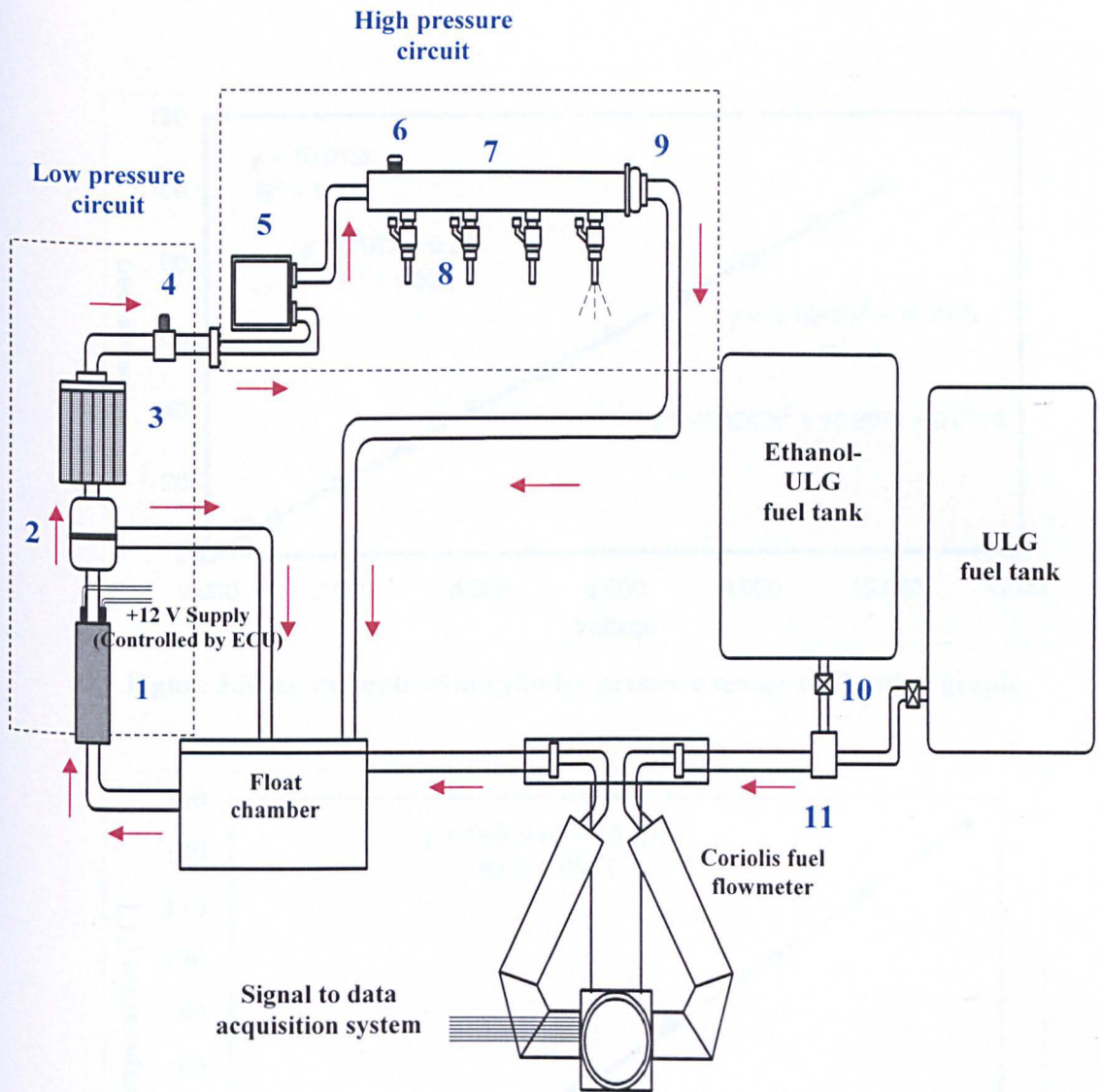


Figure 3.3. Schematic diagram of the coolant circuit of 1.6L SGDI engine test facilities.



1. Electric fuel pump
2. Pressure regulator
3. Fuel filter
4. Fuel pressure sensor (to the data acquisition system)
5. High pressure pump
6. High pressure sensor
7. Fuel rail
8. Fuel injectors
9. Pressure control valve
10. Valve
11. Three-way valve

Figure 3.4. Schematic diagram for the fuel supply system.

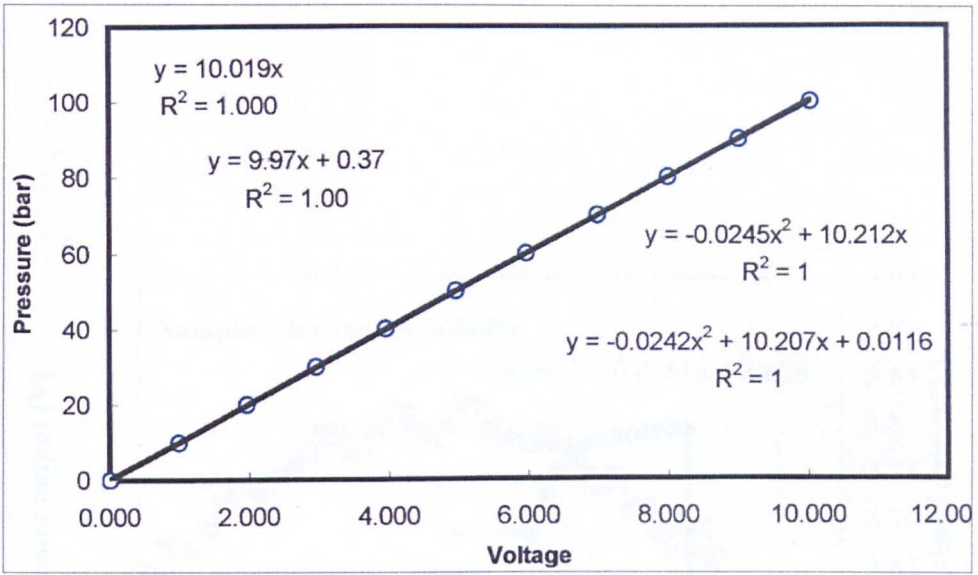


Figure 3.5. An example of in-cylinder pressure sensor calibration graph.

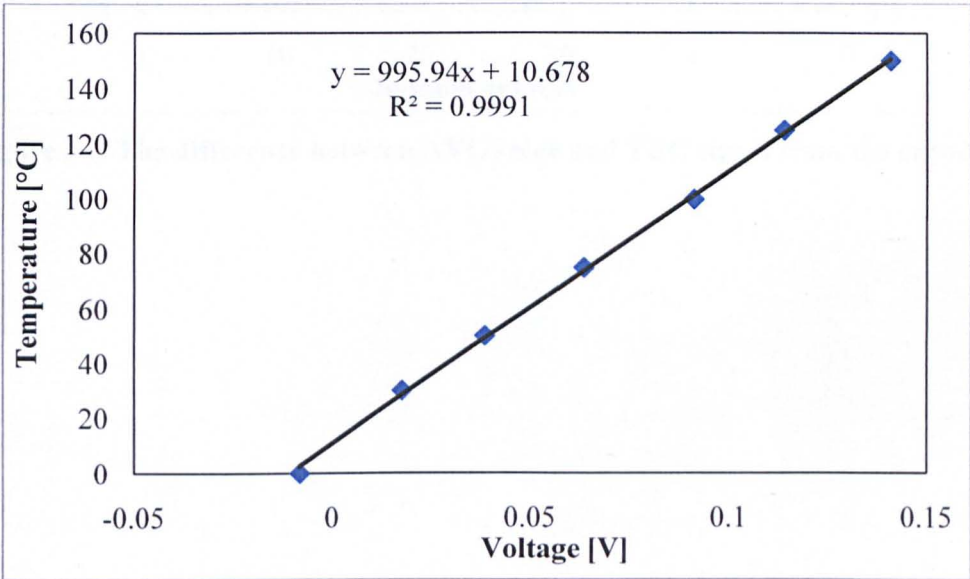


Figure 3.6. An example of a thermocouple calibration graph.

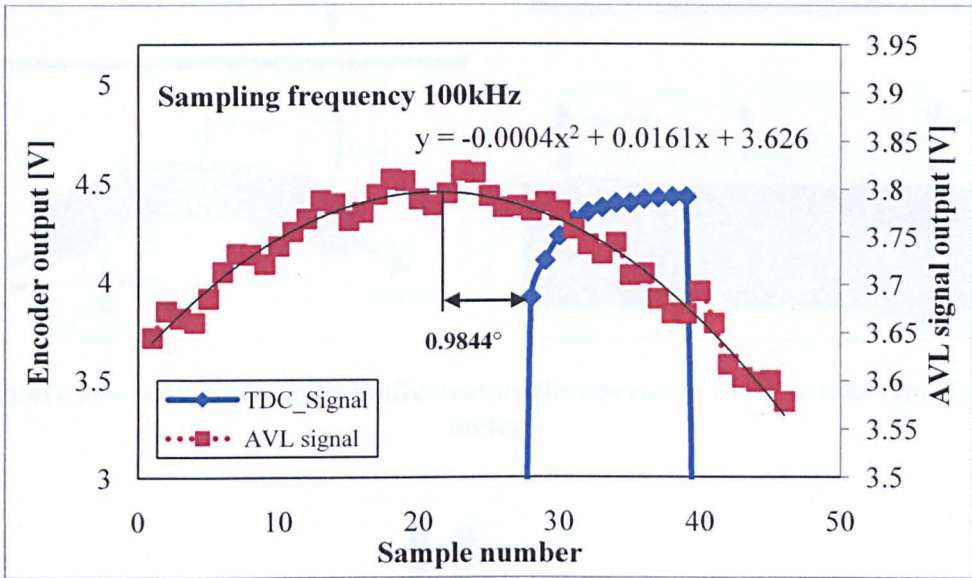


Figure 3.7. The difference between AVL value and TDC signal from the encoder.

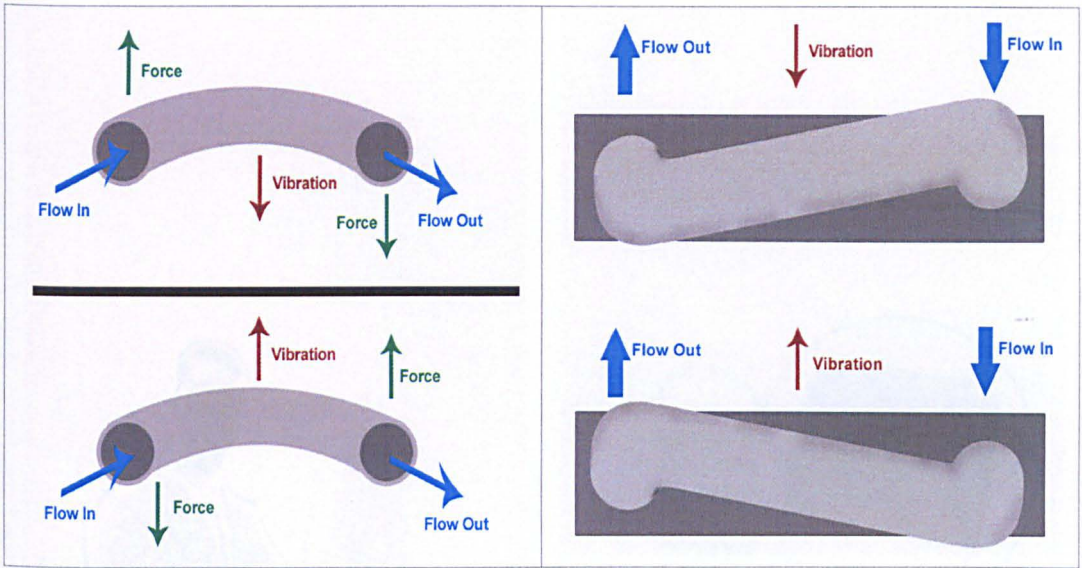


Figure 3.8. Schematic diagram illustrating the operation of a Coriolis type flow meter.

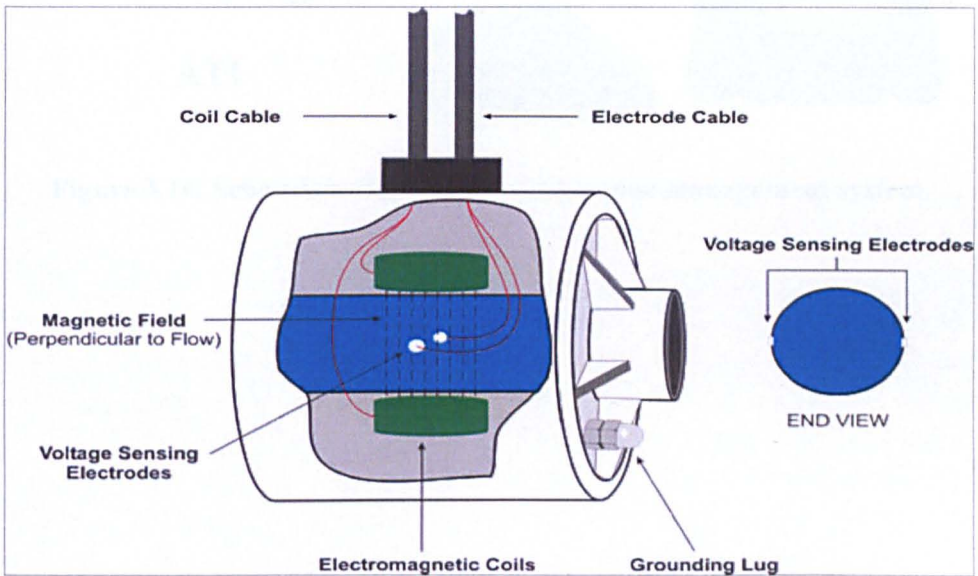


Figure 3.9. Schematic diagram illustrating the operation of an electromagnetic volume flow meter.

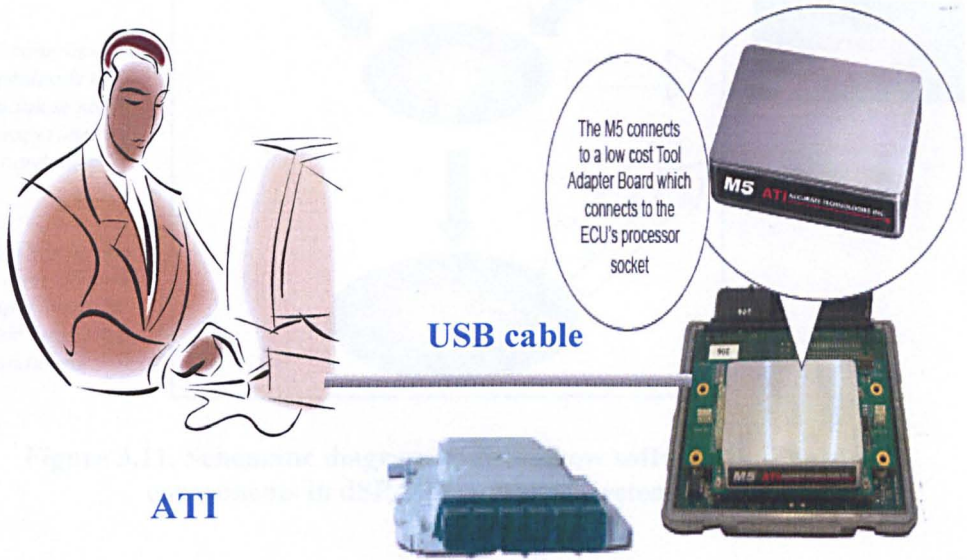


Figure 3.10. Schematic diagram for ATI engine management system.

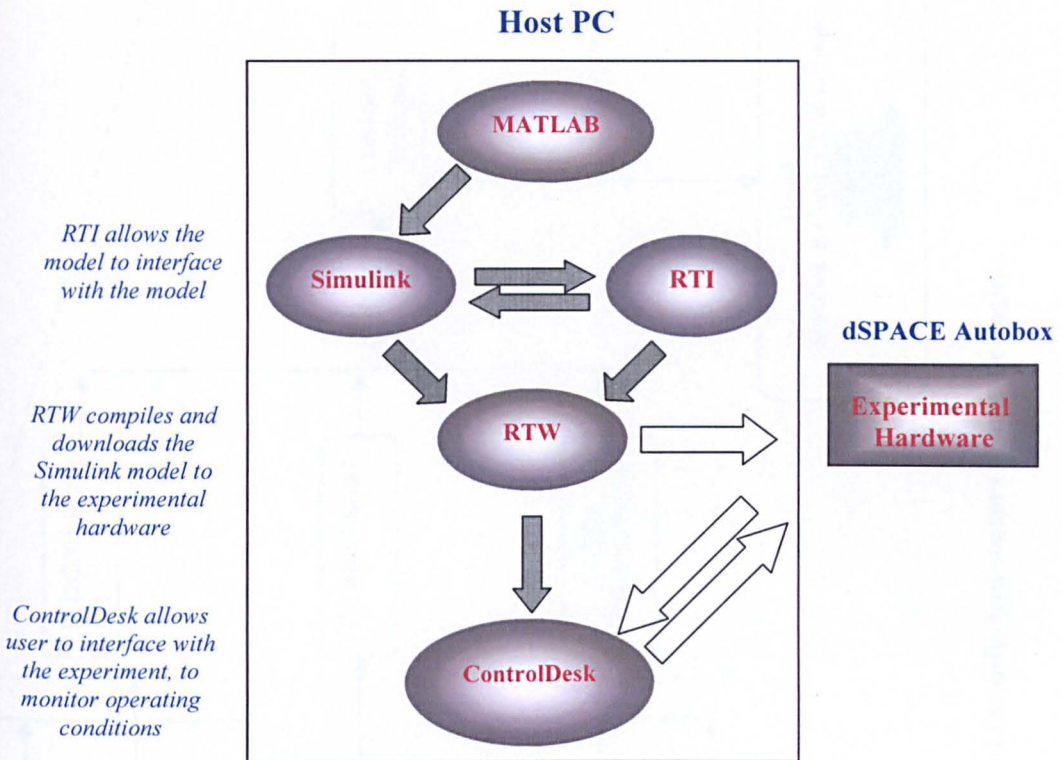


Figure 3.11. Schematic diagram showing how software and hardware components in dSPACE/Simulink system interact.

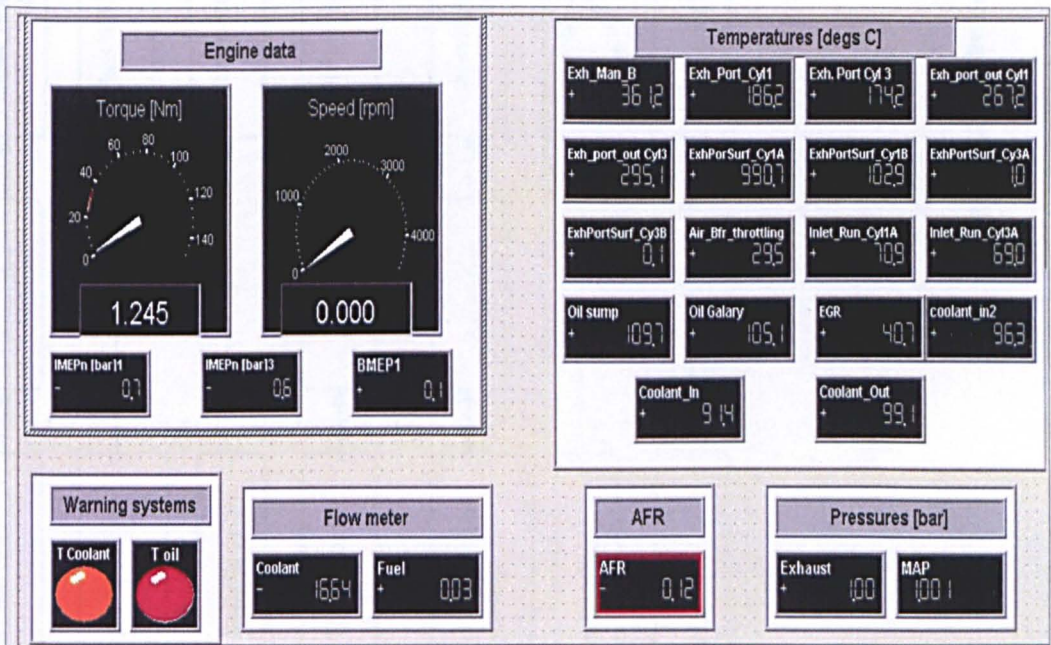


Figure 3.12. An example of ControlDesk layout utilised to monitor engine variables and output parameters.

Engine Sensors

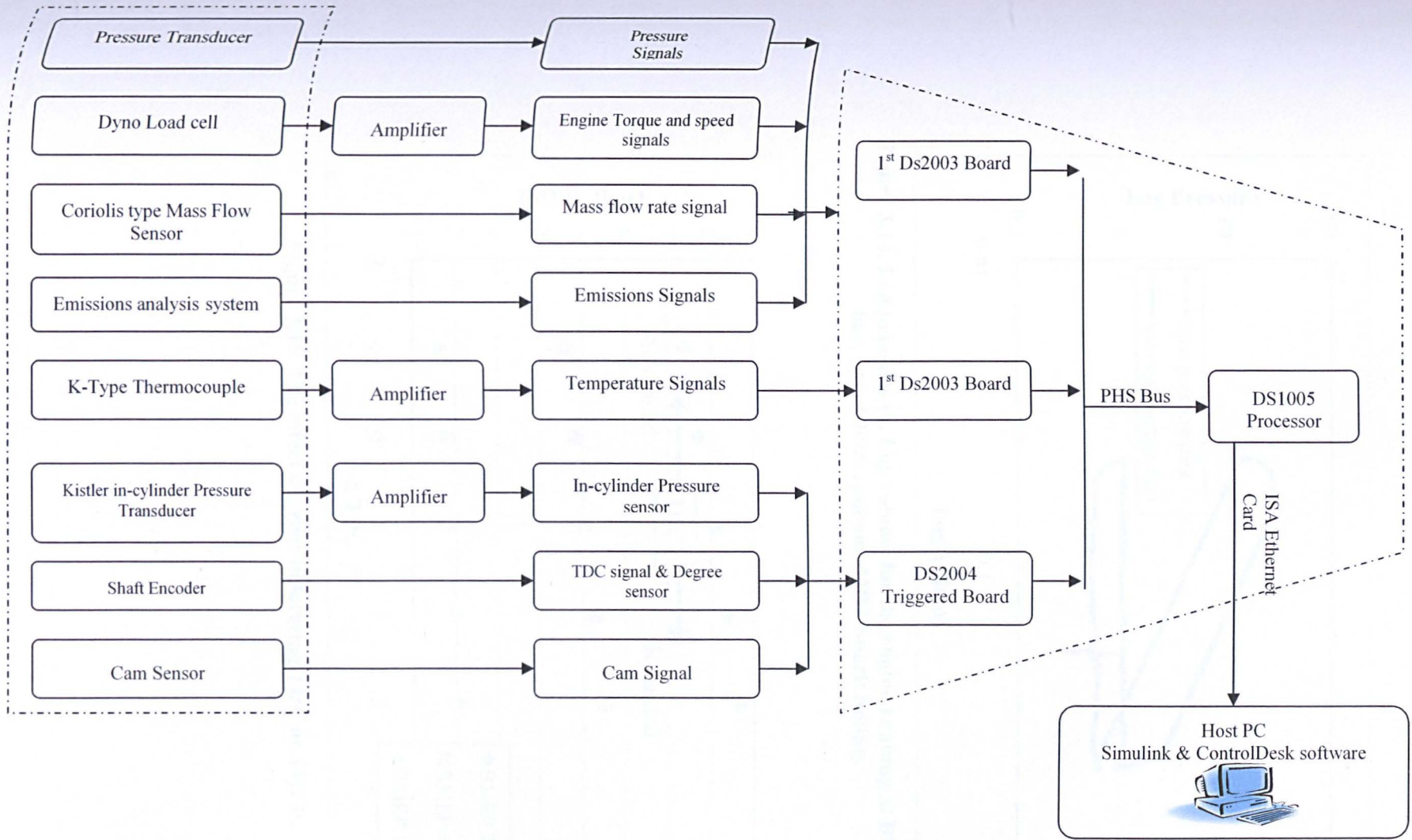


Figure 3.13. Schematic diagram of the different sensors inside the engine.

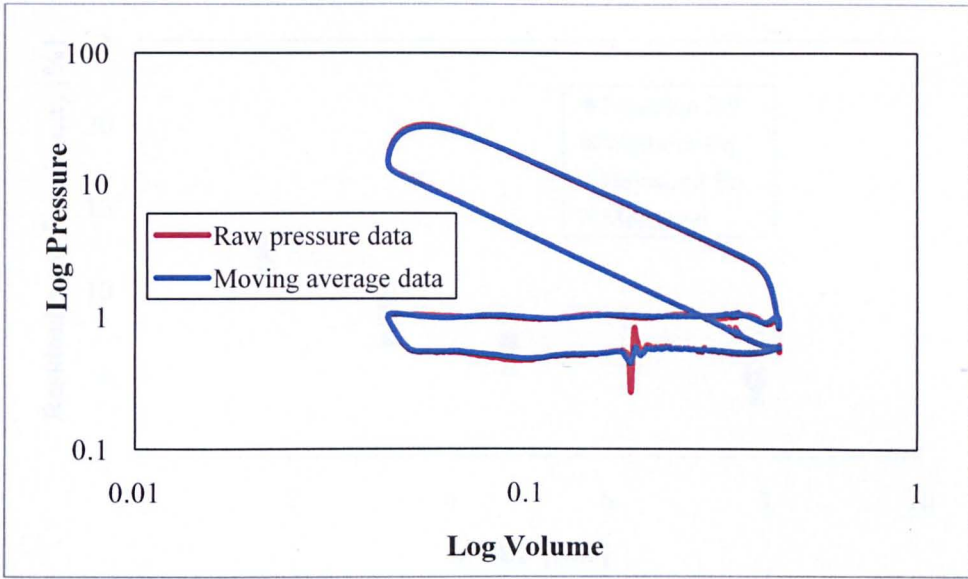


Figure 3.14. Log pressure vs. Log volume for the engine running at BMEP 4.75 bar, speed 2000 rpm and MBT Spark timing.

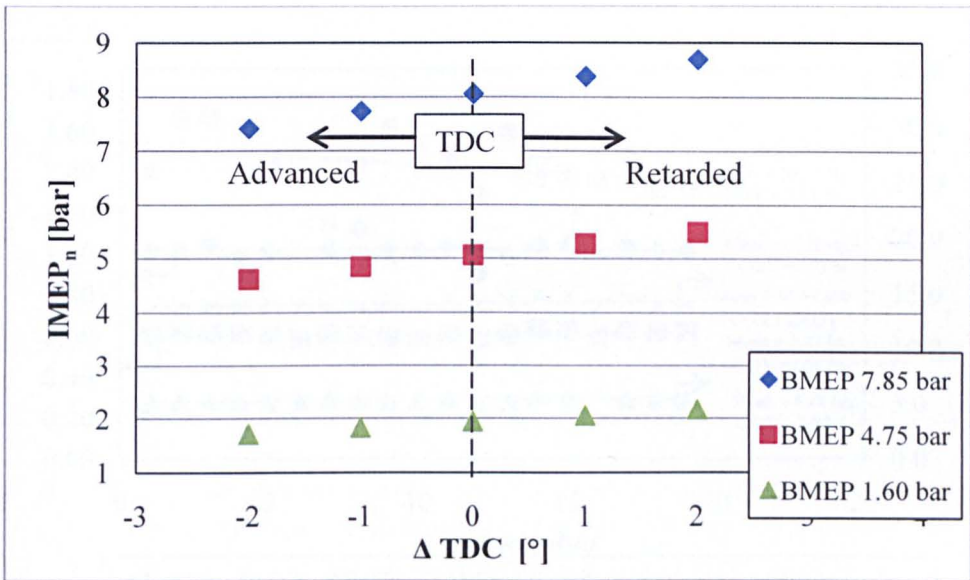


Figure 3.15. The effect of error in locating TDC on IMEP_n.

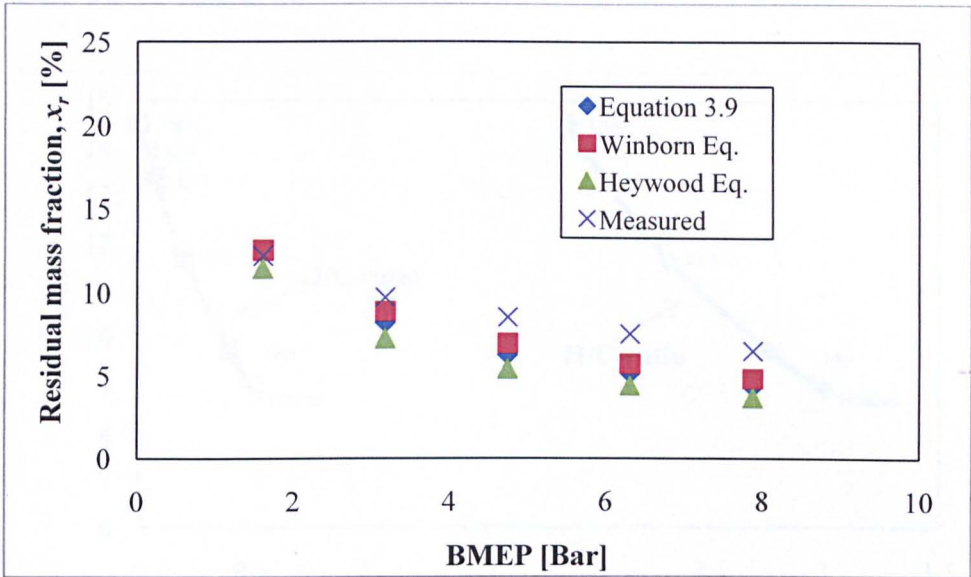


Figure 3.16. Comparison of residual mass fraction predictions made using Heywood equation[17], Winborn equation[67], Equation 3.9 and measured values from Bonatesta [68].

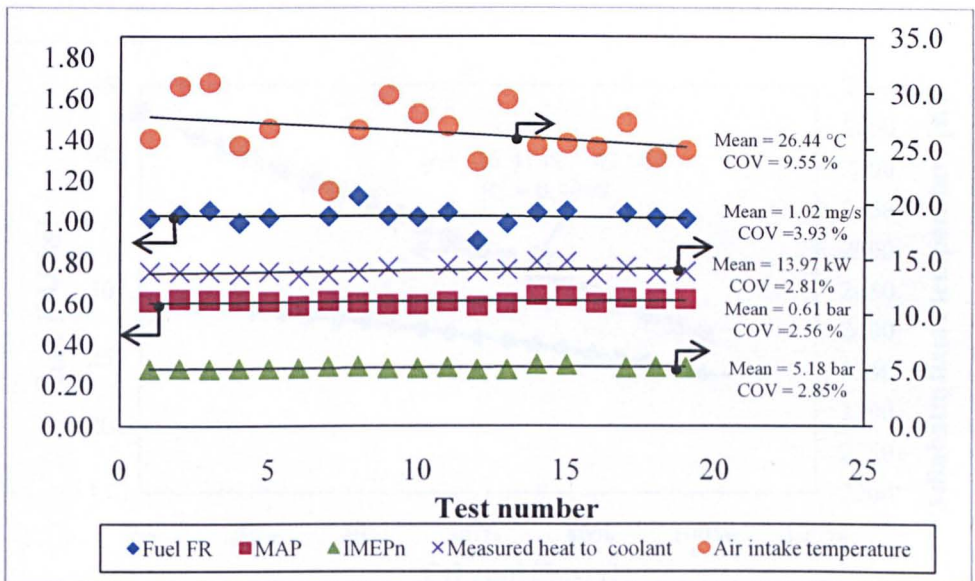


Figure 3.17. Variation of data at standard reference point, the engine is running at 4.75 bar BMEP and 2000 rpm. The data were taken over 18 months of experimental testing.

CHAPTER 4

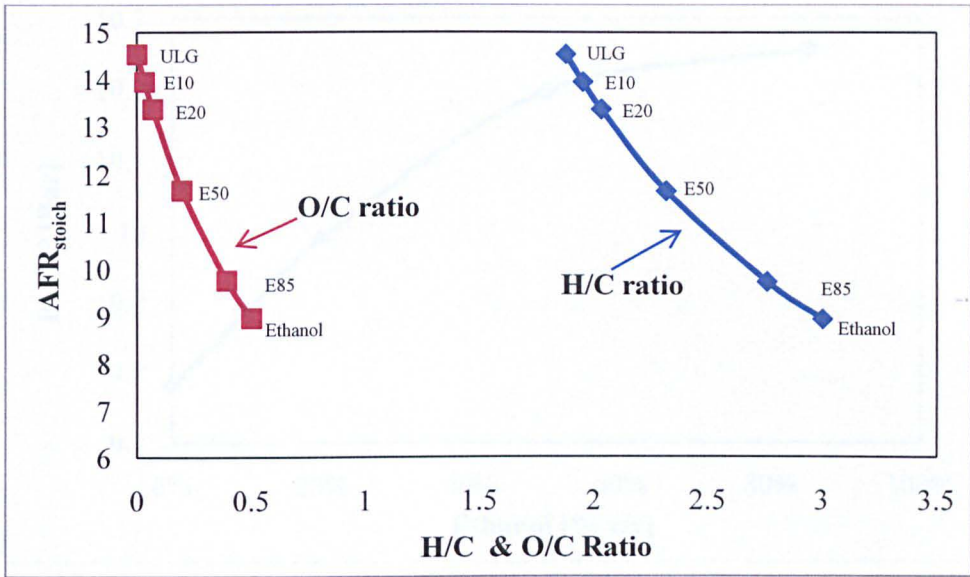


Figure 4.1. AFR_{stoich} as a function of H/C and O/C ratio, change of H/C and O/C was due to the change in ethanol percentage in the mixture.

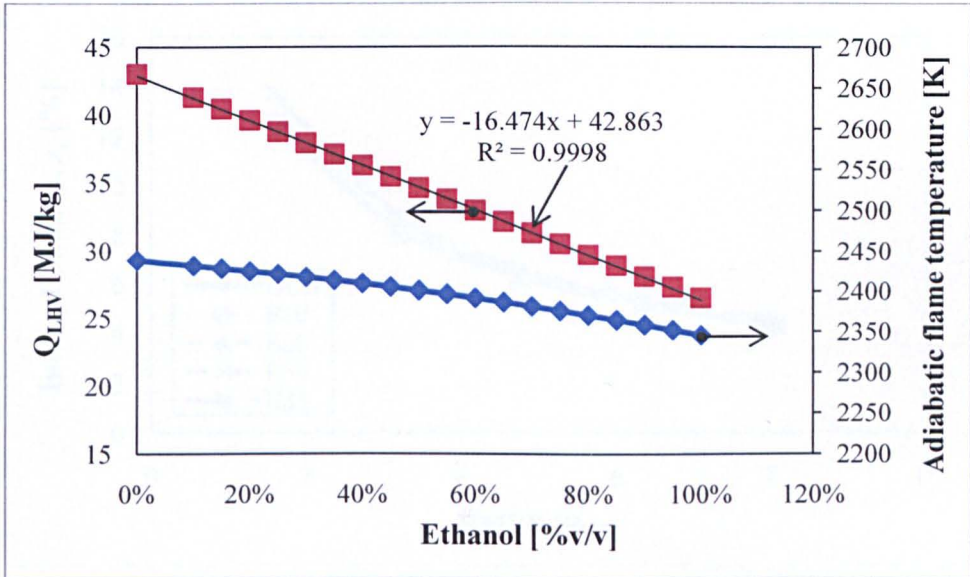


Figure 4.2. Adiabatic flame temperature and Q_{LHV} as a function of ethanol percentage in the fuel mixture.

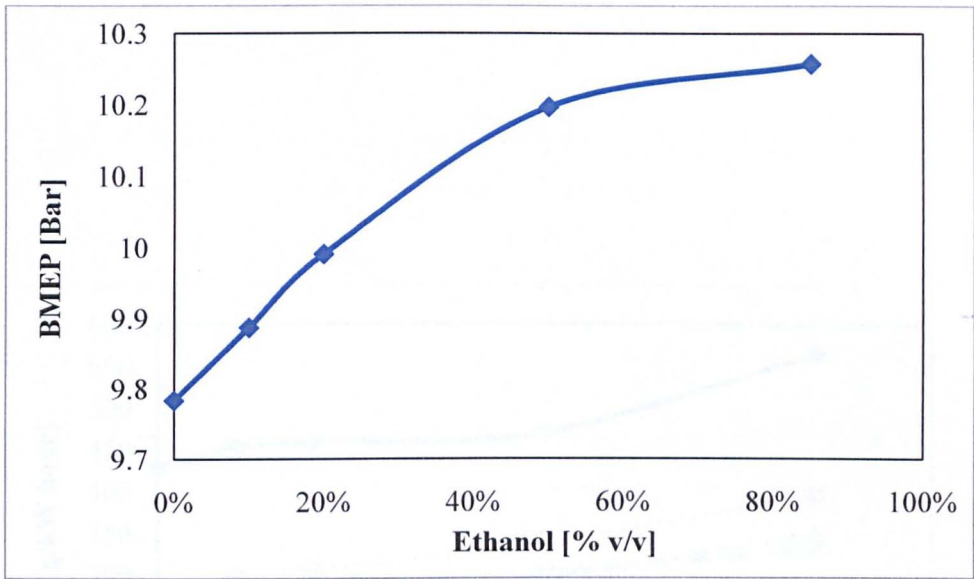


Figure 4.3. The effect of ethanol on engine performance at fixed amount of air introduced (WOT), constant ST and speed 2000 rpm.

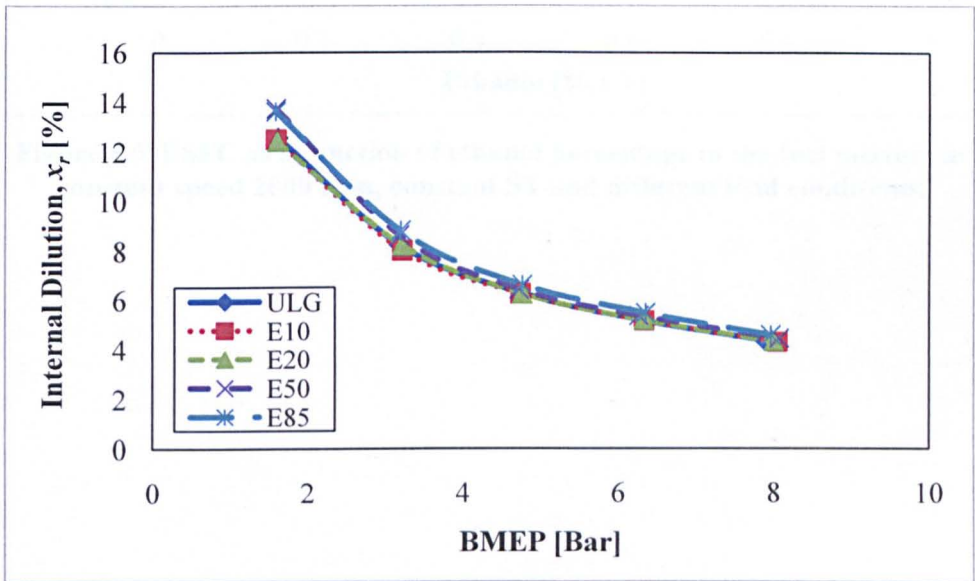


Figure 4.4. Internal dilution for different fuel mixtures as a function of BMEP.

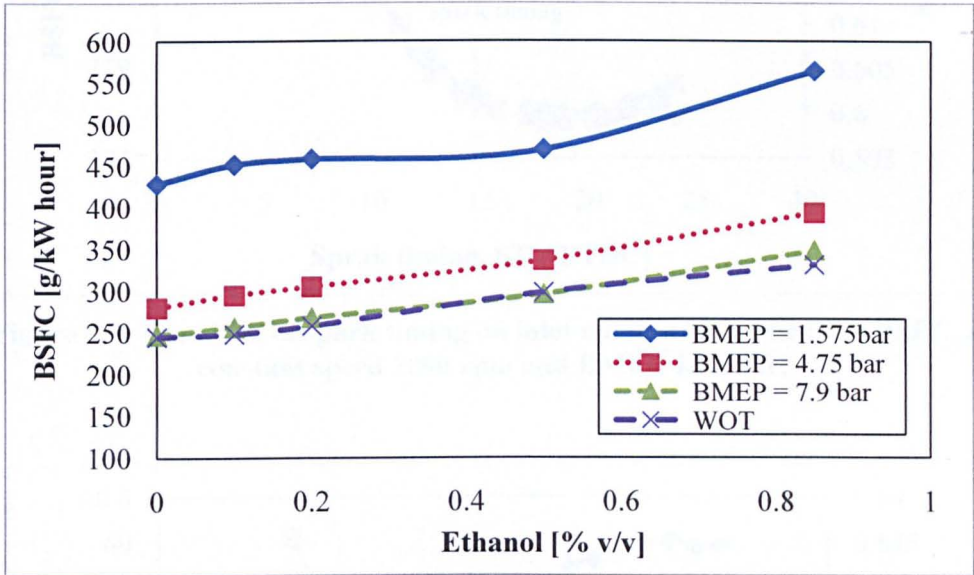


Figure 4.5. BSFC as a function of ethanol percentage in the fuel mixture at constant speed 2000 rpm, constant ST and different load conditions.

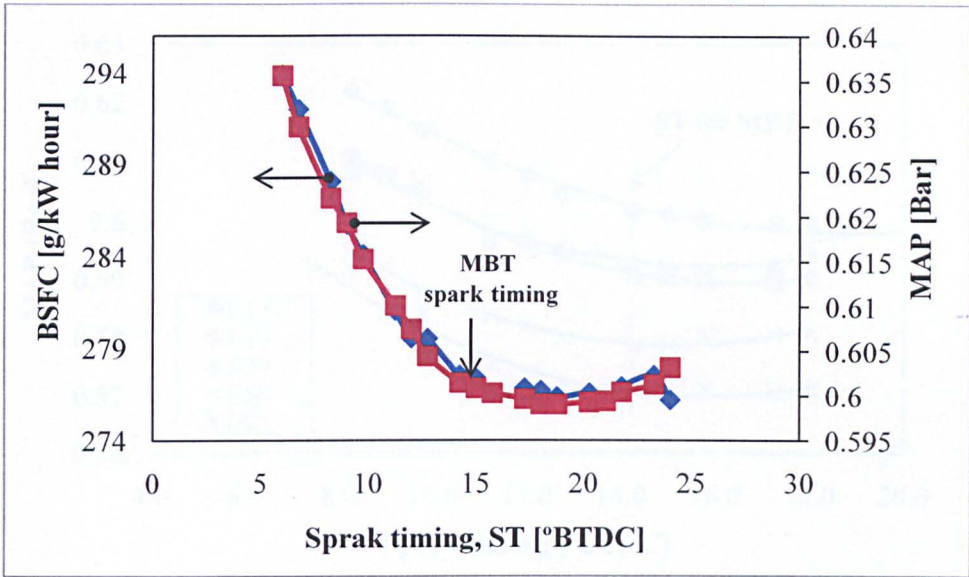


Figure 4.6. The effect of spark timing on inlet manifold pressure and BSFC, at constant speed 2000 rpm and BMEP 4.75 Bar.

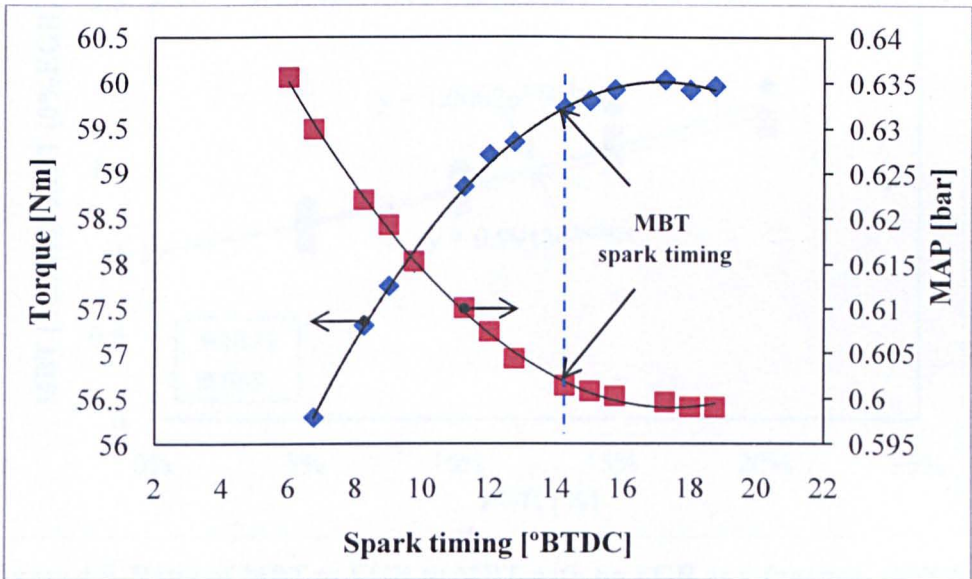


Figure 4.7. Comparison between two methods to determine MBT.

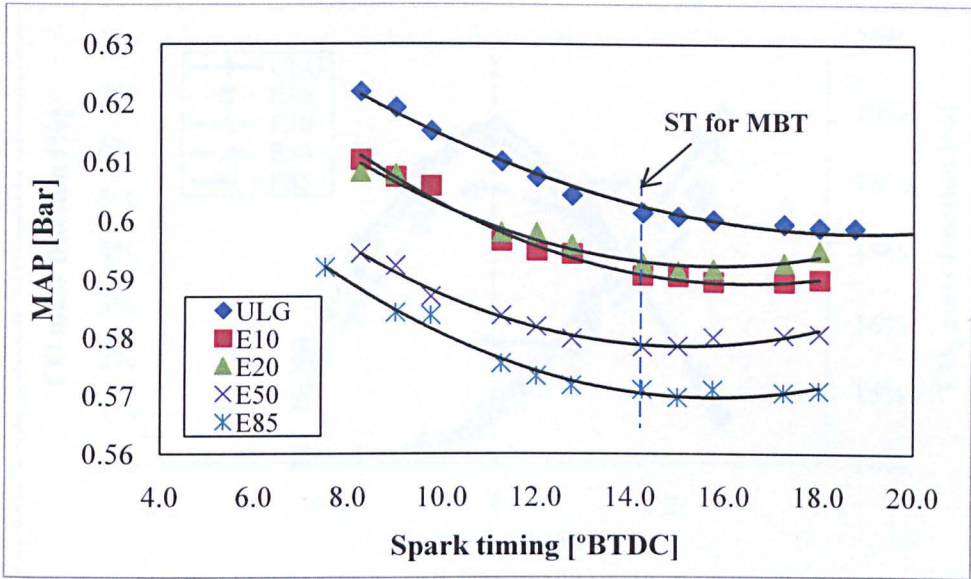


Figure 4.8. MBT for different gasoline-ethanol mixtures.

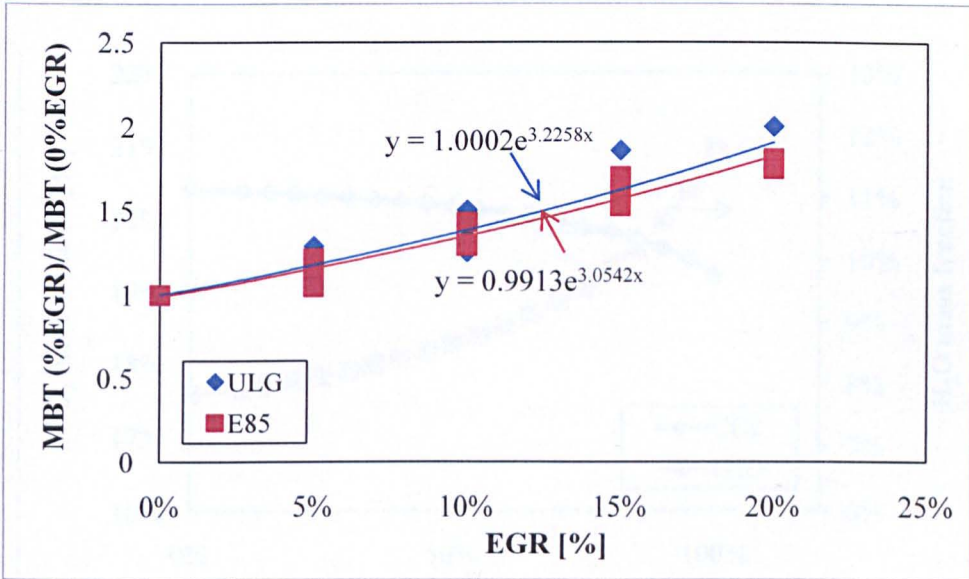


Figure 4.9. Ratio of MBT at EGR to MBT with no EGR as a function of EGR percentage.

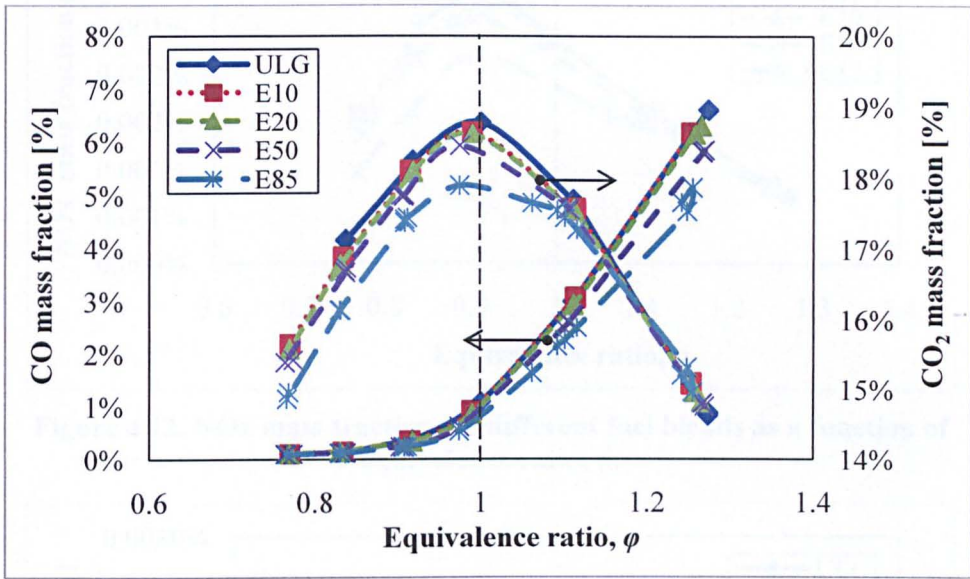


Figure 4.10. Mass fraction of CO and CO₂ for different fuel blends as a function of fuel/air equivalence ratio.

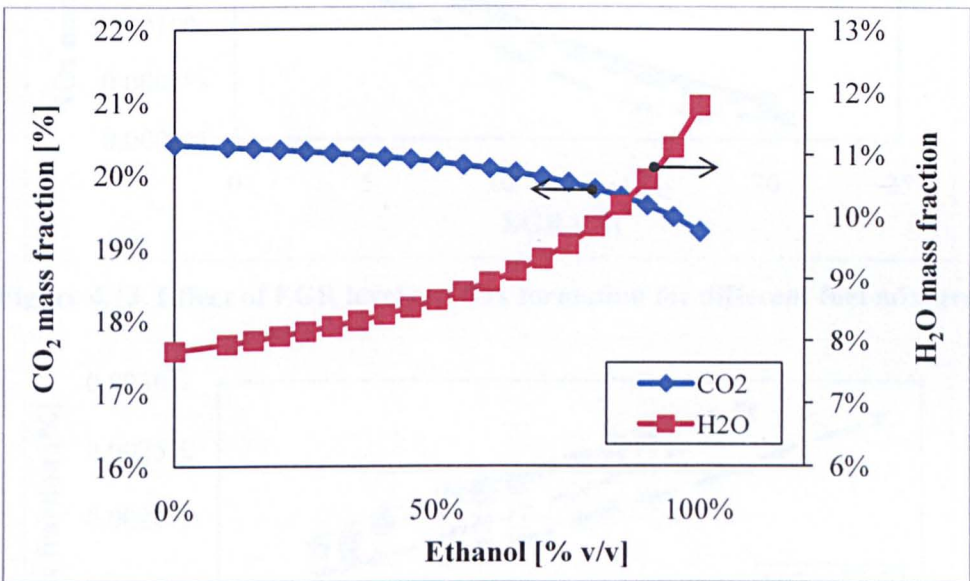


Figure 4.11. Calculated H₂O and CO₂ mass fraction assuming the fuel is fully burned.

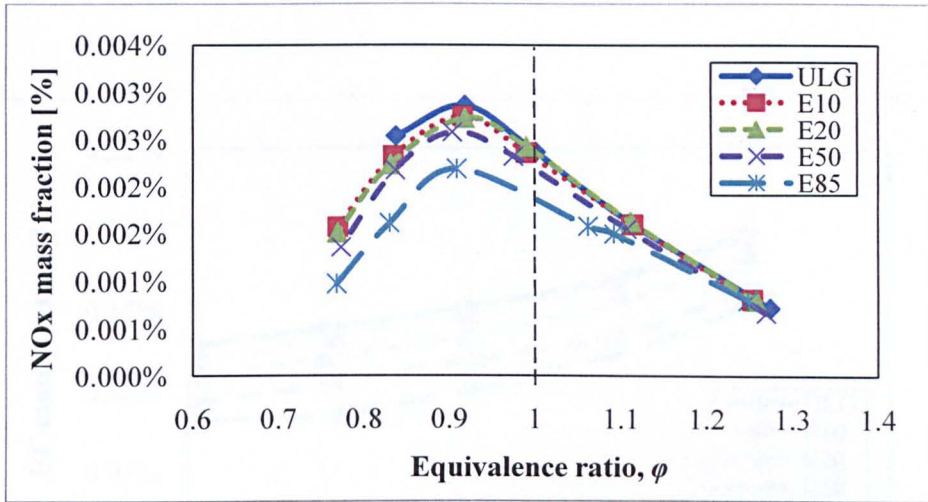


Figure 4.12. NOx mass fraction for different fuel blends as a function of equivalence ratio, ϕ .

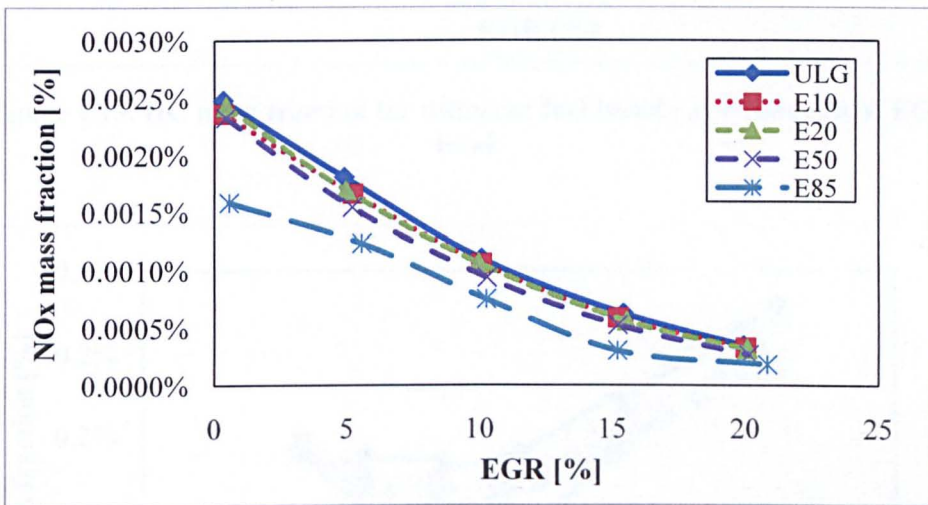


Figure 4.13. Effect of EGR level on NOx formation for different fuel mixture.

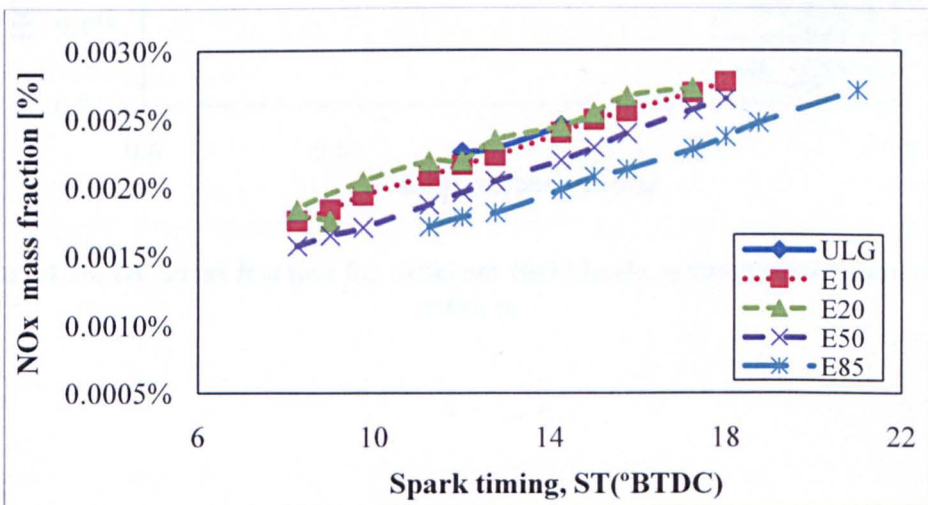


Figure 4.14. Effect of spark timing on NOx formation for different fuel mixture.

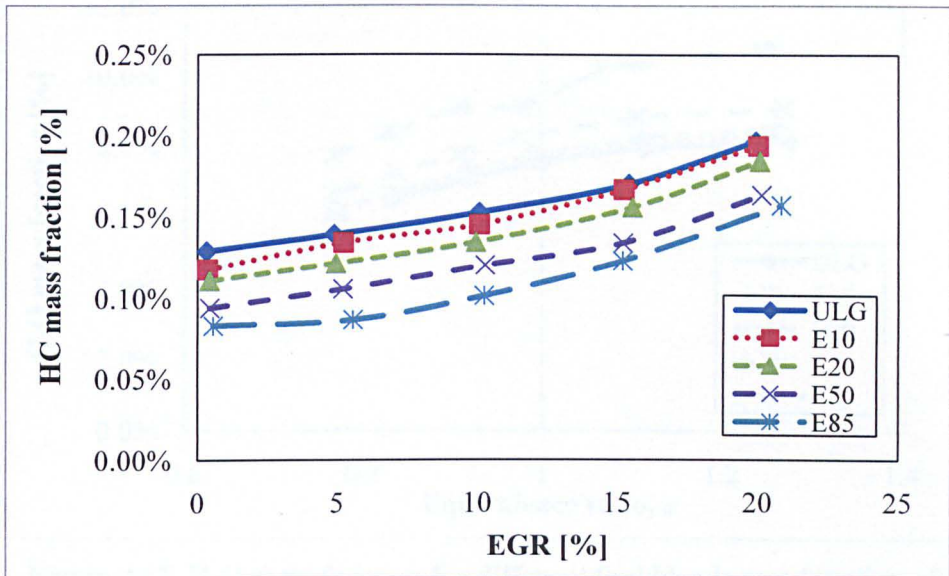


Figure 4.15. HC mass fraction for different fuel blends as a function of EGR level.

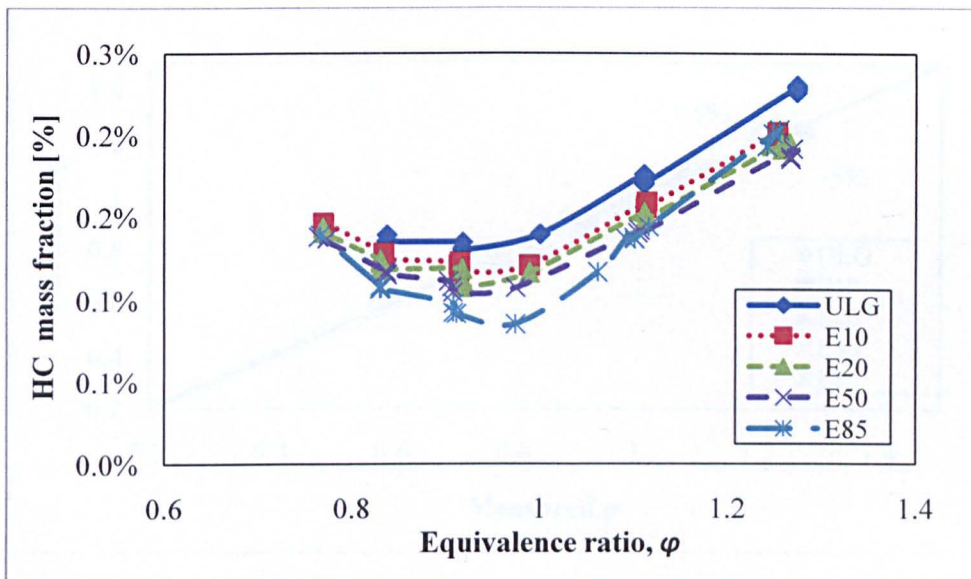


Figure 4.16. HC mass fraction for different fuel blends as function of equivalence ratio, ϕ .

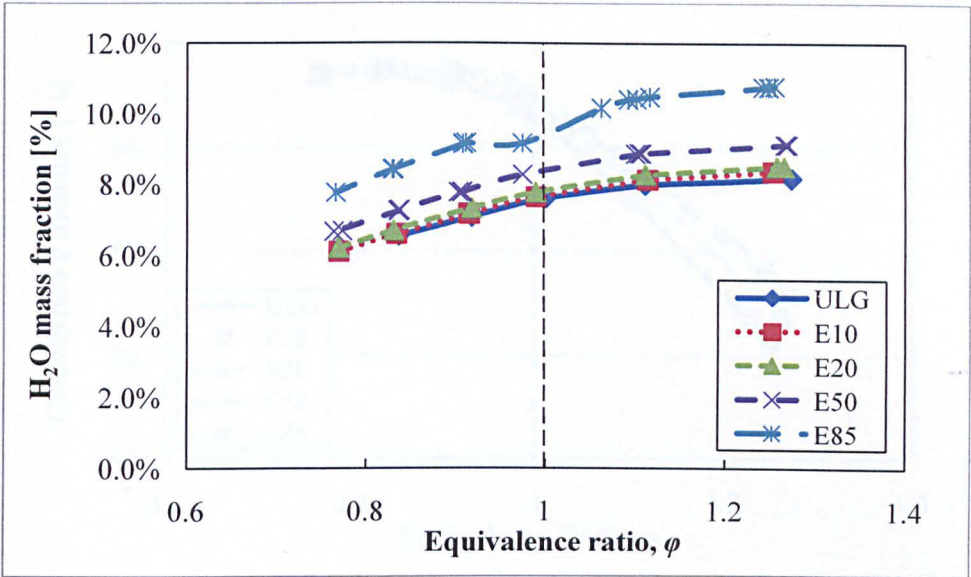


Figure 4.17. H₂O mass fraction for different fuel blends as a function of equivalence ratio ϕ .

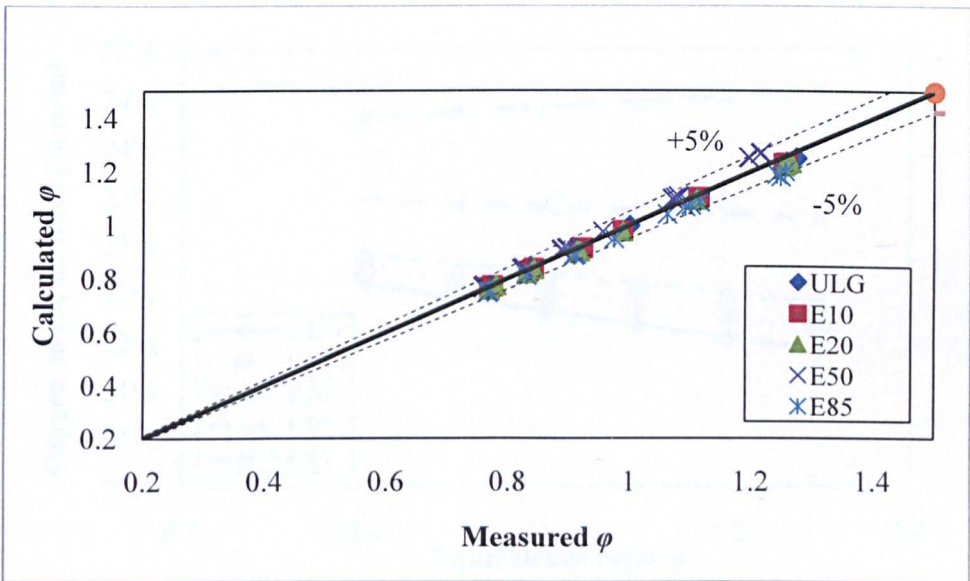


Figure 4.18. Comparison between measured and predicted equivalence ratio, ϕ .

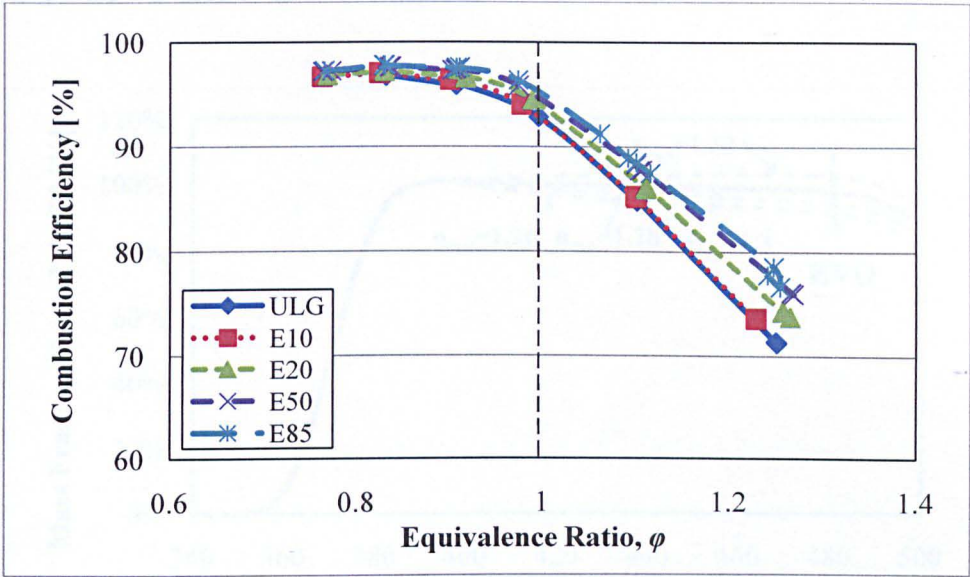


Figure 4.19. Combustion efficiency for different fuel blends as a function of equivalence ratio.

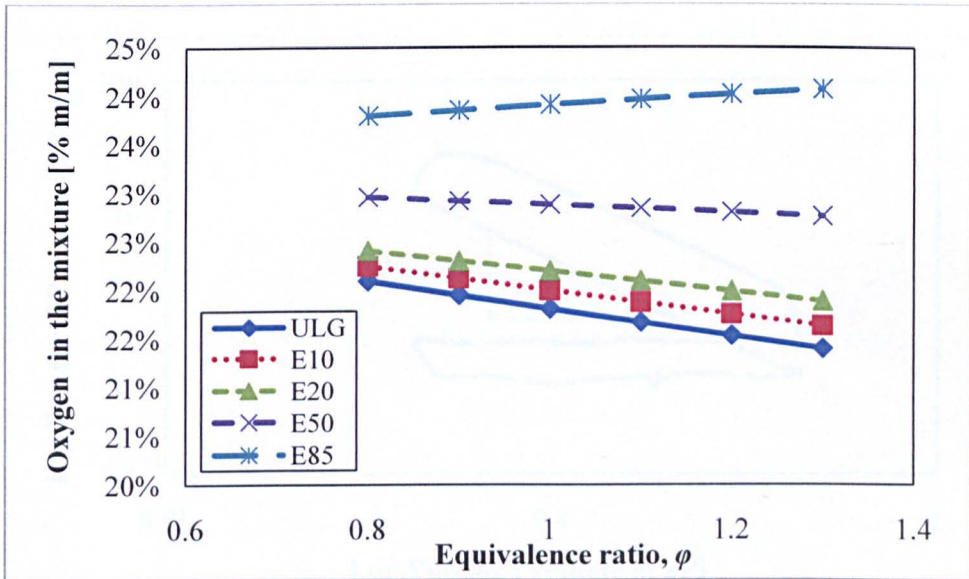


Figure 4.20. Oxygen mass fraction in the mixture as a function of ϕ for different fuel mixtures.

CHAPTER 5

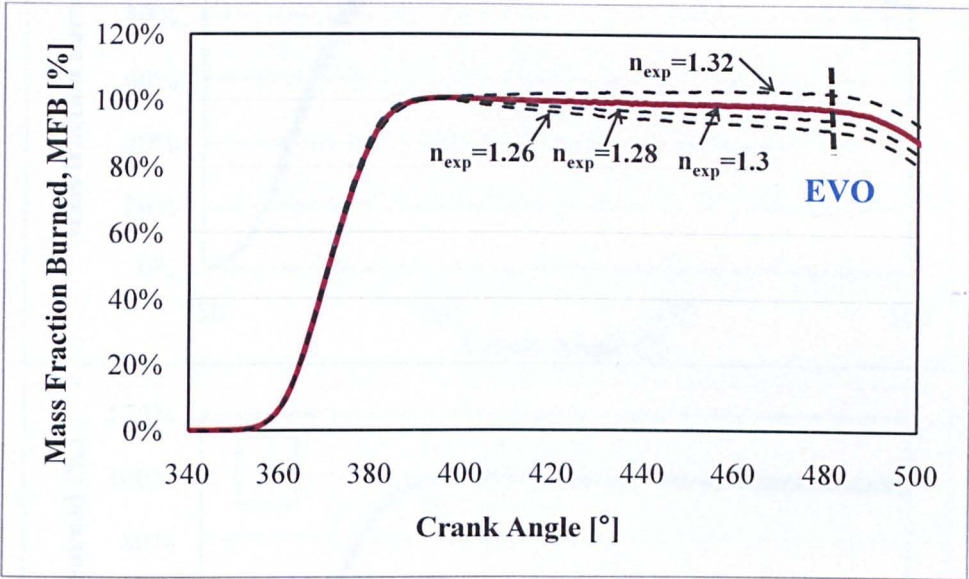


Figure 5.1. Effect of changing expansion index on MFB profile.

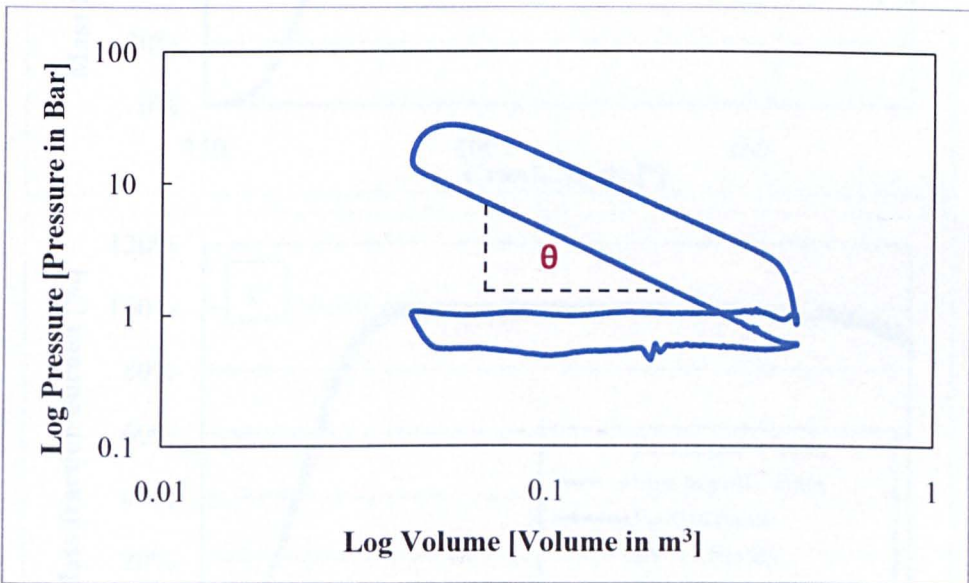


Figure 5.2. Log P-V diagram used to calculate the compression index.

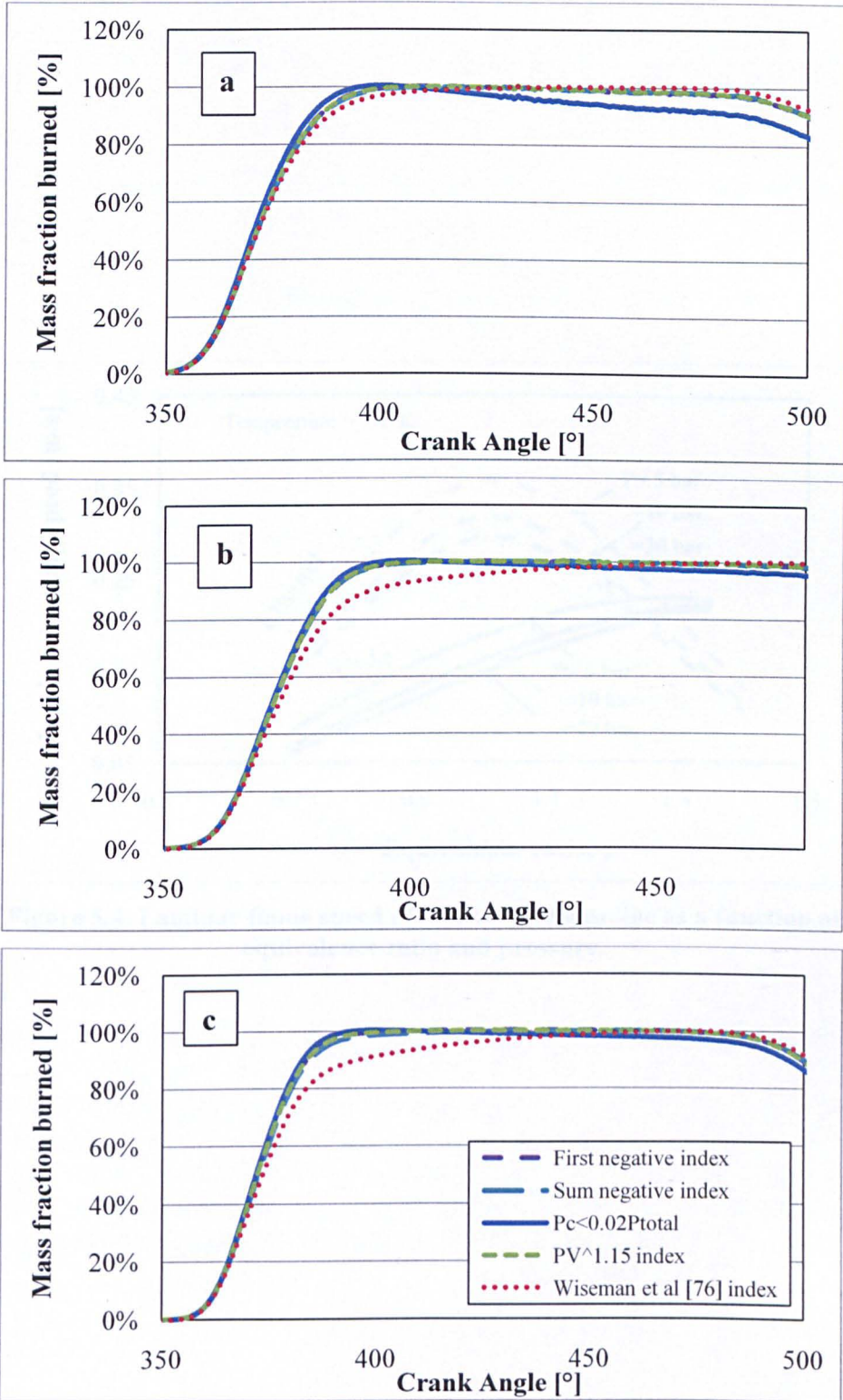


Figure 5.3. MFB profile calculated using different methods to calculate n_{exp} for engine running at a) low load and constant speed 2000 rpm b) medium load and constant speed 2000 rpm c) high load and constant speed 2000 rpm. All running at MBT Spark timing.

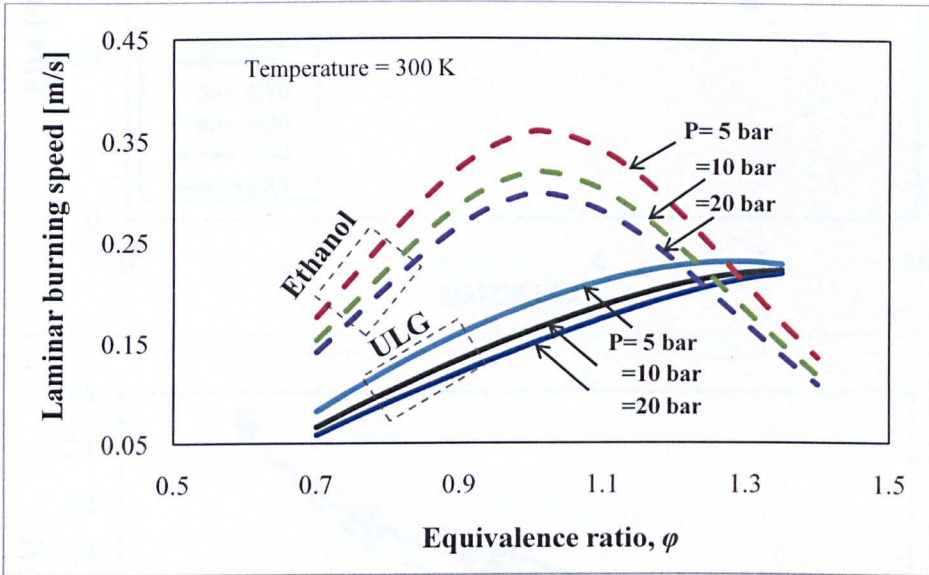


Figure 5.4. Laminar flame speed of ethanol and gasoline as a function of equivalence ratio and pressure.

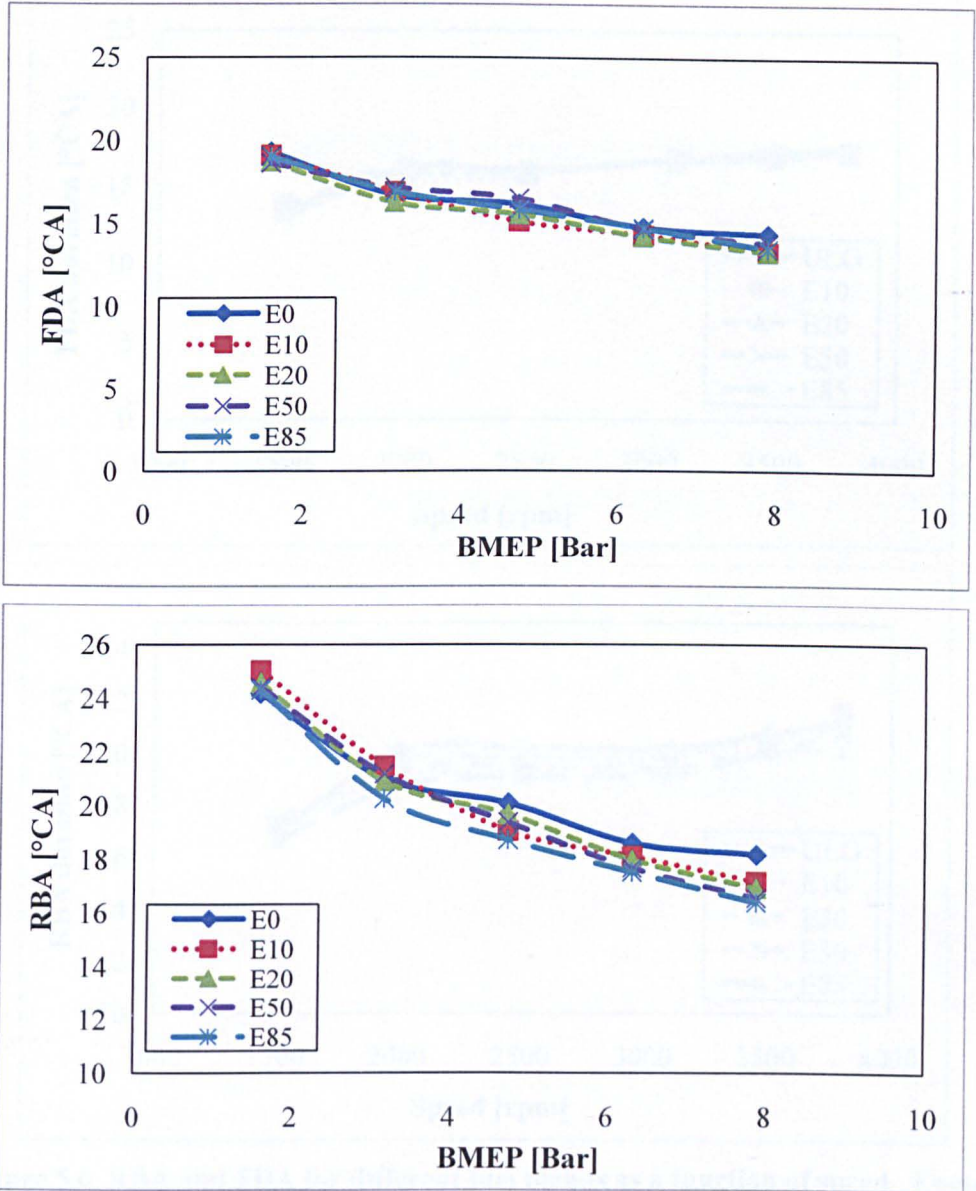


Figure 5.5. RBA and FDA for different fuel blends as a function of BMEP. Engine running at 2000 rpm and fixed ST.

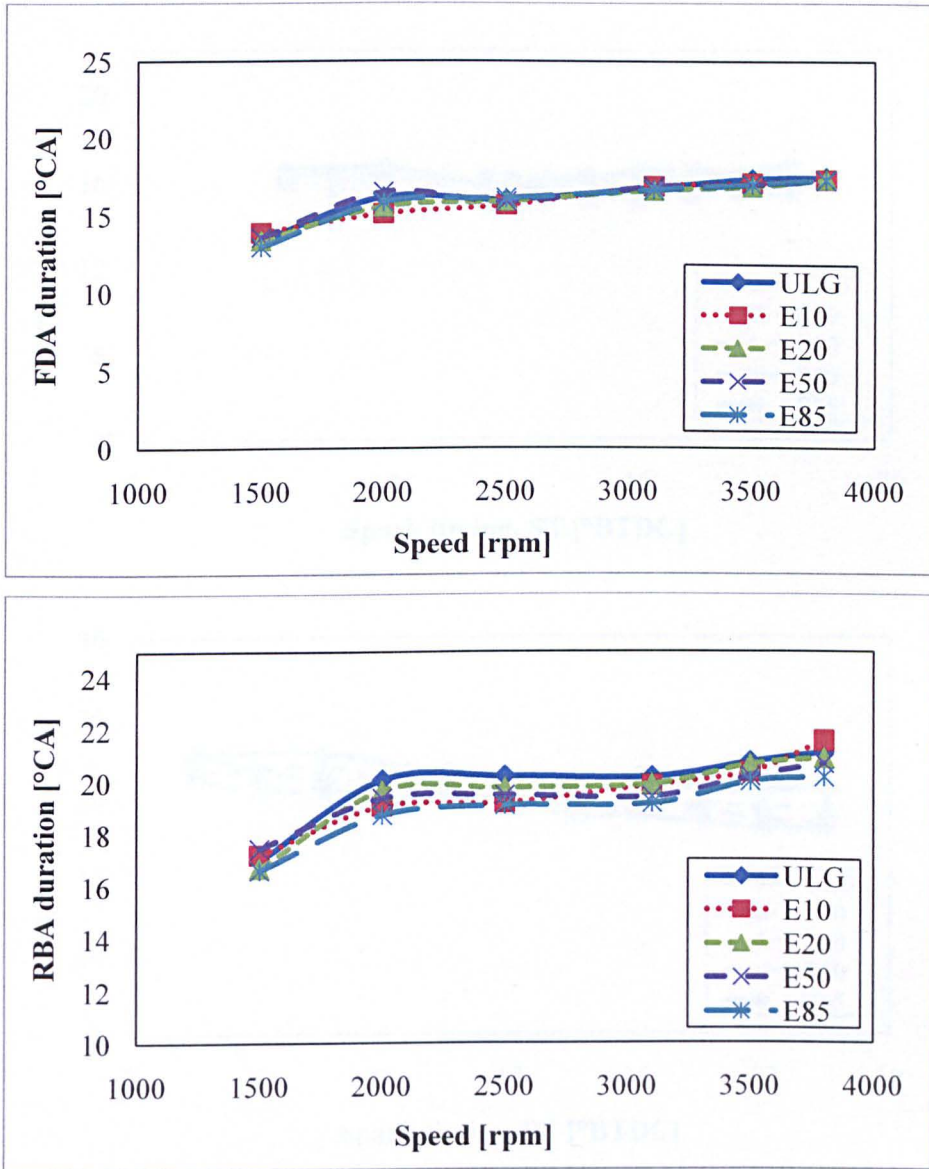


Figure 5.6. RBA and FDA for different fuel blends as a function of speed. Engine running at BMEP 4.75 bar and fixed ST.

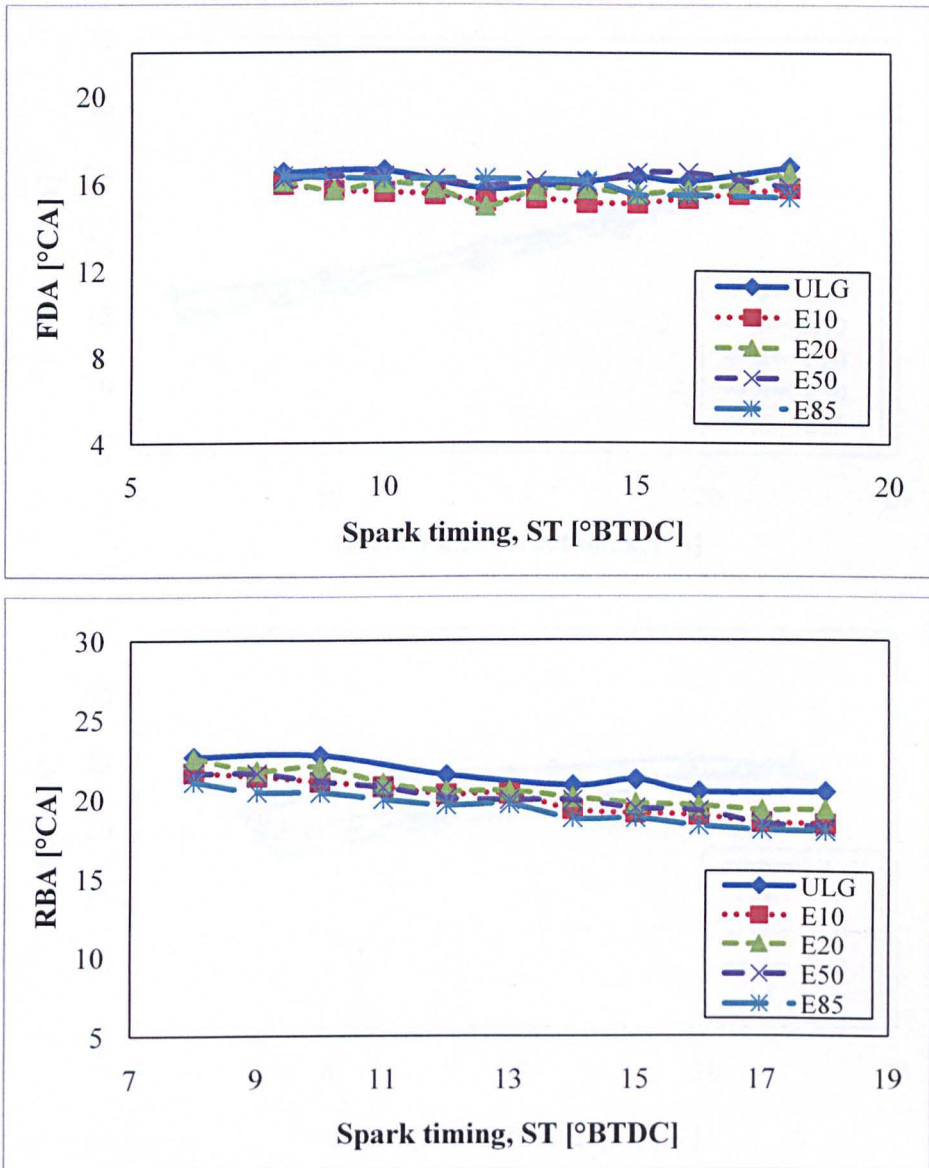


Figure 5.7. FDA and RBA for different fuel blends as a function of spark timing. Engine running at BMEP 4.75 bar and 2000 rpm.

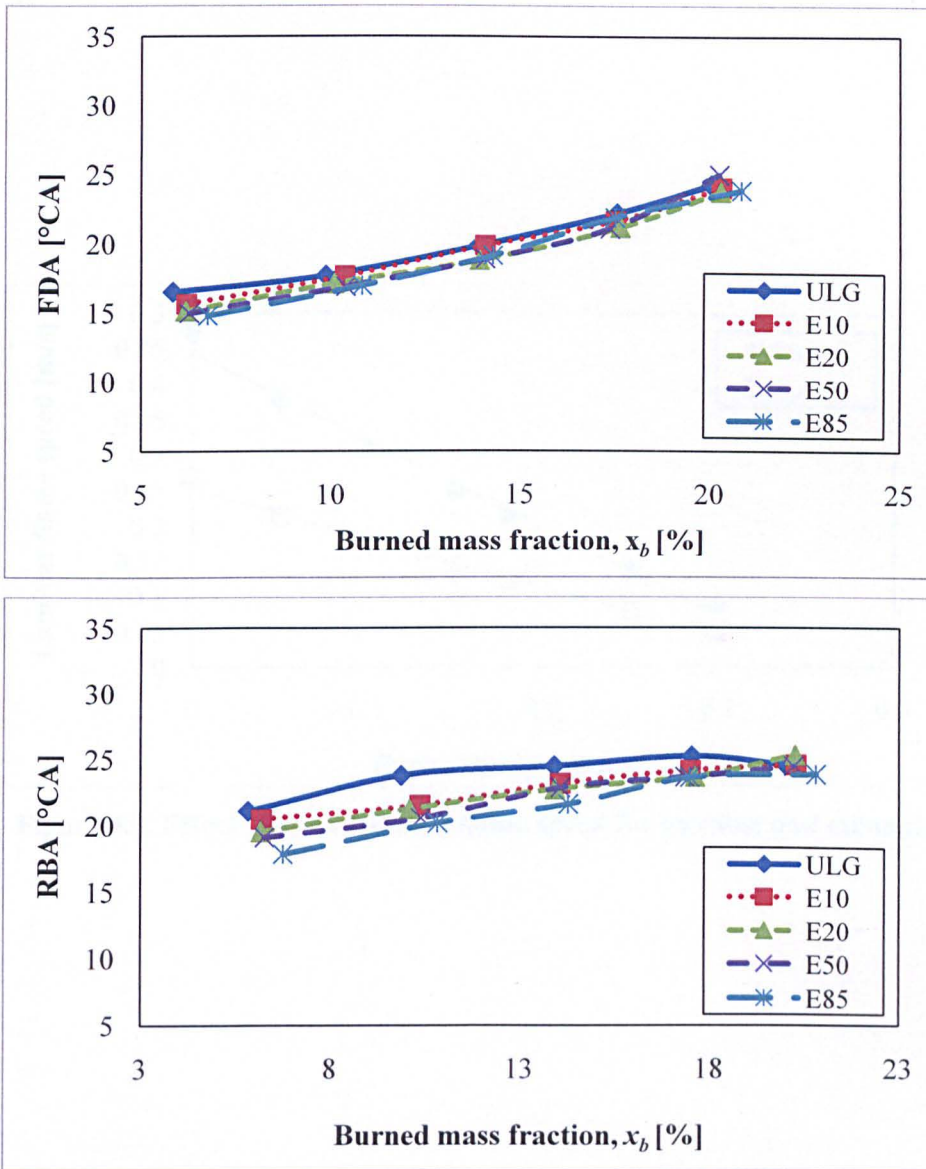


Figure 5.8. RBA and FDA for the different fuel mixtures as a function of total burned mass fraction. The engine running at constant speed 2000 rpm, constant BMEP 4.75 bar and MBT ignition timing.

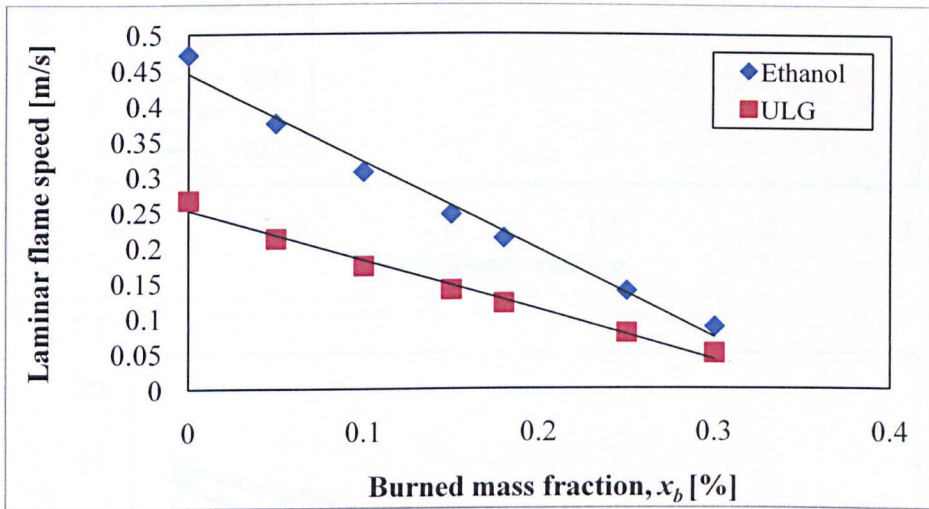


Figure 5.9. Effect of x_b on laminar flame speed for gasoline and ethanol.

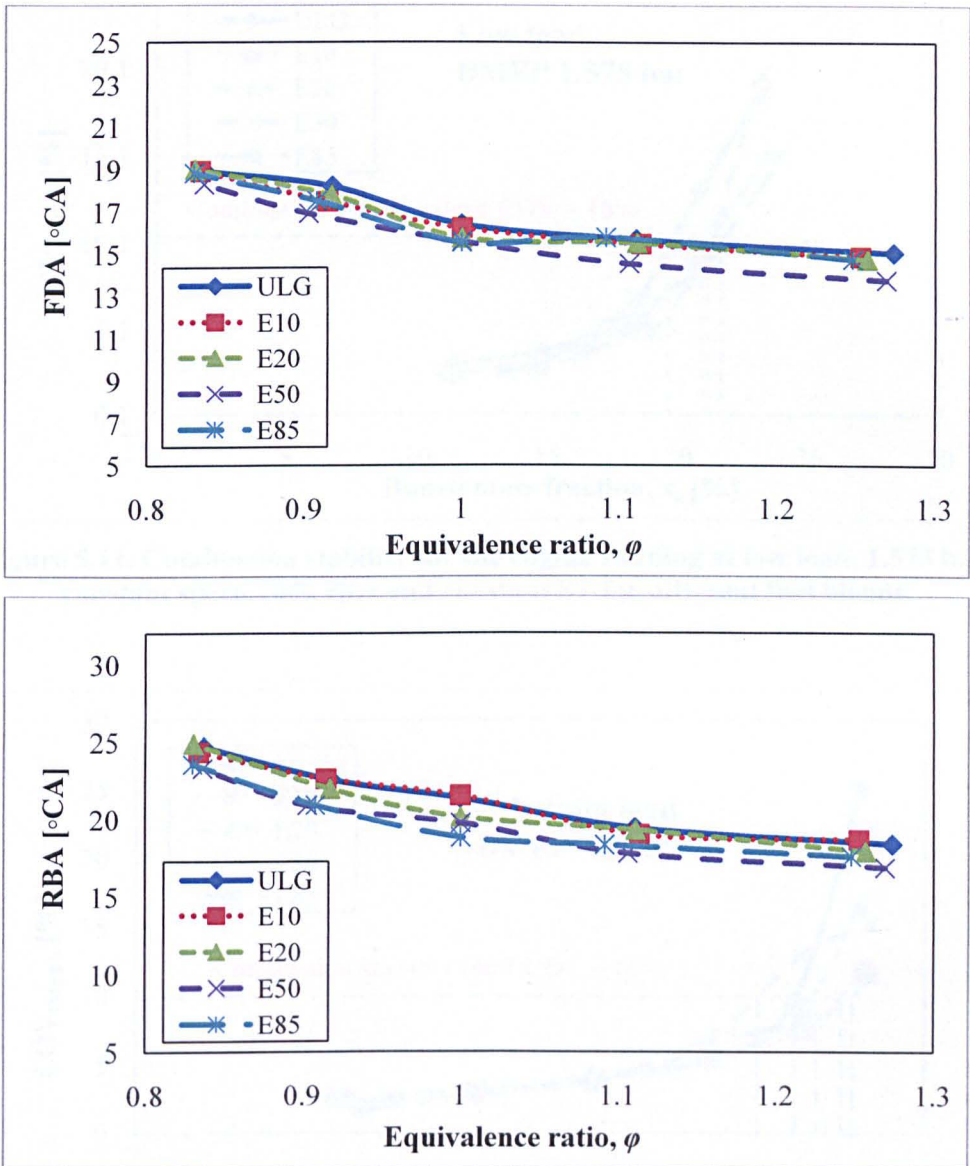


Figure 5.10. RBA and FDA for the different fuel mixtures as a function of equivalence ratio. The engine running at 2000 rpm, constant BMEP of 4.75 bar and MBT spark timing.

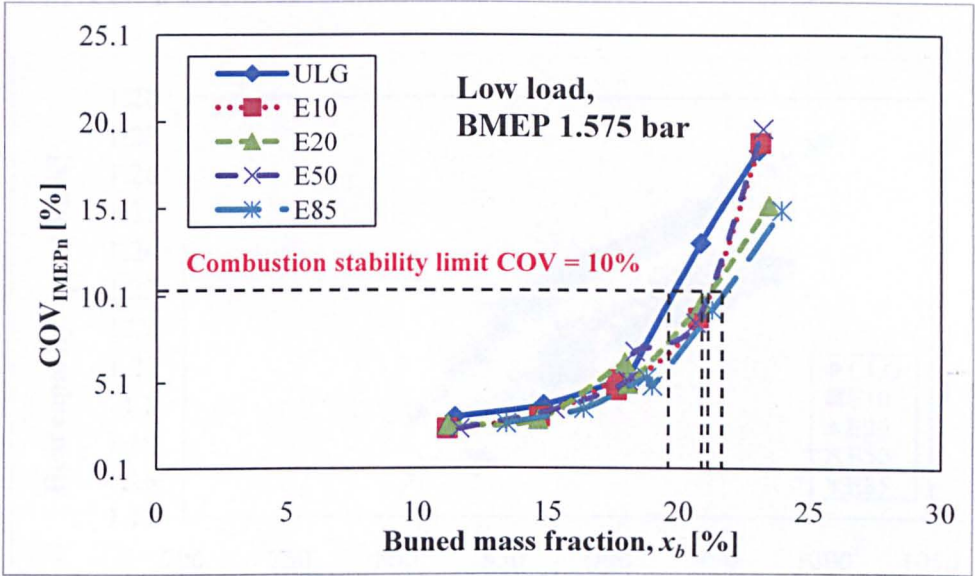


Figure 5.11. Combustion stability for the engine running at low load, 1.575 bar, constant speed 2000 rpm and constant ST for different fuel blends.

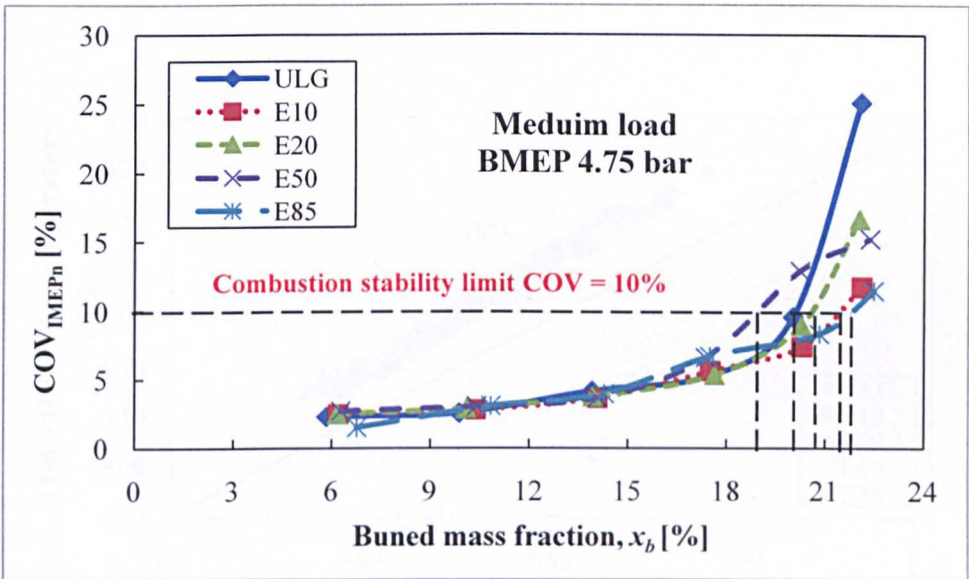


Figure 5.12. Combustion stability for the engine running at meduim load, 4.75 bar, constant speed 2000 rpm and constant ST for different fuel blends.

CHAPTER 6

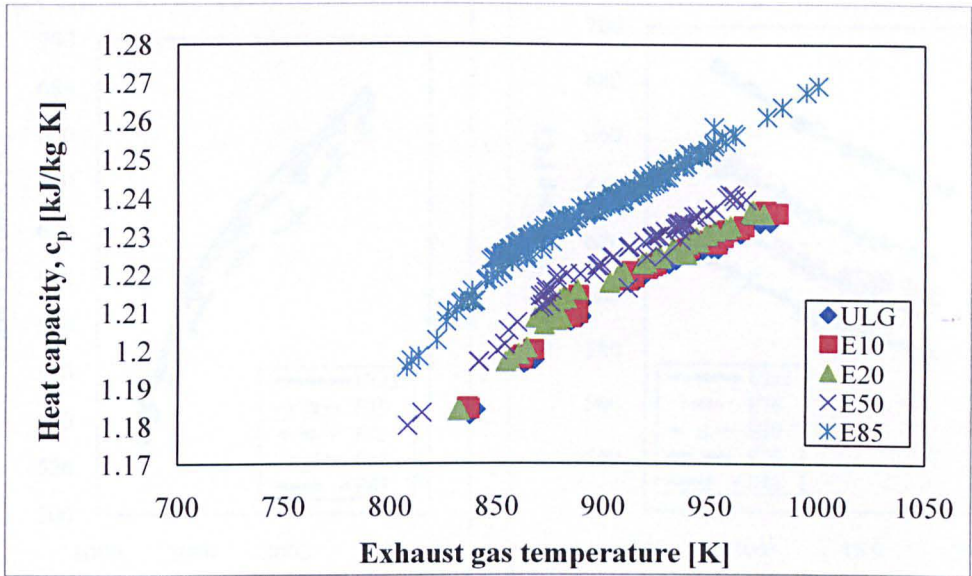


Figure 6.1. The effect of increasing ethanol ratio on $\bar{c}_{p,exh}$, various speeds, loads and EGR levels.

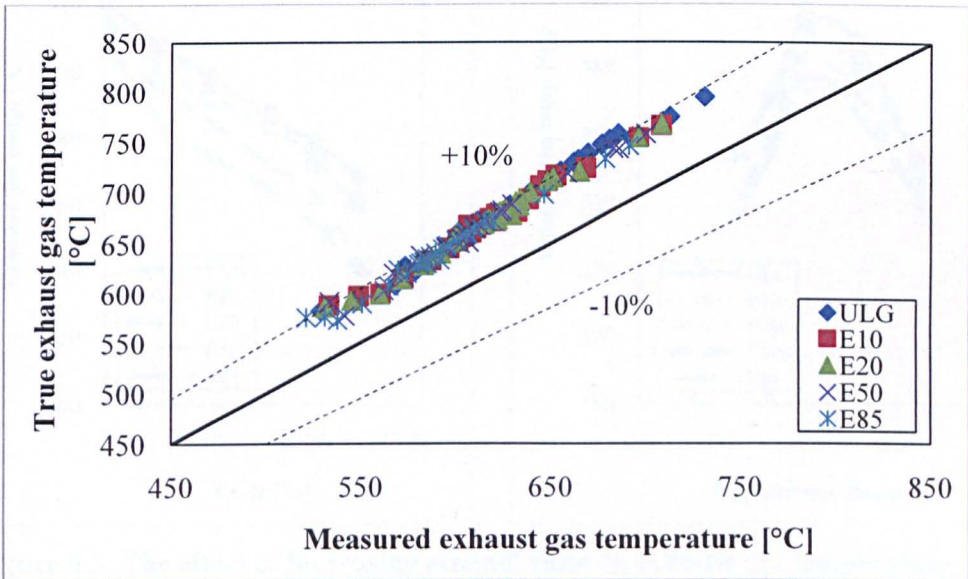


Figure 6.2. Comparison between measured and true exhaust gas temperatures.

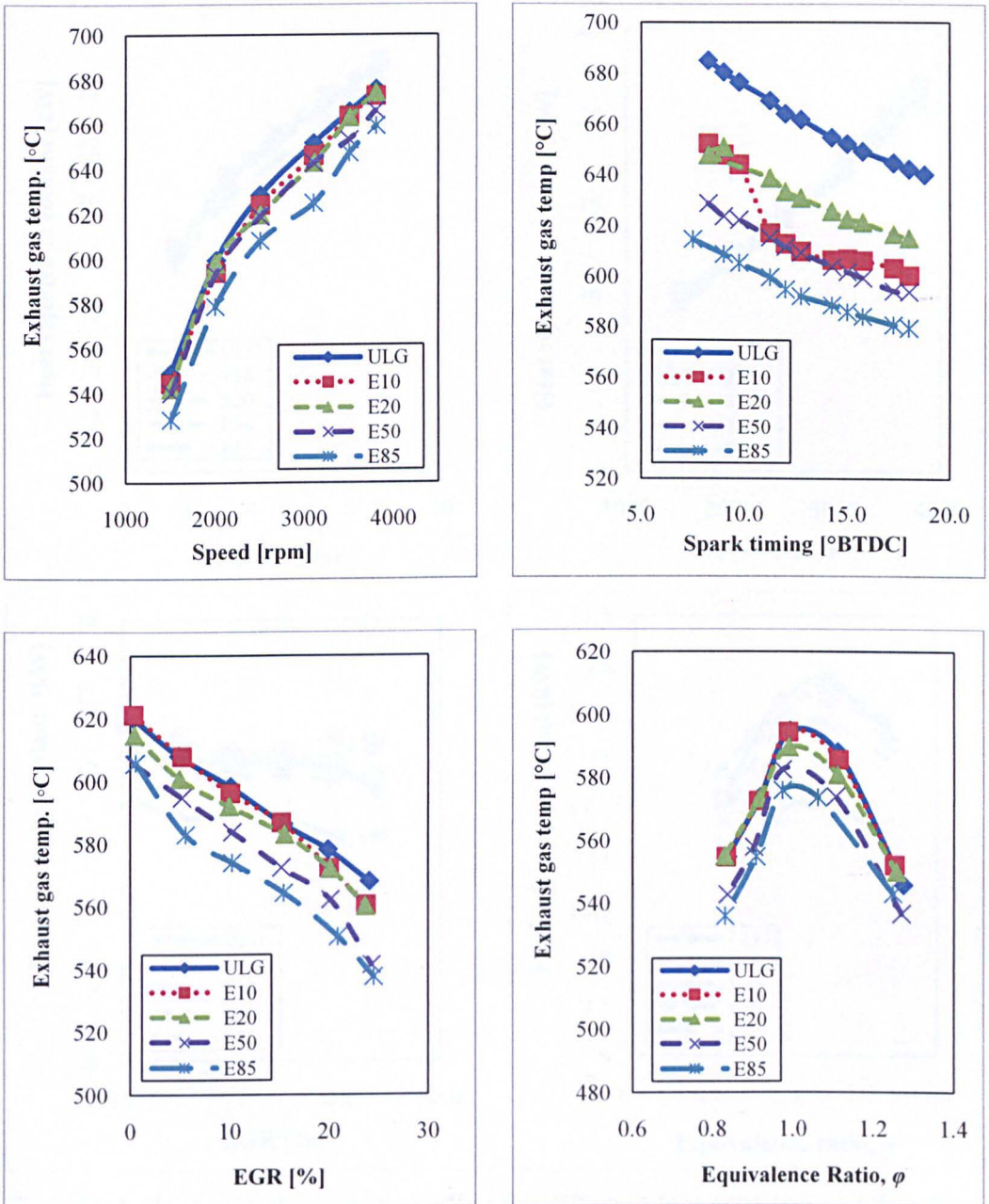


Figure 6.3. The effect of increasing ethanol ratio on exhaust gas temperature for the engine running at various conditions.

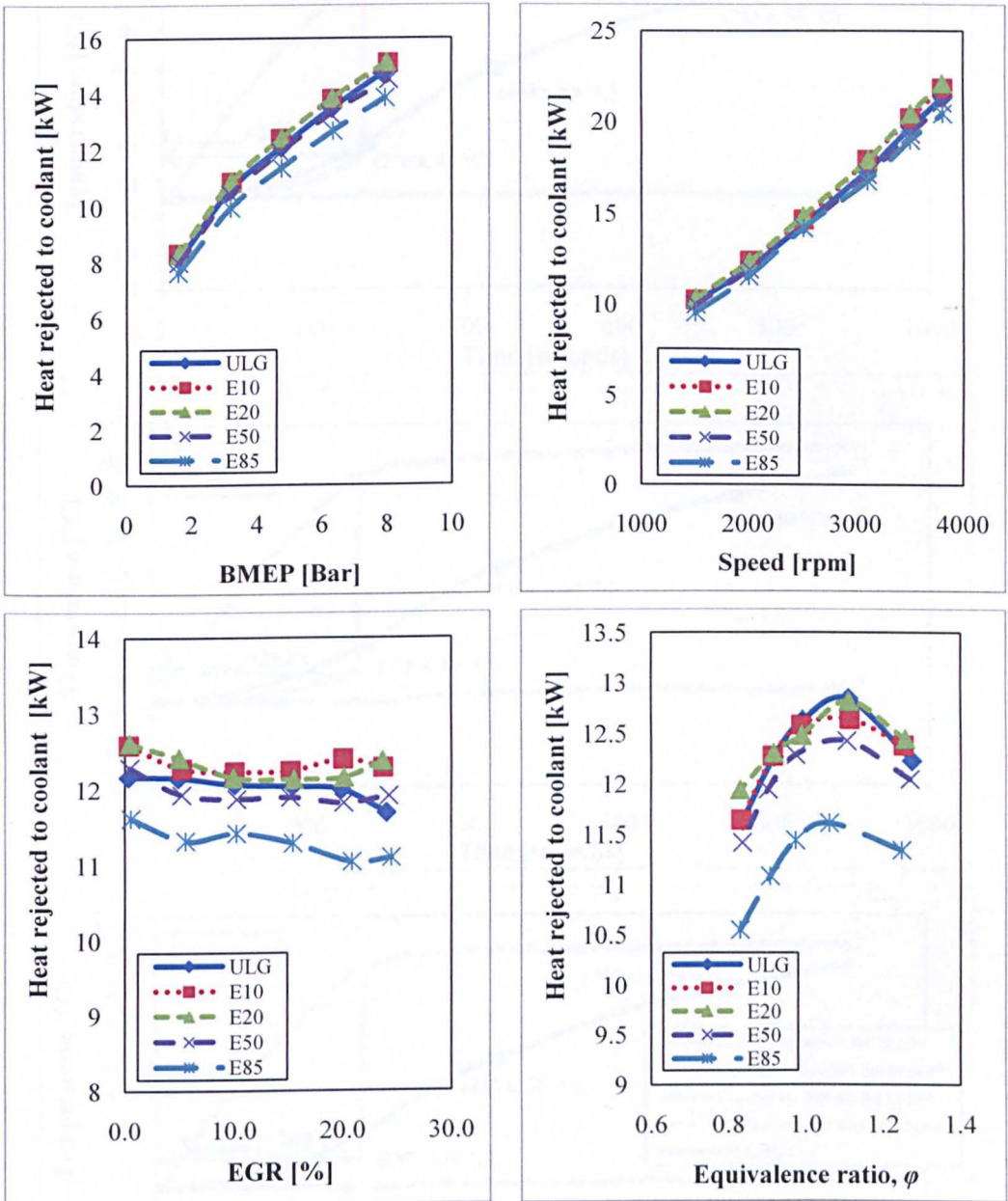


Figure 6.4. Heat rejection rate to coolant for different fuel mixtures as a function of BMEP, speed, EGR level and ϕ .

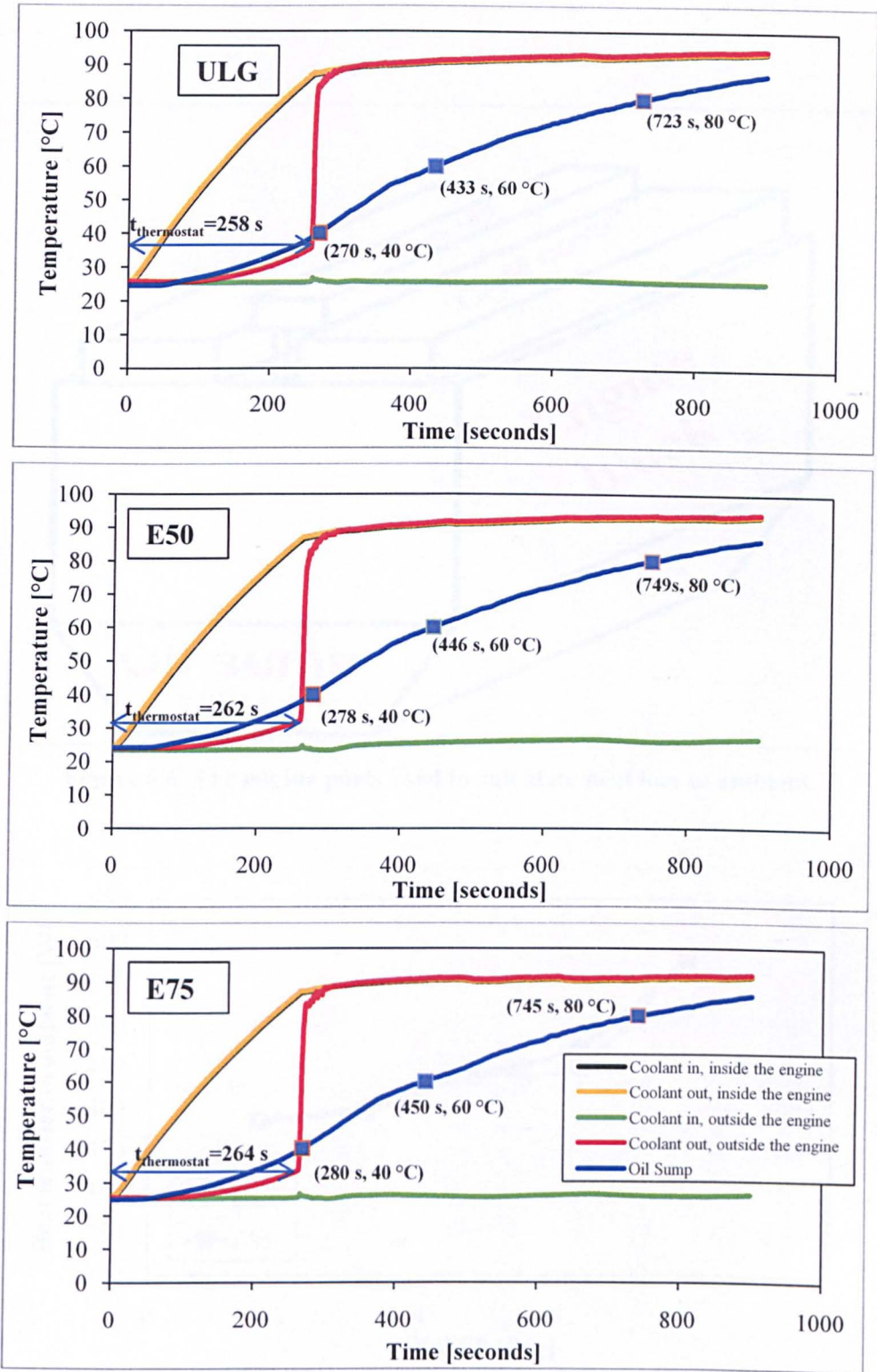


Figure 6.5. Coolant and sump oil temperatures during warm up period measured from PFI engine[86].

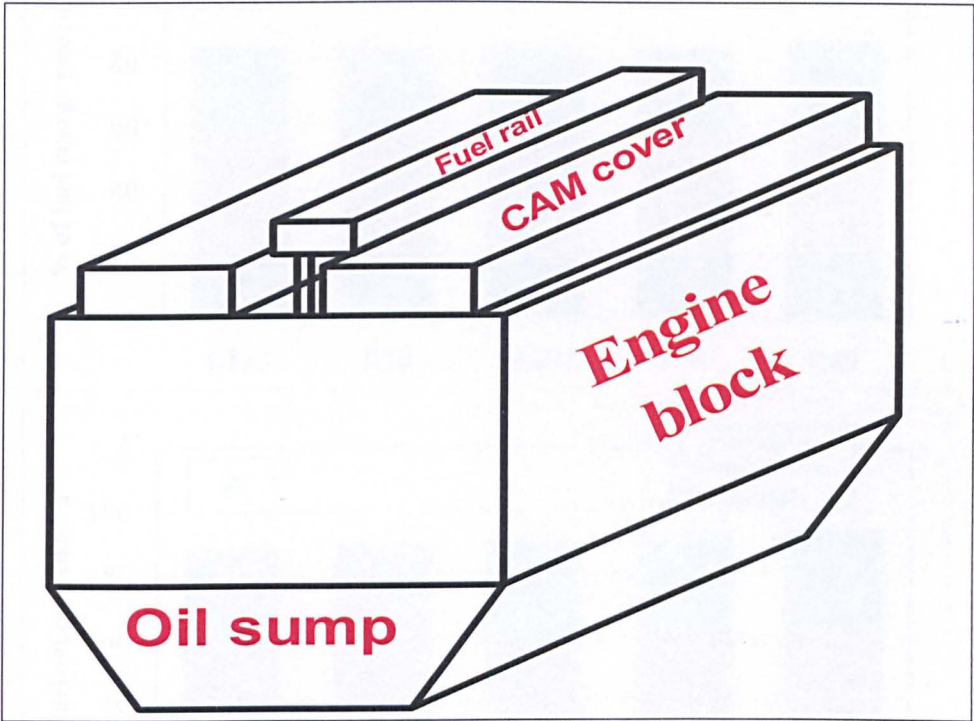


Figure 6.6. The engine parts used to calculate heat loss to ambient.

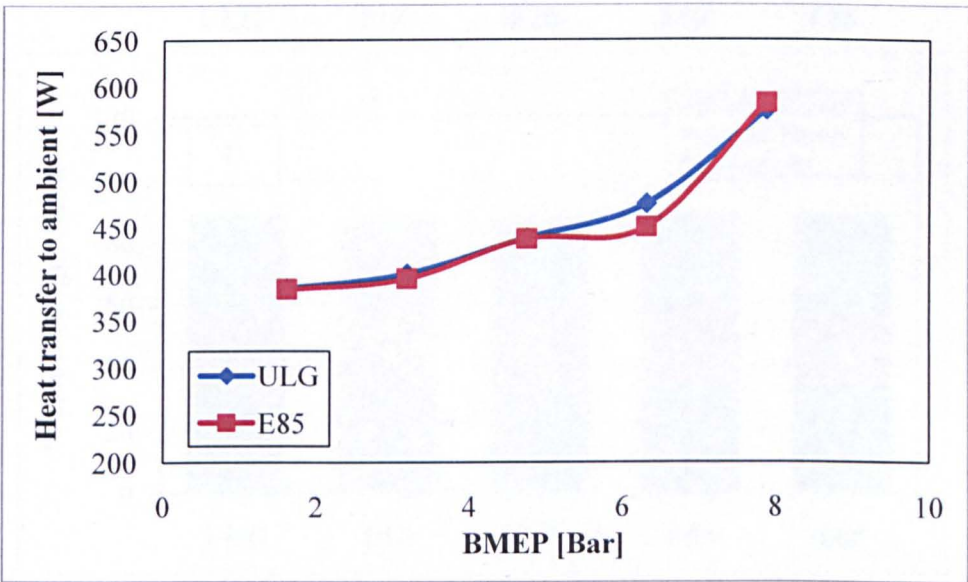


Figure 6.7. Heat loss to ambient as a function of BMEP for gasoline and E85.

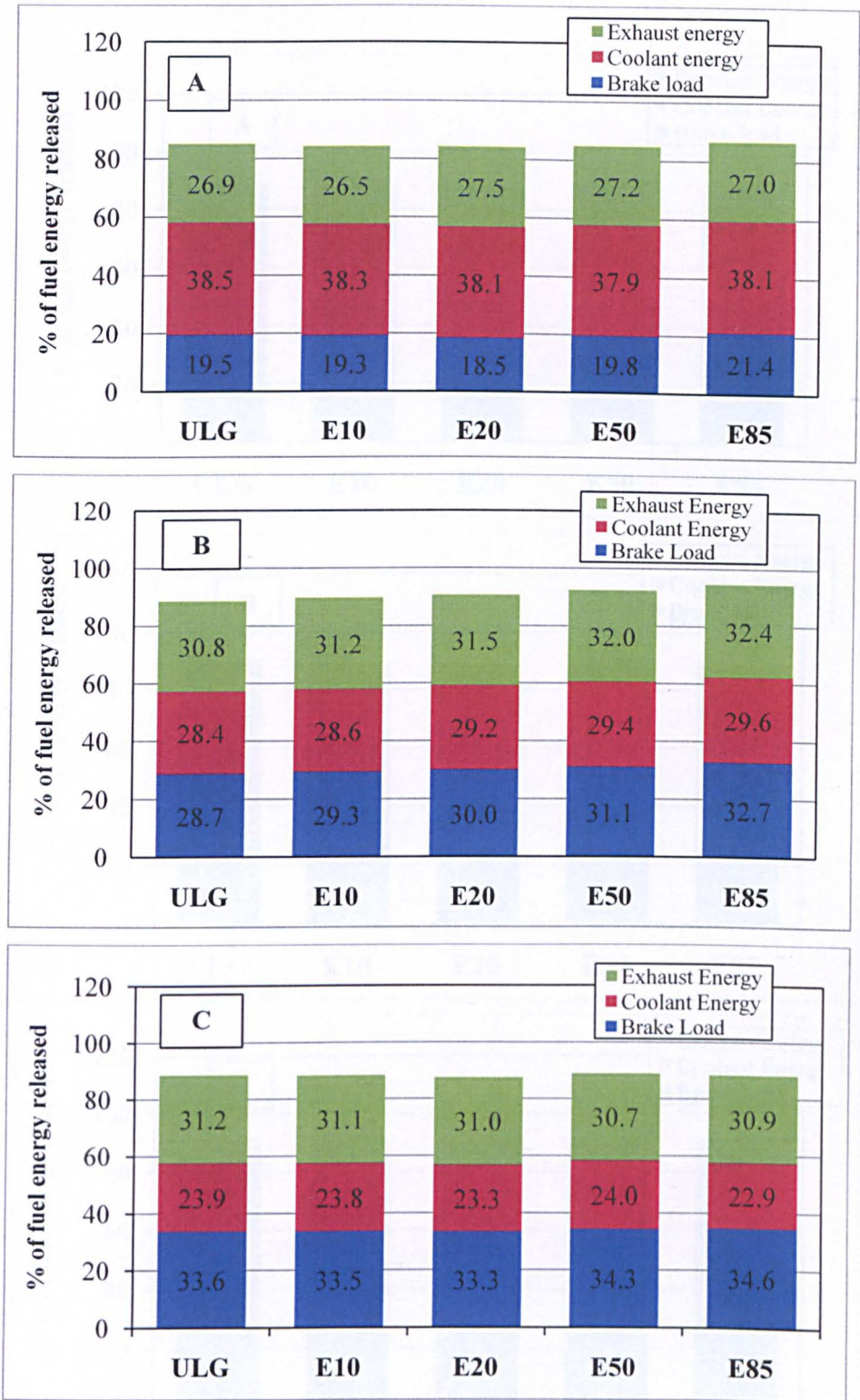


Figure 6.8. Energy balance for the engine running on different fuel mixture, 2000 rpm and BMEP of A) 1.6 bar B) 4.75 bar C) 7.95 bar.

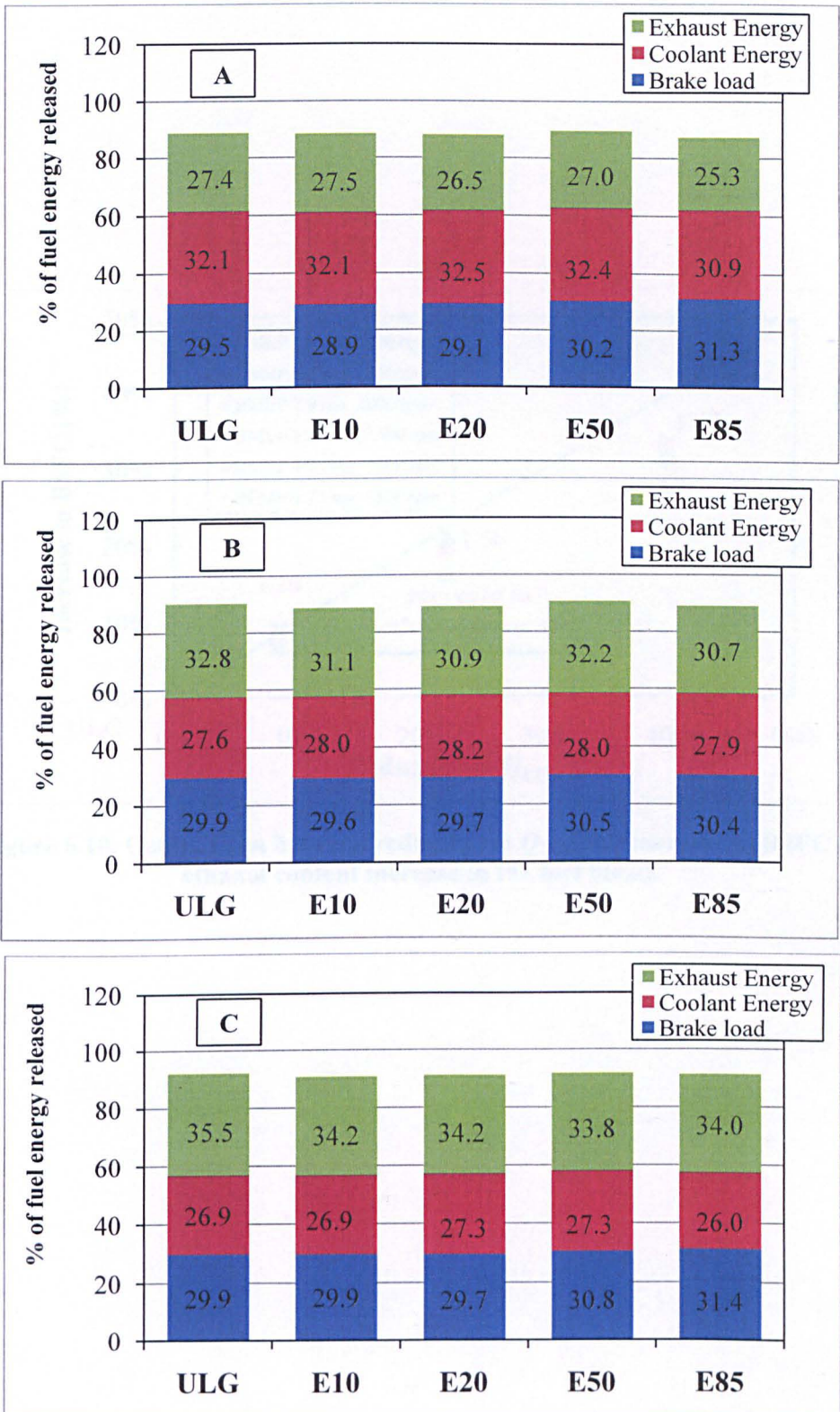


Figure 6.9. Energy balance for the engine running on different fuel blends, BMEP =4.75 bar and speed A) 1500 rpm B) 2500 rpm C) 3500 rpm

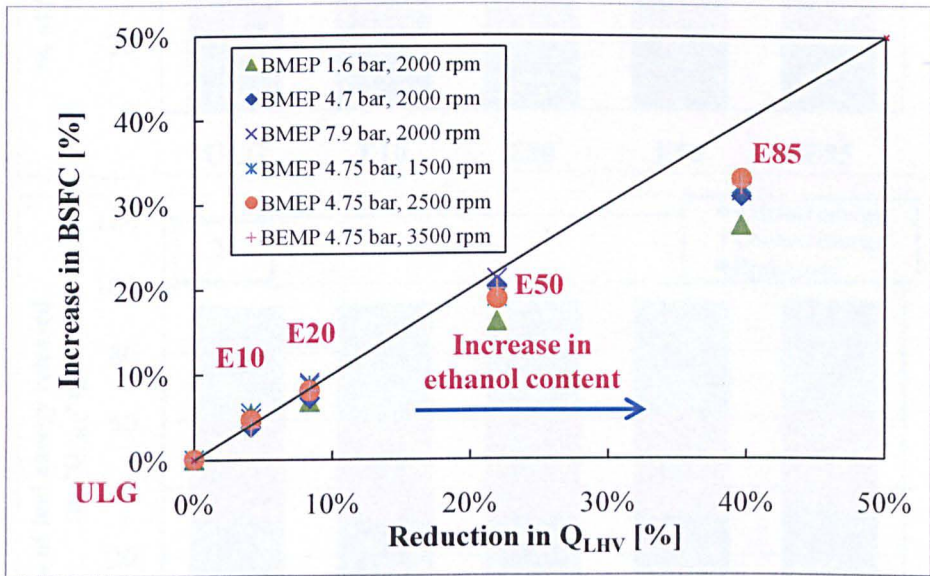


Figure 6.10. Comparison between reduction in Q_{LHV} and increase in BSFC as ethanol content increase in the fuel blend.

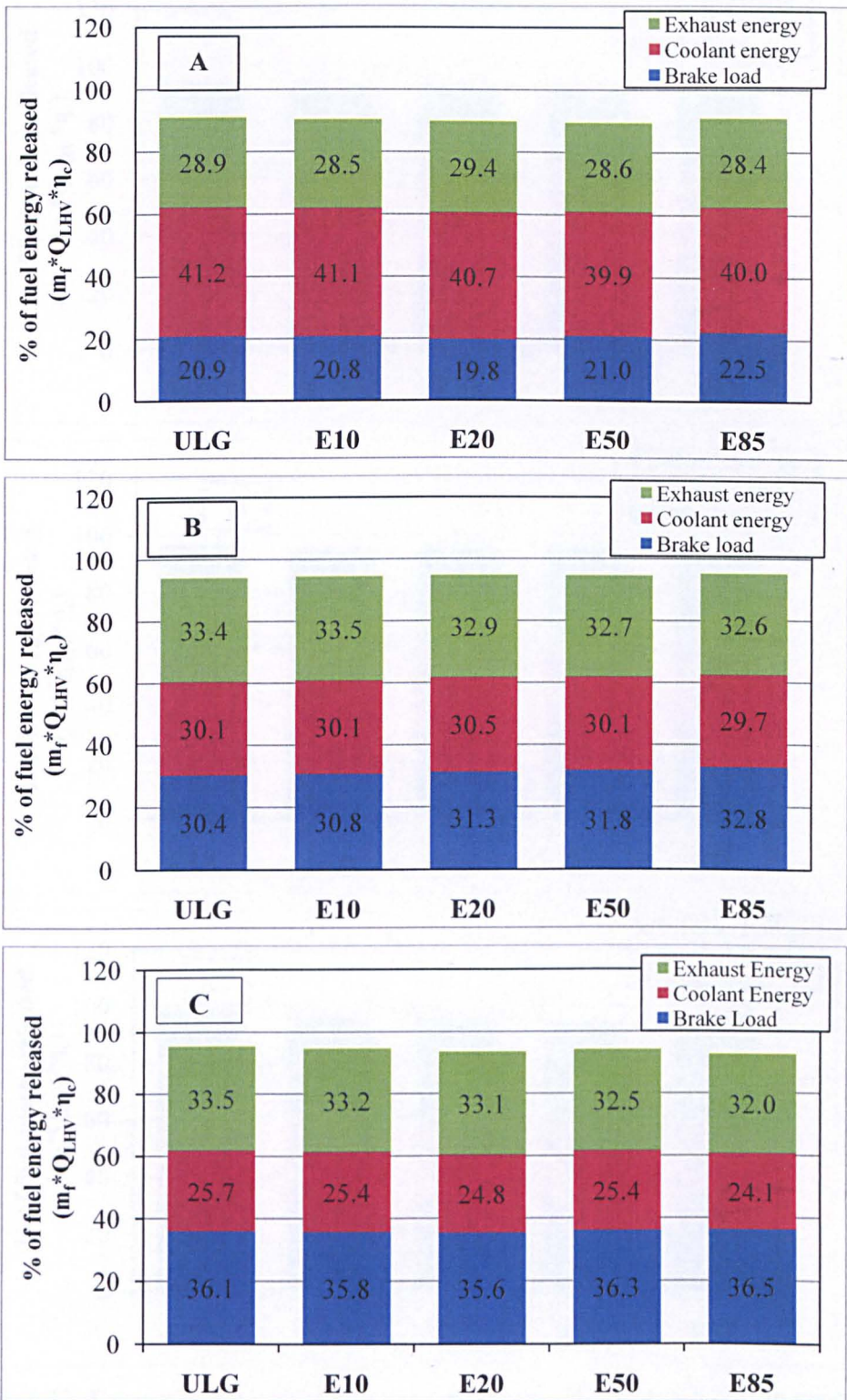


Figure 6.11. Energy balance based on heat release by the fuel taking into account combustion efficiency ($m_f \cdot Q_{LHV} \cdot \eta_c$) for the engine running on different fuel blends, 2000 rpm and BMEP of A) 1.6 bar B) 4.75 bar C) 7.95 bar

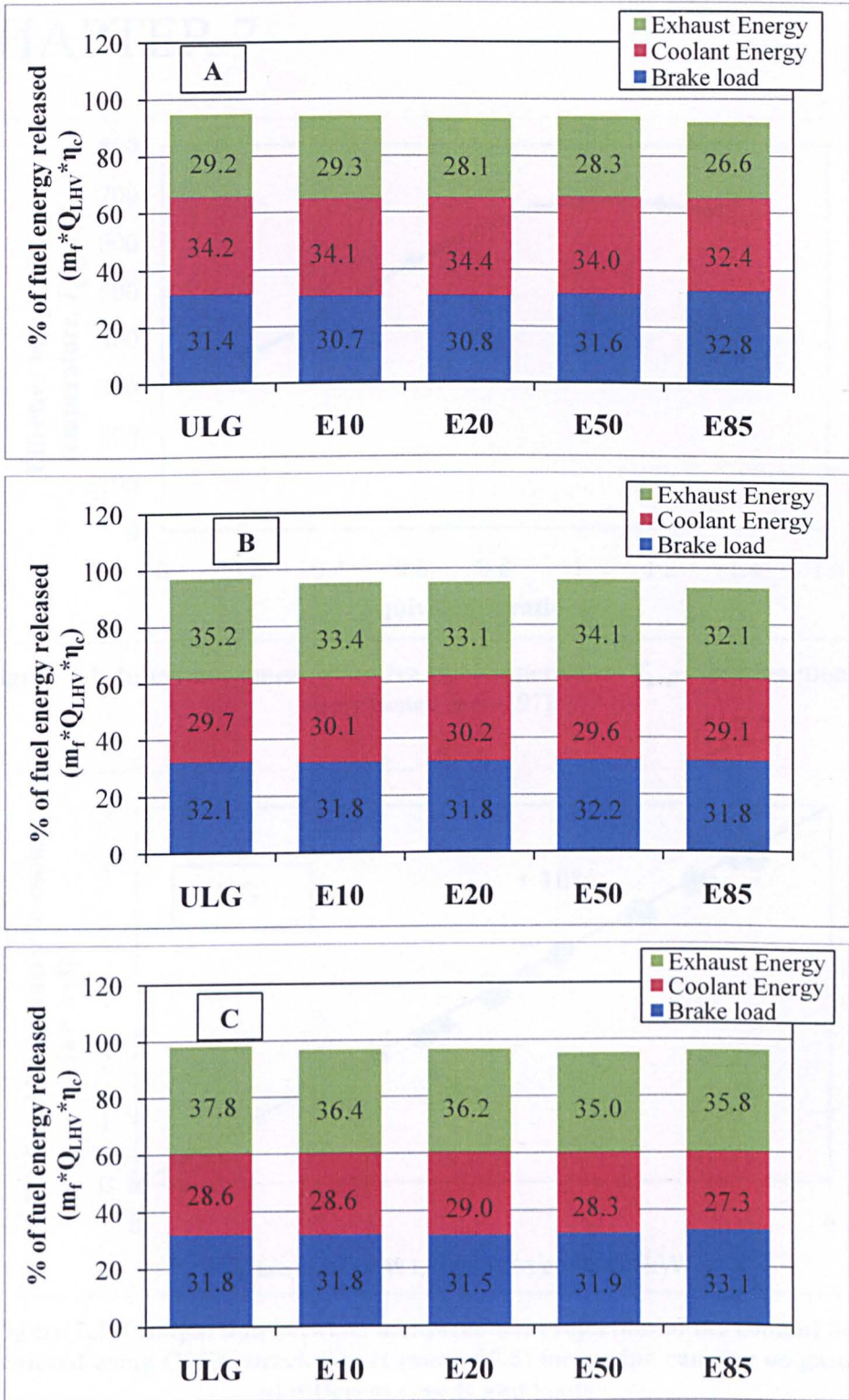


Figure 6.12. Energy balance based on heat release by the fuel taking into account combustion efficiency ($m_f * Q_{LHV} * \eta_c$) for the engine running on different fuel blends, BMEP = 4.75 bar and speed A) 1500 rpm B) 2500 rpm C) 3500 rpm

CHAPTER 7

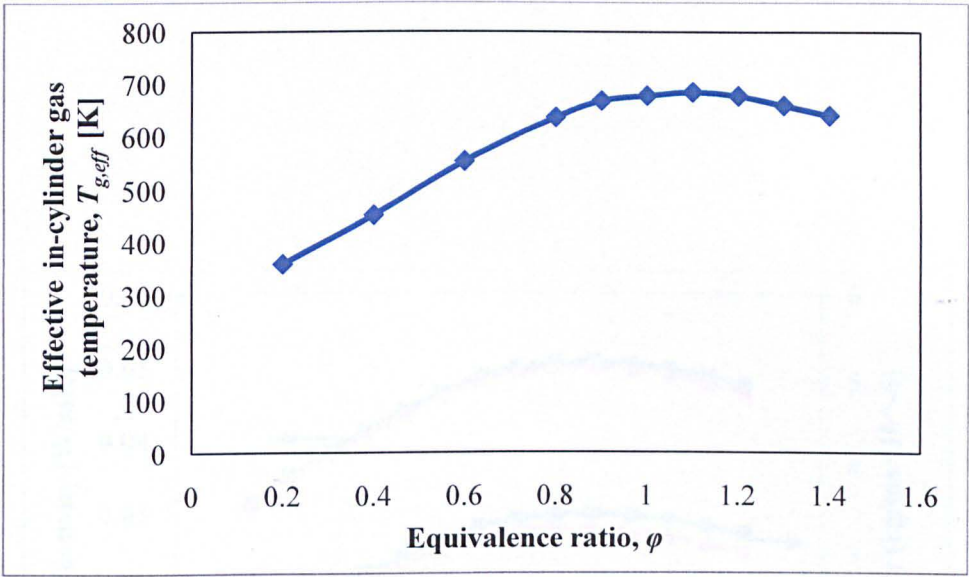


Figure 7.1. In-cylinder mean effective gas temperature, $T_{g,eff}$, as a function of equivalence ratio [97].

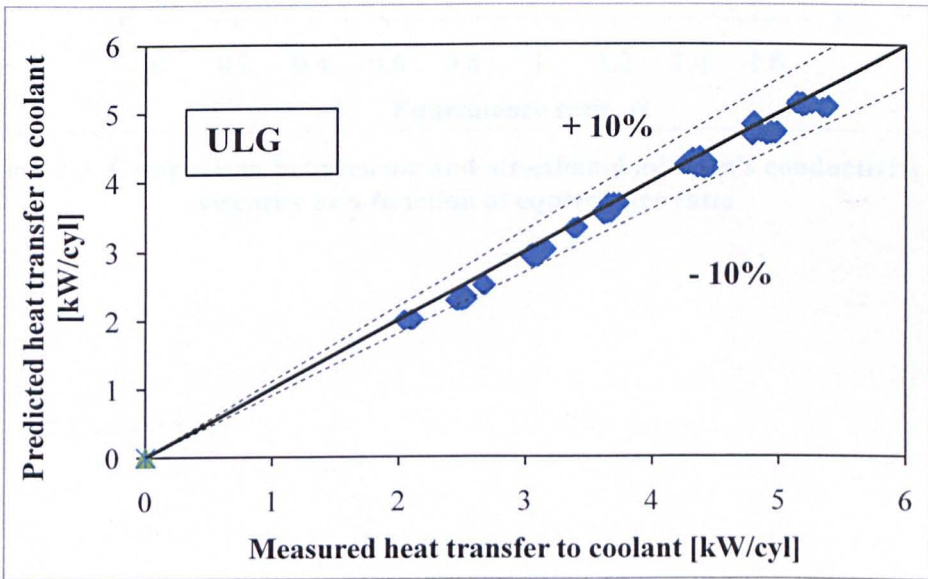


Figure 7.2. Comparison between measured heat rejection to the coolant and calculated using C1C2 correlation (equation 7.8) for engine running on gasoline at different speeds and loads.

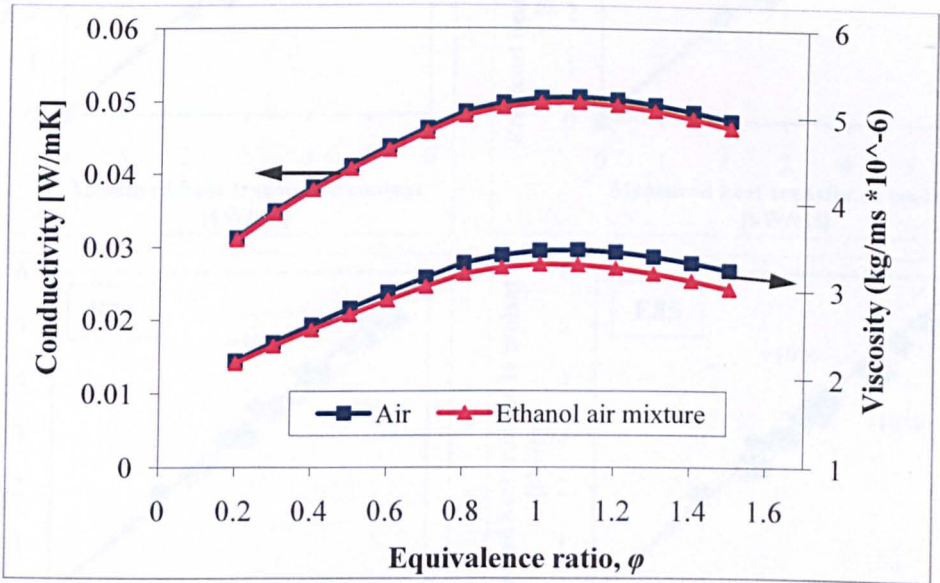


Figure 7.3. Comparison between air and air-ethanol mixture's conductivity and viscosity as a function of equivalence ratio.

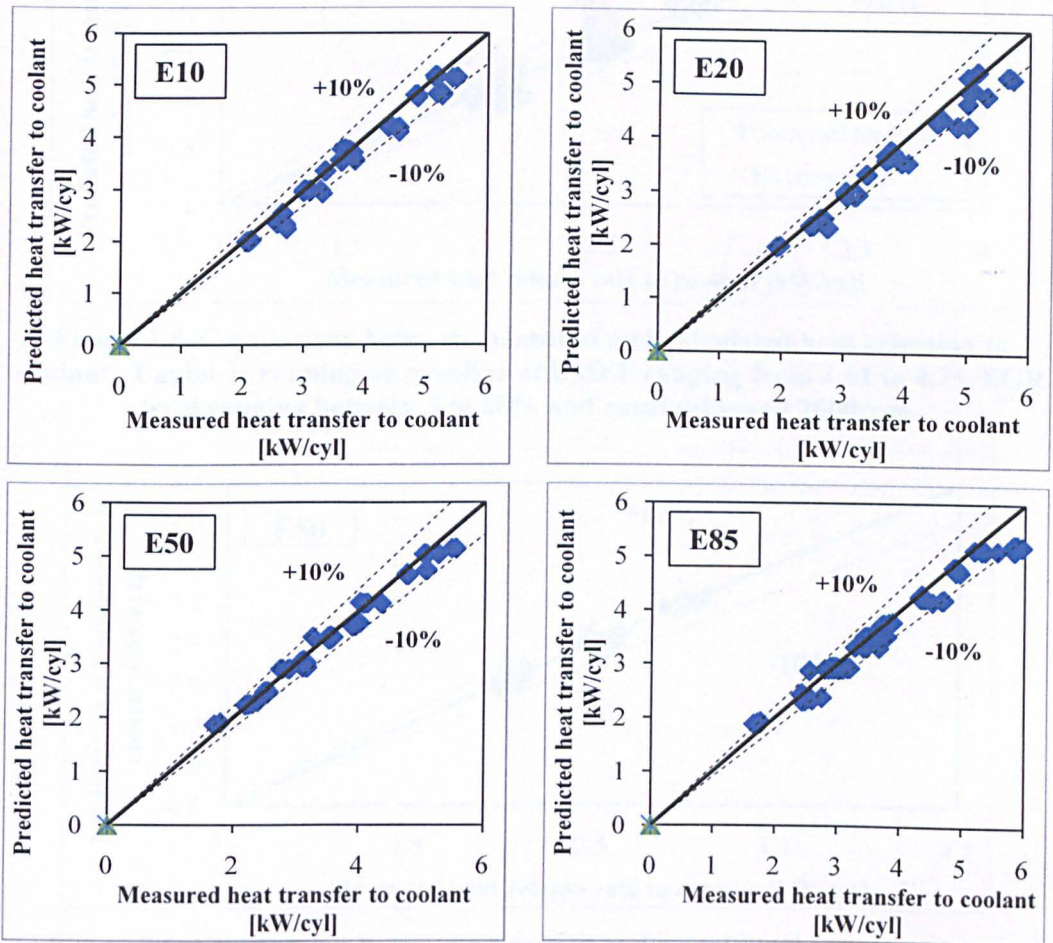


Figure 7.4. Comparison between measured heat rejection to the coolant and calculated using C1C2 correlation (equation 7.8) for engine running at different speeds and loads for different fuel mixtures.

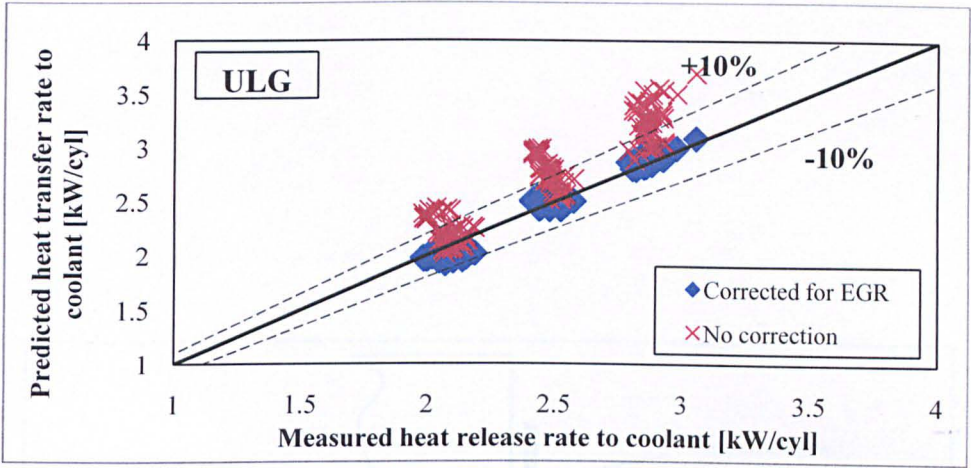


Figure 7.5. Comparison between measured and calculated heat rejection to coolant. Engine is running on gasoline at BMEP ranging from 1.61 to 4.75, EGR level ranging between 5 to 20% and constant speed 2000rpm.

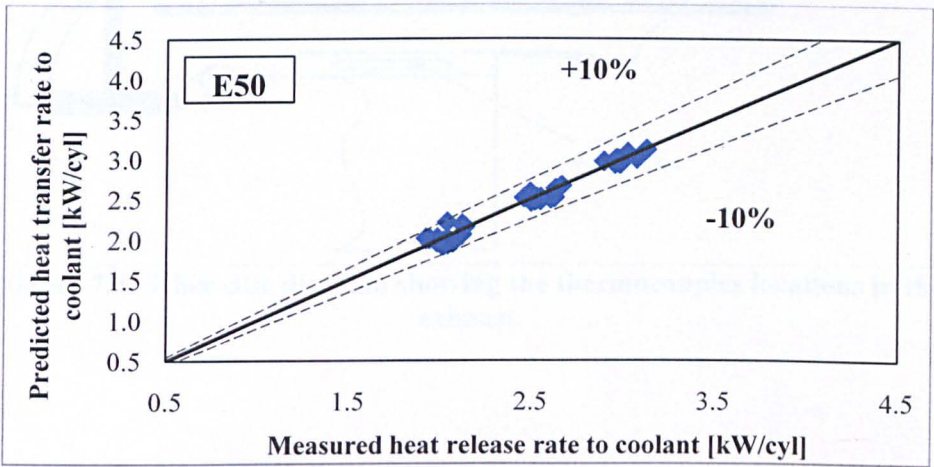


Figure 7.6. Comparison between measured and calculated heat rejection to coolant. Engine is running on E50 at BMEP ranging from 1.61 to 4.75, EGR ranging between 5 to 30% and constant speed 2000rpm.

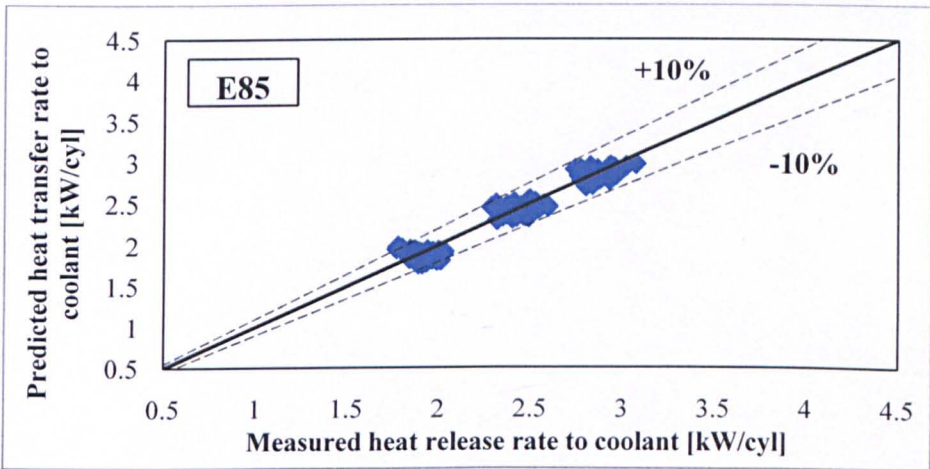


Figure 7.7. Comparison between measured and calculated heat rejected to the coolant. Engine is running on E85 at BMEP ranging from 1.61 to 4.75, EGR ranging between 5 to 30% and constant speed 2000rpm.

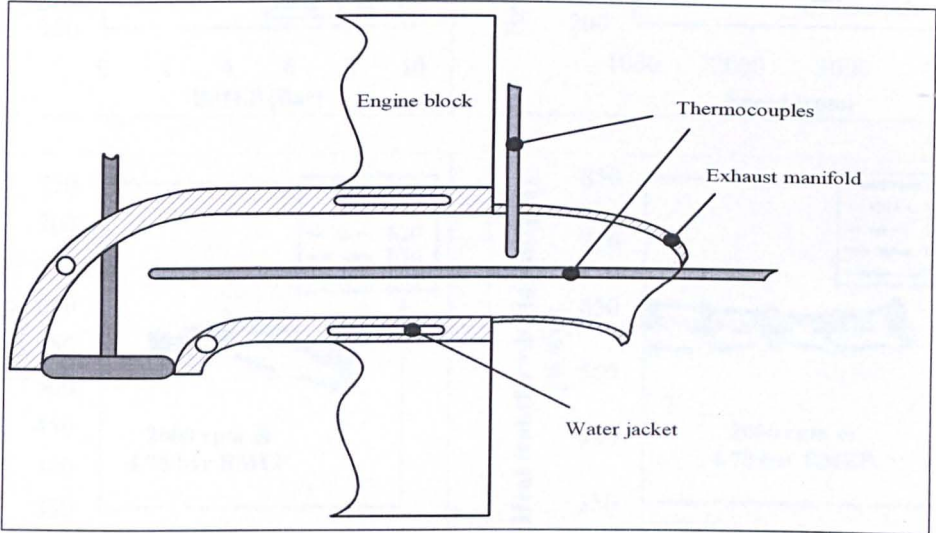


Figure 7.8. Schematic diagram showing the thermocouples locations in the exhaust.

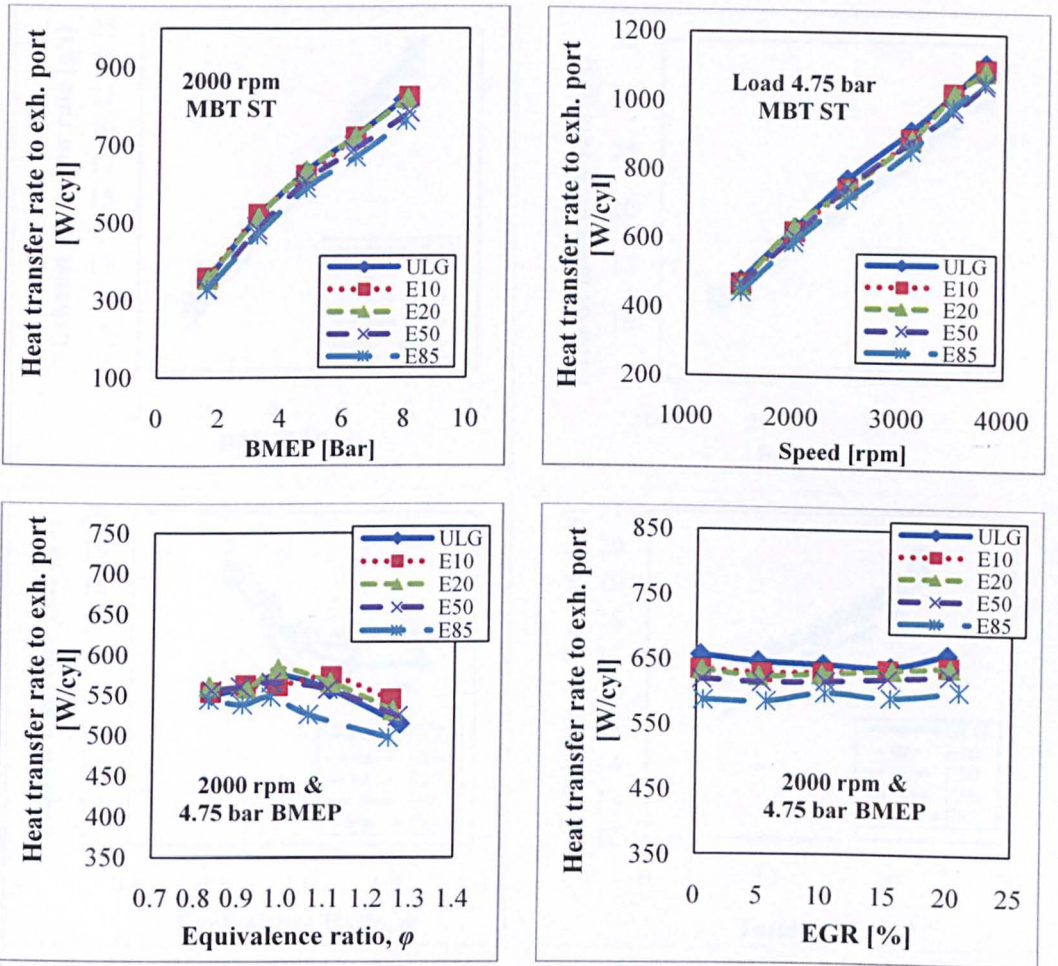


Figure 7.9. Heat transfer rate to exhaust port for different fuel blends as a function of load, speed, EGR and equivalence ratio.

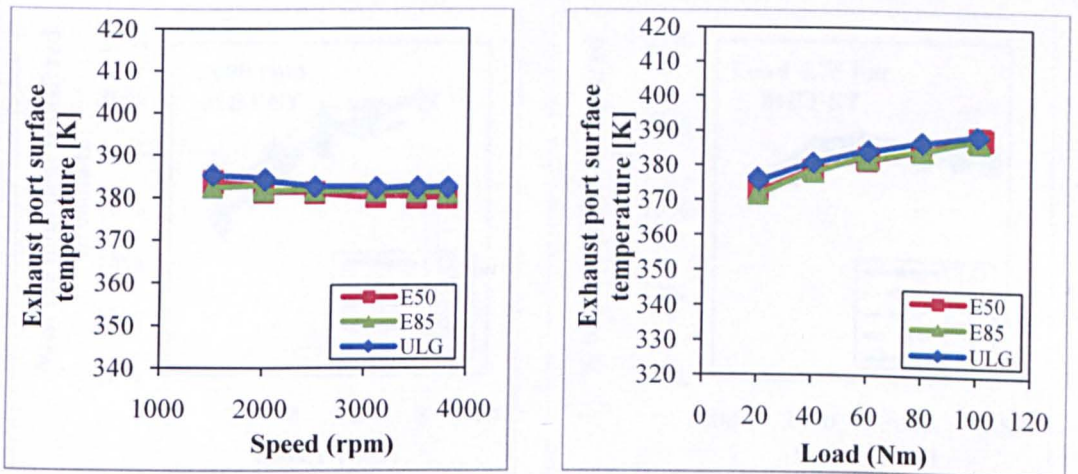


Figure 7.10. Exhaust surface temperature for different fuel mixtures as a function of speed and load.

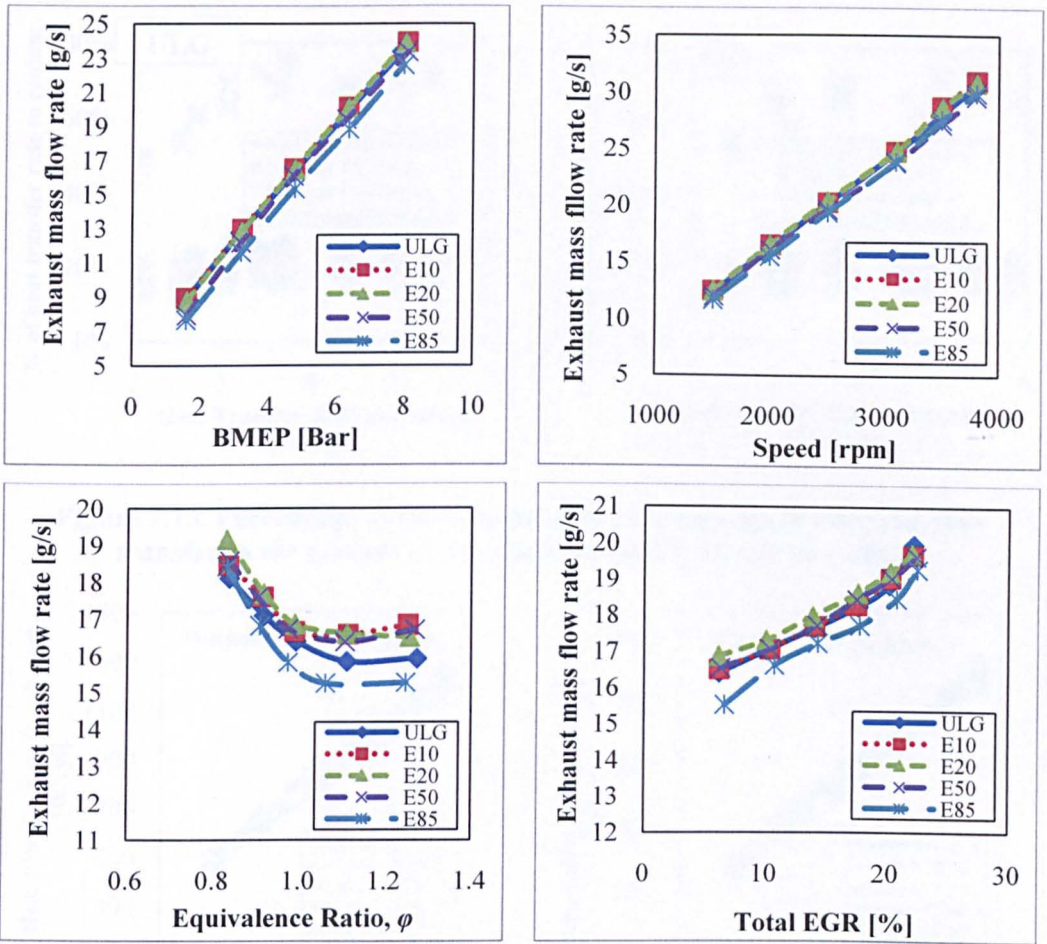


Figure 7.11. Exhaust mass flow rate for different fuel blends as function of varies running conditions.

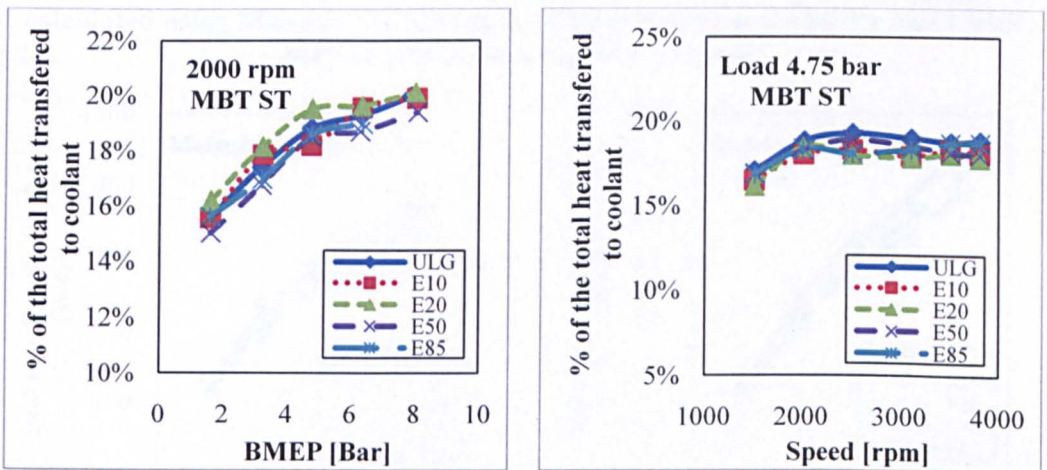


Figure 7.12. Percentage of the measured exhaust port heat rejection to the total heat transfer to the coolant as a function of speed and load.

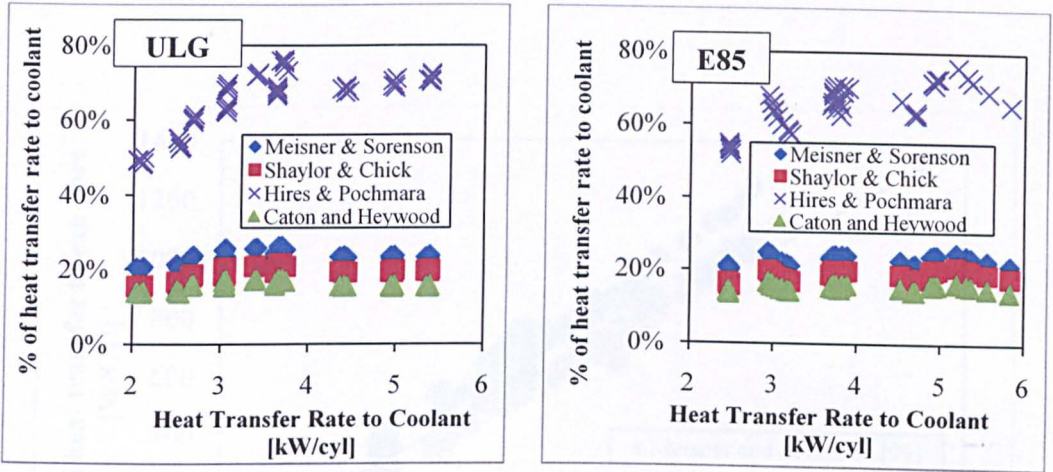


Figure 7.13. Percentage of the exhaust port heat transfer to the total heat transfer to the coolant as a function of heat rejection to coolant.

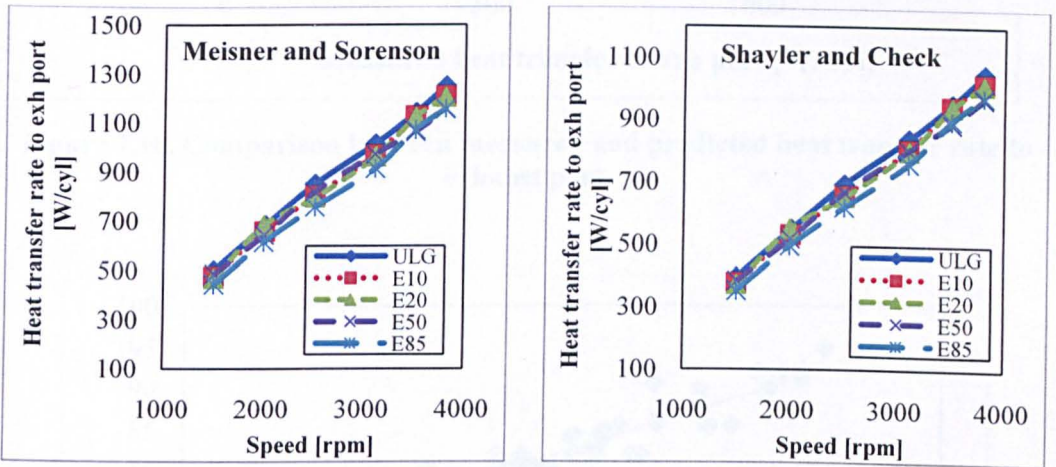


Figure 7.14. Heat rejection rate to exhaust port for different fuel blends calculated using Meisner and Sorenson [99] correlation and Shayler and Chick [88] correlation as a function of speed.

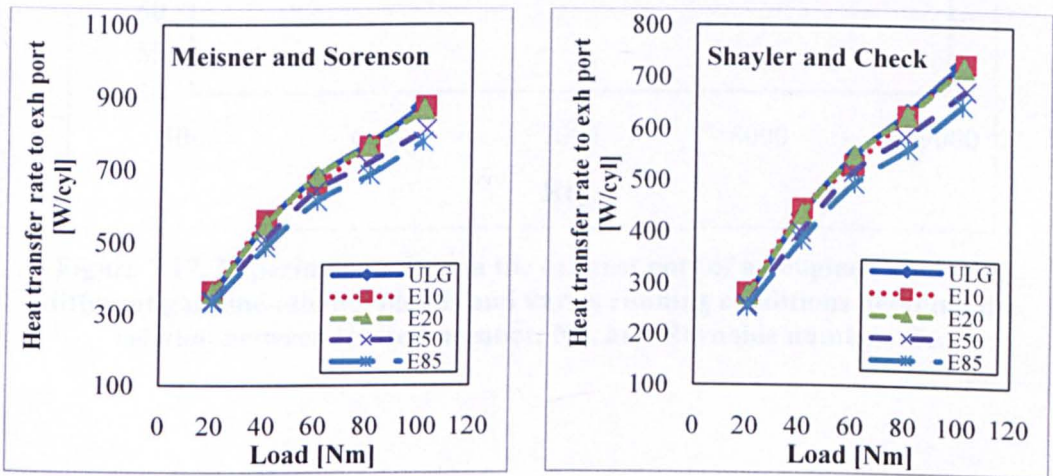


Figure 7.15. Heat rejection rate to the exhaust port calculated using Meisner Sorenson correlation [99] and Shayler and Chick correlation [88] as a function of load.

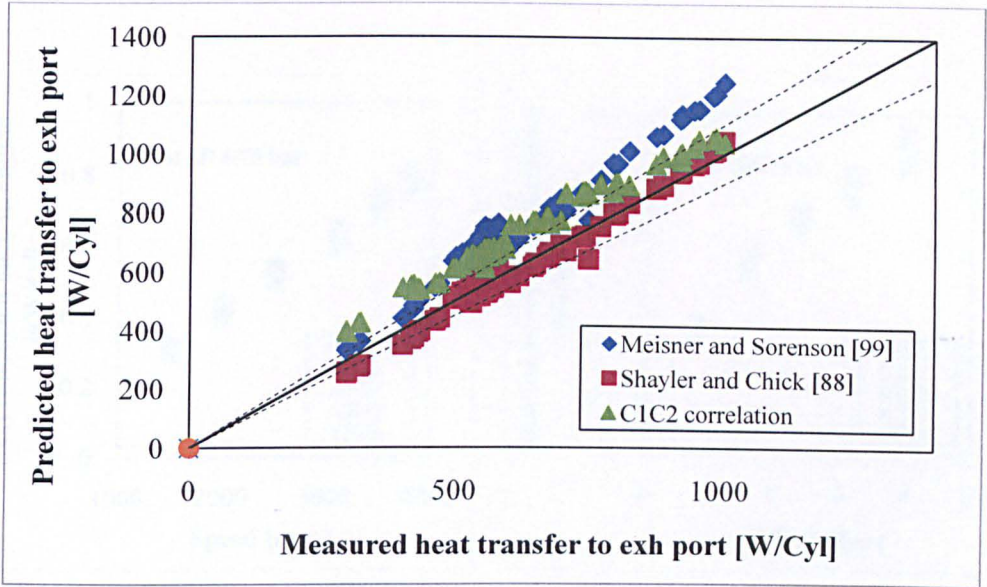


Figure 7.16. Comparison between measured and predicted heat transfer rate to exhaust port.

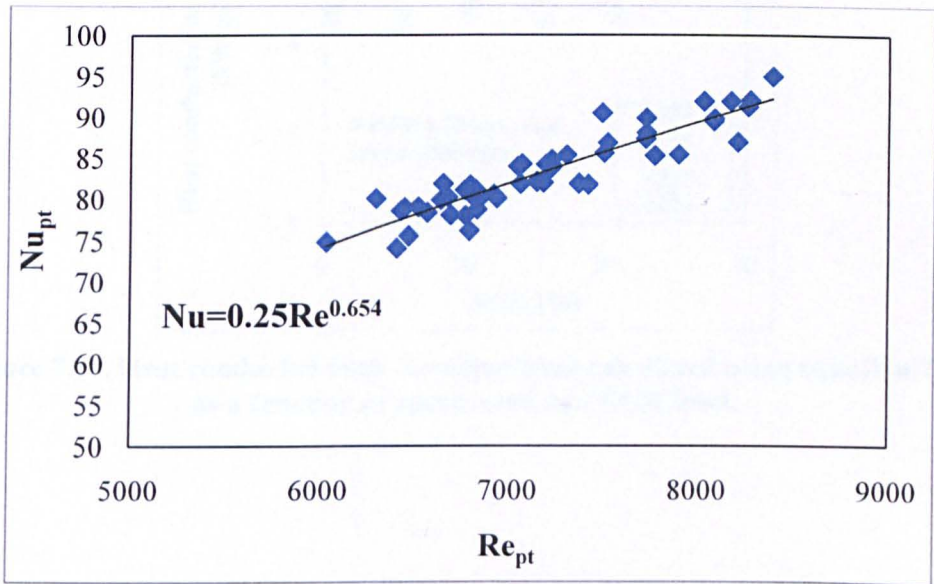


Figure 7.17. Experimental data in the exhaust port of an engine running at different gasoline-ethanol blends and varies running conditions detailing the relation between Nusselt number, Nu, and Reynolds number, Re.

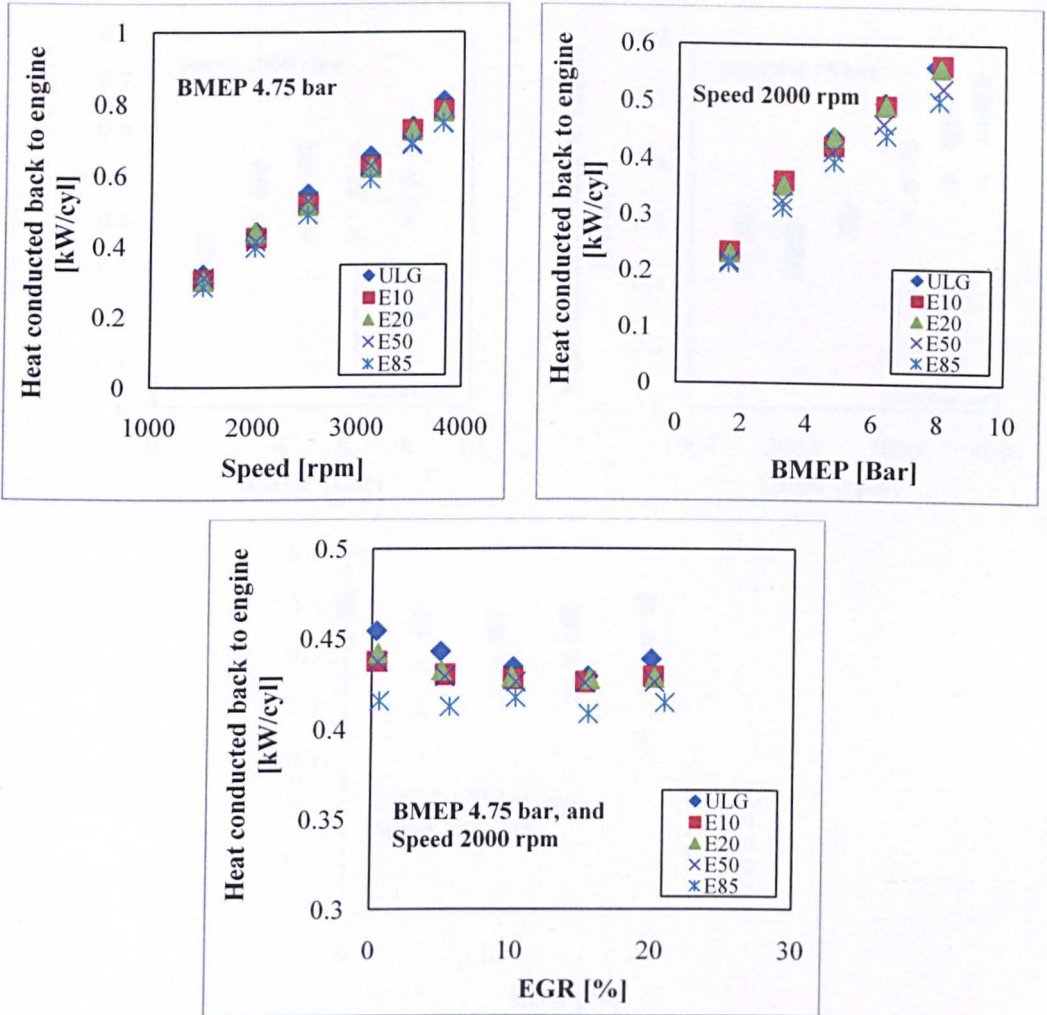


Figure 7.18. Heat conducted back to engine head calculated using equation 7.13 as a function of speed, load and EGR level.

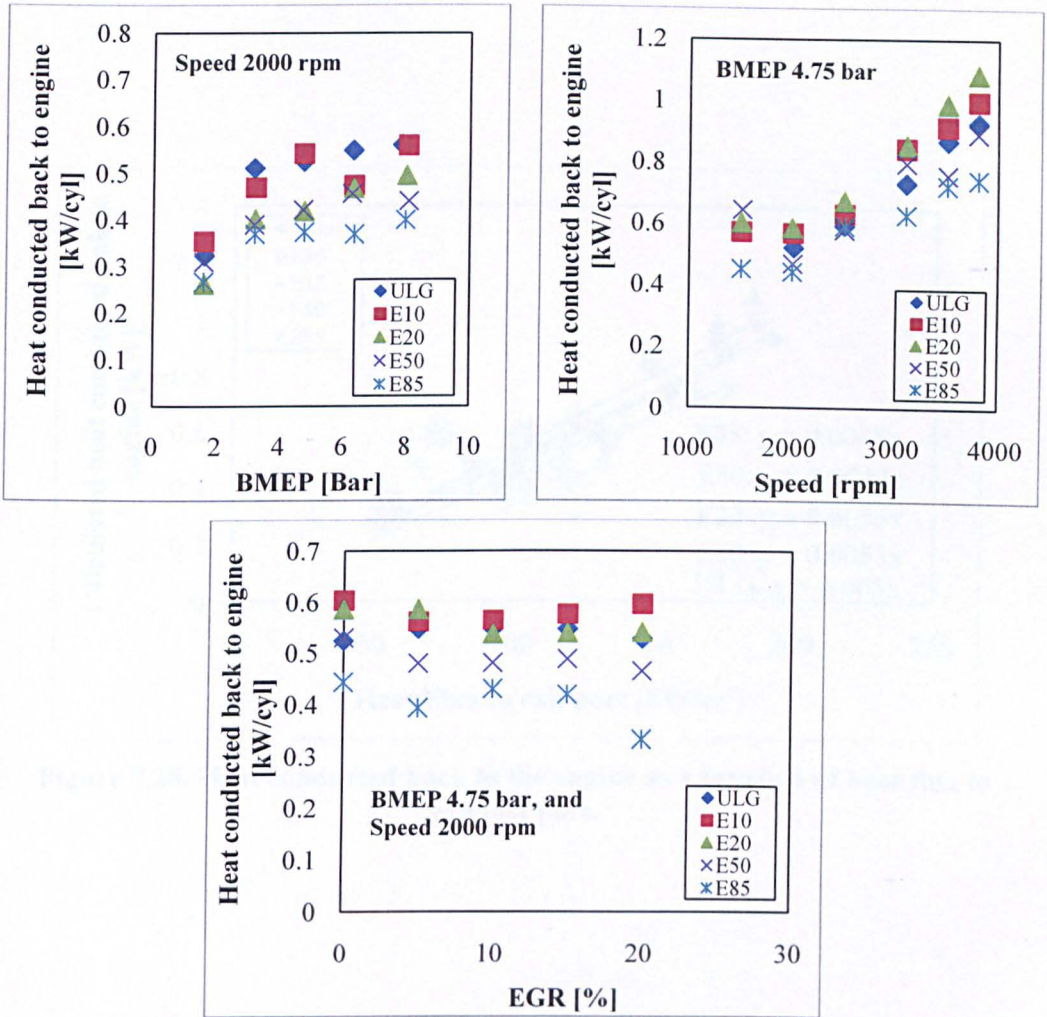


Figure 7.19. Heat conducted back to engine calculated using coolant energy balance equation as function of speed, load and EGR.

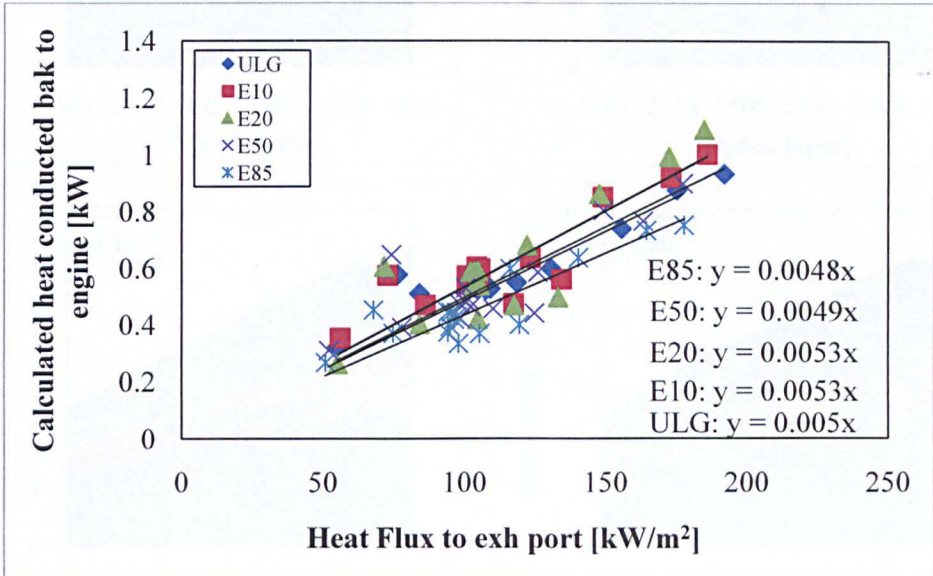


Figure 7.20. Heat conducted back to the engine as a function of heat flux to exhaust port.

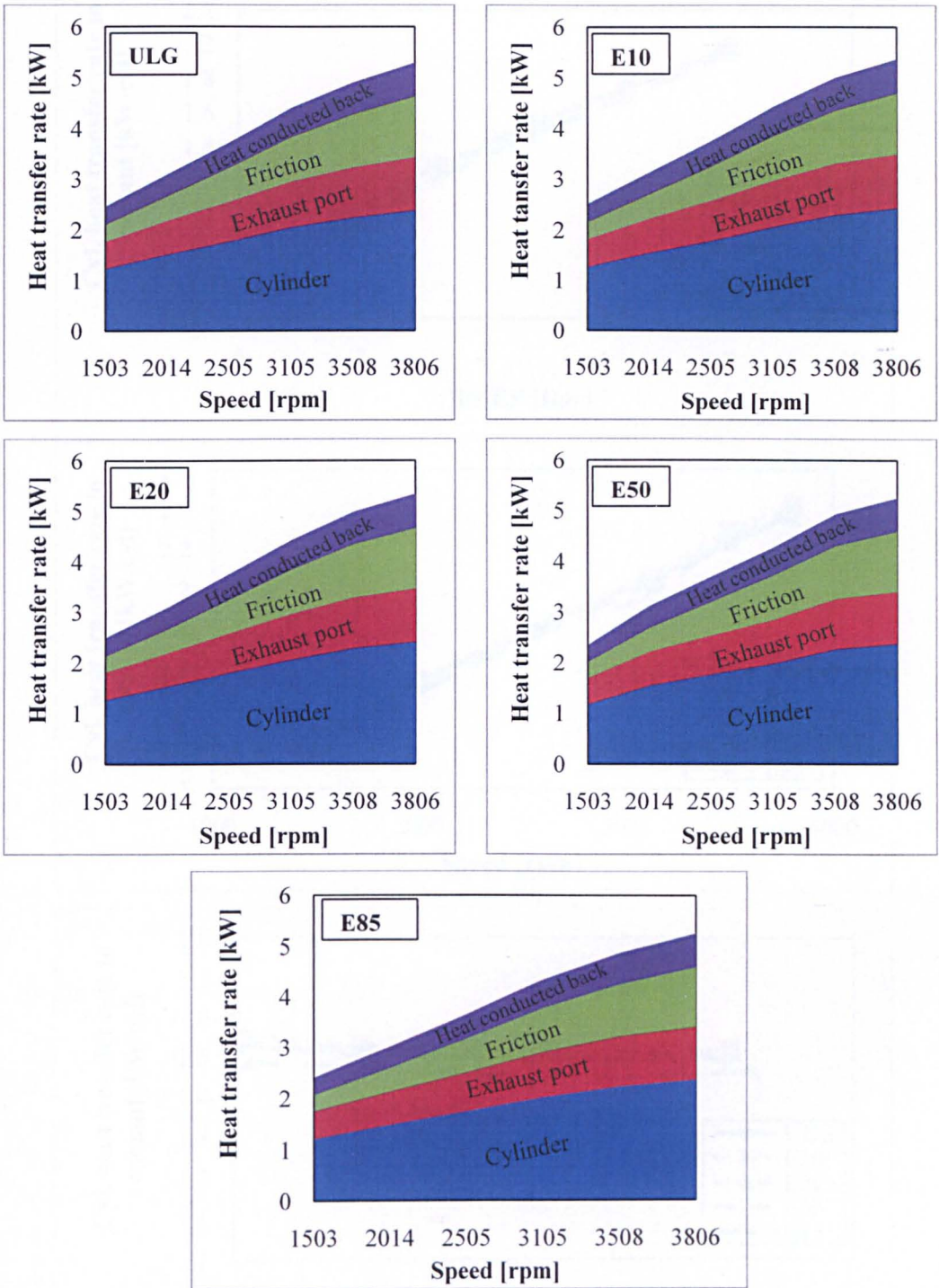


Figure 7.21. Source of heat rejection to coolant for different fuel blends as a function of speed.

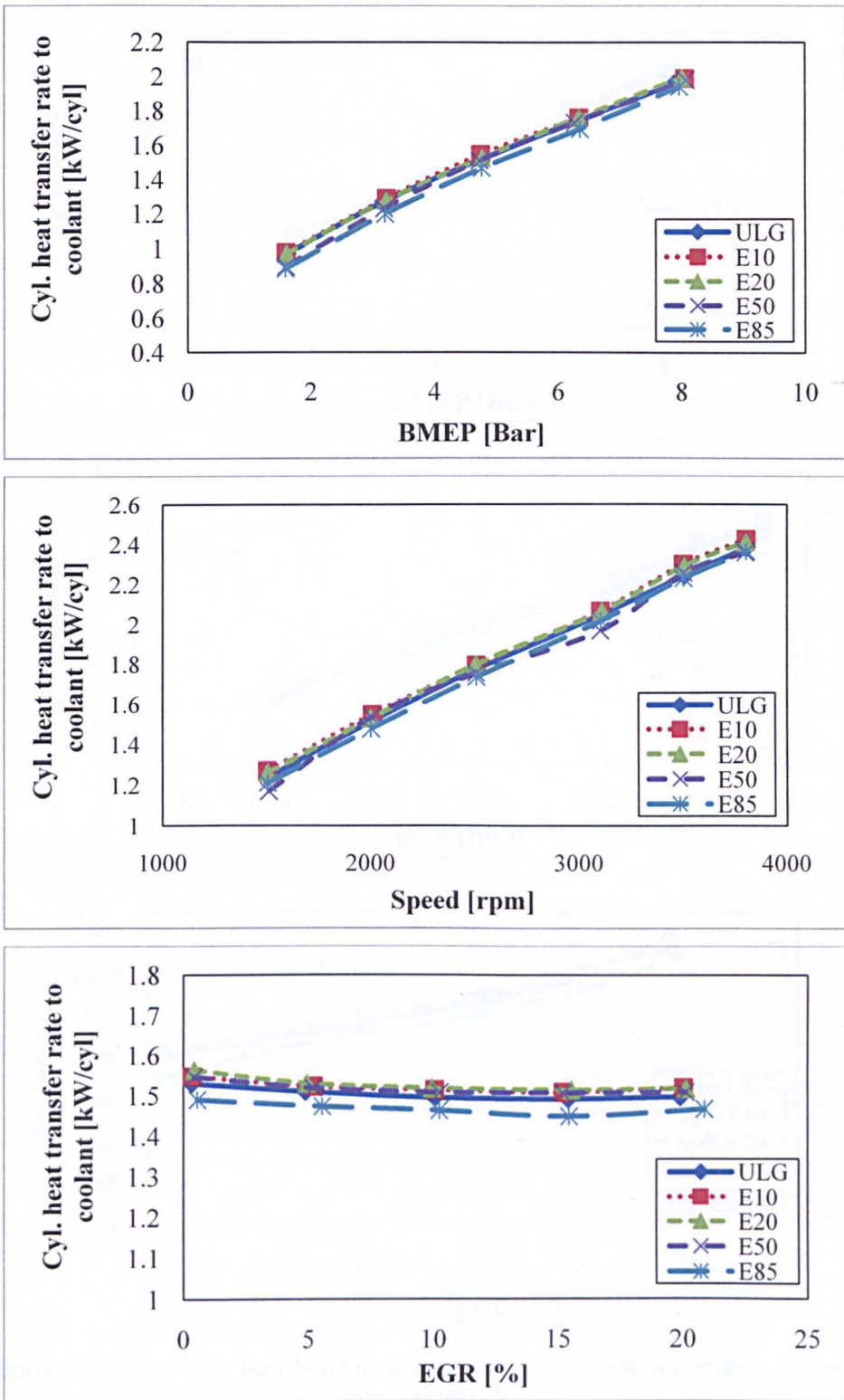


Figure 7.22. Gas side heat transfer rate to cylinder wall calculated using equation 7.6 for different fuel blends as a function of BMEP, speed and EGR levels.

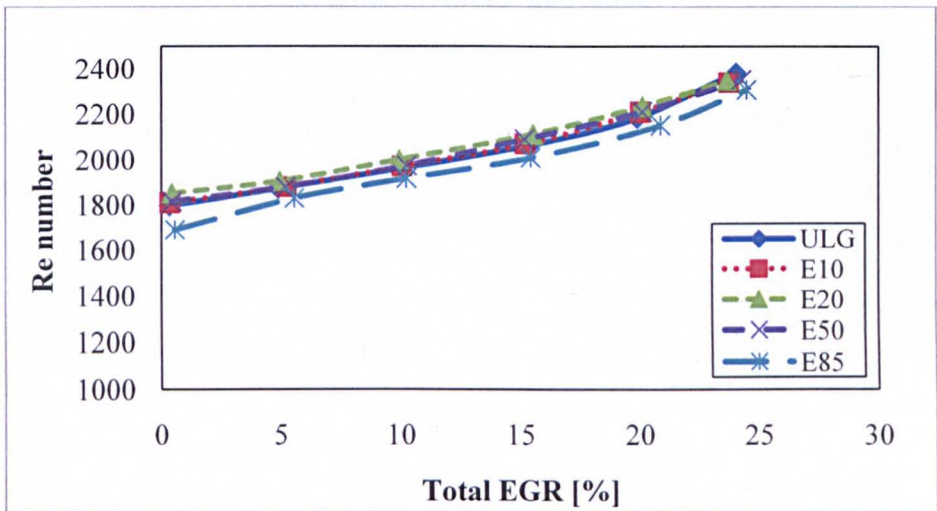
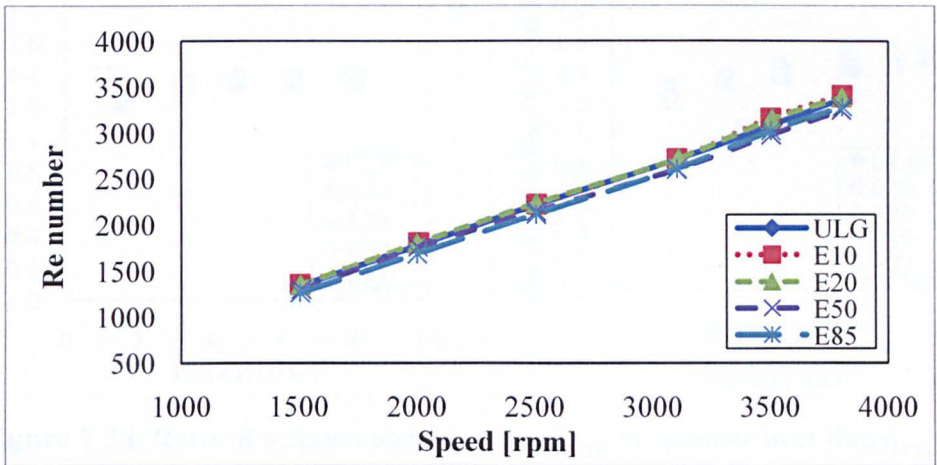
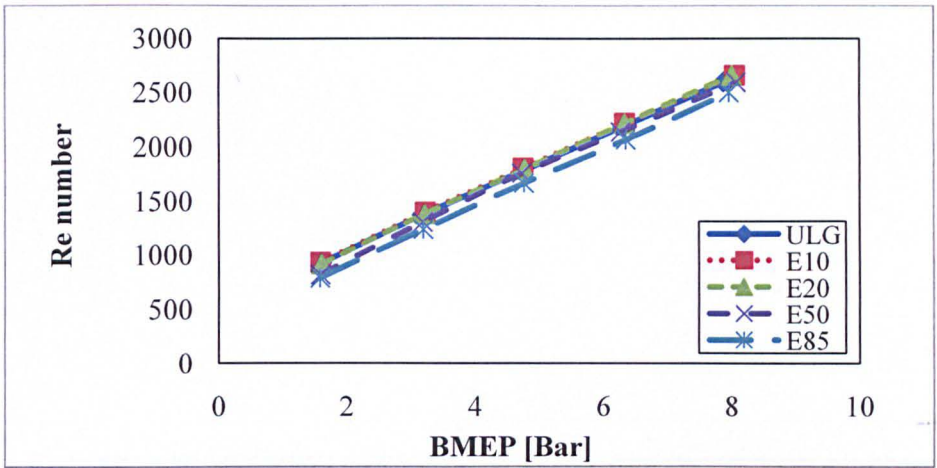


Figure 7.23. Reynolds number for different fuel blends as a function of speed, load and EGR.

CHAPTER 7

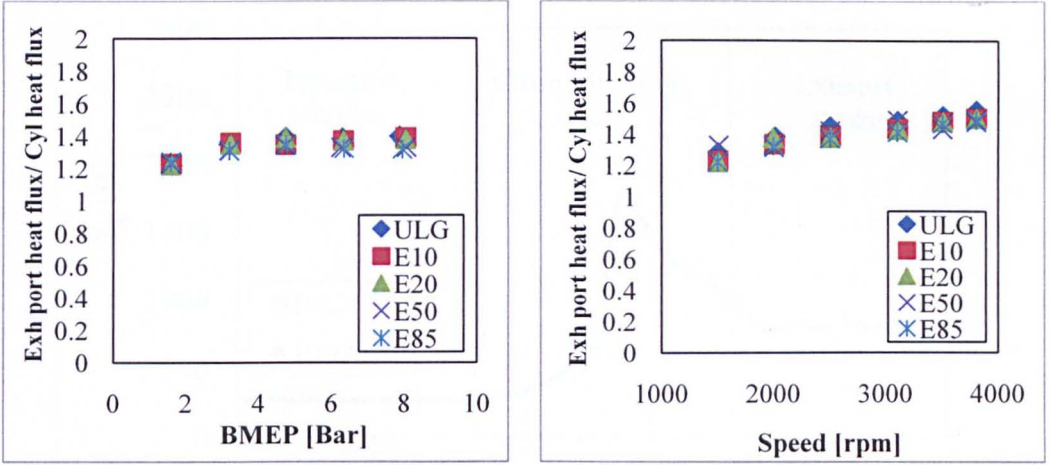


Figure 7.24. Ratio of exhaust port heat flux \dot{q}'_{exh} to cylinder heat flux \dot{q}'_{cyl} as function of BMEP and speed.

CHAPTER 8

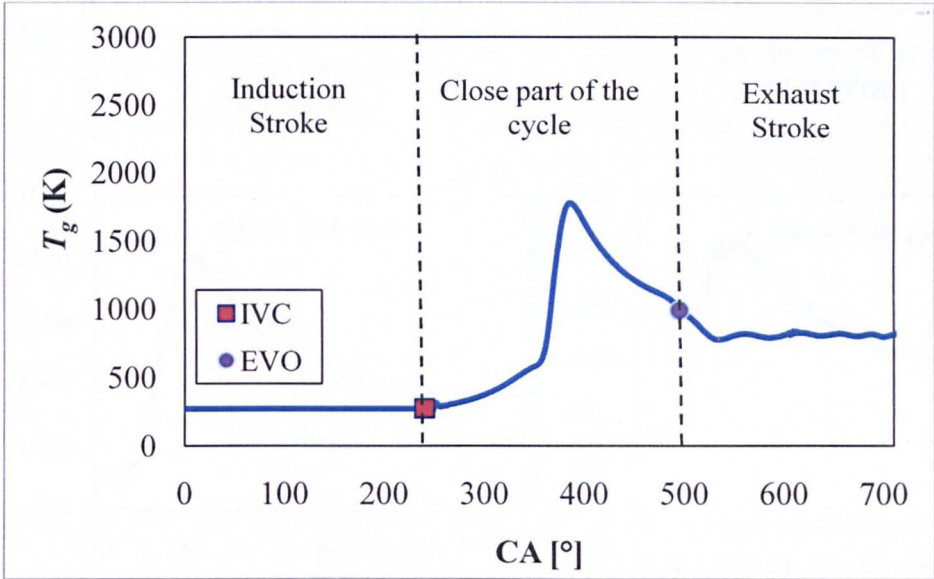


Figure 8.1. In-cylinder gas temperature, T_g , during engine cycle.

Cylinder 1

Cylinder 3

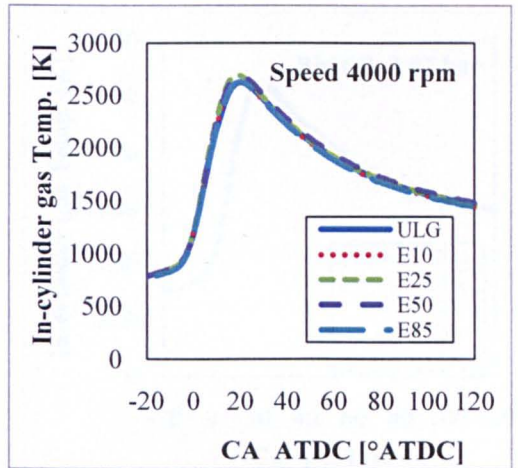
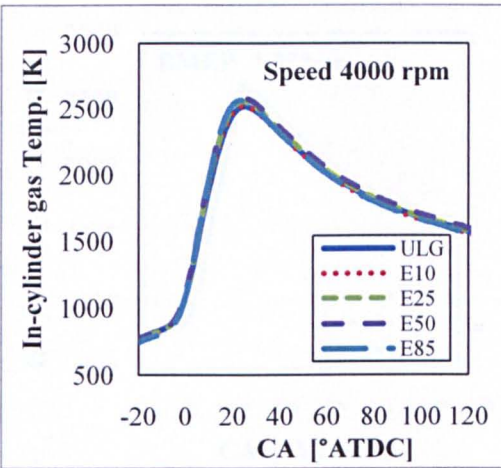
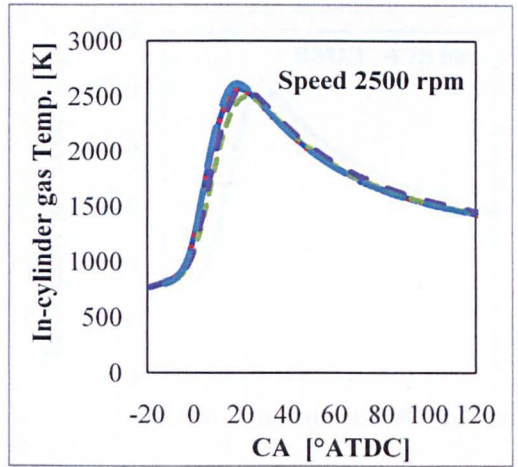
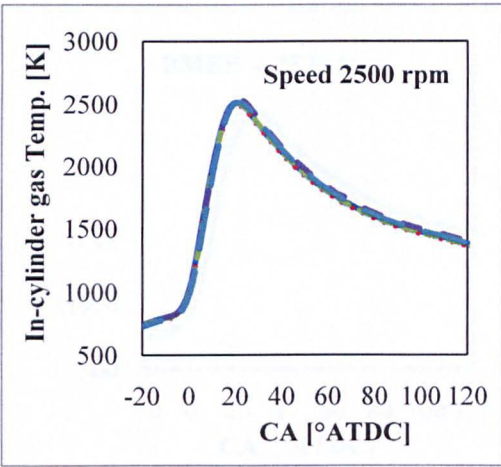
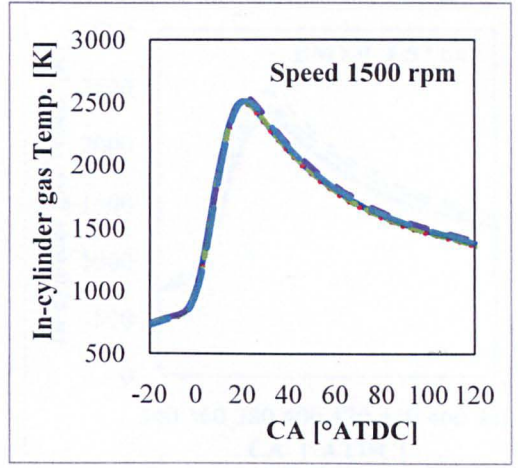
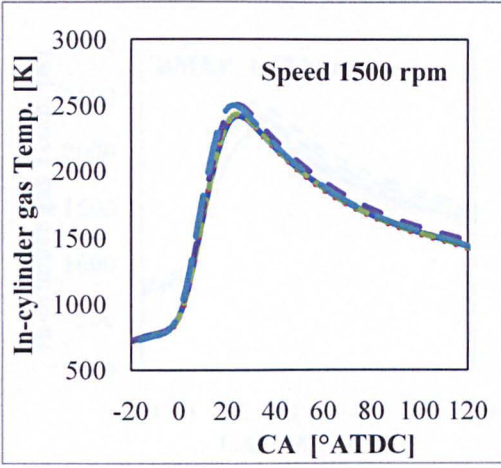
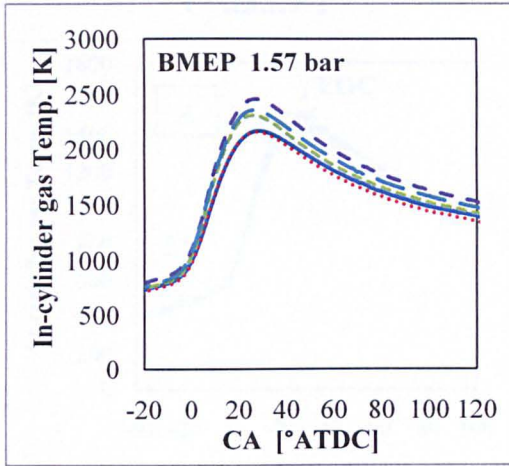


Figure 8.2. In-cylinder gas temperature for different fuel blends, different speeds, BMEP = 4.75, MBT spark timing and AFR_{stoich} .

Cylinder 1



Cylinder 3

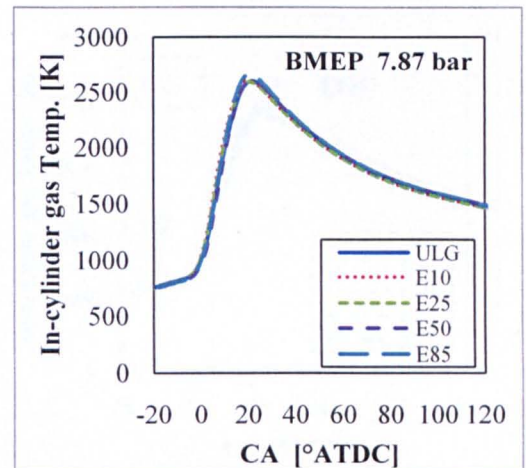
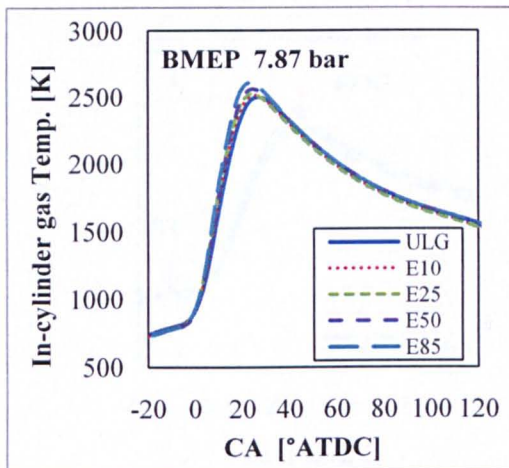
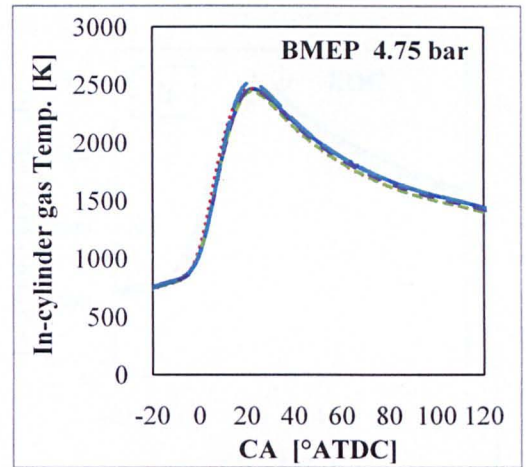
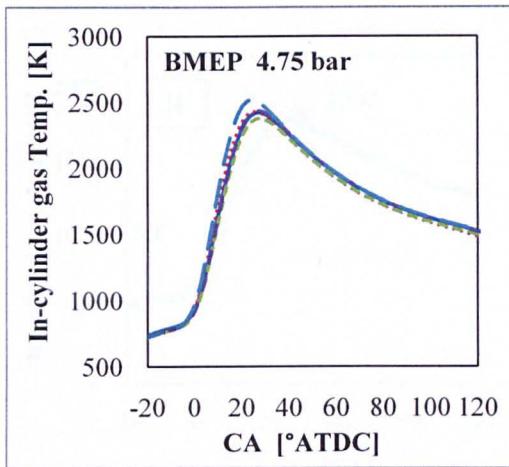
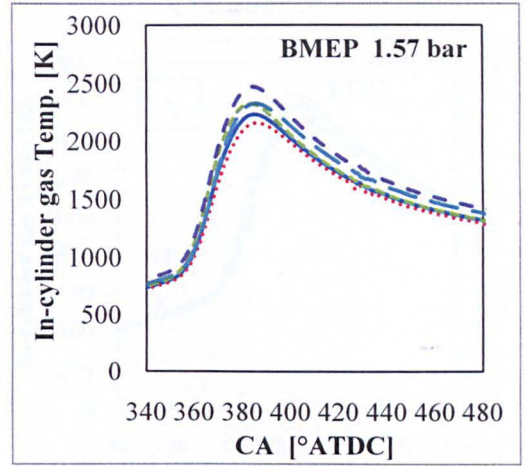


Figure 8.3. In-cylinder gas temperature for different fuel blends, different loads, constant speed 2000 rpm , MBT ST and AFR_{stoich} .

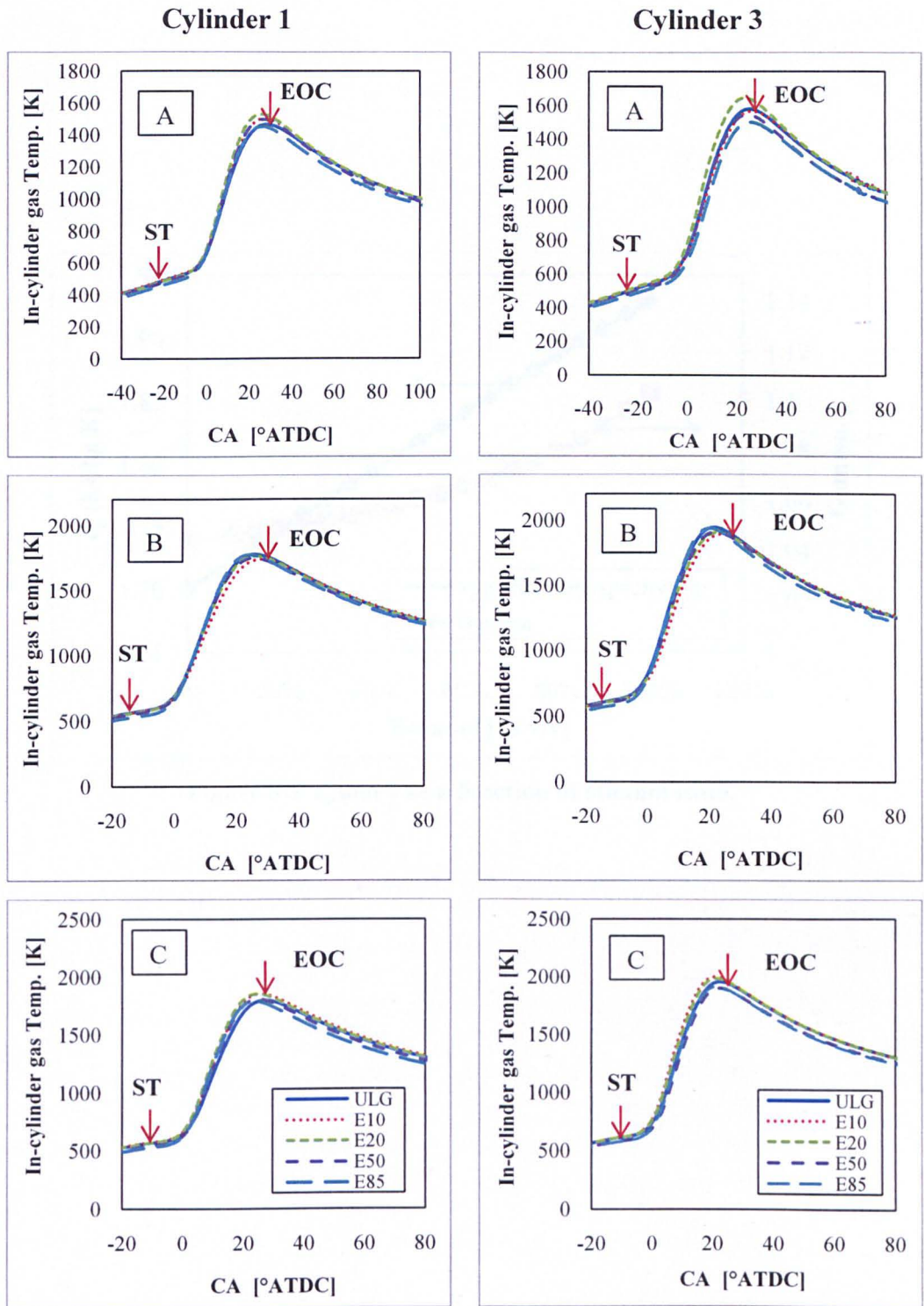


Figure 8.4. Recalculated temperature based on mass charged calculated from equation 8.3 for the engine running at constant speed and different loads at BMEP = A) 1.57 bar, B) 4.75 bar and C) 7.87 bar.

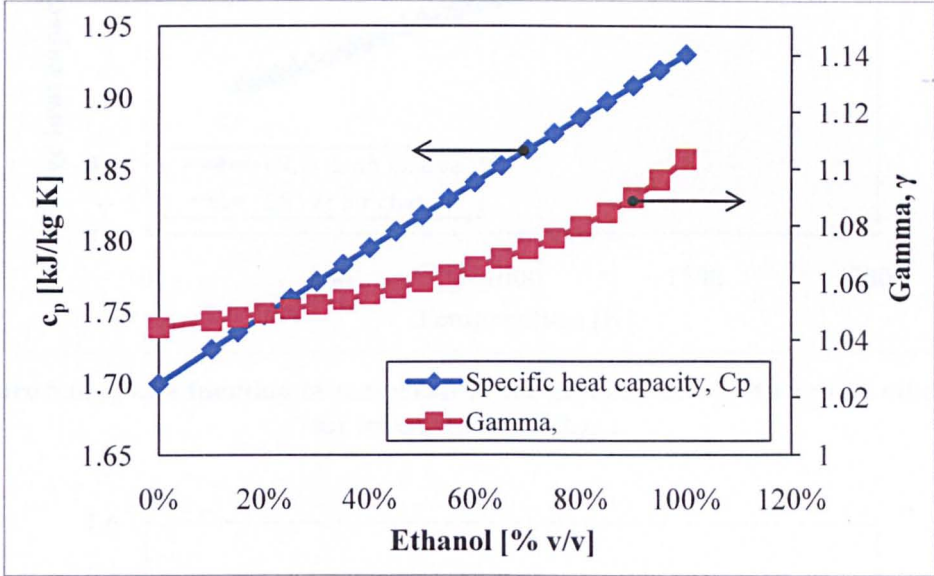


Figure 8.5. c_p and γ as a function of ethanol ratio.

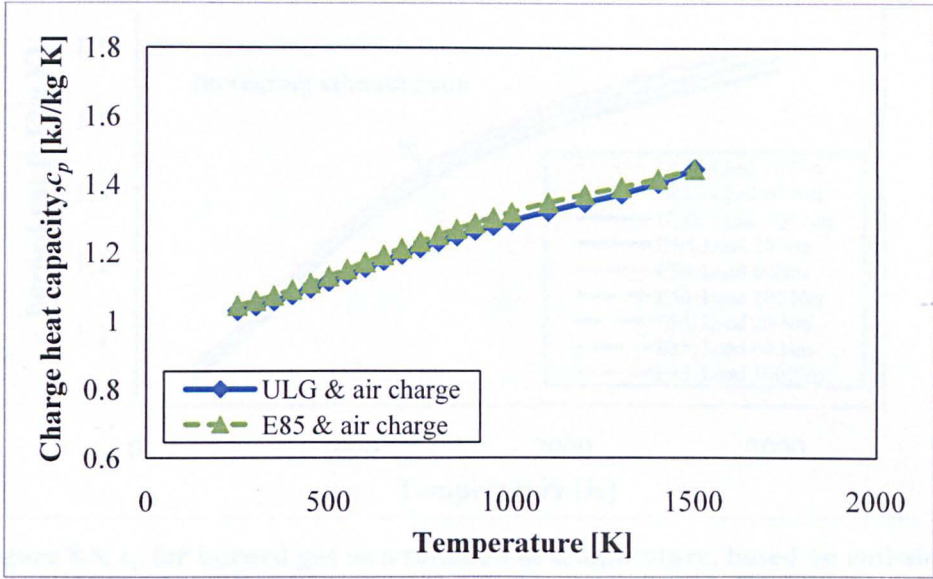


Figure 8.6. c_p as a function of temperature for gasoline-air mixtures and ethanol-air mixtures at AFR_{stoich} .

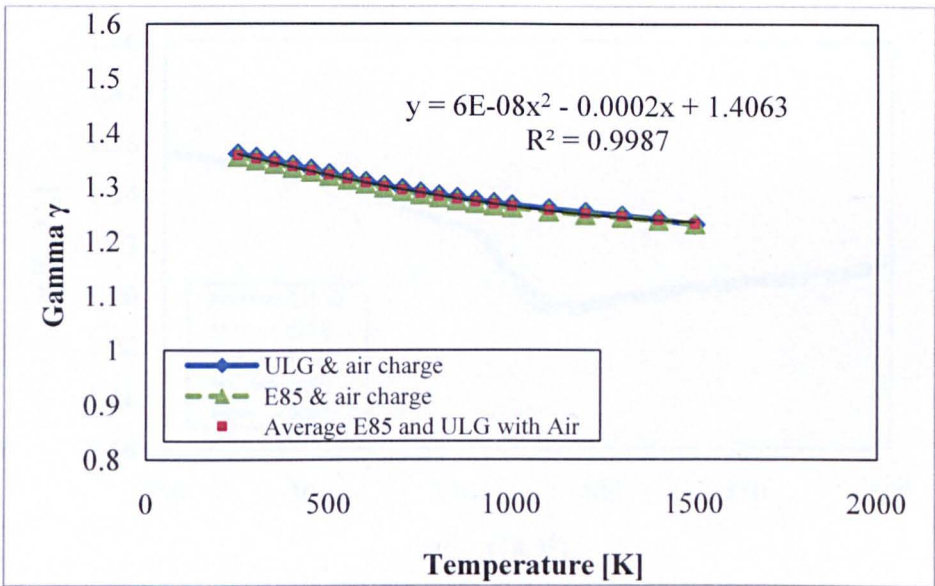


Figure 8.7. γ as a function of temperature for gasoline-air mixtures and ethanol-air mixtures at AFR_{stoich} .

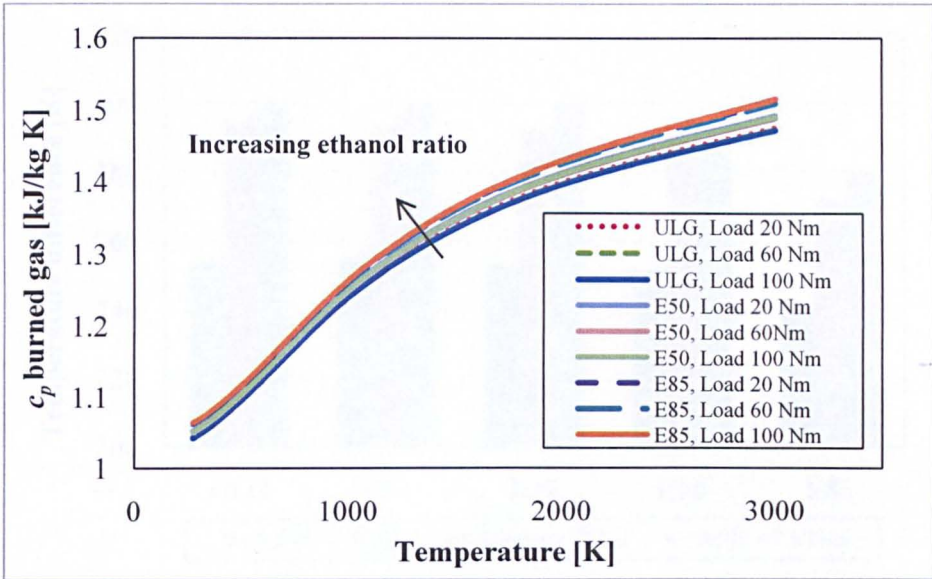


Figure 8.8. c_p for burned gas as a function of temperature, based on emissions compositions produced by the engine running at different loads and fuel compositions.

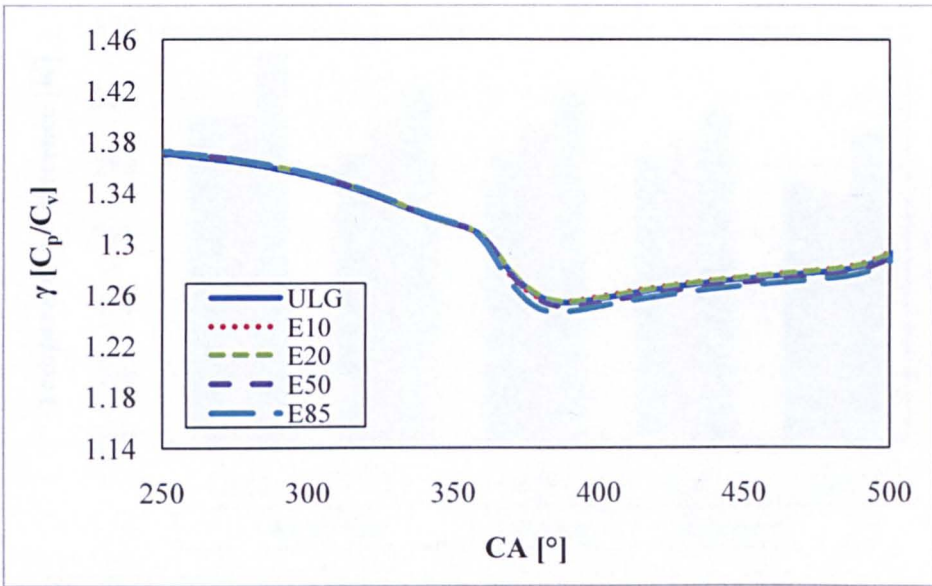


Figure 8.9. γ during the engine cycle when the engine is running at BMEP 4.75 bar and 2000rpm speed.

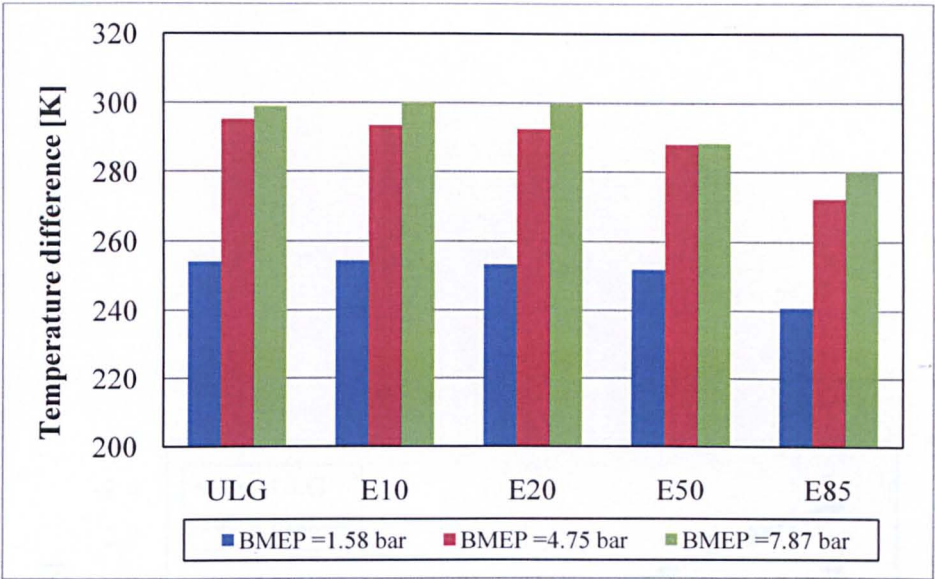


Figure 8.10. The temperature rise during compression between IVC and spark timing for different fuel mixture, at a constant engine running speed of 2000 rpm.

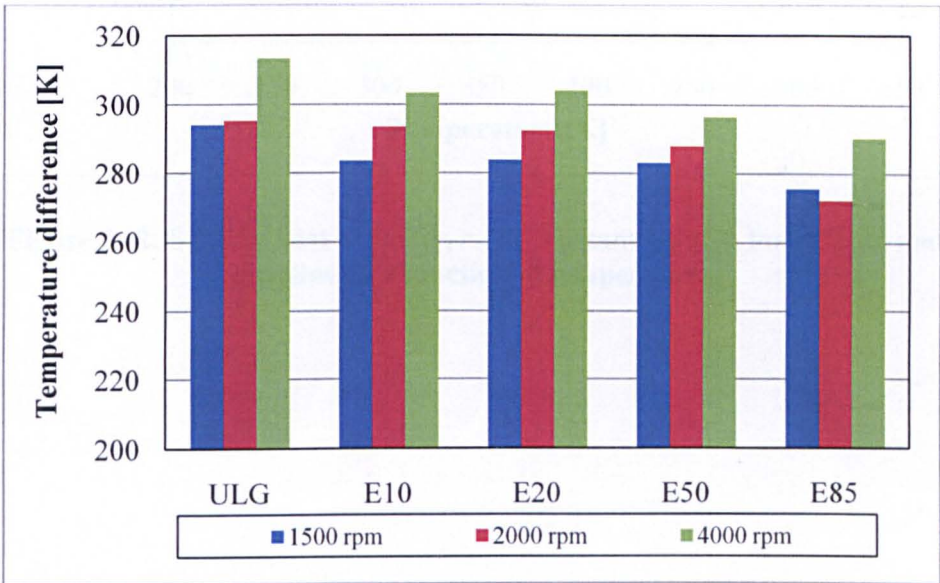


Figure 8.11. The temperature rise during compression between IVC and spark timing for different fuel mixture at a constant engine running load of 4.75 rpm.

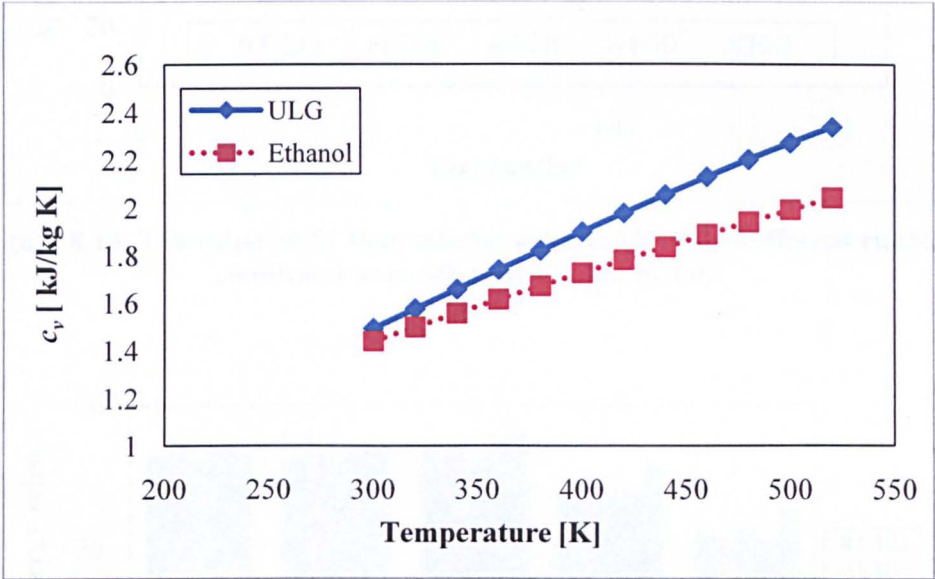


Figure 8.12. Specific heat capacity, c_v , at constant volume for ethanol and gasoline as a function of temperature.

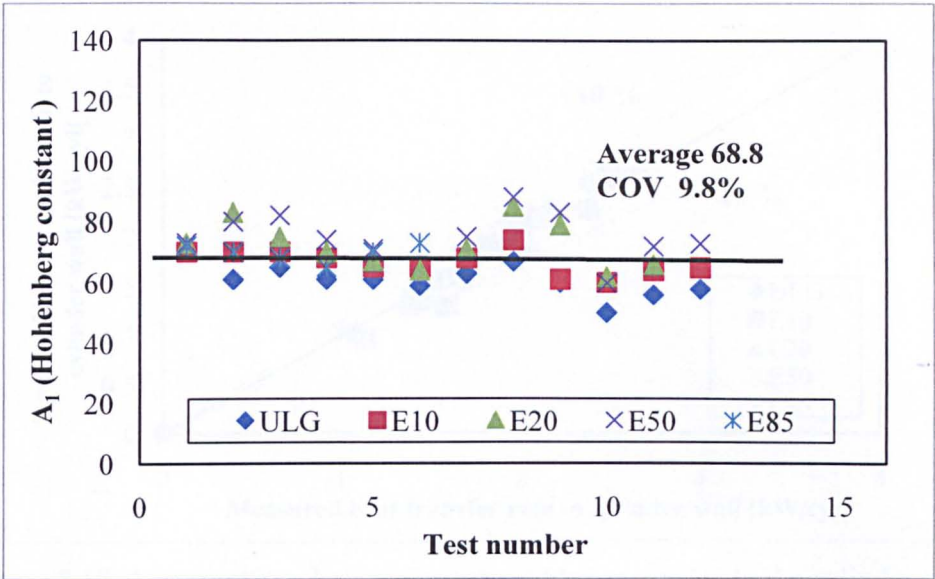


Figure 8.13. The value of A_1 that satisfies equation 8.15 for different running conditions and different ethanol blends.

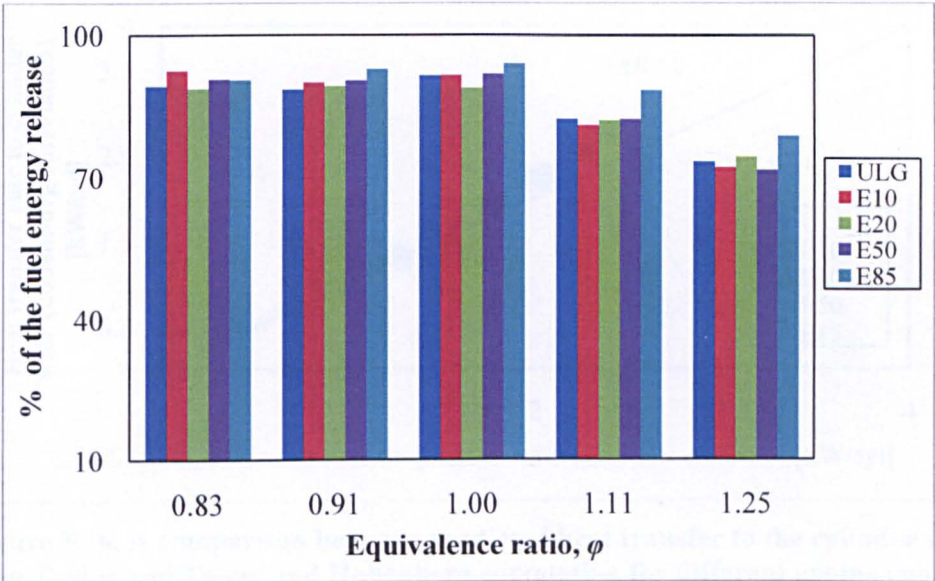


Figure 8.14. Percentage of the gross heat release to the energy released by the fuel in a cycle $\left(\frac{\dot{Q}_{gross}}{(m_f \times Q_{LHV})}\right)$ as a function of equivalence ratio.

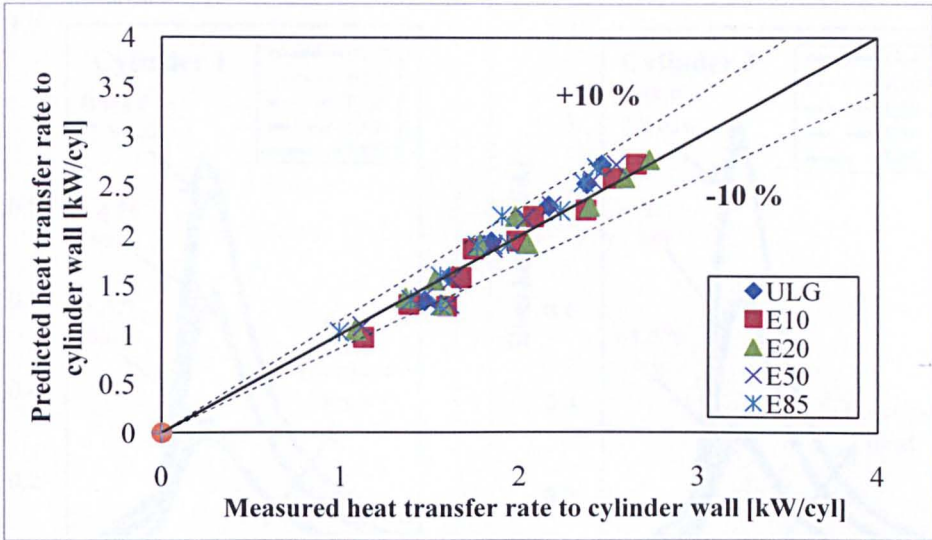


Figure 8.15. A comparison between measured heat transfer to the cylinder wall and predicted value using Hohenberg correlation for different engine running conditions.

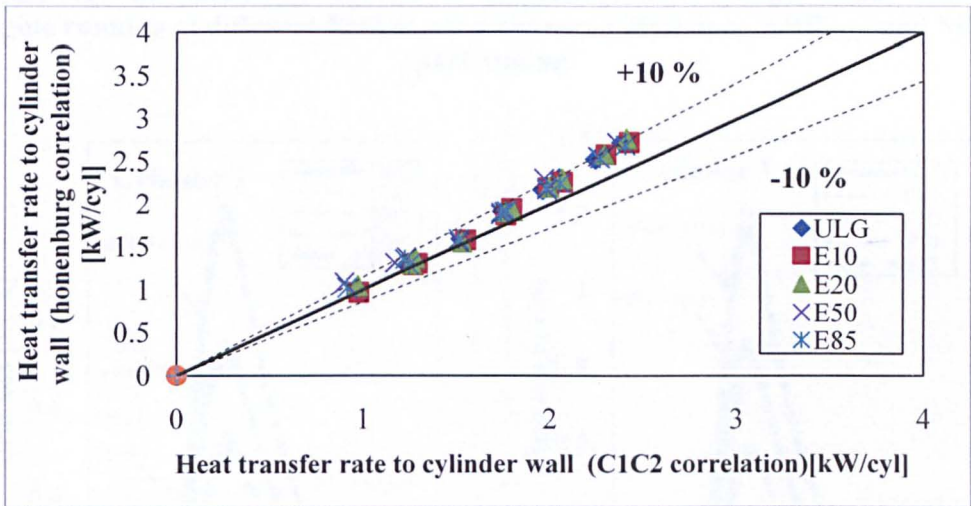


Figure 8.16. A comparison between predicted heat transfer to the cylinder wall using Taylor and Toong and Hohenberg correlation for different engine running conditions.

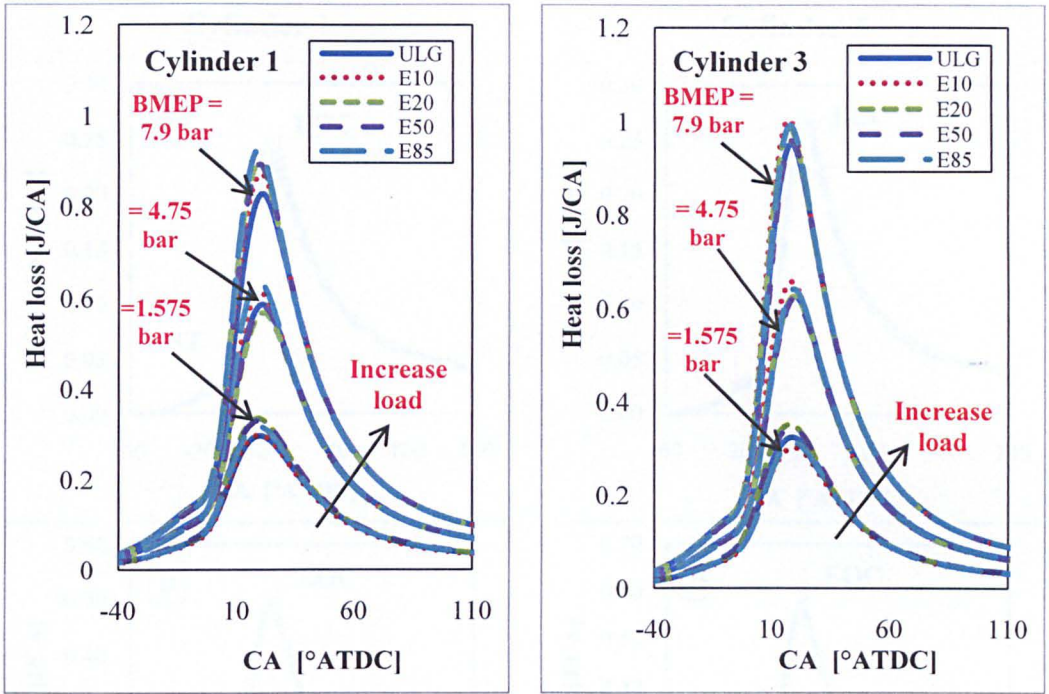


Figure 8.17. Instantaneous heat loss for different gasoline-ethanol blends with the engine running at different BMEP, constant speed 2000 rpm, ARR_{stoich} and MBT spark timing.

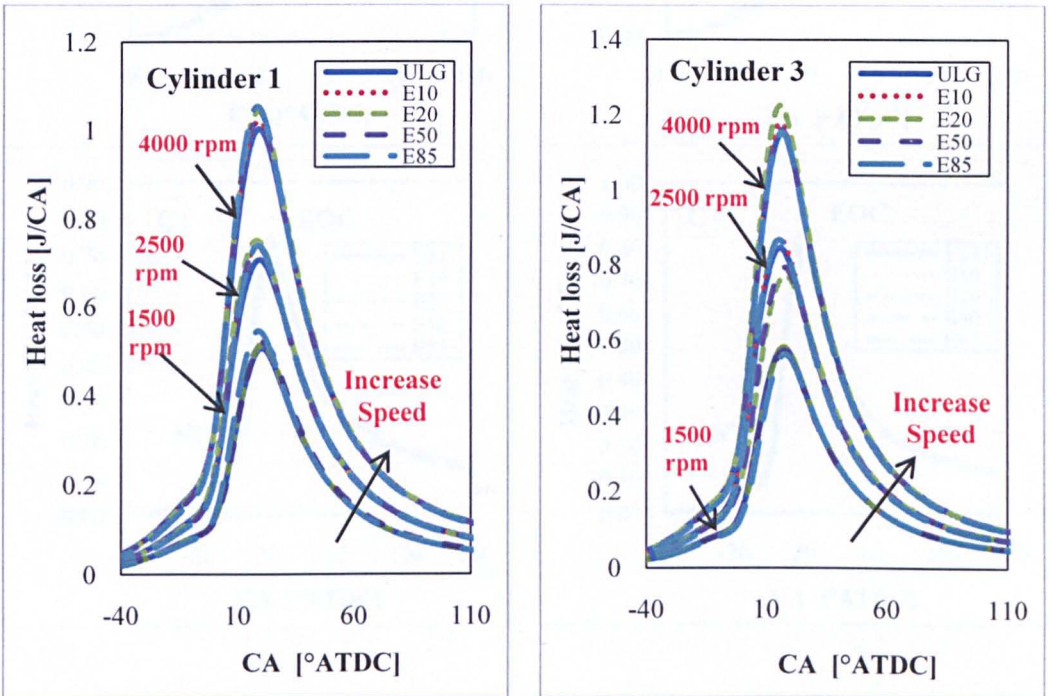


Figure 8.18. Instantaneous heat loss for different gasoline-ethanol blends with the engine running at different speed, constant BMEP 4.75 bar, ARR_{stoich} and MBT spark timing.

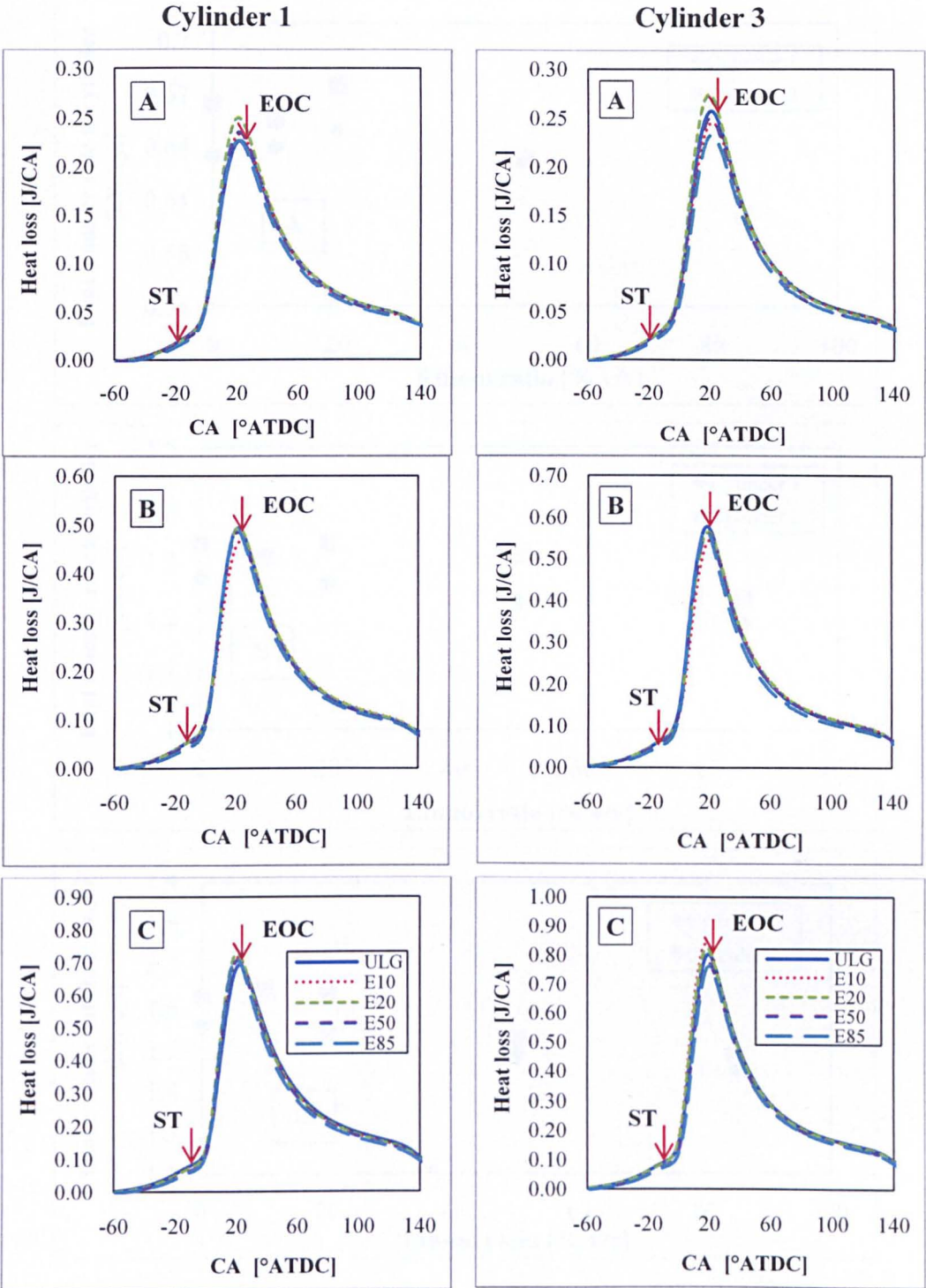


Figure 8.19. Recalculated heat loss to cylinder based on mass charged calculated from equation 8.3. Engine running at 2000 rpm and different loads, at BMEP = A) 1.57 bar, B) 4.75 bar and C) 7.87 bar.

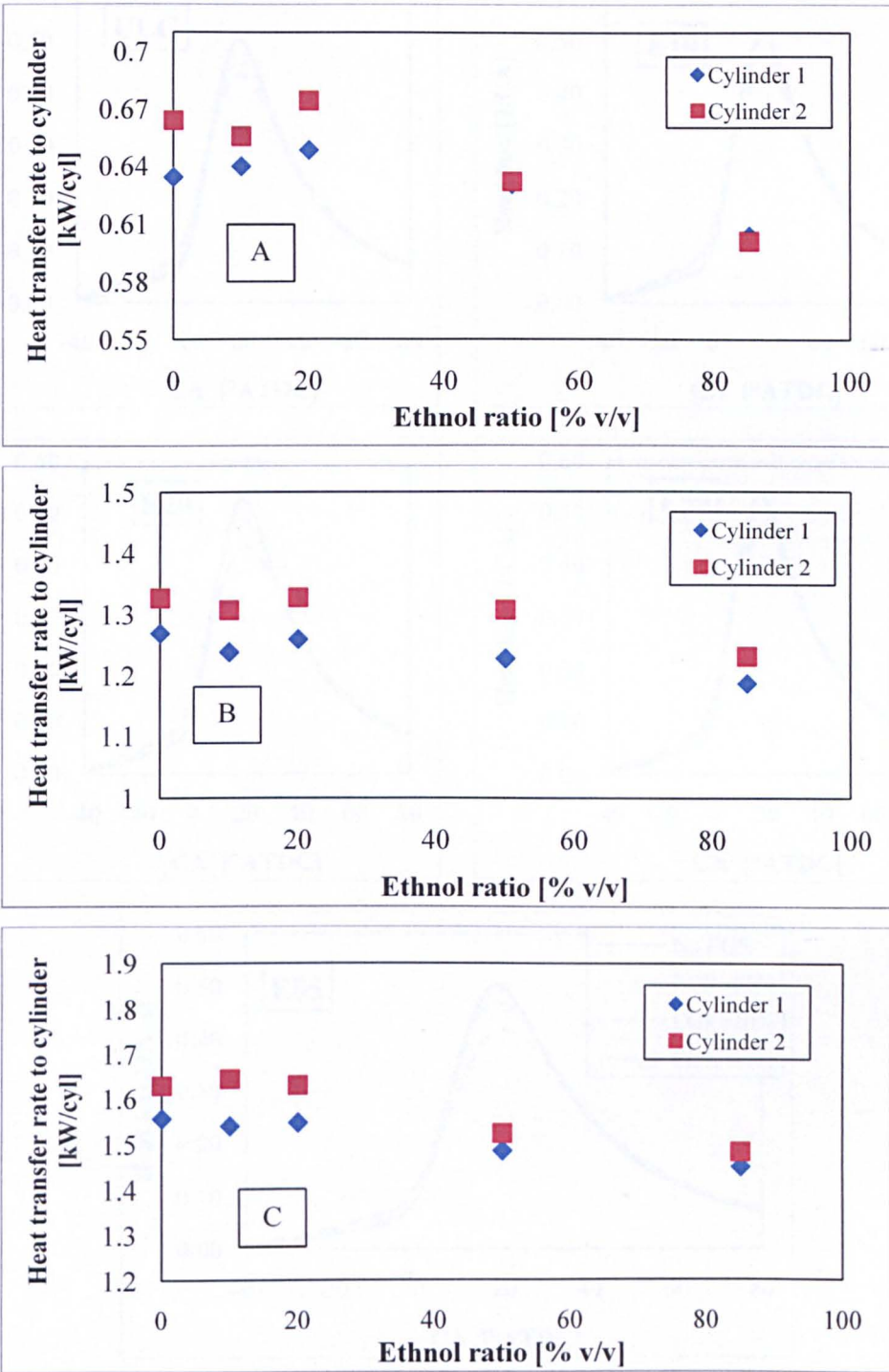


Figure 8.20. Cylinder heat transfer rate, \dot{Q}_{cyl} , based on mass charged calculated from equation 8.3. Engine running at 2000 rpm and different loads including BMEP = A) 1.57 bar, B) 4.75 bar and C) 7.87 bar.

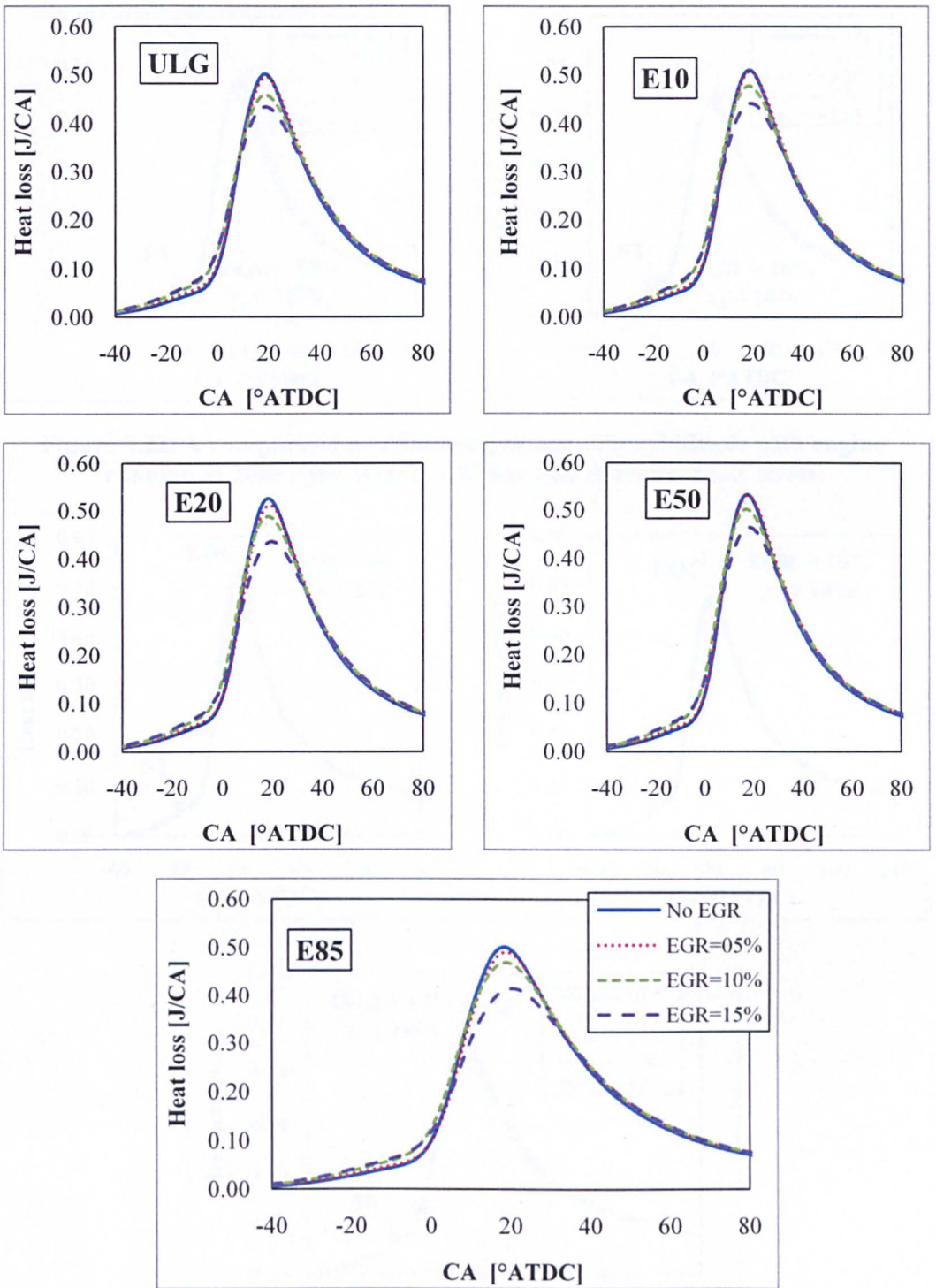


Figure 8.21. Effect of EGR on heat loss for different fuel blends.

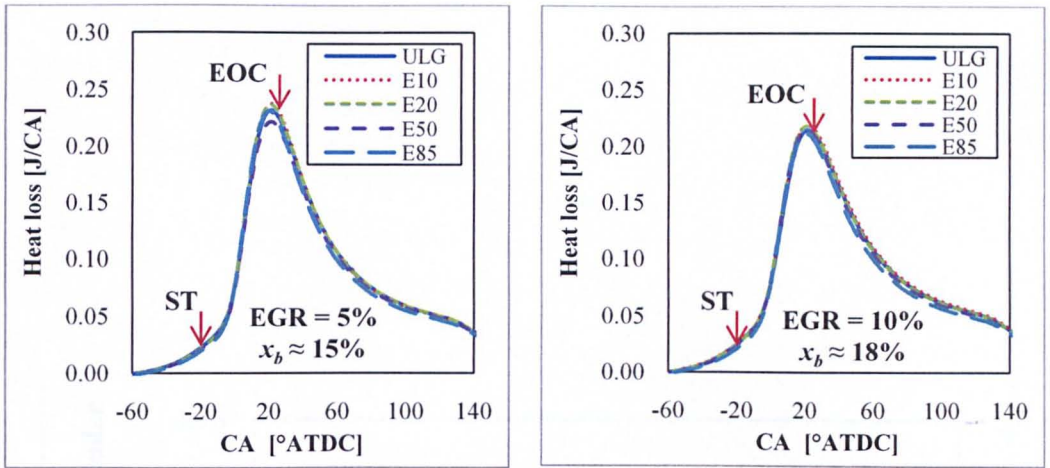


Figure 8.22. A comparison of different gasoline-ethanol blends with engine running at 2000 rpm, BMEP 1.57 bar and different EGR levels.

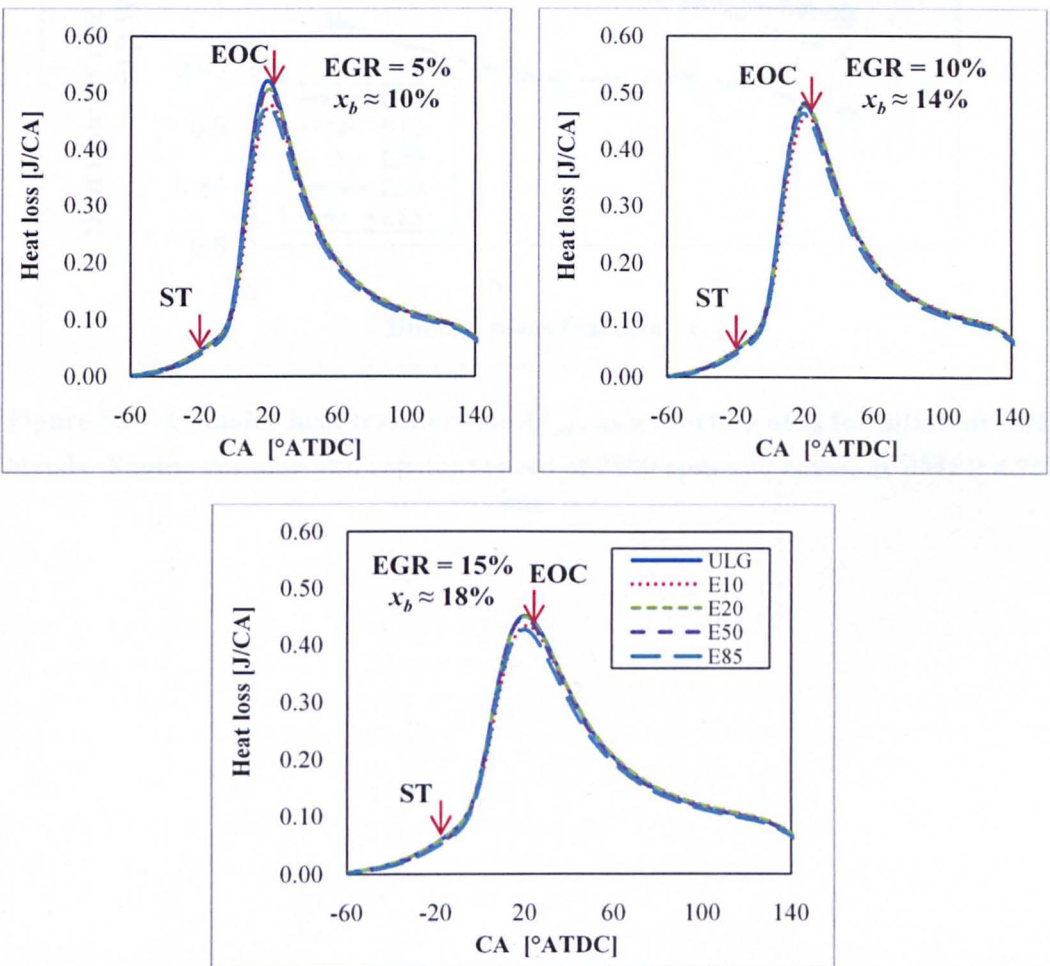


Figure 8.23. A comparison between different gasoline-ethanol blends. Engine running at 2000 rpm, BMEP 4.75 bar and different EGR levels.

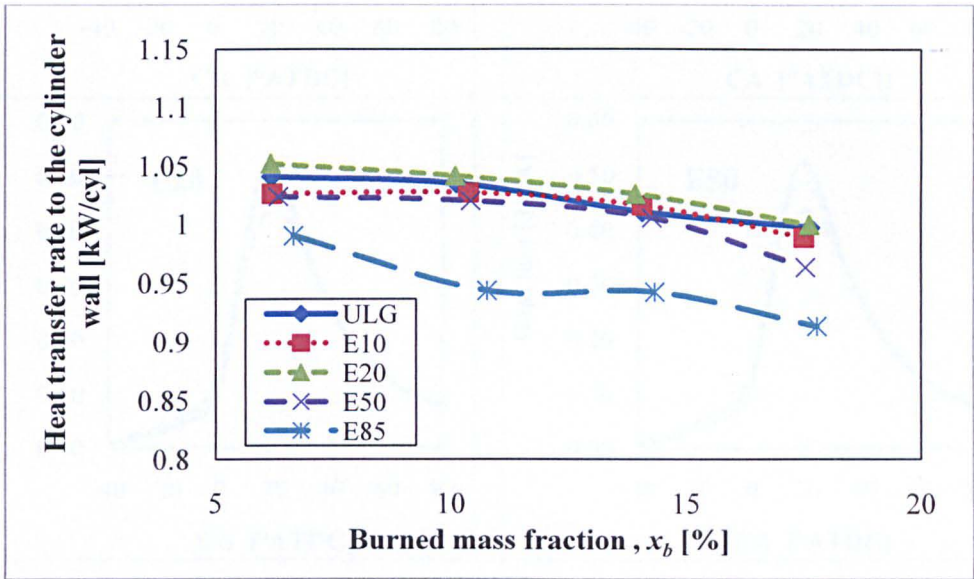


Figure 8.24. Cylinder heat transfer rate, \dot{Q}_{cyl} , as a function of x_b for different fuel blends. Engine running at a constant speed of 2000 rpm and constant BMEP 4.75 bar.

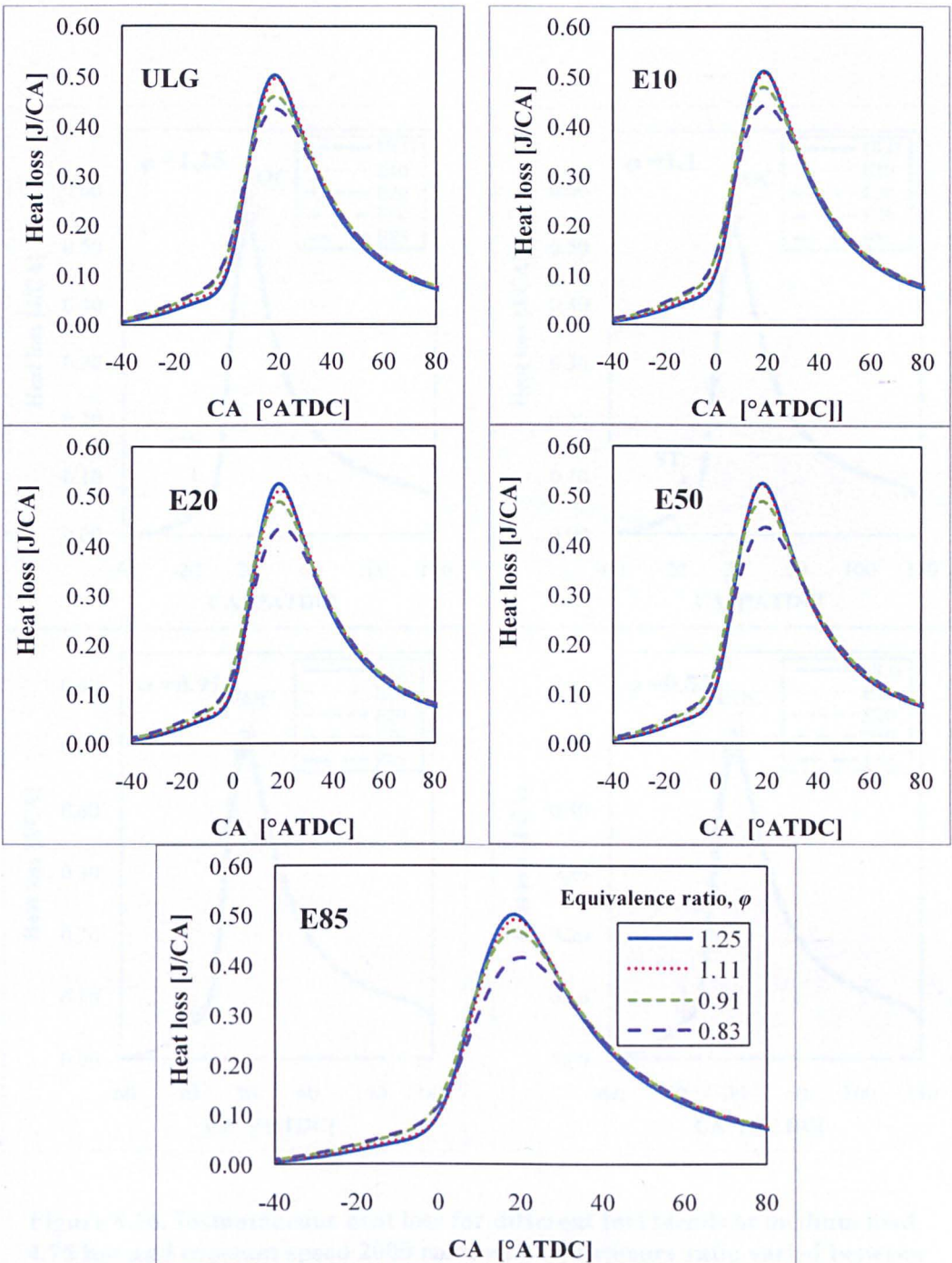


Figure 8.25. Instantaneous heat loss for different fuel blends at medium load, 4.75 bar and constant speed 2000 rpm with ϕ varied between 0.833 to 1.25.

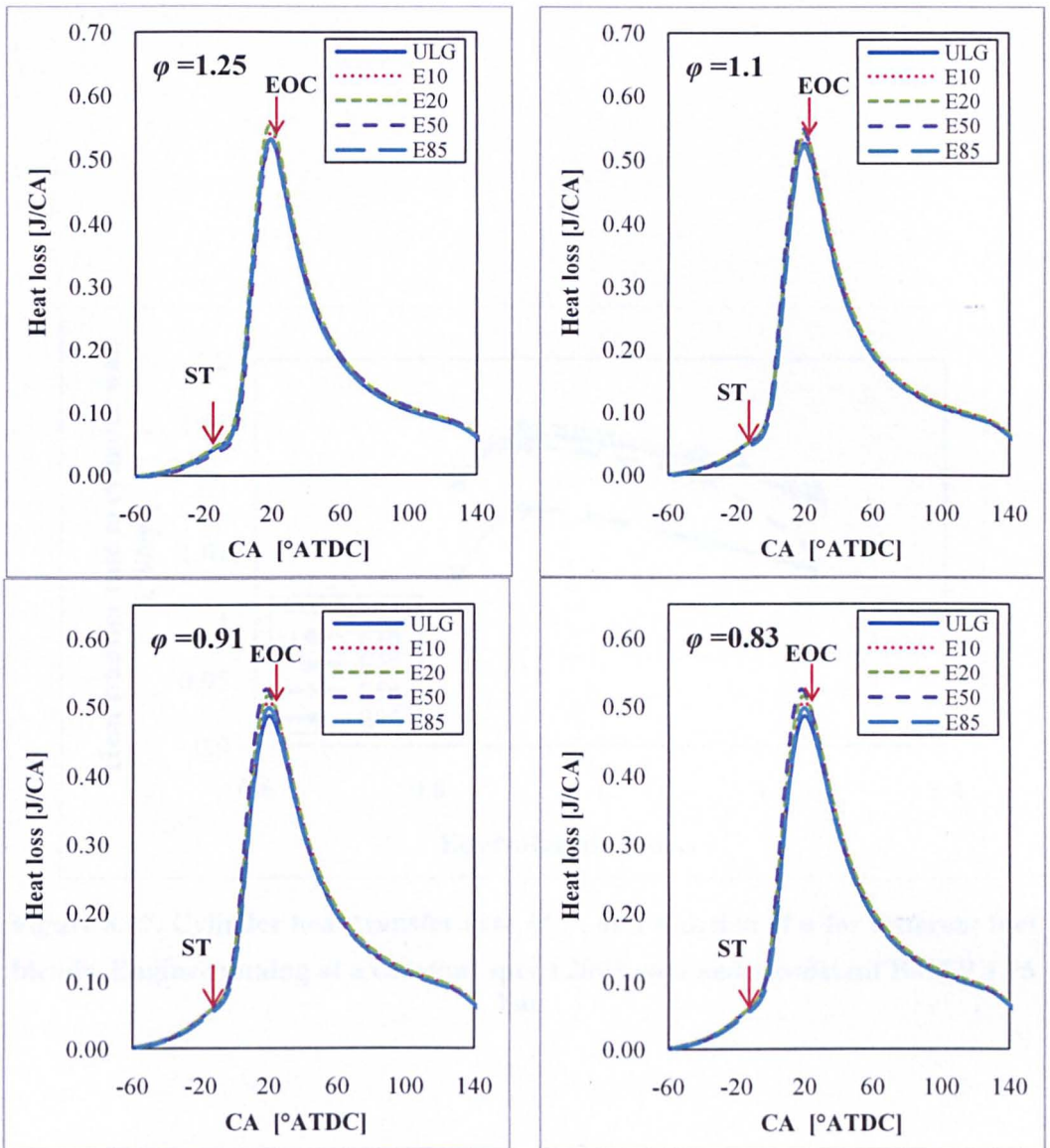


Figure 8.26. Instantaneous heat loss for different fuel blends at medium load, 4.75 bar and constant speed 2000 rpm, with equivalence ratio varied between 0.83 to 1.25.

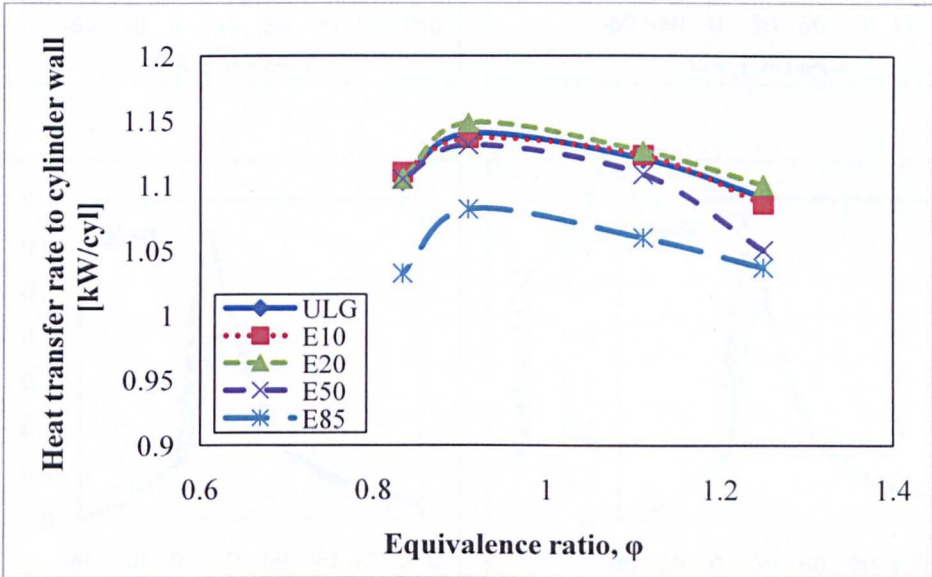


Figure 8.27. Cylinder heat transfer rate, \dot{Q}_{cyl} , as a function of ϕ for different fuel blends. Engine running at a constant speed 2000 rpm and a constant BMEP 4.75 bar.

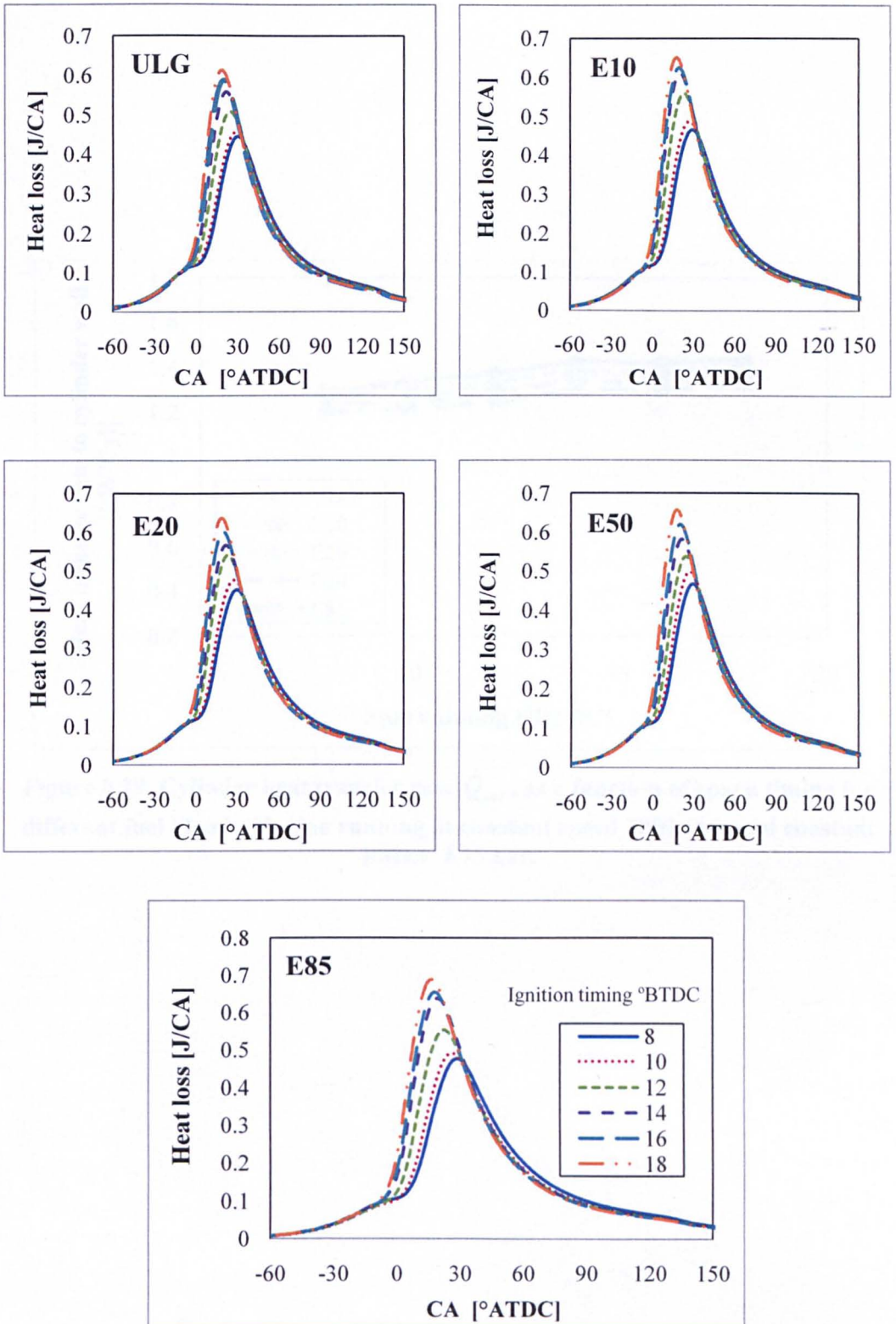


Figure 8.28. Effect of spark timing on heat loss for different fuel blends. Engine running at constant speed, 2000 rpm and constant load 4.75 bar.

Appendices

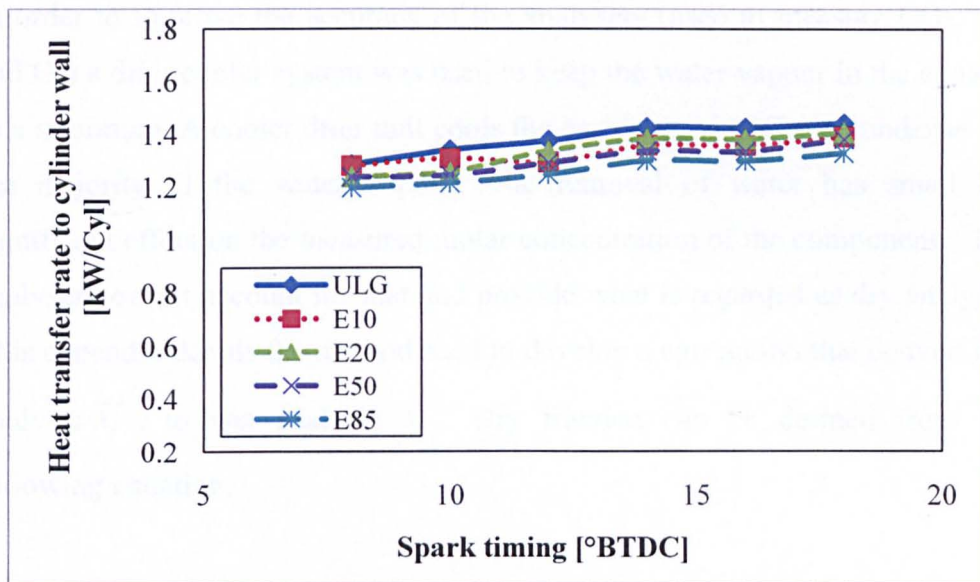


Figure 8.29. Cylinder heat transfer rate, \dot{Q}_{cyl} , as a function of spark timing for different fuel blends. Engine running at constant speed 2000 rpm and constant BMEP 4.75 bar.

Appendices

A.1 Conversion from dry to wet analysis

In order to improve the accuracy of the analysers (used to measure CO₂, CO and O₂) a drier/cooler system was used to keep the water vapour in the exhaust to a minimum. A cooler drier unit cools the gas down to 5°C and condense out the majority of the water vapour. The removal of water has small but significant effect on the measured molar concentration of the components. The analyser doesn't account for that and provide what is regarded as dry analysis. This appendix details the method used to develop a correlation that convert dry analysis \tilde{x}_i^* , to wet analysis \tilde{x}_i . Dry fraction can be defined from the following equation:

$$\tilde{x}_i^* = \frac{n_i}{n_{\text{exhaust}} - n_{\text{H}_2\text{O Lost}}} \quad (\text{A.1.1})$$

where is \tilde{x}_i^* the dry mole fraction, a wet analysis yields a wet mole fraction, given by:

$$\tilde{x}_i = \frac{n_i}{n_{\text{exhaust}}} \quad (\text{A.1.2})$$

To correct the dry analyses, knowledge of the amount of water lost in the drier is required

$$m_{(\text{H}_2\text{O})\text{Lost}} = m_{(\text{H}_2\text{O})\text{exhaust}} - m_{(\text{H}_2\text{O})\text{after drier}} \quad (\text{A.1.3})$$

The amount of water removed by the dryer can be found from the psychometric charts at ambient pressure, it can be seen that at 5°C, the relative humidity by mass can be reduced to 0.6% as shown in Figure A 1.1, which

means that 0.6% of total mass of exhaust gas that reach the analyser after leaving the drier is H₂O.

$$m_{H_2O_{after\ drier}} = 0.006m_{Gas_{after\ drier}} \approx 0.006m_{exhaust} \quad (A\ 1.4)$$

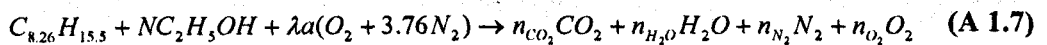
The mass of H₂O removed by cooler/drier system can be defined as,

$$m_{(H_2O)_{Lost}} = (x_{H_2O} - 0.006)m_{exhaust} \quad (A\ 1.5)$$

Using equation A1.1 and A1.2 relation between \tilde{x}_i^* & \tilde{x}_i is found to be

$$\tilde{x}_i = \frac{\tilde{x}_i^* (n_{exhaust} - n_{H_2O\ Lost})}{n_{exhaust}} = \frac{\tilde{x}_i^* \left(\frac{m_{exhaust}}{\tilde{m}_{exhaust}} - \frac{m_{H_2O\ Lost}}{\tilde{m}_{H_2O}} \right)}{\left(\frac{m_{exhaust}}{\tilde{m}_{exhaust}} \right)} \quad (A\ 1.6)$$

A total amount of water entering the drier before combustion and the total molecular weight of the exhaust gas for the different fuel mixtures can be determined considering simple and atomic balance for the overall chemical equation for complete combustion as follows,



Equation A 1.6 was used to plot the percentage difference between wet and dry

fraction, $\frac{\tilde{x}_i - \tilde{x}_i^*}{\tilde{x}_i} \times 100$, as function of lambda as show in Figure A 1.2. The

data illustrate that percentage difference is increasing as ethanol ratio increase in the mixture. A polynomial functions that relates percentage difference and lambda, λ , were extracted from data for different fuel ratio and used to develop a correlation to convert dry fraction into wet fraction as a function of λ and ethanol ratio in the fuel mixture as follows,

$$\tilde{x}_i = \frac{\tilde{x}_i^*}{(0.0733E+0.1287)\lambda^{(3E-1.1678)}} \quad (A\ 1.8)$$

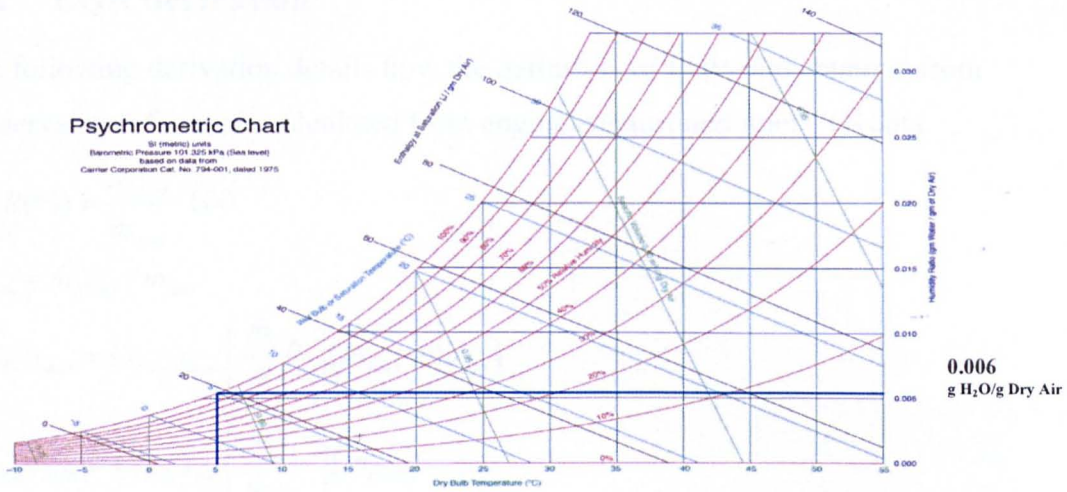


Figure A1.1. Psychrometric chart used to calculate fraction of water remaining in exhaust sample after the chiller unit.

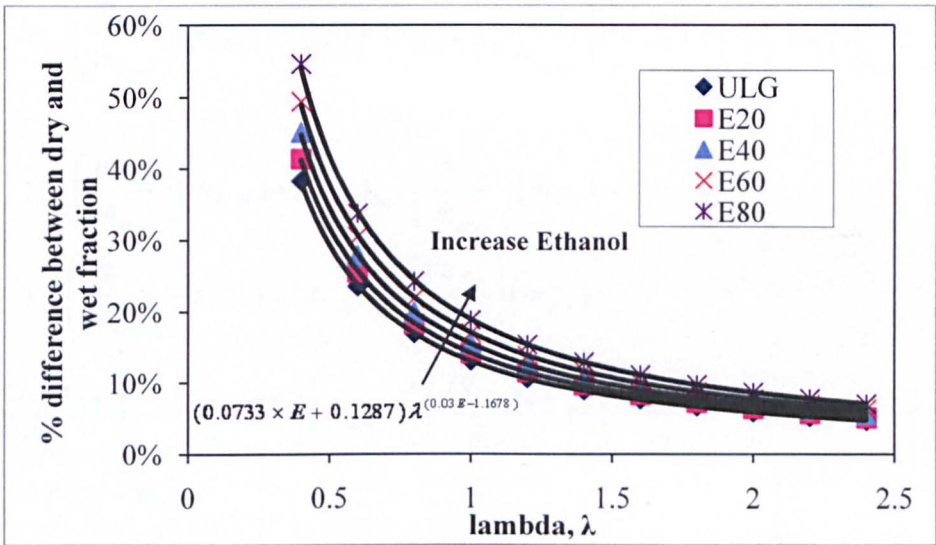


Figure A 1.2. Best fit curves to convert between dry readings to wet readings.

A.2 EGR derivation

The following derivation details how the definition of EGR rate obtained from conservation of mass is calculated from engine exhaust and inlet CO₂ data

$$EGR(\%) = \frac{\dot{m}_{EGR}}{\dot{m}_{man}} \cdot 100$$

$$\dot{m}_{man} = \dot{m}_{EGR} + \dot{m}_{atm}$$

$$(\dot{m}_{CO_2})_{man} = (\tilde{x}_{CO_2})_{man} \left(\frac{\tilde{m}_{CO_2}}{\tilde{m}_{man}} \right) (\dot{m}_{EGR} + \dot{m}_{atm})$$

$$(\dot{m}_{CO_2})_{EGR} = (\tilde{x}_{CO_2})_{exh} \left(\frac{\tilde{m}_{CO_2}}{\tilde{m}_{EGR}} \right) (\dot{m}_{EGR})$$

$$(\dot{m}_{CO_2})_{atm} = (\tilde{x}_{CO_2})_{atm} \left(\frac{\tilde{m}_{CO_2}}{\tilde{m}_{atm}} \right) (\dot{m}_{atm})$$

$$(\dot{m}_{CO_2})_{man} = (\dot{m}_{CO_2})_{EGR} + (\dot{m}_{CO_2})_{atm}$$

$$(\tilde{x}_{CO_2})_{man} \left(\frac{\tilde{m}_{CO_2}}{\tilde{m}_{man}} \right) (\dot{m}_{EGR} + \dot{m}_{atm}) = (\tilde{x}_{CO_2})_{exh} \left(\frac{\tilde{m}_{CO_2}}{\tilde{m}_{EGR}} \right) (\dot{m}_{EGR}) + (\tilde{x}_{CO_2})_{atm} \left(\frac{\tilde{m}_{CO_2}}{\tilde{m}_{atm}} \right) (\dot{m}_{atm})$$

$$(\tilde{x}_{CO_2})_{man} \left(\frac{\tilde{m}_{CO_2}}{\tilde{m}_{man}} \right) (\dot{m}_{EGR}) + (\tilde{x}_{CO_2})_{man} \left(\frac{\tilde{m}_{CO_2}}{\tilde{m}_{man}} \right) (\dot{m}_{atm}) =$$

$$(\tilde{x}_{CO_2})_{exh} \left(\frac{\tilde{m}_{CO_2}}{\tilde{m}_{EGR}} \right) (\dot{m}_{EGR}) + (\tilde{x}_{CO_2})_{atm} \left(\frac{\tilde{m}_{CO_2}}{\tilde{m}_{atm}} \right) (\dot{m}_{atm})$$

$$\left(\left(\frac{(\tilde{x}_{CO_2})_{man}}{\tilde{m}_{man}} \right) - \left(\frac{(\tilde{x}_{CO_2})_{atm}}{\tilde{m}_{atm}} \right) \right) \dot{m}_{atm} = \left(\left(\frac{(\tilde{x}_{CO_2})_{exh}}{\tilde{m}_{EGR}} \right) - \left(\frac{(\tilde{x}_{CO_2})_{man}}{\tilde{m}_{man}} \right) \right) \dot{m}_{EGR}$$

$$\dot{m}_{atm} = \dot{m}_{man} - \dot{m}_{EGR}$$

$$\left(\left(\frac{(\tilde{x}_{CO_2})_{man}}{\tilde{m}_{man}} \right) - \left(\frac{(\tilde{x}_{CO_2})_{atm}}{\tilde{m}_{atm}} \right) \right) (\dot{m}_{man} - \dot{m}_{EGR}) = \left(\left(\frac{(\tilde{x}_{CO_2})_{exh}}{\tilde{m}_{EGR}} \right) - \left(\frac{(\tilde{x}_{CO_2})_{man}}{\tilde{m}_{man}} \right) \right) \dot{m}_{EGR}$$

$$\left(\frac{(\tilde{x}_{CO_2})_{man}}{\tilde{m}_{man}} \right) \dot{m}_{man} - \left(\frac{(\tilde{x}_{CO_2})_{atm}}{\tilde{m}_{atm}} \right) \dot{m}_{man} - \left(\frac{(\tilde{x}_{CO_2})_{man}}{\tilde{m}_{man}} \right) \dot{m}_{EGR} + \left(\frac{(\tilde{x}_{CO_2})_{atm}}{\tilde{m}_{atm}} \right) \dot{m}_{EGR} =$$

$$\left(\frac{(\tilde{x}_{CO_2})_{exh}}{\tilde{m}_{EGR}} \right) \dot{m}_{EGR} - \left(\frac{(\tilde{x}_{CO_2})_{man}}{\tilde{m}_{man}} \right) \dot{m}_{EGR}$$

$$\left(\left(\frac{(\tilde{x}_{CO_2})_{exh}}{\tilde{m}_{EGR}} \right) - \left(\frac{(\tilde{x}_{CO_2})_{atm}}{\tilde{m}_{atm}} \right) \right) \dot{m}_{EGR} = \left(\left(\frac{(\tilde{x}_{CO_2})_{man}}{\tilde{m}_{man}} \right) - \left(\frac{(\tilde{x}_{CO_2})_{atm}}{\tilde{m}_{atm}} \right) \right) \dot{m}_{man}$$

Assuming $\tilde{m}_{man} = \tilde{m}_{EGR} = \tilde{m}_{atm}$;

$$\dot{m}_{EGR} = \left(\frac{(\tilde{x}_{CO_2})_{man} - (\tilde{x}_{CO_2})_{atm}}{(\tilde{x}_{CO_2})_{exh} - (\tilde{x}_{CO_2})_{atm}} \right) \dot{m}_{man}$$

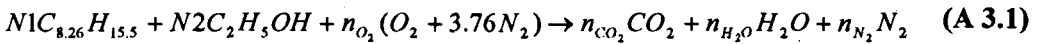
$$EGR(\%) = \frac{\dot{m}_{EGR}}{\dot{m}_{EGR} + \dot{m}_{atm}} \cdot 100 = \frac{\dot{m}_{EGR}}{\dot{m}_{man}} \cdot 100 = \left(\frac{(\tilde{x}_{CO_2})_{man} - (\tilde{x}_{CO_2})_{atm}}{(\tilde{x}_{CO_2})_{exh} - (\tilde{x}_{CO_2})_{atm}} \right)$$

A.3 Properties of the different fuel blends

This appendix details the methods that was used to calculate the different fuel blends properties such as AFR, adiabatic flame temperature, calorific value and heat capacity.

Stoichiometric Air fuel Ratio (AFR_{stoich}):

The stoichiometric quantity of an oxidizer (air) is just that amount needed to completely burn a quantity of fuel. In this case the stoichiometric Air-fuel ratio of a different mixture of Ethanol (C₂H₅OH) Gasoline blend C_{8.26}H_{15.5} is determined by writing simple atomic balance.



where N1, N2, nO₂, nCO₂, nH₂O and nN₂ are number of moles of gasoline, ethanol, air, CO₂, H₂O and N₂, respectively. The volume fraction of ethanol was transferred into number of moles because when the fuel evaporates, the ethanol ratio change in the fuel blend.

$$n_{CO_2} = 8.26 * N1 - 2 N2 \quad (A 3.2)$$

$$n_{H_2O} = \frac{15.5 N1 - 6 N2}{2} \quad (A 3.3)$$

$$n_{O_2} = \frac{2 n_{CO_2} + n_{H_2O} - N2}{2} \quad (A 3.4)$$

$$n_{N_2} = 3.76 n_{O_2} \quad (A 3.5)$$

The composition of air is assumed to be 21% O₂ and 79% N₂ (by volume) for simplicity, i.e. for each mole of O₂ there is 3.76 moles of N₂.

The stoichiometric air-fuel ratio can be found as:

$$AFRs = \frac{32 * n_{o_2} + 3.76 * 28.16 * n_{o_2}}{N2(46) + N1114.8} \tag{A 3.6}$$

Adiabatic Flame Temperature

Assuming that the fuel air mixture burns adiabatically at constant pressure, the absolute enthalpy of the reactants at initial state (say T=298 K, P= 1 atm) equals the of the products at final state (T= T_{add}, P).

$$H_{react} = \sum_{react} N_i h_i = H_{prod} = \sum_{prod} N_i h_i \tag{A 3.7}$$

| | Enthalpy of Formation @298K $\bar{h}_{f,i}^0 = (kJ / kmol)$ | Specific heat @1200K $\bar{c}_{p,i}^0 = (kJ / kmol-K)$ |
|-------------------------------------|--|---|
| C ₂ H ₅ OH | -234600 | — |
| C _{8.26} H _{15.5} | -112370 | — |
| O ₂ | 0 | — |
| CO ₂ , | -393546 | 56.21 |
| H ₂ O, | -241845 | 43.87 |
| N ₂ | 0 | 33.71 |

Table A 3.1

$$\begin{aligned}
 H_{react} &= \sum_{react} n_i h_i \\
 H_{react} &= N2(-234600) + N1(-112370) + a(0) + 3.76a(0) \\
 H_{prod} &= \sum_{prod} n_i [\bar{h}_{f,i}^0 + \bar{c}_{p,i} (T_{ad} - 298)] \\
 H_{prod} &= n_{CO_2} [-393,546 + 56.21 (T_{ad} - 298)] \\
 &+ n_{H_2O} [-241,845 + 43.87 (T_{ad} - 298)] \\
 &+ n_{N_2} [0 + 33.71 (T_{ad} - 298)] .
 \end{aligned}$$

Enthalpy of combustion and Lower heating value

The lower heating value Q_{LHV} is equal to the enthalpy of reaction,

$$\Delta H_c = H_{react} - H_{prod} \tag{A 3.8}$$

$$H_{react} = \sum_{react} N_i \bar{h}_i \quad \text{and} \quad H_{prod} = \sum_{prod} N_i \bar{h}_i .$$

Specific Heat at constant pressure (c_p) and Gamma γ for the fresh and burned gas mixture inside the engine cylinder,

The unburned gas mixture consists of the fuel and fresh air. In this study, the fuel is a mix of gasoline and ethanol at different ratios. Ethanol and gasoline have two different properties of c_p , c_v

Here is the correlations that has been used to calculate c_p for ethanol and gasoline [71],

$$c_{p,ULG} = \frac{4.184}{m_{r,ULG}} (-24.078 + 256.63A - 201.68A^2 + 64.75A^3 + 0.5808A^2) \quad (\text{A 3.9})$$

$$c_{p,Ethanol} = \frac{4.184}{m_{r,Ethanol}} 46.07(6.99 + 39.741A - 11.926A^2) \quad (\text{A 3.10})$$

where $A=T(K)/1000$, m_r is the molecular and equal 114.7 and 46.07 for gasoline and ethanol, respectively. c_p for fresh air was obtained from the following correlation based on data from[71],

$$c_{p,air} = -3 \times 10^{-10} T^3 + 7 \times 10^{-7} T^2 - 0.0003T + 1.0417 \quad (\text{A 3.11})$$

For each species (i) of the products of combustion in its standard state at temperature $T(K)$, the specific heat capacity, $c_{p,i}$, is approximated by[17],

$$\frac{c_{p,i}}{R} = \frac{(a_{i1} + a_{i2} T + a_{i3} T^2 + a_{i4} T^3 + a_{i5} T^4)}{m_{r,i}} \quad (\text{A 3.12})$$

The constant for the different species can be found from Table A 3.2 below,

| Species | T range (K) | a_{i1} | a_{i2} | a_{i3} | a_{i4} | a_{i5} |
|------------------|-------------|----------|------------|-----------|-----------|-----------|
| CO ₂ | 300-1000 | 2.40E+00 | 8.74E-03 | -6.61E-06 | 2.00E-09 | 6.33E-16 |
| | 1000-5000 | 4.4608 | 0.0030982 | -1.24E-06 | 2.27E-10 | -1.55E-14 |
| H ₂ O | 300-1000 | 4.07E+00 | -1.11E-03 | 4.15E-06 | -2.96E-09 | 8.07E-13 |
| | 1000-5000 | 2.7168 | 0.0029451 | -8.02E-07 | 1.02E-10 | 4.85E-15 |
| CO | 300-1000 | 3.7101 | -0.0016191 | 3.692E-06 | -2E-09 | 2.4E-13 |
| | 1000-5000 | 2.9841 | 0.0014891 | -5.79E-07 | 1.04E-10 | -6.94E-15 |
| O ₂ | 300-1000 | 3.6256 | -0.0018782 | 7.056E-06 | -6.8E-09 | 2.16E-12 |
| | 1000-5000 | 3.622 | 0.00073618 | -1.97E-07 | 3.62E-11 | -2.89E-15 |
| N ₂ | 300-1000 | 3.67E+00 | -1.21E-03 | 2.32E-06 | -6.32E-10 | -2.26E-13 |
| | 1000-5000 | 2.8963 | 0.0015155 | -5.72E-07 | 9.98E-11 | -6.52E-15 |

Table A 3.2 [17].

The mixture for the burned and unburned value can be found from

$$c_{p,mixture} = \frac{\sum X_i \rho_i c_{p,i}}{\sum X_i \rho_i} \text{ kJ/kg K} \tag{A 3.13}$$

Where X_i is the volume fraction and ρ_i is the density. Combustion emissions products for engine running at E85 and gasoline were used to calculate c_p using equation A 3.12 and equation A 3.13 for different emissions species. For the different the fuel blend a correlation was developed to relate c_p to temperature as shown in Figure A 3.1,

If $275 < T(K) < 1000$

$$c_{p,b} = A1T + A2 \tag{A 3.14}$$

If $T(K) > 1000$

$$c_{p,b} = B1 \ln T - B2 \tag{A 3.15}$$

Where A1, A2, B1 and B2 are constants that are dependent on the fuel mixture

| | A1 | A2 | B1 | B2 |
|-----------------|--------|--------|--------|---------|
| Gasoline | 0.0003 | 0.9563 | 0.2248 | 0.28290 |
| E10 | 0.0003 | 0.9577 | 0.2147 | 0.2259 |
| E20 | 0.0003 | 0.9585 | 0.209 | 0.195 |
| E50 | 0.0003 | 0.9635 | 0.2087 | 0.1918 |
| E85 | 0.0003 | 0.9755 | 0.2073 | 0.1838 |

Table A 3.3.

The values of the different constants as function of ethanol ratio were plotted in Figure A 3.2. These values were used to develop correlations to relate those constants to ethanol ratio,

$$A2 = 0.0222E + 0.955$$

$$B1 = 0.0205E + 0.2061$$

$$B2 = 0.0222E + 0.955$$

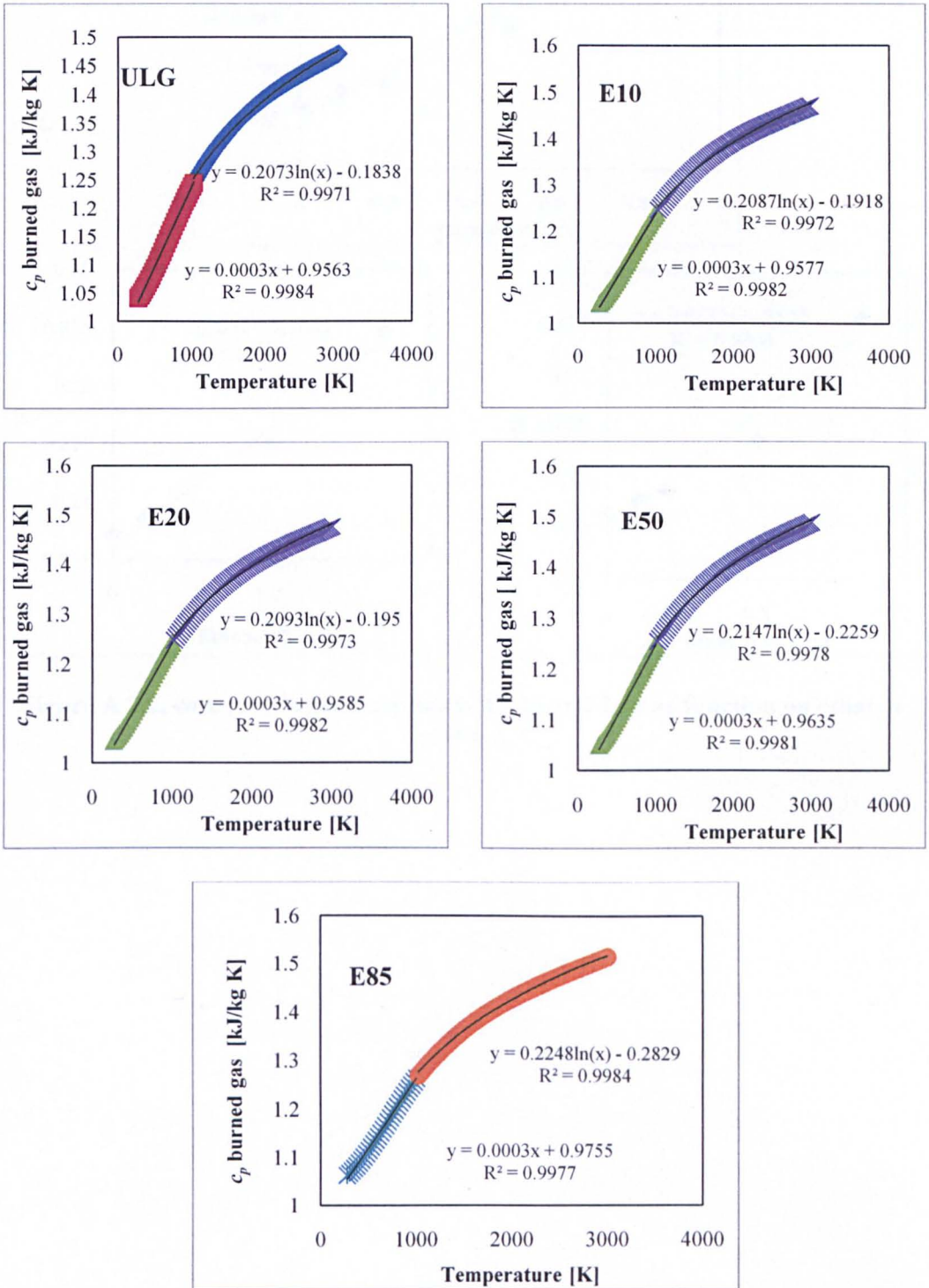


Figure A 3.1, c_p for burned gas as function when the engine is running at different fuel blends based on emissions averaged from different loads.

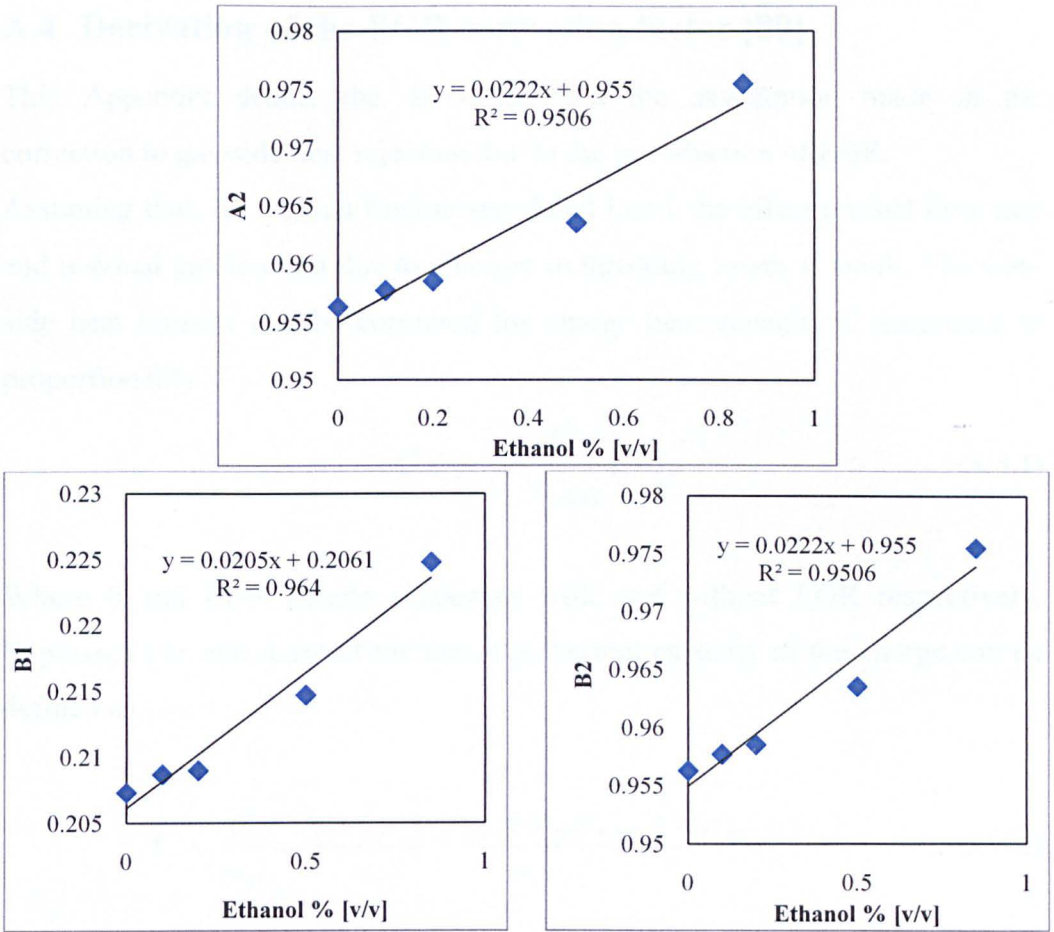


Figure A 3.2, constants used in equation A3.15 and 3.16 as function on ethanol ratio.

A.4 Derivation of the EGR correction factor [89]

This Appendix details the derivation and the assumption made in the correction to gas-side heat rejection due to the introduction of EGR.

Assuming that, for a given Engine speed and Load, the effect on fuel flow rate and residual gas fraction due to changes in throttling losses is small. The Gas-side heat transfer can be corrected for charge heat capacity C according to proportionality

$$\dot{Q}_{CIC2EGR} \propto \frac{C_0}{C_{EGR}} \dot{Q}_{CIC0} \quad (A 4.1)$$

Where 0 and EGR denote properties with and without EGR respectively. Expressed per unit mass of the fuel, the thermal capacity of the charge can be defined as:

$$C' = \frac{C}{m_f} = \frac{m_f c_{p,f} + m_a c_{p,a} + m_{exh} c_{p,exh} + m_r c_{pr}}{m_f} \quad (A 4.2)$$

Where m is the mass per cycle and c_p the specific heat capacity, while the subscript f , a , exh and r denote fuel, air, exhaust and residual, respectively.

Assuming that the heat capacity of the exhaust and the residual gases is approximately equal to that of air.

$$C' = c_{pf} + \left(AFR \left(1 + \frac{EGR}{1 - EGR} \right) + \frac{m_r}{m_f} \right) c_{pa} \quad (A 4.3)$$

The residual gas fraction, x_r , can be defined as :

$$\begin{aligned} x_r &= \frac{m_r}{m_a + m_f + m_{ex}} \\ &= \frac{m_r (1 - EGR)}{m_f (1 - EGR + AFR)} \end{aligned} \quad (A 4.4)$$

Substituting for $\frac{m_r}{m_f}$ in equation A 4.3

$$C' = c_{pf} + \left(AFR \left(1 + \frac{x_r (1 - EGR + AFR)}{1 - EGR} \right) \right) c_{pa} \quad (\text{A 4.5})$$

And the ratio $\frac{C'_{EGR}}{C'_0}$ is given by:

$$\frac{C'_{EGR}}{C'_0} = \frac{c_{pf} (1 - EGR) + (AFR + x_{r_{EGR}} (1 - EGR + AFR)) c_{pa}}{(1 - EGR) (c_{pf} + (AFR + x_{r_0} (1 + AFR)) c_{pa})} \quad (\text{A 4.6})$$

Since $AFR \gg 1$, and $EGR < 1$ equation A 4.6 can be approximated to:

$$\frac{C'_{EGR}}{C'_0} \approx \frac{c_{pf} (1 - EGR) + (AFR (1 + x_{r_{EGR}})) c_{pa}}{(1 - EGR) (c_{pf} + (AFR (x_{r_0} + 1)) c_{pa})} \quad (\text{A 4.7})$$

For spark ignition engine, the residual fraction varies typically from 7% at full load to 20% at light load. For otherwise similar operating conditions the residual fraction x_r for the case with EGR will be lower than the equivalent case without EGR because of throttling differences required maintaining the correct Air/Fuel ratio. However, since EGR is not used at full load we can assume $x_r \approx 10\%$ and equation A 4.7 can be simplified further:

$$\begin{aligned} \frac{C'_{EGR}}{C'_0} &\approx \frac{c_{pf} (1 - EGR) + 1.1 AFR c_{pa}}{(1 - EGR) (c_{pf} + 1.1 AFR c_{pa})} \\ &\approx \frac{1}{(1 - EGR)} \end{aligned} \quad (\text{A 4.8})$$

A.5 Measurements and calculation uncertainties

Because of the comparative nature of this study, any experimental error could have an effect on the data and subsequently the drawn conclusion. The difference between various fuel mixtures can be due to experimental error rather than the fuel content. For that reason, it was very important to estimate the error in the experiment.

There are mainly two types of errors associated with experimental results: the "precision" and the "accuracy". Precision is related to the random errors inside the experiment including noise. Accuracy is related to the existence of systematic error associated with the instruments used. An instrument can be assessed for systematic errors only by calibration against an appropriate standard. The systematic errors of the instruments are usually provided by the manufacturers. The random error is assessed by repeated measurements made under identical conditions[105]. As mentioned in section 3.7, at each running condition, the data were averaged over 750 samples. The standard error of the mean, E_{stand} , was used to express the precision of the mean value of repeated tests such as[105]

$$E_{stand} = \frac{s}{\sqrt{n-1}} \quad (\text{A 5.1})$$

where s is the standard deviation and n is the number of readings.

A.5.1 Estimation of the error in temperature, fuel mass flow rate, coolant flow rate and AFR.

As mentioned in section 3.7, all temperature measurements were taken using K type thermocouple. The inaccuracy of the thermocouples according to the manufacturer, associated with the systematic error, is $\pm 1.5^\circ\text{C}$ or $\pm 0.4\%$ [64]. Figure A1.1 shows standard error of the mean, $E_{stand,Temp}$, calculated from equation A 5.1, for exhaust and coolant temperatures. The data were taken from engine running at different speeds, BMEPs and fuel mixtures. The results illustrate clearly that $E_{stand,Temp}$ is lower than 0.2°C for the vast majority of the tests. For that reason, systematic error is assumed to be the major source of the temperature measurement error. Hence, thermocouples uncertainty, E_{Temp} is assumed to be $\pm 1.5^\circ\text{C}$ or $\pm 0.4\%$.

According to the manufacturers, the accuracy of the fuel and coolant flow meters are 0.05% and 0.5% respectively [106, 107]. The standard errors of the mean, E_{stand} , of both measurements are shown in Figure A 5.2 and Figure A 5.4 for different running conditions. The percentage of E_{stand} compare to the mean value of the sample is shown in Figure A 5.3 and Figure A 5.5. Percentage of E_{stand} for both fuel and coolant flow rate are lower than 0.1%. The uncertainties in the measurement for fuel and coolant flow rate, $E_{\dot{m}_{fuel}}$ & $E_{\dot{m}_{coolant}}$, are assumed to be $\pm 0.1\%$ and $\pm 0.5\%$ respectively.

According to the manufacturer, the accuracy in the measurement of CO, CO₂, HC, NO_x, and O₂ are +1%, +1%, +1%, 1.5% and 1.5% respectively [108]. The standard error of the mean and its percentage compare to the mean value are plotted in Figure A 5.6. The data illustrate that error percentage is lower than 0.2%, 0.3%, 0.4% and 0.04% for NO_x, HC, CO and CO₂ emissions. Once again those random errors are much smaller than that of the manufacturer accuracy. Consequently, the error in the experiment was assumed to be equal to the manufacturer accuracy.

A.5.2 Errors in pressure measurements

There are several sources of error that can affect in-cylinder pressure readings. These errors have been widely discussed and analysed by several researches [109, 110]. The main sources of errors are:

- Inaccurate pressure referencing (pegging).
- Thermal shock or short term drift or intra-cycle drift.
- Incorrect crank angle phasing with pressure data.
- Inaccurate transducer calibration and sensor non linearity.
- Long term drift or inter-cycle.
- Noise.

Several measures were taken to eliminate some of the error sources mentioned in the list above in order to insure accurate pressure readings. For example, to eliminate noise, pressure data was averaged over 100 consecutive cycles. Regarding transducer calibration and no linearity as a source of error, extra care was taken when calibrating both in cylinder transducer and manifold pressure sensor. In addition, modern pressure transducers are affected by small

or negligible uncertainties due to non-linearity or repeatability. Pegging, or in-cylinder pressure referencing, was performed at each cycle to eliminate inter-cycle drift as recommended. The in-cylinder pressure was referenced to the inlet manifold pressure at BDC as detailed in section 3.6.1. There are a number of pressure reference techniques that are available, both Randloph[109] and Brunt *et al* [110] carried out two separate study to evaluate different pressure referencing techniques. The two studies concluded that the main source of inaccuracy is associated with errors in the measured cylinder pressure data rather than the technique used for pegging. In this study, any error at pressure data at BDC will affect the pressure referencing since the error in the reference will propagate to the whole cycle.

The main source of error in pressure data is indeed related to thermal shock or intra-cycle variation. Thermal shock is caused by in-cylinder pressure transducer sensitivity to temperature. The Transducer drift, linked to combustion, increases the cyclic variability by amplifying the effect of the actual cyclic variation. This might continue until pressure pegging occurs, which offsets all of the referenced measurements. For that reason, it would be preferable to perform pressure pegging at point where change temperature is at its minimum i.e. at inlet BDC. Intra-cycle variation occurs between the beginning and the end of a single cycle. In this study, intra-cycle variation is assumed to be the most relevant source of in-cylinder pressure inaccuracy. The inaccuracy was estimated by calculating the difference between the pressure values of two consecutive cycles at inlet BDC as shown in Figure A 5.7. The actual pressure at inlet BDC should be constant and consequently the pressure difference in Figure A 5.7 should be zero.

Figure A 5.7 shows that the intra cycle variation for different loads, speeds and fuel content has variability of ± 0.05 bar around the mean value and a standard deviation, s_p , equals to 0.049 bar. ± 0.098 bar can reasonably assume as the inaccuracy in the in-cylinder pressure where 95% of the values lies within the range (statistics based on normal distribution).

A.5.3 Estimated error in MFB

MFB was obtained from Rassweiller and Withrow methods (see section 5.3). The main sources of error are pressure error, pressure volume phasing, and

polytropic index. Polytropic indexes for compression and expansion are linked to pressure data and pressure volume phasing, so any error with compression index is associated with those two factors. Sensitivity analysis for both pressure error and pressure-volume phasing error was carried out. The inaccuracy in pressure reading was assumed to be ± 0.098 bar (see section A.5.2). Figure A 5.8 shows the effect of ± 0.098 bar pressure error on the calculated MFB for different speeds, loads and fuel blends. MFB's error is at its maximum at FDA, and then reduces to negligible values at RBA. The results also illustrate that MFB is more sensitive to pressure error at low load than at high load. Finally MFB does not appear to be sensitive to change in Fuel blends. Figure A 5.9 shows the error in burn rate duration as result of changing pressure, the maximum difference at FDA is around $\pm 0.35^\circ$, while for RBA the maximum difference was around $\pm 0.25^\circ$.

An accurate allocation of TDC is hard. In this study, extreme care was taken in allocating TDC for volume pressure phasing (see section 3.3.2). However there ought to be some error in TDC allocation, an error of $\pm 0.25^\circ$ was found to be a reasonable assumption. The effect of changing volume-pressure phasing on MFB can be shown from Figure A 5.10. The error was not affected by load, speed or fuel content. It is also illustrated that FDA is more sensitive to any change in pressure-volume phasing than RBA. Figure A 5.11 illustrates that the maximum error for FDA is $\pm 0.25^\circ$, and for RBA is around $\pm 0.15^\circ$.

In conclusion, Rassweiller and Withrow appears to be a robust method to calculate combustion duration and it is not very sensitive to pressure error (due to thermal shock or pressure referencing error) or to pressure-volume phasing. In the worst case scenario the error occurs simultaneously, then the total error can be evaluated by adding the two source of error. Hence, the maximum error is 0.6° for FDA and 0.4° for RBA.

A.5.4 Estimated error in heat transfer to the coolant calculations,

$$\dot{Q}_{coolant} :$$

The main source of uncertainty in $\dot{Q}_{coolant}$ calculation comes from coolant flow rate and temperatures errors as illustrated in equation 6.4.1. The combined error in $\dot{Q}_{coolant}$, $E_{\dot{Q}_{coolant}}$, is calculated as following,

$$E_{\dot{Q}_{coolant}} = \sqrt{\left(\frac{\partial \dot{Q}_{coolant}}{\partial \dot{m}_{coolant}}\right)^2 E_{\dot{m}_{coolant}}^2 + \left(\frac{\partial \dot{Q}_{coolant}}{\partial T_{coolant\ before}}\right)^2 E_{Temp}^2 + \left(\frac{\partial \dot{Q}_{coolant}}{\partial T_{coolant\ after}}\right)^2 E_{Temp}^2} \quad (A\ 5.2)$$

where $E_{\dot{m}_{coolant}}$ and E_{Temp} equal to 0.5% and 0.4 % respectively. Figure A 5.12 shows the error for $\dot{Q}_{coolant}$ for different speeds, loads, and different fuel mixtures. The results demonstrate that $E_{\dot{Q}_{coolant}}$ is between 1.2% at low speed to 1.5% at high speed.

A.5.5 Estimated error in the exhaust mass charge, $\dot{m}_{exhaust}$:

The exhaust mass charge, are calculated from the following equation,

$$\dot{m}_{exhaust} = \dot{m}_{fuel} (1 + AFR) \quad (A\ 5.3)$$

Subsequently the error is calculated as following,

$$E_{\dot{m}_{exhaust}} = \sqrt{\left(\frac{\partial \dot{m}_{exhaust}}{\partial \dot{m}_{fuel}}\right)^2 E_{fuel}^2 + \left(\frac{\partial \dot{m}_{exhaust}}{\partial AFR}\right)^2 E_{AFR}^2} \quad (A\ 5.4)$$

where E_{AFR} , according to the manufacturer, is equal to 1.2% and E_{fuel} is equal to 0.5% (see section A.5.1). Figure A 5.13 shows the error in $\dot{m}_{exhaust}$ at different engine running conditions (different BMEPs and speeds). The results illustrate that $E_{\dot{m}_{exhaust}}$ is around 1.2% for all running conditions and fuel mixtures.

A.5.6 Estimated error in exhaust heat capacity calculation, $\bar{c}_{p,exh}$

Exhaust heat capacity, $\bar{c}_{p,exh}$, is calculated from the exhaust composition. Subsequently, the major source of inaccuracy is coming from errors in emission measurements. The estimated error in $\bar{c}_{p,exh}$, $E_{\bar{c}_{p,exh}}$, is calculated as follows,

$$E_{\bar{c}_{p,exh}} = \sqrt{\left(\frac{\partial \bar{c}_{p,exh}}{\partial x_{CO}}\right)^2 E_{x_{CO}}^2 + \left(\frac{\partial \bar{c}_{p,exh}}{\partial x_{CO_2}}\right)^2 E_{x_{CO_2}}^2 + \left(\frac{\partial \bar{c}_{p,exh}}{\partial x_{N_2}}\right)^2 E_{x_{N_2}}^2 + \left(\frac{\partial \bar{c}_{p,exh}}{\partial x_{O_2}}\right)^2 E_{x_{O_2}}^2 + \left(\frac{\partial \bar{c}_{p,exh}}{\partial x_{H_2O}}\right)^2 E_{x_{H_2O}}^2} \quad (\text{A 5.5})$$

Figure A 5.14 illustrates that $E_{\bar{c}_{p,exh}}$ is around 1.95 to 2%.

A.5.7 Estimated error in exhaust gas energy calculations, $\dot{H}_{exh,s}$:

Exhaust energy was calculated from equation 6.2. Estimated error in exhaust energy, $\dot{H}_{exh,s}$, is calculated from:

$$E_{\dot{H}_{exh,s}} = \sqrt{\left(\frac{\partial \dot{H}_{exh,s}}{\partial \dot{m}_{exh}}\right)^2 E_{\dot{m}_{exh}}^2 + \left(\frac{\partial \dot{H}_{exh,s}}{\partial \bar{c}_{p,exh}}\right)^2 E_{\bar{c}_{p,exh}}^2 + \left(\frac{\partial \dot{H}_{exh,s}}{\partial T_{exh}}\right)^2 E_{Temp}^2} \quad (\text{A 5.6})$$

Figure A 5.15 demonstrates that $E_{\dot{H}_{exh,s}}$ is around 2%.

A.5.8 Estimated error in energy balance (thermal efficiency, coolant loss and exhaust energy percentages):

The error in energy balance estimation is associated with errors in load reading, calculated coolant energy, calculated exhaust energy and fuel flow rate reading. In the energy balance, thermal efficiency error (E_{η_t}), coolant energy percentage error ($E_{\dot{Q}_{coolant}\%}$), exhaust energy percentage ($E_{\dot{H}_{exh,s}\%}$) are calculated from the following:

$$E_{\eta_t} = \sqrt{\left(\frac{\partial \eta_t}{\partial \dot{m}_{fuel}}\right)^2 E_{\dot{m}_{fuel}}^2 + \left(\frac{\partial \eta_t}{\partial T}\right)^2 E_T^2} \quad (\text{A 5.7})$$

$$E_{\dot{Q}_{coolant} \%} = \sqrt{\left(\frac{\partial \dot{Q}_{coolant} \%}{\partial \dot{m}_{fuel}}\right)^2 E_{\dot{m}_{fuel}}^2 + \left(\frac{\partial \dot{Q}_{coolant} \%}{\partial \dot{Q}_{coolant}}\right)^2 E_{\dot{Q}_{coolant}}^2} \quad (\text{A 5.8})$$

$$E_{\dot{H}_{exh,s} \%} = \sqrt{\left(\frac{\partial \dot{H}_{exh,s} \%}{\partial \dot{m}_{fuel}}\right)^2 E_{\dot{m}_{fuel}}^2 + \left(\frac{\partial \dot{H}_{exh,s} \%}{\partial \dot{H}_{exh,s}}\right)^2 E_{\dot{H}_{exh,s}}^2} \quad (\text{A 5.9})$$

Figure A 5.16 illustrates that E_{η_t} is ranging between 0.5% at low load to 1.5% at high load. Changing speed does not appear to be affecting the error value. Figure A 5.17 shows that the estimated error in coolant energy percentage of the total fuel energy is between 1 to 1.5%. Finally, Figure A 5.18 demonstrates that the estimated error in the exhaust energy percentage of the total fuel energy is between 0.6% at low speed to 0.9% at high speed.

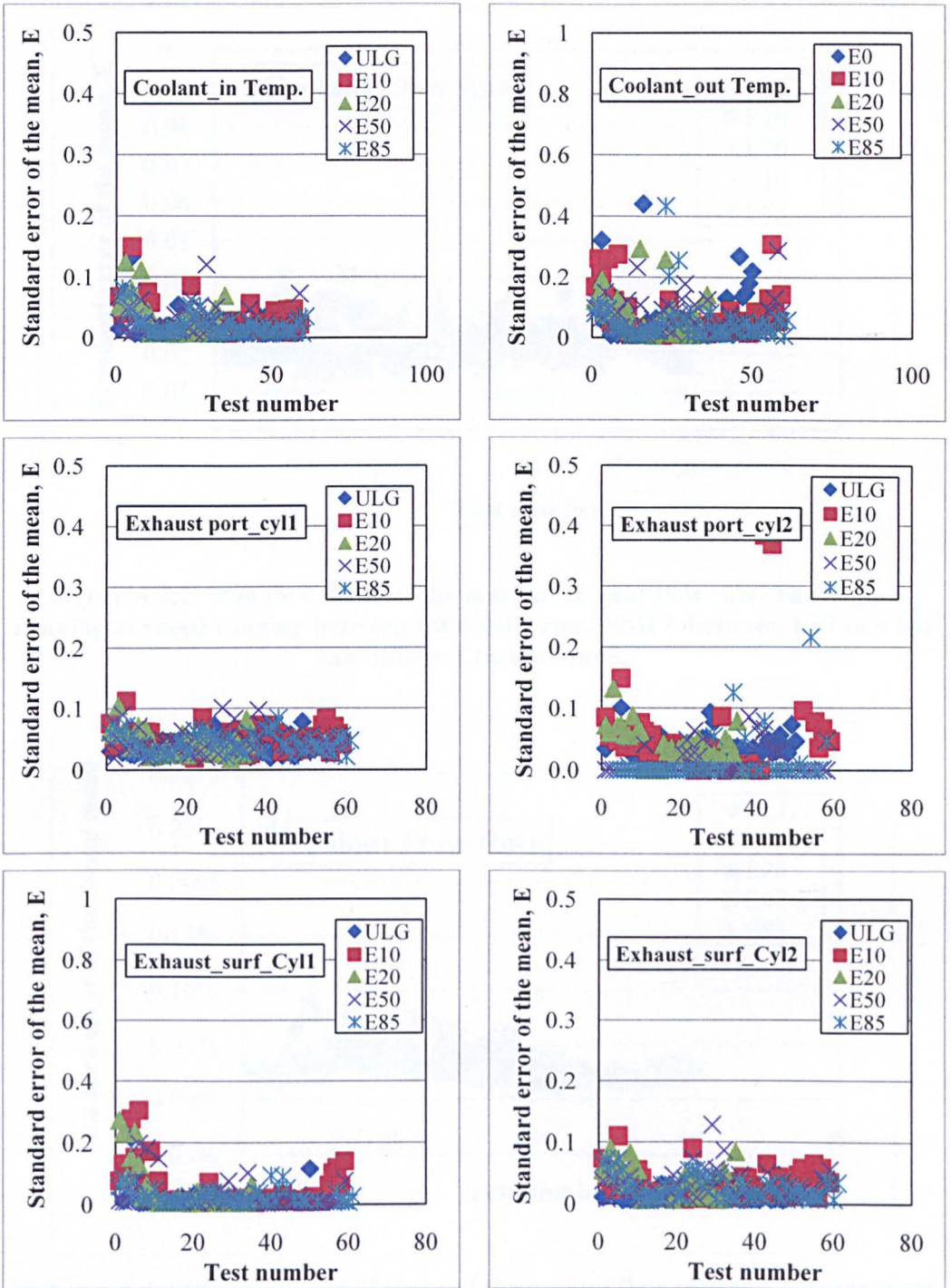


Figure A 5.1. Standard error of the mean of the temperature at different locations. The engine running at speed ranging between 1500-4000 rpm, BMEP between 1.57 to 8 bar, and different fuel mixtures.

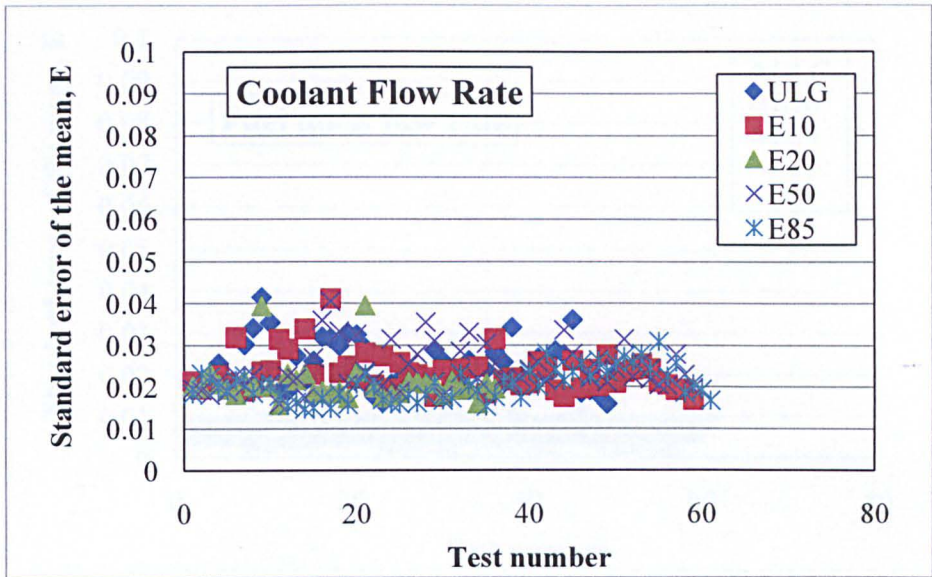


Figure A 5.2. Standard error of the mean of coolant flow rate. The engine running at speed ranging between 1500-4000 rpm, BMEP between 1.57 to 8 bar and different fuel mixtures.

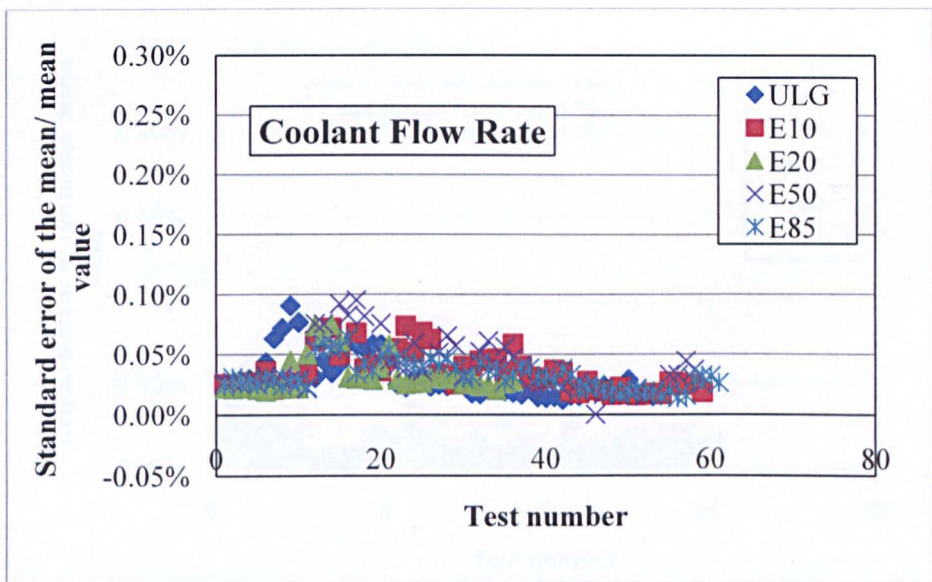


Figure A 5.3. Standard error of mean of the coolant flow rate as a percentage of the mean value.

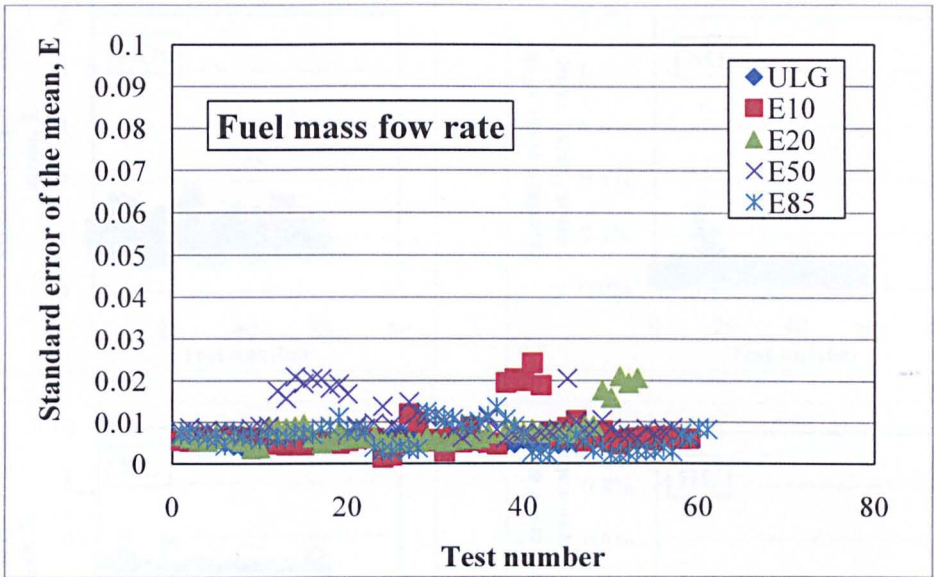


Figure A 5.4. Standard error of the mean of the fuel flow rate. The engine running at speed ranging between 1500-4000 rpm, BMEP between 1.57 to 8 bar and different fuel mixtures.

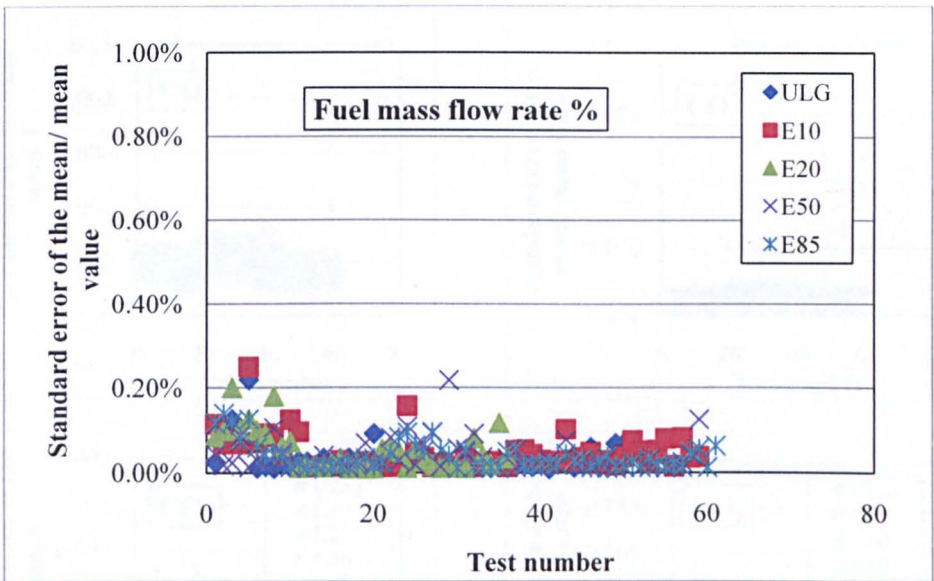


Figure A 5.5. Standard error of mean of the fuel flow rate as a percentage of the mean value.

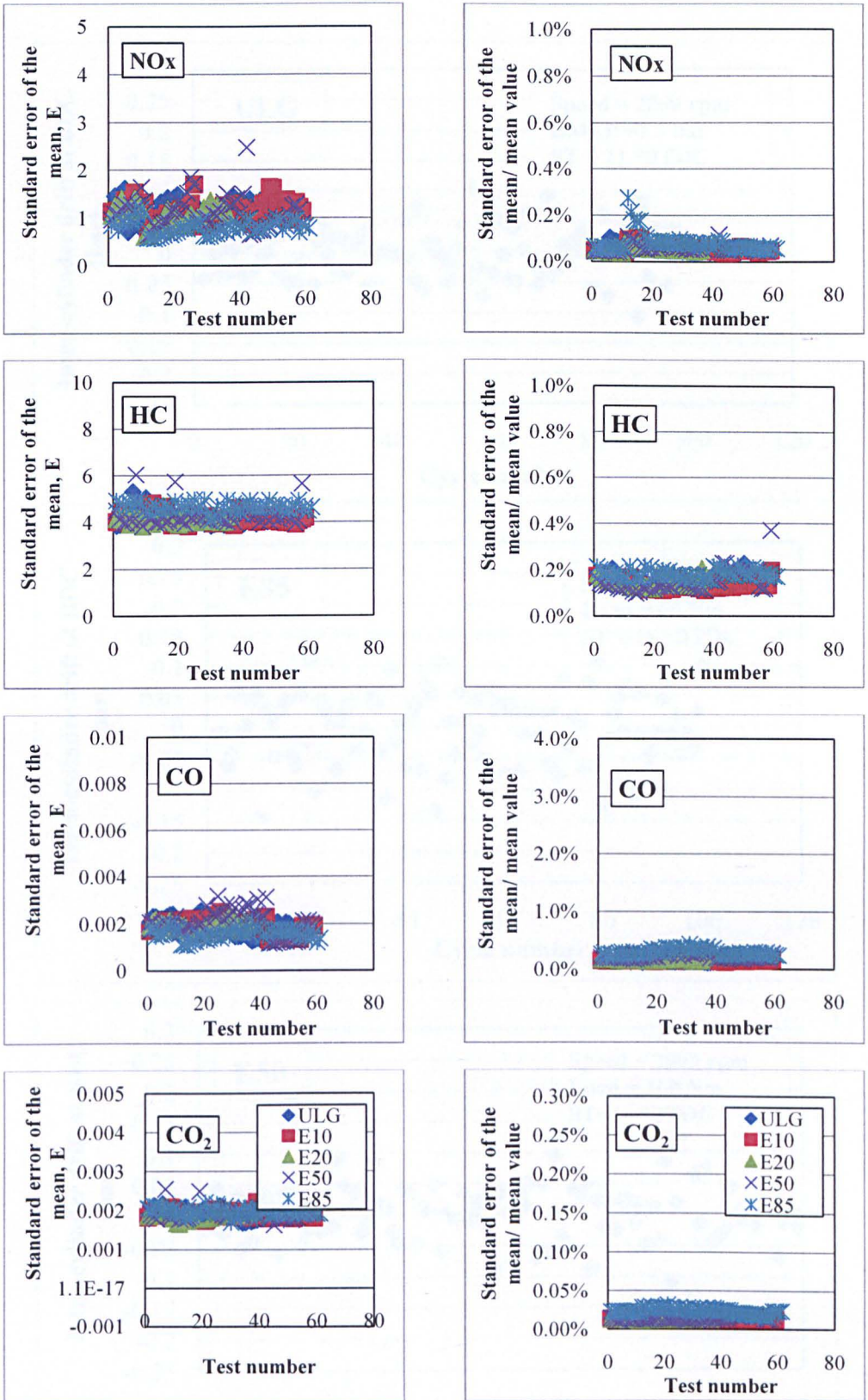


Figure A 5.6. Standard error of the mean of the emissions constituent and its percentage of the mean value. The engine running at speed ranging between 1500-4000 rpm, BMEP between 1.57 to 8 bar and different fuel mixtures.

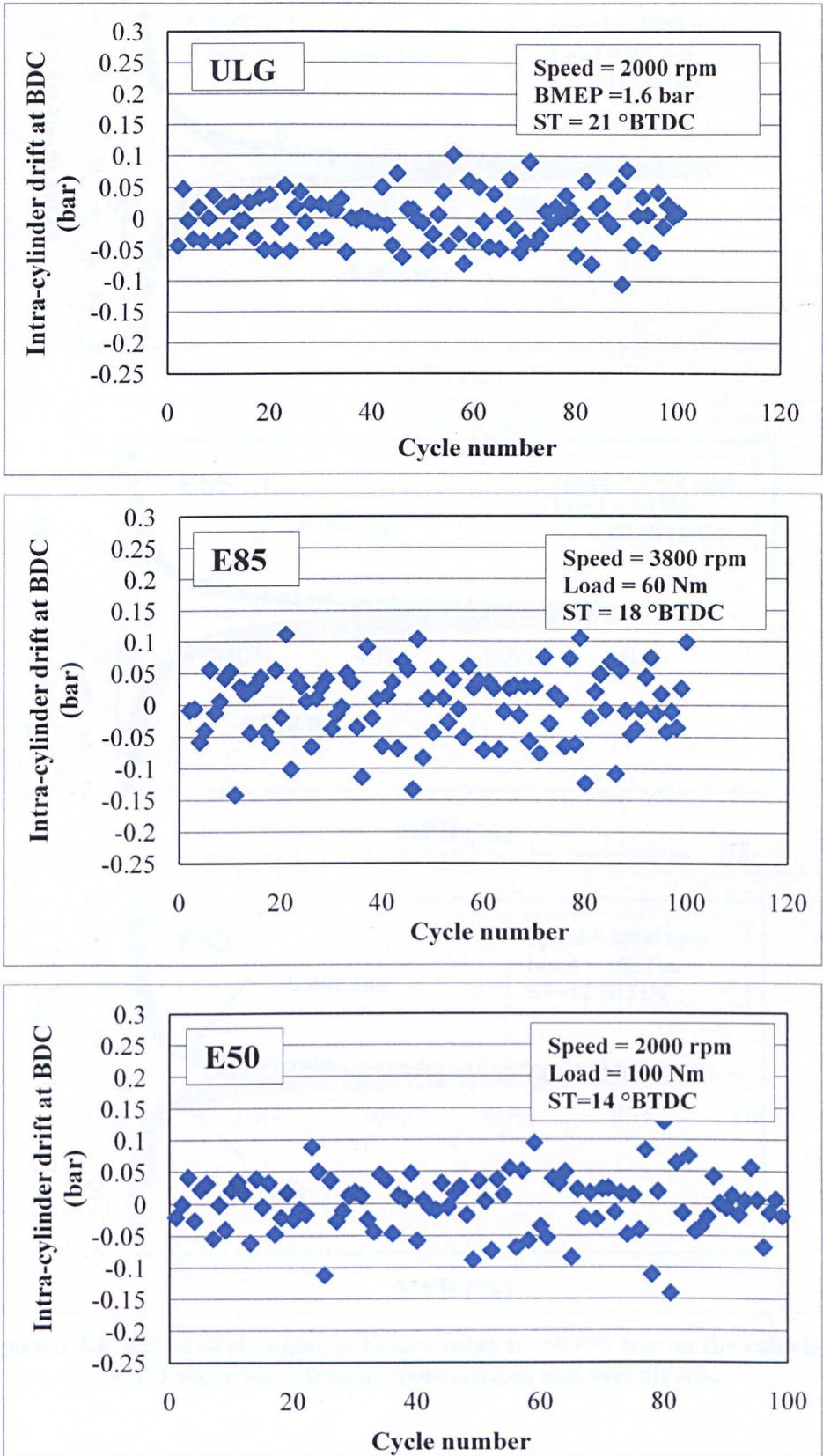


Figure A 5.7. Intra-cycle change in transducer output at inlet BDC over 100 consecutive cycles for different loads, speeds and fuel content.

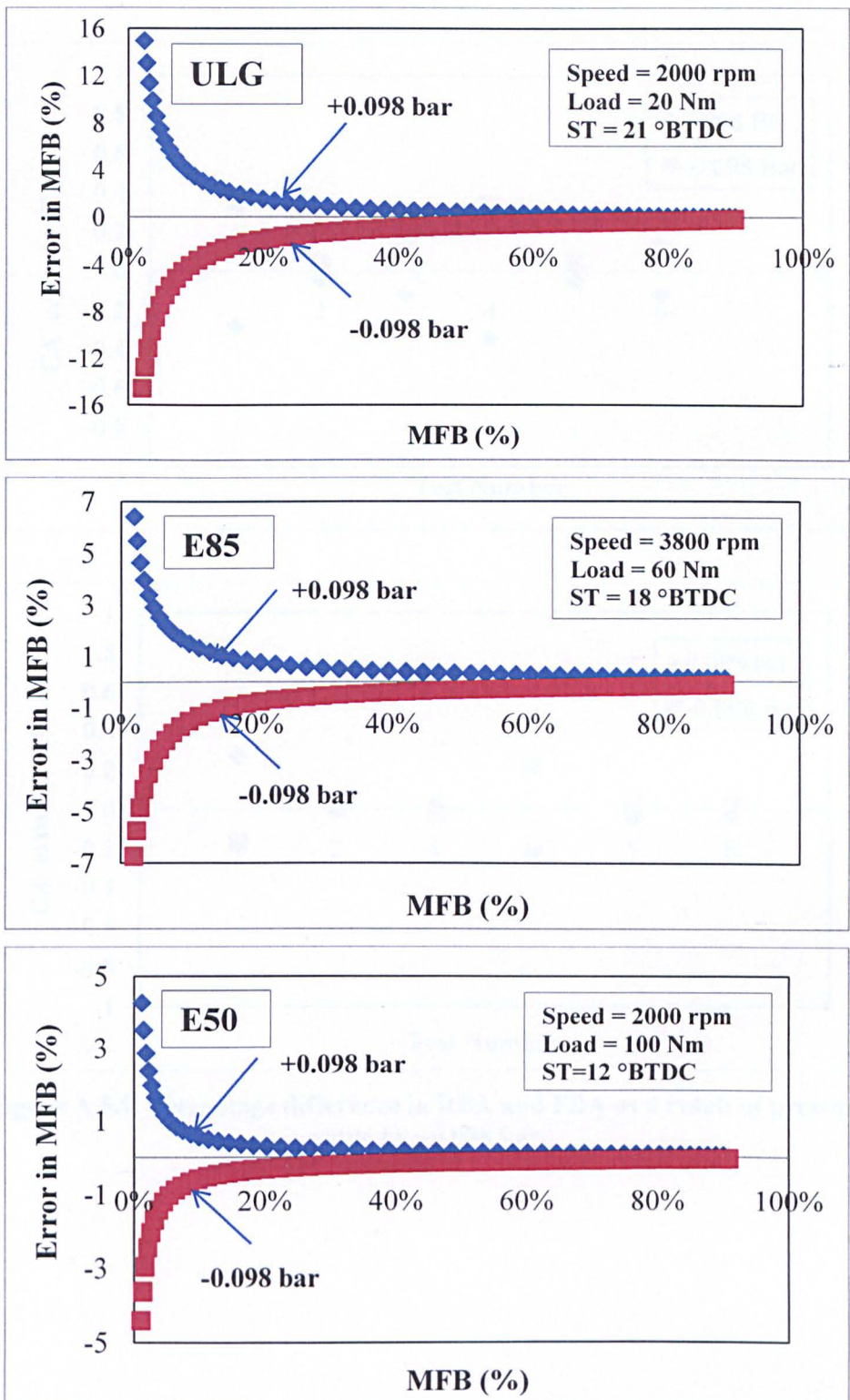


Figure A 5.8. Effect of changing pressure value by ± 0.098 bar on the calculated MFB error for different speeds, loads and fuel blends.

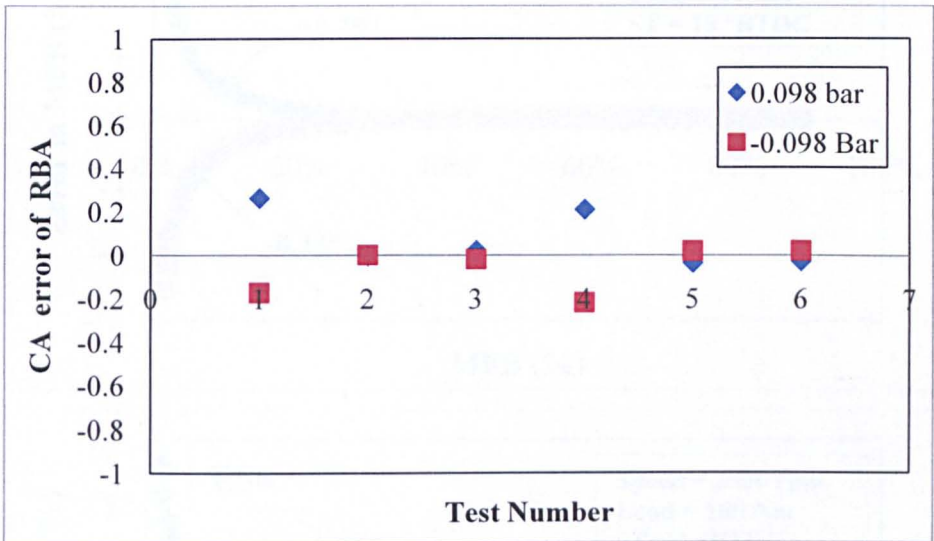
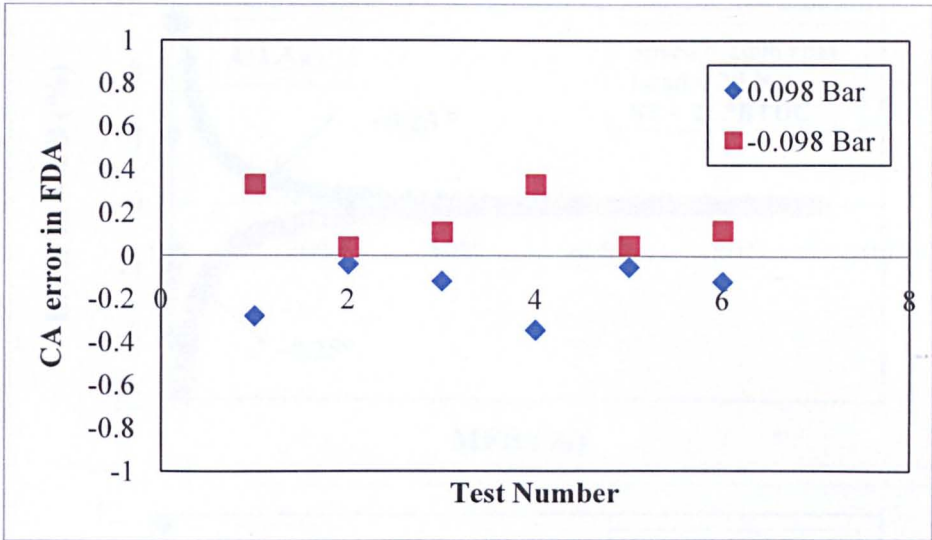


Figure A 5.9. Percentage difference in RBA and FDA as a result of pressure value by ± 0.098 bar.

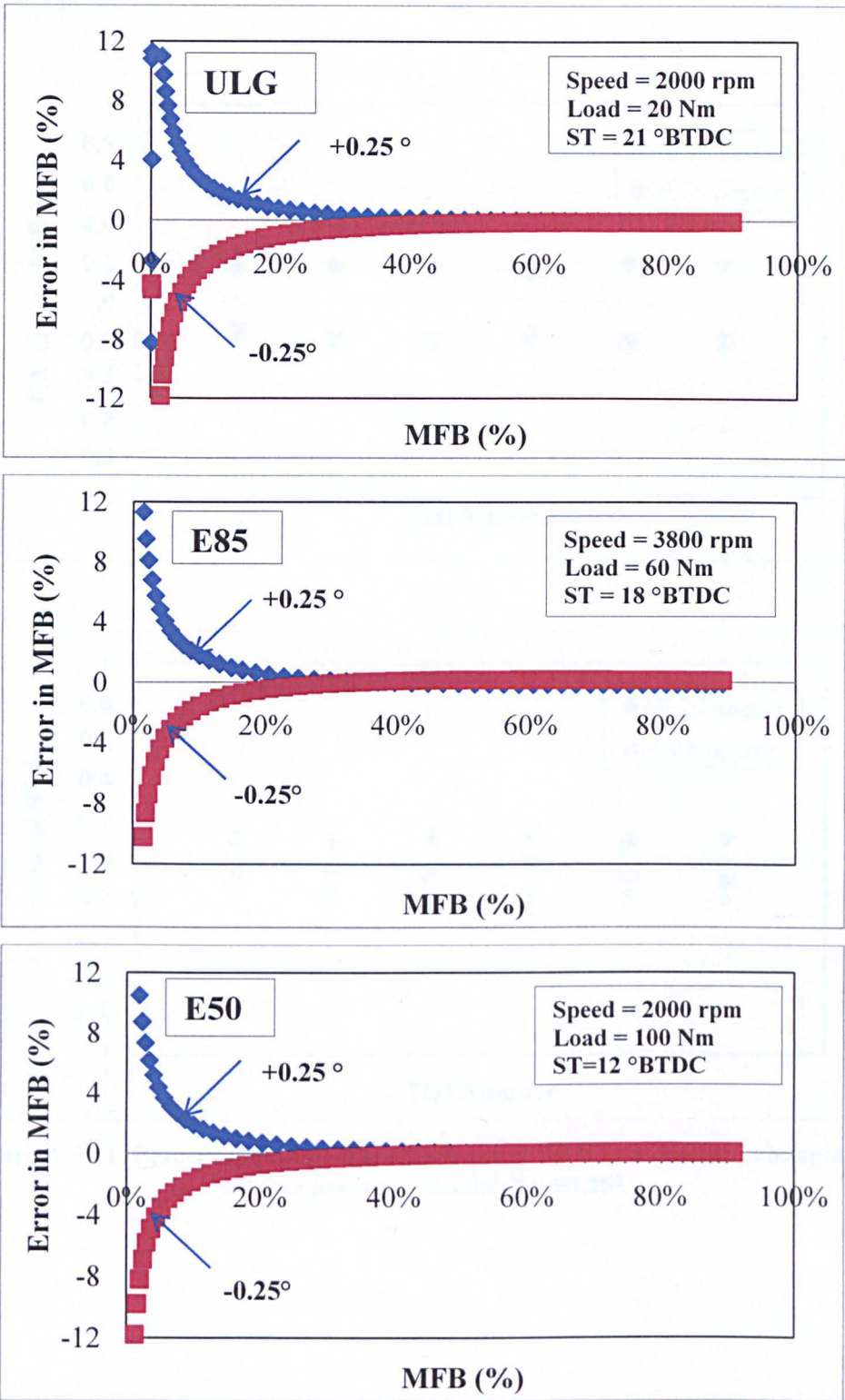


Figure A 5.10. Effect of changing of volume pressure phasing by $\pm 0.25^\circ$ on the calculated MFB error for different speeds, loads and fuel blends.

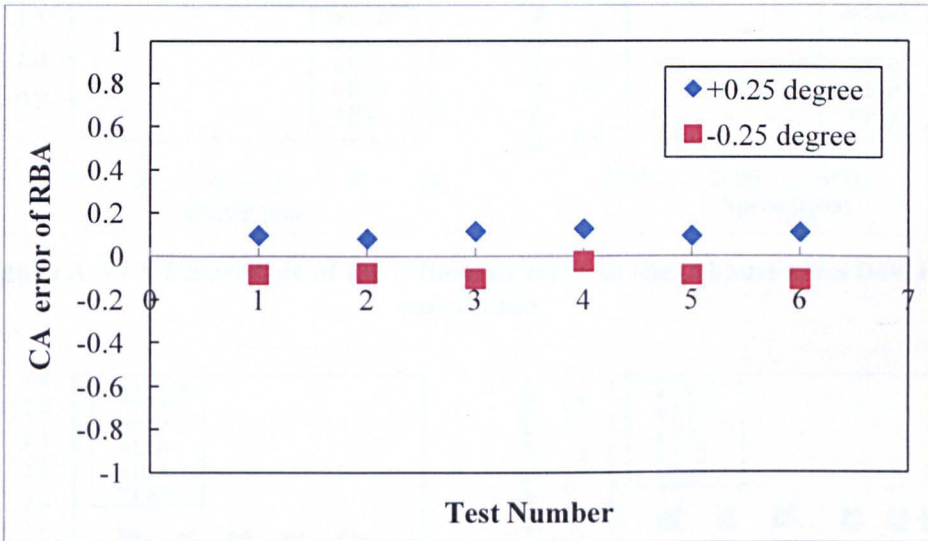
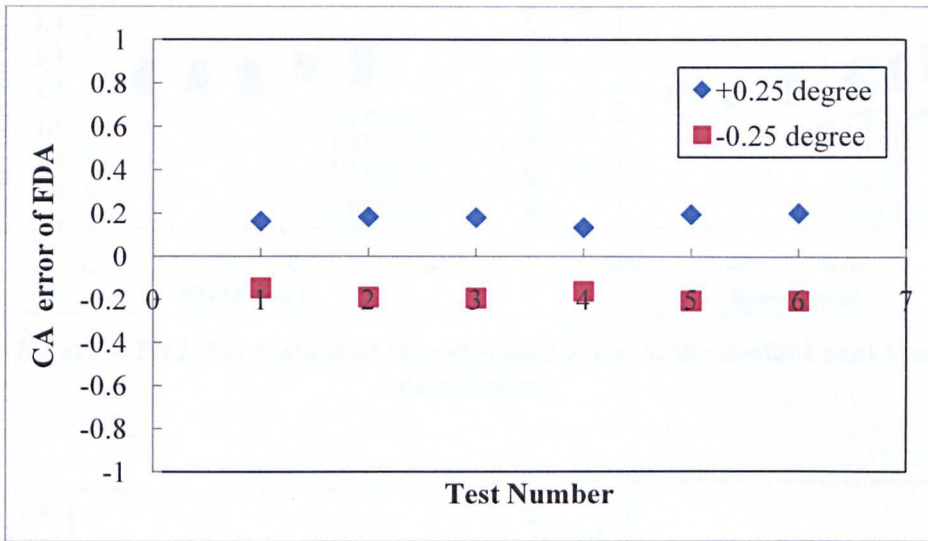


Figure A 5.11. Percentage difference in RBA and FDA as a result of changing of volume pressure phasing by $\pm 0.25^\circ$.

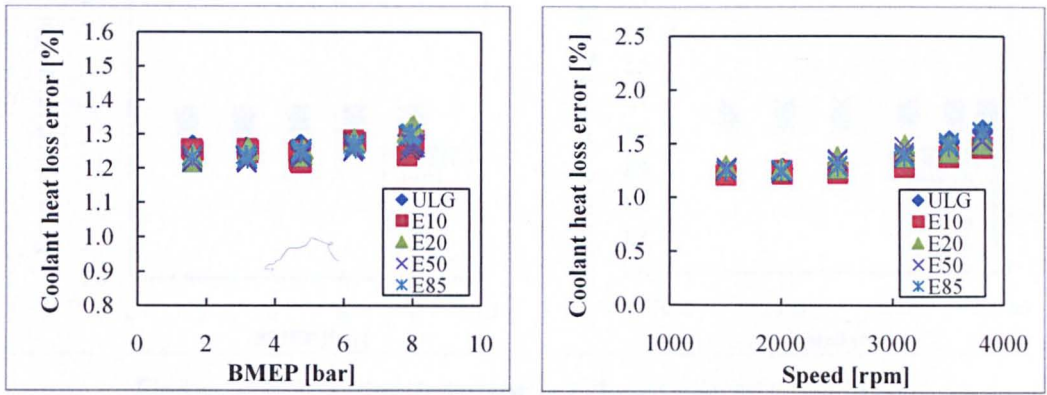


Figure A 5.12. Percentage of the estimated error in the coolant heat loss calculation.

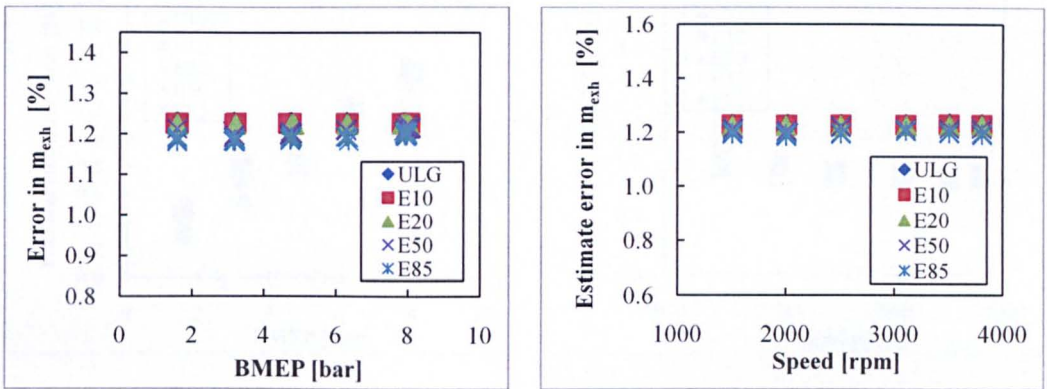


Figure A 5.13. Percentage of the estimated error in the exhaust mass flow rate calculation.

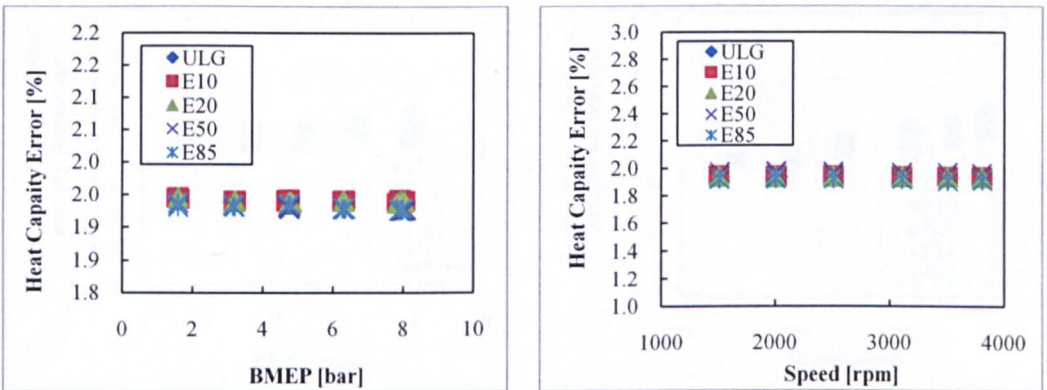


Figure A 5.14. The estimated error in the heat capacity calculation.

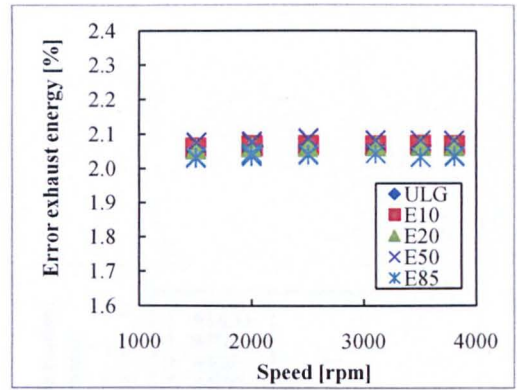
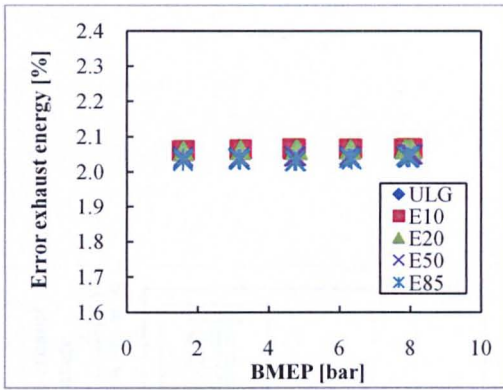


Figure A 5.15. Estimated error in exhaust energy calculation.

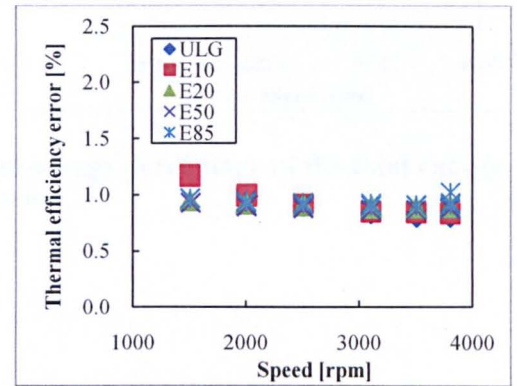
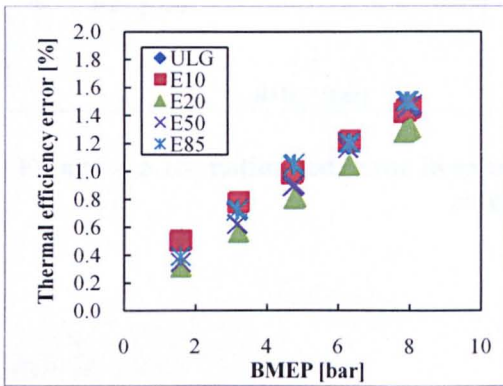


Figure A 5.16. Estimated error in the thermal efficiency calculation.

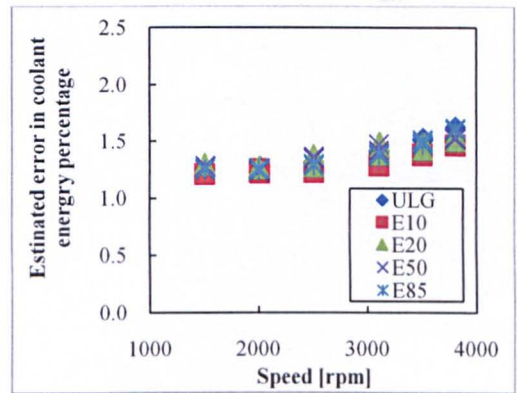
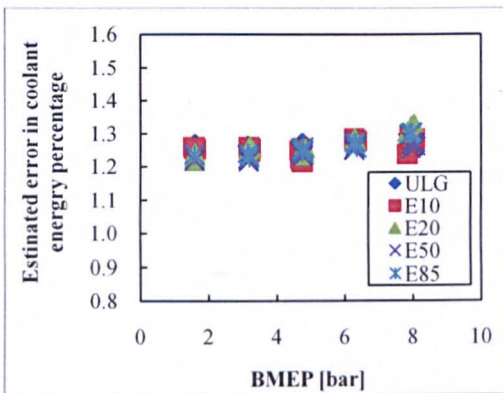


Figure A 5.17. Estimated error in coolant energy percentage of the total energy calculation.

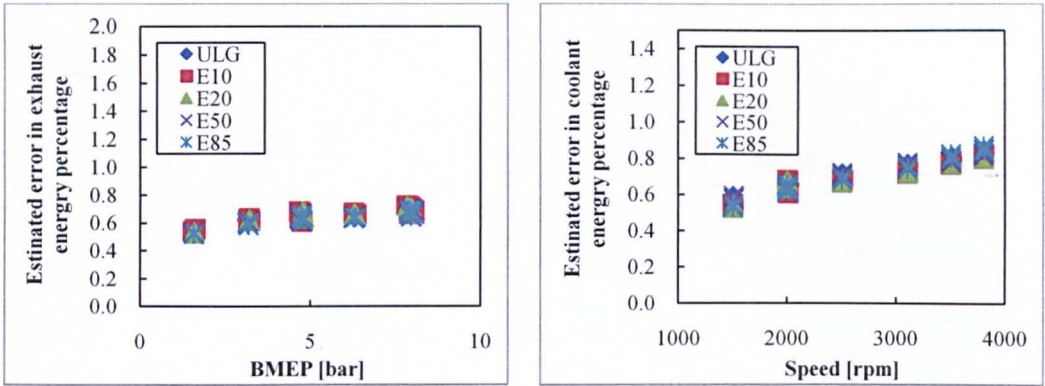


Figure A 5.18. Estimated error in exhaust energy percentage of the total energy calculation.